



**FUNDAMENTAL STUDIES OF  
ENANTIOSELECTIVE CATALYTIC  
HYDROGENATION OF ETHYL PYRUVATE AT  
SUPPORTED PLATINUM**

**A thesis submitted to  
Cardiff University  
for the degree of  
Philosophiae Doctor**

**By**

**Salem Farag Elkhaseh**

**School of Chemistry  
Cardiff University**

**December 2008**

UMI Number: U585183

All rights reserved

INFORMATION TO ALL USERS

The quality of this reproduction is dependent upon the quality of the copy submitted.

In the unlikely event that the author did not send a complete manuscript and there are missing pages, these will be noted. Also, if material had to be removed, a note will indicate the deletion.



UMI U585183

Published by ProQuest LLC 2013. Copyright in the Dissertation held by the Author.  
Microform Edition © ProQuest LLC.

All rights reserved. This work is protected against  
unauthorized copying under Title 17, United States Code.



ProQuest LLC  
789 East Eisenhower Parkway  
P.O. Box 1346  
Ann Arbor, MI 48106-1346

## ABSTRACT

Enantioselective heterogeneous catalysis is an important and growing area of research. One of the most commonly studied examples of this type of catalysis is the hydrogenation of ethyl pyruvate (EP) to *R*-ethyl lactate on chirally modified Pt catalysts, first reported in 1979 by Orito and co-workers. The hydrogenation of ethyl pyruvate over cinchona alkaloid-Pt/graphite, alumina and silica catalysts has been investigated in different solvents.

The effect of pre-heating the Pt/graphite and Pt/alumina in 5% H<sub>2</sub>/Ar at 700K was also investigated. Cyclic voltammetry has been used to investigate (i) the surface morphology of Pt particles of the terraces, steps and kinks present in as-received and conditioned catalysts and (ii) the adsorption of bismuth at Pt surfaces. By the selective blocking of Pt adsorption sites using bismuth adatoms it is shown that the modifiers hydroquinine 4-chlorobenzoate (CD-der) and hydroquinidine 4-chlorobenzoate (CN-der) give rise to novel catalytic behaviour in relation to the enantioselective hydrogenation of ethyl pyruvate. It is reported that hydrogenation of ethyl pyruvate affords an enantiomeric excess to *R*-(*S*-) ethyl lactate in DCM if CD-der (CN-der) is adsorbed at step/defect sites whereas an excess of *S*-(*R*-) ethyl lactate results from adsorption of CD-der (CN-der) at Pt{111} terrace sites. The variation of *ee* with modifier amount may also be explained within this model, as previously speculated by Hutchings *et al* [1]. In addition, hydrogenation experiments using CD-der, CN-der and CD in acetic acid demonstrate a complete collapse of *ee* for reaction occurring on Pt{111} terraces. Various structural models are proposed to interpret this behaviour. In particular, in order to rationalise the enantiodifferentiation results obtained in acetic acid it is necessary to speculate that a tilting of the quinoline substituent of the modifier when adsorbed on Pt{111} planes is occurring. Such a phenomenon is absent in the presence of aprotic solvents. Rationalisation of the effect of molecular tilting of modifier on *ee* is obtained by invocation of a recent model by McBreen *et al* [2] which states that hydrogen bonding interactions between the

substrate and the quinoline substituent of the modifier are crucial for enantioselection. It is proposed that tilting of the quinoline ring weakens  $\pi$ -interactions with the  $d$ -orbitals of the Pt catalyst and hence attenuates the magnitude of hydrogen bonding of the aromatic hydrogens with the carbonyl group of the substrate leading to a loss of  $ee$ .

- [1] N.F.Dummer, R. Jenkins, X. Li, S.M. Bawaked, P. McMorn, A. Burrows, C.J. Kiely, R.P.K. Wells, D.J. Willock, G. Hutchings, *J. Catal.*, **243** (2006) 165.
- [2] S. Lavoie, M.-A. Laliberte, I. Temprano, P.H. McBreen, *J. Am. Chem. Soc.*, **128** (2006) 7588.

## **ACKNOWLEDGEMENT**

It is with pleasure that I would like to acknowledge and express particular thanks to my supervisor, Prof. Gary A. Attard, for his constant support, guidance, encouragement, and patience throughout the course of this thesis.

I also would like to thank my employer, The Libyan Government, for funding my study.

Also thanks go to the people in lab 0.117 for their help and support during this study.

Also I would like to thank all the chemistry academic staff and the technical staff in the School of Chemistry for their continued support and help.

I would like to thank my family for their endless patience and understanding throughout the course of this study.

Finally, this study could not have been completed without the help, guidance and inspiration of Allah.

## **DEDICATION**

To my late father

To my mother, brothers and sisters and

To my wife

To my sons, Farag and Fearahs

## DECLARATION


This work has not previously been accepted in substance for any degree and is not being concurrently submitted in candidature for any degree.

Signed..........(Candidate)

Date... 27.03.2009.....

## STATEMENT 1

This thesis is the result of my own investigations, except where otherwise stated. Other sources are acknowledged by footnotes giving explicit references. A bibliography is appended.

Signed..........(Candidate)

Date... 27.03.2009.....

## STATEMENT 2

I hereby give consent for my thesis, if accepted, to be available for photocopying and for inter-library loan, and for the title and summary to be made available to outside organisations.

Signed..........(Candidate)

Date... 27.03.2009.....

# TABLE OF CONTENTS

<b>CHAPTER ONE: INTRODUCTION</b>		<b>1</b>
<b>1</b>	<b>Introduction</b>	<b>2</b>
1.1	Historical background	2
<b>1.2</b>	<b>Terms and Definitions</b>	<b>5</b>
1.2.1	Catalyst and catalysis	5
1.2.2	Heterogeneous and homogenous catalysis	6
1.2.2.1	Homogenous catalysis	6
1.2.2.2	Heterogeneous catalysis	10
1.2.2.2.1	Langmuir-Hinshelwood mechanism	11
1.2.2.2.2	Eley-Rideal mechanism	12
1.2.2.3	Advantages of heterogeneous catalysis over homogeneous catalysis	14
1.2.3	Adsorption of molecules at the catalyst surface	14
1.2.3.1	Chemisorption	15
1.2.3.2	Physisorption	17
1.2.4	Selectivity and activity	18
<b>1.3</b>	<b>Asymmetric catalysis</b>	<b>21</b>
<b>1.4</b>	<b>Chirality</b>	<b>22</b>
<b>1.5</b>	<b>The Orito reaction</b>	<b>25</b>
1.5.1	Experimental aspects of the Orito reaction	28
<b>1.6</b>	<b>Cinchona alkaloids</b>	<b>28</b>
<b>1.7</b>	<b>Substrates</b>	<b>31</b>
<b>1.8</b>	<b>Models of enantioselectivity</b>	<b>36</b>
1.8.1	The Wells model	36
1.8.2	The Baiker model	38
1.8.3	The Augustine model	41
1.8.4	The Margitfalvi model	42



1.8.5	The McBreen model	44
<b>1.9</b>	<b>Solvents</b>	<b>47</b>
<b>1.10</b>	<b>Background to experimental methods used</b>	<b>48</b>
1.10.1	Electrochemical methods	48
1.10.2	Voltammetry	48
1.10.3	Cyclic voltammetry	48
1.10.4	Characterization of Pt surfaces from CV	50
<b>1.11</b>	<b>Miller indices</b>	<b>53</b>
<b>1.12</b>	<b>Objectives</b>	<b>58</b>
<b>1.13</b>	<b>References</b>	<b>59</b>
 <b>CHAPTER TWO: EXPERIMENTAL</b>		 <b>69</b>
<b>2.1</b>	<b>Introduction</b>	<b>70</b>
<b>2.2</b>	<b>Materials</b>	<b>71</b>
2.2.1	Catalysts	71
2.2.2	Reactants and reagents	71
<b>2.3</b>	<b>Apparatus</b>	<b>73</b>
2.3.1	Autoclave reactor	73
2.3.2	Control tower	76
2.3.3	Process gas flow diagram	77
2.3.4	Control system	78
<b>2.4</b>	<b>Experimental procedure</b>	<b>79</b>
<b>2.5</b>	<b>Product recovery</b>	<b>81</b>
<b>2.6</b>	<b>Product analysis</b>	<b>81</b>
2.6.1	Chiral gas chromatograph	81
<b>2.7</b>	<b>Analysis</b>	<b>84</b>
2.7.1	Determination of enantiomeric excess ( <i>ee</i> )	84
2.7.2	Determination of conversion	84
<b>2.8</b>	<b>The electrochemical cell and data collection</b>	<b>85</b>

2.8.1	Electrochemical cell preparation procedure	87
<b>2.9</b>	<b>Ultra-pure water purification system</b>	<b>89</b>
<b>2.10</b>	<b>Distillation of ethyl pyruvate</b>	<b>89</b>
<b>2.11</b>	<b>Apparatus used for catalyst reduction</b>	<b>91</b>
<b>2.12</b>	<b>Addition of bismuth <math>\text{Bi}(\text{NO}_3)_3</math> to platinum surface</b>	<b>93</b>
<b>2.13</b>	<b>Calculation of adsorbate coverage</b>	<b>94</b>
2.13.1	Adsorbate coverage of Bi	94
<b>2.14</b>	<b>References</b>	<b>96</b>

## CHAPTER THREE: RESULTS

<b>ENANTIOSELECTIVE HYDROGENATION OF ETHYL PYRUVATE CATALYSED BY PLATINUM ON GRAPHITE, SILICA AND ALUMINA</b>		<b>97</b>
<b>3.1</b>	<b>Introduction</b>	<b>98</b>
<b>3.2</b>	<b>Results of enantioselective hydrogenation of ethyl pyruvate (distilled and non-distilled) using Cinchonidine-derivative and Cinchonine-derivative modified 5% Pt/G</b>	<b>88</b>
3.2.1	Standard reaction on graphite	88
3.2.2	Thermal annealing of Pt/G and its influence on enantioselective hydrogenation	103
3.2.3	Enantioselective hydrogenation of distilled ethyl pyruvate over CD-derivative and CN-derivative-modified 5% Pt/G catalyst sintered at 700K in dichloromethane and acetic acid	106
3.2.4	Adsorption of bismuth onto unsintered 5% Pt/G	109
3.2.5	Adsorption of bismuth onto 5% Pt/G at 700K	120
3.2.6	The influence of solvent on <i>ee</i> using cinchonidine (CD) and cinchonine (CN) as modifiers	133
3.2.7	Reaction of bismuthated catalysts in acetic acid	134
3.2.8	The influence of Pt metal loading on enantiomeric excess	143
<b>3.3</b>	<b>Enantioselective hydrogenation using EUROPT-1</b>	<b>145</b>
3.3.1	Standard reaction over EUROPT-1	145
<b>3.4</b>	<b>Enantioselective hydrogenation using 5% Pt/<math>\text{Al}_2\text{O}_3</math></b>	<b>151</b>

3.4.1	Comparison of CD-derivative and CN-derivative on values of enantiomeric excess of ethyl pyruvate hydrogenation over 5% Pt/Al <sub>2</sub> O <sub>3</sub> catalyst at 300K in dichloromethane (DCM)	152
3.4.2	Comparison of CD-derivative and CN-derivative on values of enantiomeric excess of ethyl pyruvate hydrogenation over 5% Pt/Al <sub>2</sub> O <sub>3</sub> catalyst at 700K in acetic acid	157
3.5	<b>References</b>	<b>168</b>
 <b>CHAPTER FOUR: DISCUSSION</b>		<b>170</b>
4.1	<b>Introduction</b>	<b>171</b>
4.2	<b>The structural reaction model used to interpret <i>ee</i> change</b>	<b>171</b>
4.2.1	Reaction in DCM of CD-derivative and CN-derivative	171
4.2.2	Reaction in DCM of CD and CN	172
4.2.3	Reaction in the presence of acetic acid of CD-derivative and CN-derivative	172
4.2.4	Reaction in presence of acetic acid of CD and CN	173
4.2.5	Model justification	173
4.2.5.1	Justification of assumptions listed in 4.2.2 and 4.2.4	173
4.2.5.2	Justification of assumptions 4.2.1 and 4.2.3	176
4.2.6	The impact of EP distillation on enantiomeric excess	183
4.2.7	Particle size effects	186
4.2.8	Variation of catalyst support	187
4.2.8.1	Pt/silica	188
4.2.8.2	Pt/alumina	191
4.3	<b>Possible configuration of modifier in controlling enantioselectivity</b>	<b>198</b>
4.4	<b>References</b>	<b>205</b>

<b>CHAPTER FIVE: SUMMARY AND FUTURE WORK</b>	<b>208</b>
<b>5.1 Summary and future work</b>	<b>209</b>
<b>5.2 References</b>	<b>212</b>

**CHAPTER ONE**

**INTRODUCTION**

## 1. Introduction

### 1.1. Historical background

Catalytic reactions play a fundamental role in all of our lives. Most biological reactions in our bodies are catalytic and are vital for our survival. The incorporation of catalytic methods in organic synthesis has also become a major feature of modern synthetic chemistry. The preservation and restoration of the environment are among the most pressing economic, technological, political, environmental and scientific challenges of our time and catalysis offers a means of carrying out highly energy and material efficient chemical processes and therefore will impact enormously on all of these issues. The term “catalysis” was first coined in the early nineteenth century when many important discoveries in chemistry and physics were being made. Kirchhoff noted that acids aided the hydrolysis of starch to glucose [1]. Faraday (1813) was the first to explore the reasons for the increase in the rate of reaction when he studied the effect of platinum on oxidation reactions. In 1825 Döbereiner discovered that platinum could be used to catalyse the oxidation of hydrogen at room temperature. By mixing platinum sponge with clay, he anticipated the methods for supporting the active metal which came into widespread use almost a century later [2]. The term catalysis was coined by Berzelius (1836) [3]. Ostwald defined catalysts as “*agents which accelerate chemical reaction without affecting the chemical equilibrium*”. Catalysis is essentially a chemical phenomenon and the ability of a substance to act as a catalyst in a specified system depends on its chemical nature. In heterogeneous catalysis, the catalyst

is not present in the same phase as the reactants. Hence, one is concerned with specific chemical properties of, for example, the surface of the catalytic substance in order to rationalise the heterogeneous catalytic effect. Some important milestones in the history of heterogeneous catalysis are outlined in Table 1.1.

*Table 1.1 Important dates marking advances in catalysis at surfaces [4].*

Year	Investigator (s)	Phenomenon
1796	van Marum	Dehydrogenation of alcohols contacted with metal surfaces.
1817	Davy & Döbereiner	Glowing of metals in contact with mixtures of air and combustible gases.
1825	Faraday	Surface induced combustion of hydrogen.
1831	Phillips	Patent for sulphur dioxide oxidation on platinum.
1836	Berzelius	Definition of catalysis.
1869	von Hoffmann	Partial oxidation of methanol to formaldehyde on silver.
1875	Squire, Messel	Industrial scale oxidation of sulphur dioxide on platinum.
1894	Takamine	First patent for an extracted enzyme catalyst.
1905	Sabatier & Sanderens	Hydrogenation of unsaturated hydrocarbons on nickel.
1913	Sabatier & Sanderens	First ammonia synthesis plant operated at Oppau, (Germany) ( $1.3 \times 10^8$ kg fixed nitrogen per annum).
1915	Langmuir	First quantitative theory of adsorption.
1925	H.S.Taylor	First detailed theory of contact catalysis.

Table 1.2 Important dates marking advances in enantioselective catalysis [5]

Year	Investigator (s)	Phenomenon
1932	Schwab & Rudolph	Explored supporting the Group 10 metals on cleaved quartz; these catalysts showed enantiomeric discriminations of up to 10% in the dehydration of secondary butanol.
1956	Akabori	Studies of metals supported on silk.
1959	Balandin	Polysaccharides.
1970	Harada	Cellulose.
1920	Erlenmeyer	First reported an enantiomeric excess of 50% in the bromination of cinnamic acid catalysed by ZnO modified by fructose and later a positive result was obtained in the bromination of the hydrocinchonine salt of cinnamic acid in homogeneous solution.
1939	Lipkin & Stewart	Investigated whether a hydrocinchonine salt would modify a Pt surface so as to induce enantioselective hydrogenation and they reported the enantioselective hydrogenation of hydrocinchonine $\beta$ -methylcinnamate to $\beta$ -phenylbutyric acid catalysed by Adams Pt.
1978	Orito, Imai, and Niwa	Foundation for extensive studies of noble metals modified by cinchona alkaloids that have appeared over the last decade and in which values of the enantiomeric excess of up to 98% have been reported in $\alpha$ -ketoester hydrogenations over cinchona-modified Pt.



## 1.2 Terms and Definitions

### 1.2.1 Catalyst and catalysis

Transition metals are of paramount importance in catalysis. Transition metal elements can form one or more stable ions which have incompletely filled  $d$  orbitals. One of the key features of transition metal chemistry is a wide range of oxidation state (oxidation numbers) that the metal can show. Because they can readily gain and lose electrons without a high energetic penalty, oxidation states of transition–metal complexes may be changed smoothly and intervene upon a system to push reactions forward [6].

As originally stated by Ostwald, the role of a catalyst is to achieve a rapid equilibrium for a chemical reaction by increasing the rate of forward and reverse reaction (*i.e.* increasing the rate constants of the reaction,  $k_1$  and  $k_2$ ).



The rate constant,  $k$ , is defined by the Arrhenius equation:

$$k = A \exp(-\Delta E_a/RT) \quad (1.2)$$

where,  $A$  is the collision frequency,  $E_a$  is the activation energy,  $R$  is the gas constant and  $T$  is the temperature. A catalyst lowers the activation barrier of the process, *i.e.* it provides a more energetically favourable pathway for conversion of reactants to product (Figure 1.1). Hence, catalysis is a purely kinetic effect. In Figure 1.1 a hypothetical reaction coordinate for a process which is catalysed is superimposed on the coordinate for the same process which is not catalysed. Regeneration of the active species or site is another feature of catalysis. Consequently, significantly less than one equivalent of catalyst is

usually required to transform the reactant to product. In terms of performance, the use of a small amount of catalyst and simpler reaction conditions constitute two great advantages of catalytic reactions.

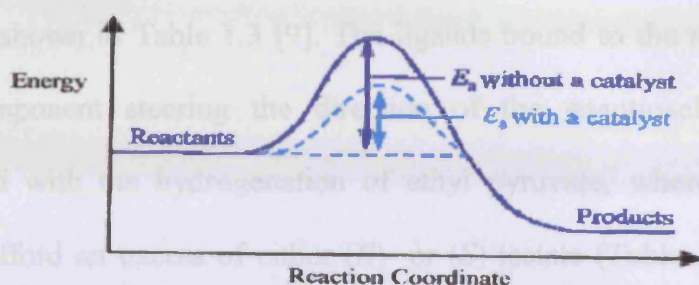


Figure 1.1 Activation energy barriers of a catalysed and uncatalysed chemical reaction.

## 1.2.2. Heterogeneous and homogenous catalysis

### 1.2.2.1 Homogenous catalysis

Homogenous catalysts work in the same phase as the reactants. Often the reactants, products and catalysts are all dissolved in the same solvent. Consequently, reactants can achieve good “contact” with the catalyst [7]. In homogeneous catalysis, the chemistry of the metal atom at the heart of the homogenous catalyst is directly influenced by the environment of the ligands surrounding it which at the same time provides the active site for the reaction [8]. Ligand substituents play an important role in tuning the selectivity of a catalyst. By this, it is meant that not only may the catalyst accelerate chemical reactions, but that different possible products may be accelerated to different extents. A special case of selectivity exhibited by homogeneous catalysts is enantioselectivity. An enantioselective catalyst by its action facilitates the

production of one chiral product over and above the production of the other enantiomer. The Binap-Ru (see Table 1.3) catalysts are examples of excellent ligand-metal complexes that allow efficient enantioselective hydrogenation of functionalized olefins and ketones producing a high enantiomeric excess (up to 99%) as shown in Table 1.3 [9]. The ligands bound to the metal centre are a vital component steering the direction of the enantioselectivity. This is illustrated with the hydrogenation of ethyl pyruvate, where different chiral ligands afford an excess of either (*R*)- or (*S*)-lactate (Table 1.3 entry 1) [10]. Both catalysts contain a ruthenium centre but for an excess of (*S*)-ethyl lactate, the ligand (2*S*, 3*S*)-NORPHOS is used whereas to achieve an *ee* in (*R*)-lactate the ligand (2*S*, 4*S*)-BPPM is used. Other examples of this behaviour include the enantioselective hydrogenation of aromatic ketones (Figure 1.2) [11]. Homogeneous chiral catalysts exhibit high activity and selectivity and the reaction mechanism can be investigated *via* spectroscopic methods such as NMR [12]. Hence a good deal of insight concerning the catalytic action of metal complexes has been obtained [13]. However, difficulties of separation, handling and re-use constitute major disadvantages associated with homogeneous catalysts.

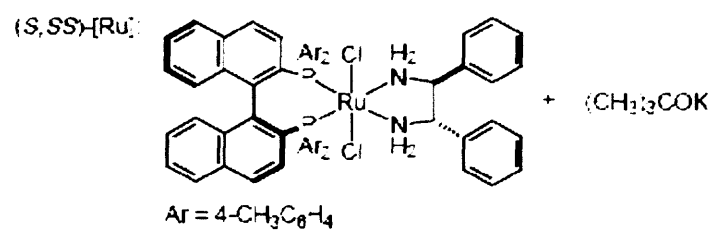
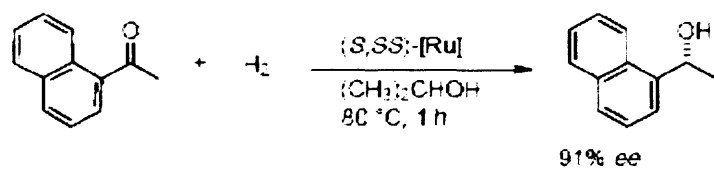


Figure 1.2 Example of enantioselective hydrogenation of aromatic ketones using homogeneous metal complexes. Reproduced from reference [11].

Table 1.3 Values of enantiomeric excess for hydrogenation reactions conducted using homogeneous catalysts.

Entry	Reactant	Enantiomeric excess (%)	Catalyst	Reference
1		89 ( <i>S</i> )	Rh (nbd)Cl <sub>2</sub> + (2 <i>S</i> ,3 <i>S</i> )-NORPHOS <sup>a</sup>	10
2		71 ( <i>R</i> )	Rh (nbd)Cl <sub>2</sub> + (2 <i>S</i> ,4 <i>S</i> )-BPPM <sup>b</sup>	13
		1. 97 ( <i>S</i> ) 2. 99 ( <i>R</i> )	Ru-( <i>S</i> )-BINAP <sup>c</sup> Ru-( <i>R</i> )-MeO-BIPHEP <sup>d</sup>	
3		99 ( <i>R</i> )	Ru-( <i>R</i> )-xylyl-PhanePhos <sup>e</sup> (+( <i>S,S</i> )-DPEN <sup>f</sup> )	15
		98 ( <i>S</i> )	Ru-( <i>S</i> )-xylyl-PhanePhos <sup>e</sup> (+( <i>R,R</i> )-DACH <sup>g</sup> )	
4		72 ( <i>R</i> )	Rh-( <i>R</i> )-BINAP <sup>c</sup>	16
		90 ( <i>R</i> )	Rh-( <i>R</i> )-MeO-BIPHEP <sup>d</sup>	
5		96 ( <i>R</i> )	( <i>R,R</i> )-Ru-BICP <sup>h</sup> (+ ethylthioethylamine)	17
		93 ( <i>S</i> )	( <i>S,S</i> )-Ru-BICP <sup>h</sup> (+ ethylthioethylamine)	
6		91 ( <i>R</i> )	Soluble di-Rh <sup>i</sup>	18
		91 ( <i>R</i> )	Silica supported di-Rh <sup>j</sup>	

nbd = norbornadiene; a = (2,3)-bis-(diphenylphosphino)-bicyclo-[2.2.1]-hept-5-ene;

b = (2,4)-bis-(para-phosphophenyl)methane;

c = 2,2'-bis(diphenylphosphino)-1,1'-binaphthyl;

d = 6,6'-dimethoxy-2,2'-bis(diphenylphosphino)-1,1'-biphenyl; e = 4,12-

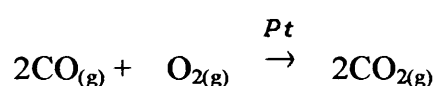
bis(diphenylphosphino)-[2.2]paracyclopane; f = 1,2-diphenylethylenediamide; g = trans-1,2-

diaminocyclohexane; h = (2,2')-bis(diphenylphosphanyl)-(1,1')-dicyclopentane;

i=di( $\mu$ -carboxylato)bis(aminophosphinephosphinite)dirhodium; j= silica supported-i.

### 1.2.2.2. Heterogeneous catalysis

Heterogeneous catalysts participate in chemical reactions by being present in a different phase from the reactants, (*i.e.* the addition of the catalyst to a reaction increases the number of phases present). The catalysed reactions proceed through adsorption of the reactants onto the catalyst surface, followed by molecular or atomic level rearrangement of reactants forming products, and desorption of the final products from the catalyst surface [19]. In catalysis, it is desirable to obtain a fundamental understanding of the catalytic process, *i.e.* reaction mechanisms and reaction kinetics. Unfortunately, many of the spectroscopic methods available to study homogeneous catalysis such as *in situ* NMR become inapplicable to studies of molecular interactions at solid surfaces although solid state NMR can observe surface behaviour in high surface area solids. Hence, heterogeneous catalysts are intrinsically more difficult to study at a fundamental, molecular level. An example of a “simple” heterogeneous catalyst reaction would be the oxidation of carbon monoxide to carbon dioxide at platinum surfaces (scheme 1.1):

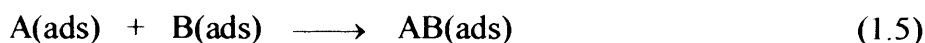


Scheme 1.1 Reaction of carbon monoxide with oxygen to form carbon dioxide using platinum as heterogeneous catalyst.

In heterogeneous catalysis, two main reaction mechanisms have been proposed to interpret this “simple” reaction: these are Langmuir-Hinshelwood [20] and Eley-Rideal [21]. For the vast majority of surface catalytic reactions, the Langmuir-Hinshelwood mechanism is observed. For catalytic CO oxidation

on Pt{111} it is indeed the case that a Langmuir-Hinshelwood mechanism applies.

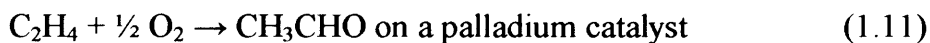
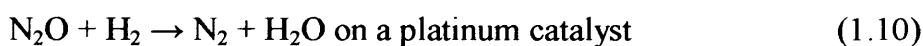
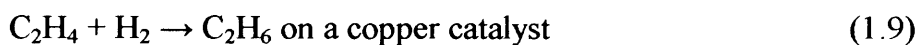
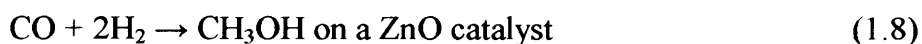
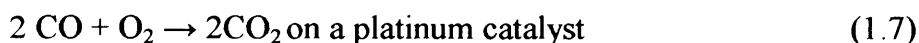
#### 1.2.2.2.1 Langmuir- Hinshelwood mechanism



The Langmuir-Hinshelwood mechanism consists of the following steps:

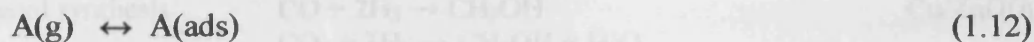
- i. Adsorption of reactant molecules from the gas phase onto the surface.
- ii. Dissociation of molecules on the surface.
- iii. Reaction between adsorbed molecules.
- iv. Desorption of the reaction product(s) to the gas phase.

Other examples of reactions following surface catalysed reactions are reported to follow Langmuir- Hinshelwood kinetics are listed below [22-26]:



## 1.2.2.2 Eley-Rideal mechanism

In contrast, the Eley-Rideal reaction mechanism for surface catalytic CO oxidation may be summarized as follows: [21].



In this mechanism, if a gas-phase molecule strikes a previously adsorbed molecule, there is a possibility that the collision leads to reaction and that the product escapes directly into the gas phase as shown in Figure 1.3b. Great efforts have been made to prove experimentally that this mechanism actually occurs [27, 28]. Rettner provided the most convincing evidence for an E-R mechanism by investigating the hydrogen-deuterium exchange at Cu{111} surface [29]:

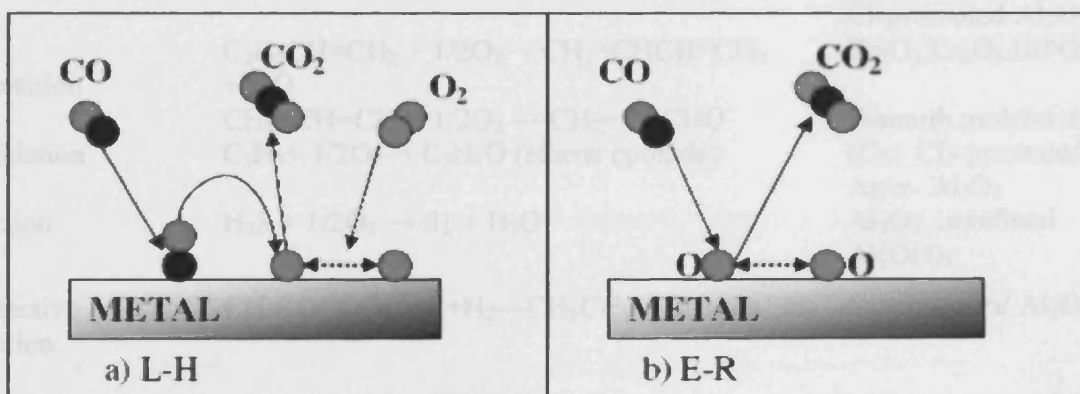


Figure 1.3 Schematic representations of the Langmuir-Hinshelwood mechanism (a) and the Eley-Rideal mechanism (b) for the catalytic oxidation of CO. Dark balls correspond to the carbon atoms and grey balls correspond to the oxygen atoms.



Table 1.4 Examples of heterogeneous catalysts used in industry [30].

Process	Chemical transformation <sup>a</sup>	Catalyst
Steam reforming	$\text{CH}_4 + \text{H}_2\text{O} \rightarrow \text{CO} + 3\text{H}_2$ $\text{C}_n\text{H}_m + n\text{H}_2\text{O} \rightarrow n\text{CO} + (n + m/2)\text{H}_2$	Ni/Al <sub>2</sub> O <sub>3</sub> Ni/Ca Al <sub>2</sub> O <sub>3</sub>
Methanol synthesis	$\text{CO} + 2\text{H}_2 \rightarrow \text{CH}_3\text{OH}$ $\text{CO}_2 + 3\text{H}_2 \rightarrow \text{CH}_3\text{OH} + \text{H}_2\text{O}$	Cu/ZnO/Al <sub>2</sub> O <sub>3</sub>
Hydrocarbon synthesis (Fischer Tropsch)	$n\text{CO} + 3\text{H}_2 \rightarrow \text{C}_n\text{H}_{2n} + n\text{H}_2\text{O}$ $n\text{CO} + (3n + 1)\text{H}_2 \rightarrow \text{C}_n\text{H}_{2n} + n\text{H}_2\text{O}$	Alkali-promoted Fe Alkali-promoted Co
Low temperature water gas shift	$\text{CO} + \text{H}_2\text{O} \rightarrow \text{CO}_2 + \text{H}_2$	Ni/Al <sub>2</sub> O <sub>3</sub>
Nitrogen fixation (Haber process)	$\text{N}_2 + 3\text{H}_2 \rightarrow 2\text{NH}_3$	K-promoted Fe
Selective hydrogenation	Partial hydrogenation of esters of glycerol with C <sub>18</sub> -acids ( <i>e.g.</i> linolic)	Ni/SiO <sub>2</sub>
Ammonia oxidation	$4\text{NH}_3 + 5\text{O}_2 \rightarrow 4\text{NO} + 6\text{H}_2\text{O}$	Pt-Rh gauze
Hydrodenitrogenation	$\text{C}_4\text{H}_4\text{S}(\text{thiophen}) + 2\text{H}_2 \rightarrow \text{C}_4\text{H}_6 + \text{H}_2\text{S}$	Co- or Ni-promoted MoS <sub>2</sub> /Al <sub>2</sub> O <sub>3</sub> or WS <sub>2</sub> / Al <sub>2</sub> O <sub>3</sub>
Hydrodesulfurisation	$\text{C}_5\text{H}_4\text{N}(\text{pyridine}) + 5\text{H}_2 \rightarrow \text{C}_5\text{H}_{12} + \text{NH}_3$	As above
Hydrodemetallation	Ni-porphyrin + NH <sub>2</sub> → Ni↓ + hydrocarbons	As above
Alkane cracking	$\text{C}_n\text{H}_{2n} + \text{H}^+(\text{ads}) \rightarrow [\text{C}_n\text{H}_{2n+1}]^+(\text{ads})$ $[\text{C}_{2n}\text{H}_{2n+1}]^+(\text{ads}) \rightarrow [\text{C}_n\text{H}_{2n-3}]^+(\text{ads}) + \text{C}_2\text{H}_4(\text{g})$	Type Y faujasite
Reforming	<i>e.g.</i> $2\text{C}_6\text{H}_{14} \rightarrow \text{C}_6\text{H}_6 + \text{C}_6\text{H}_{12} + 5\text{H}_2$	Rh-promoted Pt Supported on Cl-promoted Al <sub>2</sub> O <sub>3</sub>
Oxidative dehydrogenation	$\text{C}_2\text{H}_5\text{CH}=\text{CH}_2 + 1/2\text{O}_2 \rightarrow \text{CH}_2=\text{CHCH}=\text{CH}_2 + \text{H}_2\text{O}$	Fe <sub>2</sub> O <sub>3</sub> ; Cr <sub>2</sub> O <sub>3</sub> ; BiPO <sub>4</sub>
Oxidation	$\text{CH}_3-\text{CH}=\text{CH}_2 + 1/2\text{O}_2 \rightarrow \text{CH}_2=\text{CHCHO}$	Bismuth molybdate
Ethene oxidation	$\text{C}_2\text{H}_4 + 1/2\text{O}_2 \rightarrow \text{C}_2\text{H}_4\text{O}(\text{ethene epoxide})$	(Cs+ Cl)-promoted Ag/α- Al <sub>2</sub> O <sub>3</sub>
Claus reaction	$\text{H}_2\text{S} + 1/2\text{O}_2 \rightarrow \text{S}\downarrow + \text{H}_2\text{O}$	Al <sub>2</sub> O <sub>3</sub> , unrefined Al(OH) <sub>3</sub>
Enantioselective hydrogenation	$\text{CH}_3\text{COCOOC}_2\text{H}_5 + \text{H}_2 \rightarrow \text{CH}_3\text{CH}(\text{OH})\text{COOC}_2\text{H}_5$	Cinchona/Pt/ Al <sub>2</sub> O <sub>3</sub>

<sup>a</sup>for reaction conditions see Handbook of Heterogeneous Catalysis (Ertl *et al.* 1997) [30].

### *1.2.2.3 Advantages of heterogeneous catalysis over homogeneous catalysis*

As mentioned previously, the major advantage of a heterogeneous catalytic reaction over a homogeneous system is the ability to readily separate product from the catalyst. This represents a cost advantage, as separation is replaced by simple filtration in the case of the heterogeneous system. There are also advantages with respect to 'green' chemistry and application of continuous operation. In addition, other advantages, including ease of handling, ease of catalyst preparation, no solvent restrictions and a greater potential for regeneration and re-use make the quest for more active and selective catalysts a challenging but important goal.

However, the inability to control activity and selectivity by systematically altering the active site poses a major disadvantage of heterogeneous catalysts compared to homogeneous catalysts based on inorganic metal complexes. Some important examples of heterogeneous catalysts used in industry are shown in Table 1.4.

### *1.2.3 Adsorption of molecules at the catalyst surface*

Adsorption is the term used to describe the process whereby a molecule (adsorbate) can form a bond to the surface (the adsorbent). Moreover, there are two principal modes of adsorption of molecules on surfaces; chemisorption and physisorption. One may distinguish between both types by considerations of the bonding between the molecule and the surface. The adsorption phenomenon itself was discovered over two centuries ago by C.W. Scheele (1773) who studied the uptake of gases by charcoal. Priestley (1775) and Abbé

Fontana (1777) also studied independently of Scheele this phenomenon. In addition, charcoal was found to decolorize solutions by a surface adsorption mechanism (1785) [31].

#### *1.2.3.1. Chemisorption*

A chemical bond formed between the adsorbate and the substrate involves substantial rearrangement of electron density on both the metal and the adsorbate molecule. The nature of this bond may lie anywhere between the extremes of a virtually completely ionic or completely covalent bond. Chemisorption is an important step in terms of activation of a molecule for reaction. For a molecule to react catalytically at a solid surface it must first be chemisorbed and this can also take one of two forms. The first form is dissociative adsorption which is adsorption of a molecule with dissociation into two or more molecular fragments (for example H<sub>2</sub> adsorption on Pt) (Figure 1.4).

The second is associative adsorption in which no fragmentation of the adsorbate molecule occurs (for example CO adsorption on Pt).

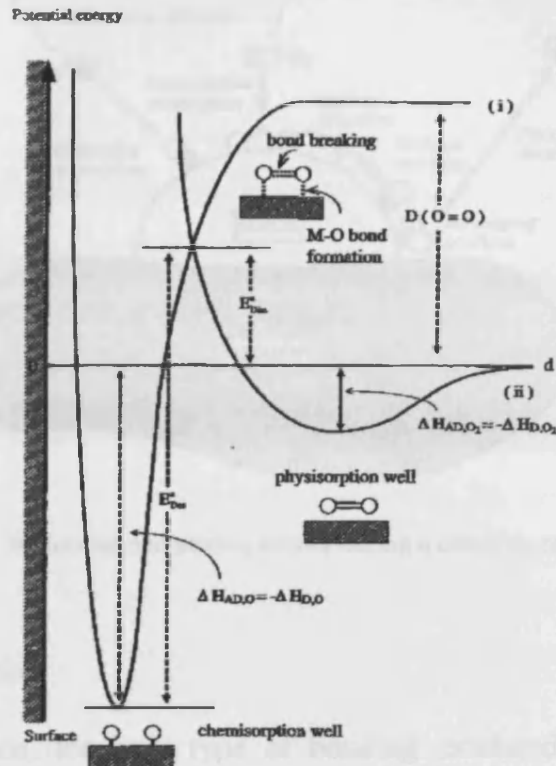


Figure 1.4 Schematic of dissociative adsorption of  $O_{2(g)}$  and the energetics of the adsorption process [32].

The reaction between  $O_2$  and CO on Pt metal is shown schematically in Figure 1.5. Note that in this case, CO adsorbs associatively on the metal surface whereas oxygen adsorbs dissociatively. For transition metals on the right hand side of the Periodic Table, CO tends to adsorb associatively whereas CO will tend to adsorb dissociatively on transition metals to the left hand side of the Periodic Table such as tungsten. This reflects the strength of interaction of CO with different metal surfaces.

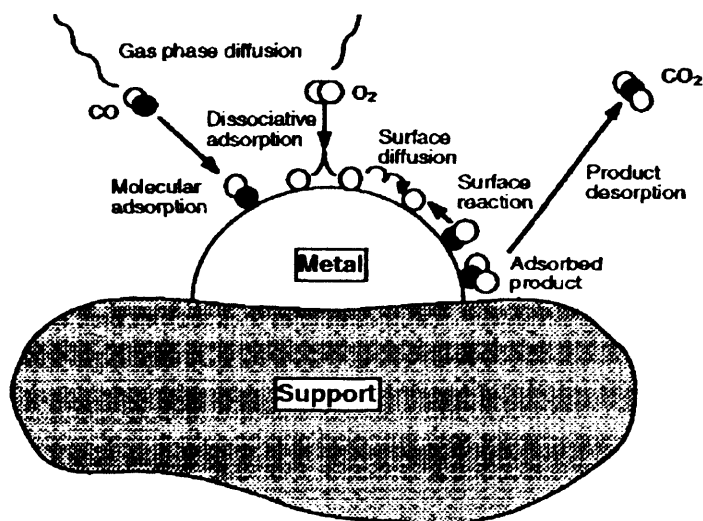


Figure 1.5 Molecular and atomic events during a catalytic reaction [33].

### 1.2.3.2 Physisorption

In physisorption, the only type of bonding exhibited is weak Van der Waals-type interactions. There is minimal redistribution of electron density either on the adsorbate molecule or on the solid surface. Comparison of chemisorption and physisorption at solid surfaces is shown in the Table 1.5.

*Table 1.5 Comparison of chemisorption and physisorption properties at solid surfaces.*

Criterion	Chemisorption	Physisorption
Temperature range (over which adsorption occurs)	Virtually unlimited (but a given molecule may effectively adsorb only over a small range)	Near or below the condensation point of the gas ( <i>e.g.</i> Xe < 100 K, CO <sub>2</sub> < 200K ).
Adsorption enthalpy	Wide range (related to the chemical bond strength typically 40-800 kJ mol <sup>-1</sup> )	Related to factors like molecular mass and polarity but typically 5-40 kJmol <sup>-1</sup> .
Crystallographic specificity (variation between different surface planes of the same crystal)	Marked variation between crystal planes.	Virtually independent of surface atomic geometry.
Nature of adsorption	Often dissociative, adsorption may be irreversible.	Non-dissociative and reversible.
Saturation uptake	Limited to one monolayer	Multilayer.
Kinetics of adsorption	Very variable-often an activated process.	Fast-since it is a non-activated process.

#### *1.2.4 Selectivity and activity*

The success of a catalytic chemical reaction can be viewed in terms of two factors: selectivity [34] and activity [35]. In addition, based on selectivity, chemical reactions can be categorized into four types [36]. The first one is termed chemoselectivity. An example of chemoselectivity is reduction of a carbon-carbon double bond in the presence of a carbon-oxygen double bond during hydrogenation. Regioselectivity refers to the control of orientation of

reactants with respect to each other. The third and fourth types of selective reactions are stereoselective reactions, which involve controlling relative stereochemistry (called diastereoselectivity) and absolute stereochemistry, known as enantioselectivity. The selectivity towards product A is defined as the percentage of A relative to the total amount of products formed. However, the activity of a catalyst is defined as the rate of consumption of reactant, although the activity to a particular product could also be specified [37]. Thus, the same reaction over different catalysts can result in different products, due to the different low energy pathways afforded by a particular metal. An example of this phenomenon is the catalytic reaction of carbon monoxide and hydrogen over different metals as shown in Table 1.6.

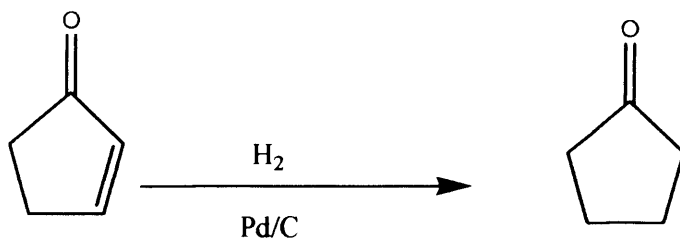
*Table 1.6 Selectivity towards different products from catalytic reactions of carbon monoxide and hydrogen over different metals.*

Reactants	Metal	Products	Industrial Company
CO + 3 H <sub>2</sub>	Ni	CH <sub>4</sub> + H <sub>2</sub> O	British Gas, UK
CO + 2 H <sub>2</sub>	Cu/ZnO/alumina	CH <sub>3</sub> OH	ICI, UK
12 CO + 6 H <sub>2</sub>	Ru, Fe	C <sub>6</sub> H <sub>12</sub> + 6 CO <sub>2</sub>	By-products of Fischer-Tropsch synthesis. SASOL
11 CO + 7 H <sub>2</sub>	Ru, Fe	C <sub>6</sub> H <sub>13</sub> OH + 5 CO <sub>2</sub>	SASOL

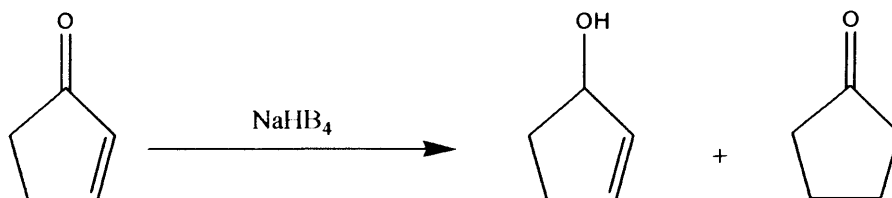
Furthermore, all the above processes have negative values of  $\Delta G_{\text{reaction}}$  and therefore they are all thermodynamically feasible. Hence, it is again emphasised that differences in metal catalyst behavior are caused by differences in the kinetics which is the origin of reaction selectivity.

Some examples of chemoselective and enantioselective:

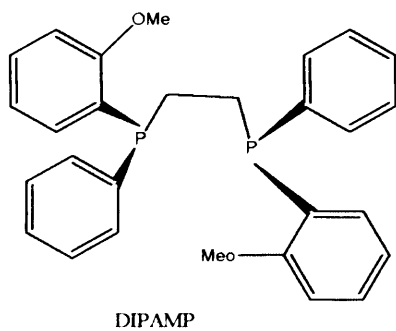
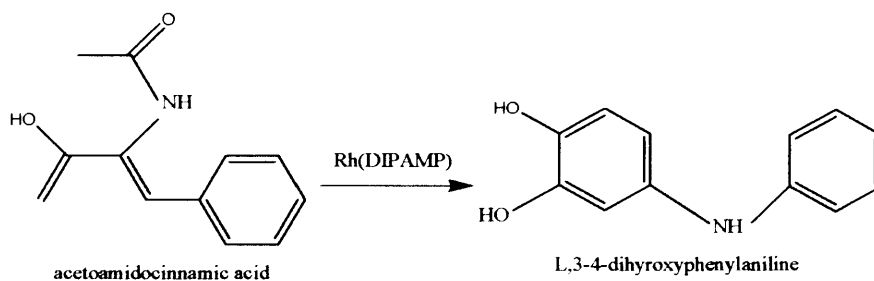
Chemoselective reduction of C=C over C=O:



Chemoselective reduction of C=O over C=C:



The enantioselective hydrogenation of acetamidocinnamic acid to L-3,4-dihydroxyphenylalanine





### 1.3 Asymmetric catalysis

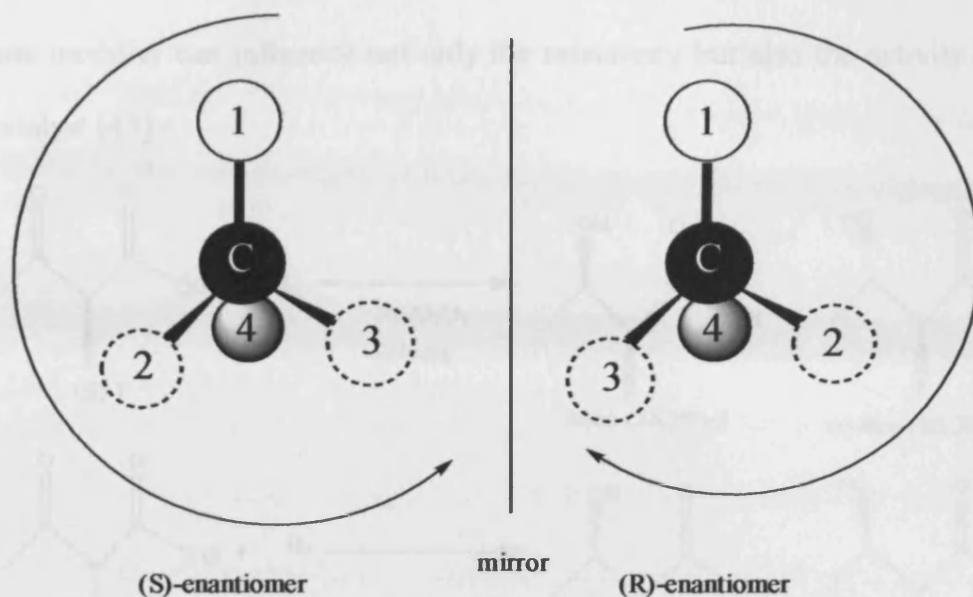


Figure 1.6 The mirror images of chiral molecules are not superimposable on each other. The substituents around the *S*-enantiomer are viewed as having a counter clockwise rotation, while the substituents around the *R*-enantiomer are viewed as having a clockwise rotation.

Many of the pharmaceuticals found in the market place are enantiomeric compounds, *i.e.* a single isomer that has been separated from a racemic mixture [38, 39]. Often, one enantiomer offers the desired therapeutic effect, while the other is ineffective or can cause harmful side effects. In addition, the necessity of producing a specific isomer has led synthetic chemists to research catalytic mechanisms that selectively yield the desired compound. Today, some pharmaceuticals and agrochemicals are developed as chemicals from a single enantiomer [40, 41]. Selective synthesis results in a dramatic reduction of environmental waste and increase in atom economy and energy efficiency.

The heterogeneous hydrogenation of  $\alpha$ -ketoesters is catalysed by noble metals, such as platinum or palladium [42], but the ability to function as an enantiomeric catalyst also requires the presence of an asymmetric modifier

molecule otherwise racemic product is always observed (as shown in Figure 1.7) since adsorption is racemic. For  $\alpha$ -ketoester hydrogenation, the chiral organic modifier can influence not only the selectivity but also the activity of the catalyst [43].

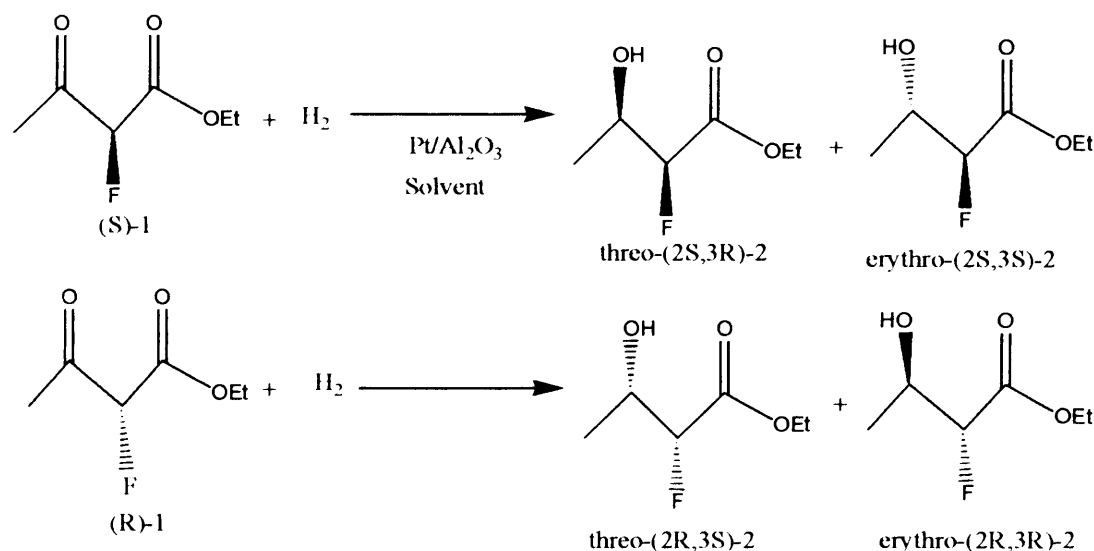


Figure 1.7 General scheme of the hydrogenation of racemic ethyl 2-fluoroacetoacetate.

In the next section, the hydrogenation of  $\alpha$ -ketoesters will be discussed in more detail since it along with the enantioselective hydrogenation of  $\beta$ -ketoesters constitute the two model reactions for understanding of chiral selectivity at metal surfaces [44].

## 1.4 Chirality

Chirality (handedness) is a key element in nature [45]. Due to of their molecular structure (based on *sp*<sup>3</sup> hybridised carbon atoms in particular), a wide range of organic substances consist of two non-superimposable mirror-image structures called enantiomers (Figure 1.6). Biot was the first to observe this phenomenon in 1815 when he observed the rotation of plane-polarised

light upon passing through solutions of sugar and tartaric acid [46]. Pasteur (1848) deduced that this property had a molecular basis which depended on the structure of the molecule. When he examined the crystallisation of sodium ammonium para-tartrate, he found two types of crystal [47]. He realised that there are left- and right-handed molecules and each was a mirror image of the other. He suggested that a pure enantiomer could be prepared in the laboratory in the presence of a directing agent. Van't Hoff and Le Bel [48, 49] described optical activity in organic molecules using the tetrahedron arrangement model of substituent atoms around the stereogenic centre. They recognised that the four substituent atoms arranged tetrahedrally around the carbon atom must be different in order to generate two different *enantiomers*. Dextrorotation and levorotation refer, respectively to the properties of rotating plane polarized light clockwise (for dextrorotation) or counter clockwise (for levorotation). A compound with dextrorotation is called dextrorotatory, while a compound with levorotation is called levorotary. Compounds with these properties are said to possess optical activity and consist of chiral molecules. A dextrorotary compound is often prefixed “(+)-” or “d-”. Likewise, a levorotary compound is often prefixed “(-)-” or “l-”. These “d-” and “l-” prefixes should not be confused with the “D-” and “L-” prefixes based on the actual configuration of each enantiomer, with the version synthesized for naturally occurring (+)-glyceraldehyde being considered the D- form. In 1966, Cahn, Ingold, and Prelog addressed the nomenclature of chiral molecules [50]. A molecule can be chiral if it is not superimposable on its mirror image. Molecules which are not

superimposable on each other, but are mirror images of each other, are called enantiomers. In addition, chiral molecules have the property to rotate plane-polarised light so they are optically active. When a molecule can be superimposed on its mirror image then it is called achiral. Furthermore, a racemic mixture is a mixture that contains two enantiomers in equal amounts. Enantiomers have the same chemical and physical properties. Cahn-Ingold-Prelog rules are used to assign the absolute configuration of a stereogenic centre [51]. The highest atomic number around the stereogenic centre will have the highest priority; it will be assigned Number 1. A lower atomic number substituent will be given No.2, *etc.* In the case where two atoms directly bonded to the stereogenic centre are the same, for instance, if  $-\text{CH}_3$  and  $-\text{CO}$  are bonded to the stereogenic centre,  $-\text{CO}$  will have the highest priority because the carbon is bonded to O, which has a higher atomic number than H on the  $-\text{CH}_3$  substituent. The molecule is then positioned such that the substituent of lowest priority is pointing down. If viewed from above with the sequence from the highest to the lowest priority substituent in a clockwise direction, the molecule will be designated an *R*-enantiomer whereas if the same sequence in an anti-clockwise direction, the molecule will be designated an *S*-enantiomer (Figure 1.6).

### 1.5 The Orito reaction

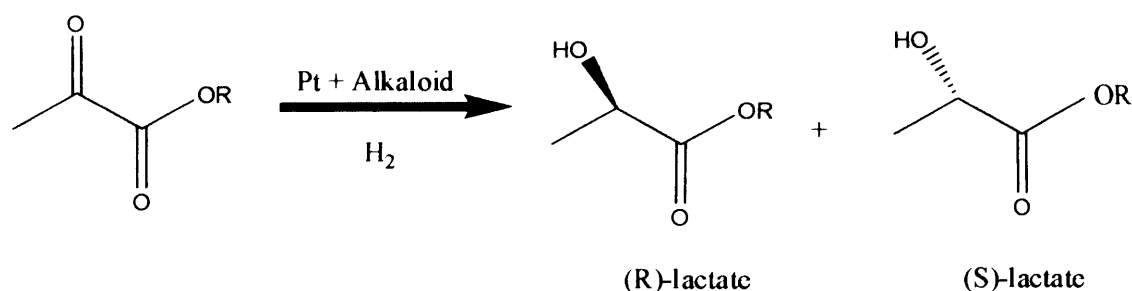


Figure 1.8 The Orito reaction where,  $R = \text{CH}_3$ ; (methyl pyruvate),  $\text{C}_2\text{H}_5$ ; (ethyl pyruvate).

In 1979, Orito and co-workers first reported the enantioselective hydrogenation of  $\alpha$ -ketoesters over cinchona modified platinum, (Figure 1.8) [52-54], with high values of the enantiomeric excess (*ee*) [52]. Orito, Imai and Niwa investigated the enantioselective hydrogenation of methyl pyruvate (Mepy) using graphite supported platinum catalysts (Pt/G) to the corresponding lactate ester. Enantioselectivity is conferred on the reaction by the adsorption of a cinchona alkaloid (the modifier), onto the supported Pt-metal catalyst. The reaction has been shown to take place in a wide variety of both protic and aprotic solvents. The highest enantioselectivities obtained thus far have been achieved using acetic acid [55]. The experimental procedure as used by Orito *et al* [44, 53], consisted of a number of steps:

- The reduction of the Pt/G catalyst.
- The modification of catalyst by immersion in a 1% solution of the alkaloid modifier.
- Washing.
- The transfer of the modified catalyst to a high pressure reactor.

In later studies highest enantioselectivity was obtained using acetic acid as solvent [56]. In addition, the platinum could be supported on alumina, silica,

titania, carbon, or zeolites [57] with alumina exhibiting the greatest *ee*. This supported catalyst could be used to hydrogenate methyl pyruvate to give (*R*) (+)-methyl lactate in high enantiomeric excess when CD or quinine (CD, QN; Figure 1.9a and b, respectively) was used as the modifier.

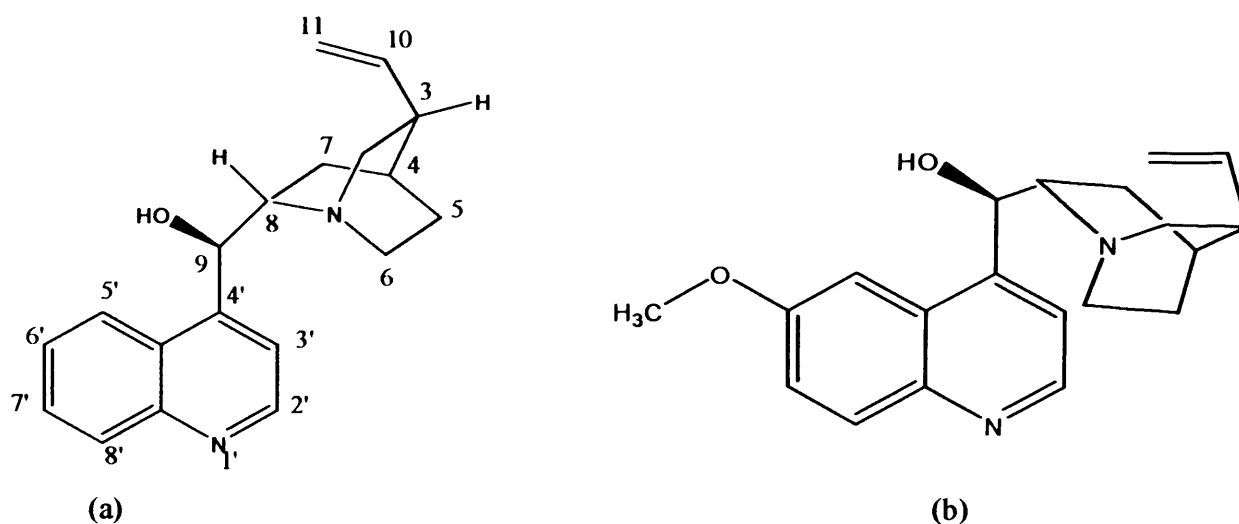


Figure 1.9a) Structure of cinchonidine (CD), b) structure of quinine (QN).

Switching to the epimers of CD and QN namely cinchonine (CN) and quinidine (QD) (Figure 1.10a and b, respectively) [53], the (*S*) (-)-methyl lactate could be preferentially obtained. Modifier molecules contain three distinct functional parts, these being the quinoline ring, the asymmetric region at C<sub>8</sub> and C<sub>9</sub> and the vinylic bi-cyclic quinuclidine ring system. The double bond at C<sub>10</sub>-C<sub>11</sub> is hydrogenated under reaction conditions. One of the characteristics of the cinchona-modified Pt system is the enhanced rate that accompanies enantio-differentiation in the presence of the chiral modifier. [58]. The stereogenic centres in the cinchona alkaloid are located at C<sub>3</sub>, C<sub>4</sub>, C<sub>8</sub>, and C<sub>9</sub>. It has been observed that C<sub>8</sub> and C<sub>9</sub> play an important role in controlling the sense of enantioselectivity. For example, CD (where C<sub>8</sub> and C<sub>9</sub> are configured

as *S* and *R*, respectively) produced an *R*- excess, while CN (possessing the opposite configuration at C<sub>8</sub> and C<sub>9</sub>) produces the *S*-enantiomer in excess. The configuration at C<sub>8</sub> was found to be responsible for the sense of enantioselectivity, and the substituent at C<sub>9</sub> to be important for high *ee* (OH and OMe substituent groups are the best whereas large bulky groups will reduce or even invert enantioselectivity [55, 59]. Partial hydrogenation of the aromatic ring weakens the bond to the metal which leads to lowering of the *ee*; and the alkylation of quinuclidine-N leads to a complete loss of *ee* [59, 60]. Interestingly, in the absence of a cinchona alkaloid, the racemic reaction is relatively slow. Furthermore, according to their initial findings and extending their range of enantioselective hydrogenation reactions, the Orito group was further able to demonstrate that a variety of polar and non-polar solvents could be used to optimize *ee* including toluene, dichloromethane and ethanol.

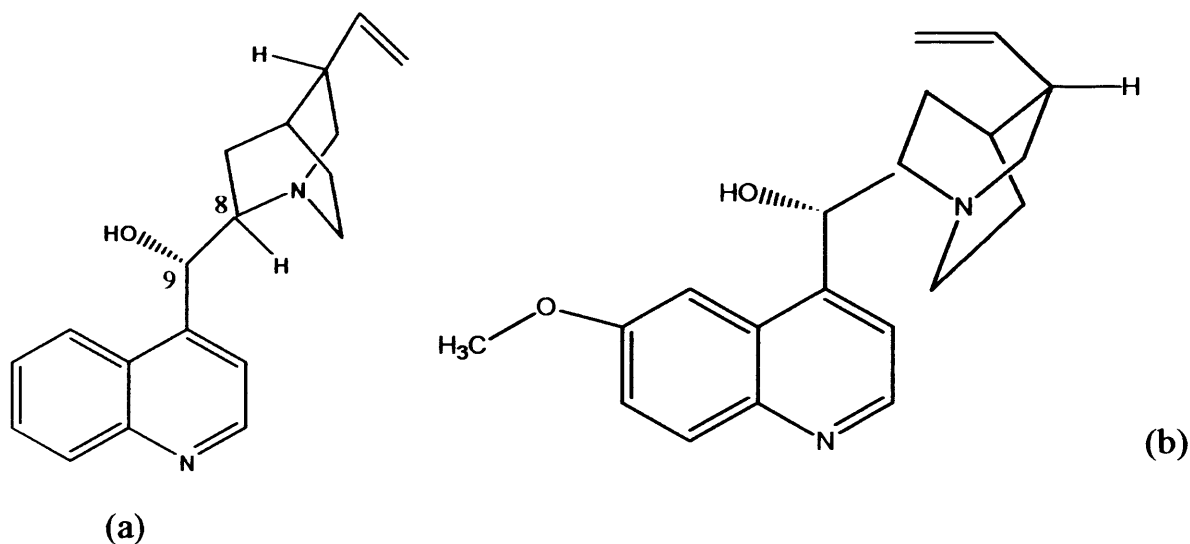


Figure 1.10 a) Structure of cinchonine (CN), b) structure of quinidine (QD).

### 1.5.1 Experimental aspects of the Orito reaction

Based on a larger body of published work [52-54], the following remarkable features of the Orito reaction procedure may be stated:

- Enantioselective reaction showed a 10 to 50-fold rate enhancement over racemic reaction (*i.e.* reaction in the absence of alkaloids) [61].
- Minute quantities of alkaloid suffice, considerable enantioselectivity being obtained when the Pt surface is only partially covered with alkaloid [62].
- Enantioselectivity was lost at temperatures above about 45°C [61].

The sensitivity of the optical yields obtained (defined as % *ee* *R* and % *ee* *S* and *vice versa* depending on the choice of modifier) were found to depend on the catalyst support [61], the activation of the catalyst [56], the temperature [61], the solvent [57], and the concentration of the alkaloid [62] used in the reaction mixture. Upon optimization of the above catalysis conditions, activity/selectivity with the Pt-cinchona system was further found to depend on: (i) the structure and nature of the modifier [63] and (ii) the platinum particle size, morphology and support [64]. These aspects will be discussed further below.

### 1.6 Cinchona alkaloids

Studies of cinchona alkaloids in enantioselective hydrogenation on Pt concluded that an increase in the amount of modifier, at low modifier concentration, leads to an increase in both enantiomeric excess (*ee*) and reaction rate [65-68]. Blaser *et al* also noted that many related studies [65-68]



have experimentally confirmed both enantiomeric excess and rate as being functions of the modifier concentration. Hence initial results indicated that rate and *ee* appeared to be connected. The aromatic based molecules that provided the best results obtained thus far was based on two or more interconnected flat rings such as quinolines. This functionality was needed to allow the modifier to bond to the Pt surface *via* its  $\pi$ -system [69]. In addition, several other natural and synthetic compounds have been investigated, mainly for the hydrogenation of  $\alpha$ -ketoesters, but only a few of these afforded a high *ee* (Figure 1.11) [65].

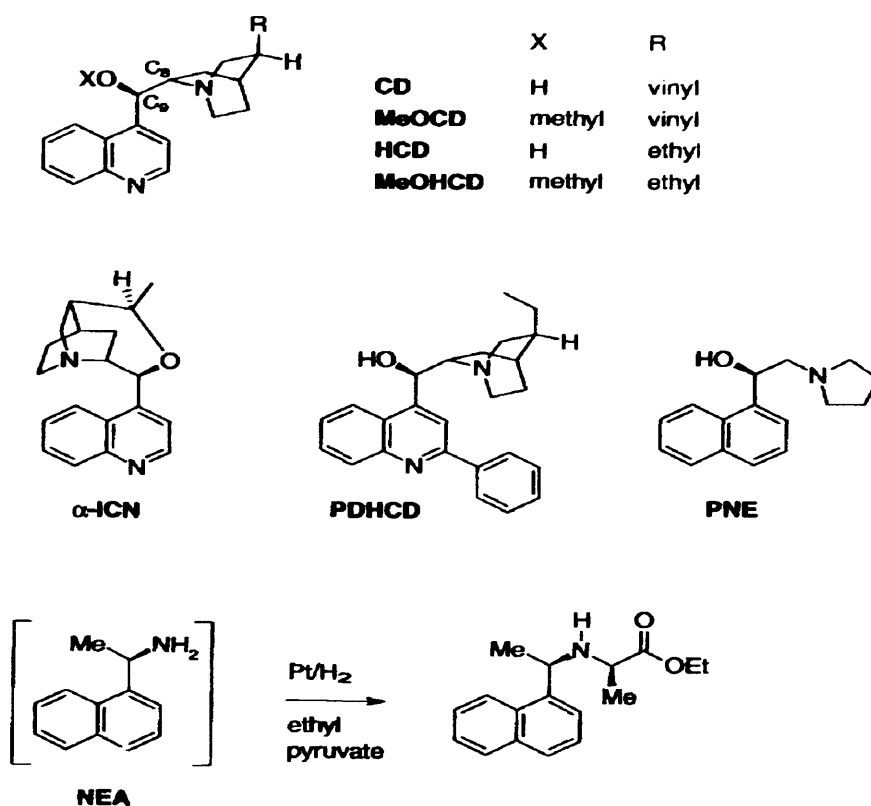


Figure 1.11 Some natural and synthetic chiral modifiers for enantioselective hydrogenation over Pt [65]. Where  $\alpha$ -ICN =  $\alpha$ -isocinchonine, PDHCD = 2-Phenyl-9-deoxy-10,11-dihydrocinchonidine, PNE = (*R*)-2-(Pyrrolidin-1-yl)-1-(1-naphthyl) ethanol, and NEA = 1-(1-naphthyl) ethylamine.

It should be noted that all successful modifiers for the Orito reaction contain the following structural elements:

i) A naphthalene or quinoline rings thought to be essential for adsorption of the modifier to the platinum surface during reaction,

ii) A tertiary, secondary or primary amine substituent to activate the carbonyl group on the substrate *via* H-bonding,

iii) A chiral centre close to the basic nitrogen atom of the amine substituent.

The cinchonidine (CD) modifier can exist in many conformations, and it is thought that only one of these stable conformations in solution is the active agent during enantioselective hydrogenation [70].

The various conformations in solution available to CD are depicted in Figure 1.12 and are referred to as the “closed (1)”, “closed (2)”, “open (3)” and “open (4)” conformations.

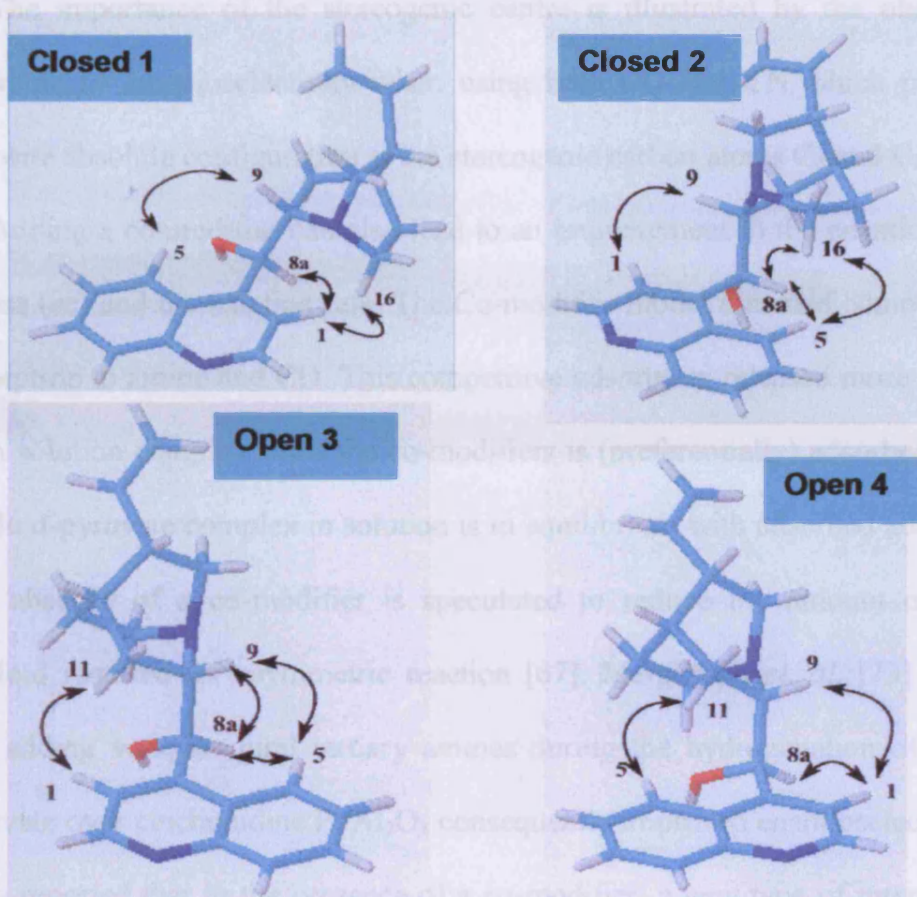


Figure 1.12 Molecular simulations of the four low energy conformers of cinchonidine. Figure reproduced from reference [71].

The terms “open” and “closed” [69] are used to indicate whether the quinuclidine *N* points away (open) or toward (closed) the quinoline ring.

Several theoretical studies and references have focused on the conformational behavior of cinchona alkaloids using various computational methods [72]. According to Baiker, the open conformation was found to be the most stable and has demonstrated higher values of enantiomeric excess when present under reaction conditions in solution.

The importance of the stereogenic centre is illustrated by the observed inversion of enantioselectivity when using both CD and CN which possess opposite absolute configuration at the stereogenic carbon atoms C<sub>8</sub> and C<sub>9</sub>.

Adding a co-modifier can also lead to an improvement in the enantiomeric excess (*ee*) and the reaction rate. The Co-modifier model assumed competitive adsorption to amine and CD. This competitive adsorption released more CD to form solution complex since the co-modifiers is (preferentially) adsorbed. The alkaloid-pyruvate complex in solution is in equilibrium with adsorbed alkaloid. The absence of a co-modifier is speculated to reduce the amount of free alkaloid required for asymmetric reaction [67]. Margitfalvi *et. al.* [73] noted that adding various chiral tertiary amines during the hydrogenation of ethyl pyruvate over cinchonidine Pt/Al<sub>2</sub>O<sub>3</sub> consequently improved enantioselectivity. They reported that in the presence of a co-modifier, a new type of interaction (alkaloid co-modifier interaction) resulted in an increase in the amount of free alkaloid required, thought necessary by those authors to be crucial for asymmetric reaction.

## 1.7 Reactant

Modified hydrogenation catalysts transform specific substrates with high enantioselectivity. Only a few types of substrate exhibit the specificity needed for technical enantioselective hydrogenations. For cinchona alkaloid-platinum catalysts, the preferred substrates, as stated by Blaser *et. al.* [72], are  $\alpha$ -ketoesters. The most common model compound used in experimentation, which is also used as the primary reaction in this work, is ethyl pyruvate (Figure 1.13).

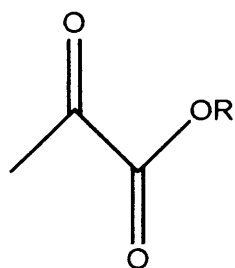


Figure 1.13 Ethyl pyruvate ( $C_5O_3H_8$ ).

The two enantiomeric hydroxyesters (*R*)-ethyl lactate and (*S*)-ethyl lactate, produced as result of ethyl pyruvate hydrogenation are shown in Figures 1.14 and 1.15, respectively.

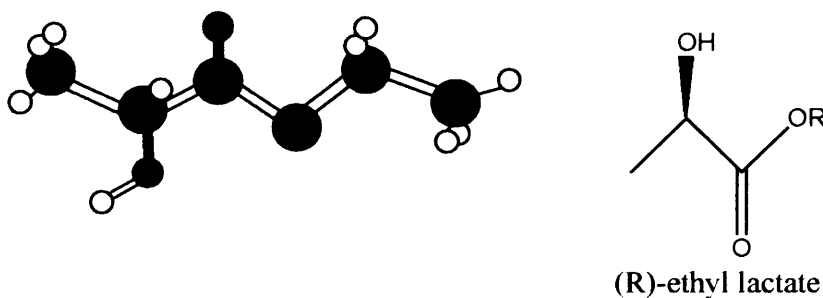


Figure 1.14 (*R*)-ethyl lactate ( $C_5O_3H_{10}$ ).

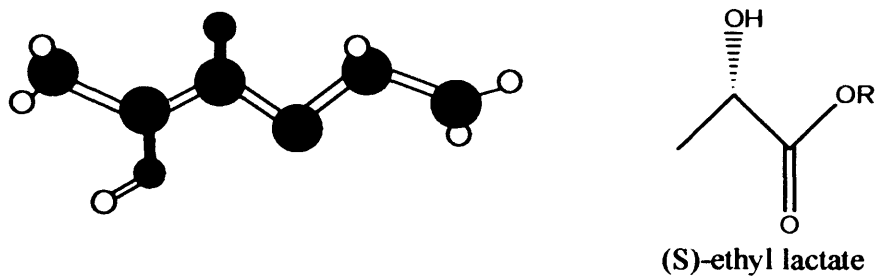

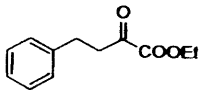
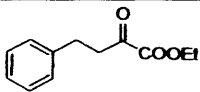
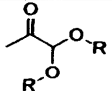
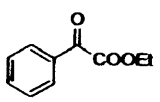
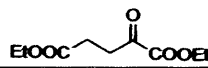
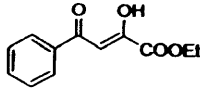

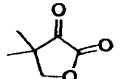
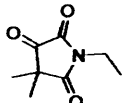
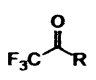
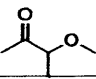
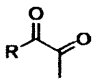


Figure 1.15 (S)-ethyl lactate ( $C_5O_3H_{10}$ ).

Table 1.7 shows various substrates suitable for enantioselective hydrogenation using the Orito reaction.

Table 1.7 The best value of enantiomeric excess (*ee*) obtained for various substrates used for the Orito reaction.

Substrate	Enantiomeric excess ( <i>ee</i> ) %	Catalyst	Reference
 R = Me R = Et	98 97	Pt colloids 5%Pt/Al <sub>2</sub> O <sub>3</sub>	[74] [75]
	96	5%Pt/Al <sub>2</sub> O <sub>3</sub>	[75]
	94	1%Pt/Al <sub>2</sub> O <sub>3</sub>	[76]
 R = Me R = (CH <sub>3</sub> ) <sub>3</sub>	97 97	5%Pt/Al <sub>2</sub> O <sub>3</sub> 5%Pt/Al <sub>2</sub> O <sub>3</sub>	[77] [78]
	98	5%Pt/Al <sub>2</sub> O <sub>3</sub>	[79]
	96	5%Pt/Al <sub>2</sub> O <sub>3</sub>	[80]
	86	5%Pt/Al <sub>2</sub> O <sub>3</sub>	[81]
	60	5%Pt/Al <sub>2</sub> O <sub>3</sub>	[82]
	92	5%Pt/Al <sub>2</sub> O <sub>3</sub>	[83]
	91	5%Pt/Al <sub>2</sub> O <sub>3</sub>	[83]
 R = CH <sub>2</sub> COOEt R = Ph	93 92	5%Pt/Al <sub>2</sub> O <sub>3</sub> 5%Pt/Al <sub>2</sub> O <sub>3</sub>	[84] [84]
	98	5%Pt/Al <sub>2</sub> O <sub>3</sub>	[85]
 R = Ph R = Me	65 50	5%Pt/Al <sub>2</sub> O <sub>3</sub> 5%Pt/Al <sub>2</sub> O <sub>3</sub>	[86] [87]

## 1.8 Models of enantioselective mechanism

Several theoretical studies and considerable effort over the last decade or so have focused on the mechanism for enantioinduction in the presence of cinchona modifier. All models are limited by the need to make assumptions regarding the adsorption mode of the reactant and the modifier involved. These models have recently been reviewed by Baiker [88].

### 1.8.1 The Wells model

In this model, Wells and co-workers (1990) originally proposed that the enantiodifferentiation was due to an ordered array of cinchonidine molecules on the platinum surface which generated the active chiral phase, with special emphasis on the enantioselective hydrogenations of ethyl and methyl pyruvate to the corresponding lactate [89]. The ordered array model (generating chiral pockets) was eventually abandoned since it could not explain other aspects of the kinetics [69, 90]. However, other studies have been conducted by the same group and a later model was proposed describing the importance of a 1:1 interaction between reactant and modifier. In addition, in this approach they assumed that an N-H-O type H-bond interaction between cinchonidine in its most stable open 3 conformation and *S* trans pyruvate ester was occurring, as shown in Figure 1.16. A key feature includes restricted rotation for the half hydrogen state (by Pt surface) leading to *R*-lactate. Adsorption of CD on Pt *via* quinoline ring system was consistent with H/D exchange reactions [69]. Rate enhancement (typically 20 fold) was ascribed to hydrogen transfer to half-



hydrogenated state (hhs) being faster compares to racemic reaction leading to the high *ee* observed.

In presence of CD *R*-lactate formed in  $\approx 70\%$  *ee* with a reaction rate  $\approx 1000$  mmol g<sup>-1</sup> h<sup>-1</sup>

In the presence of CN, *S*-lactate formed in  $\approx 65\%$  *ee* with a reaction rate  $\approx 800$  mmol g<sup>-1</sup> h<sup>-1</sup>

In the absence of modifier, *ee* = 0% (as expected) with a reaction rate  $\approx 50$  mmol g<sup>-1</sup> h<sup>-1</sup> [69].

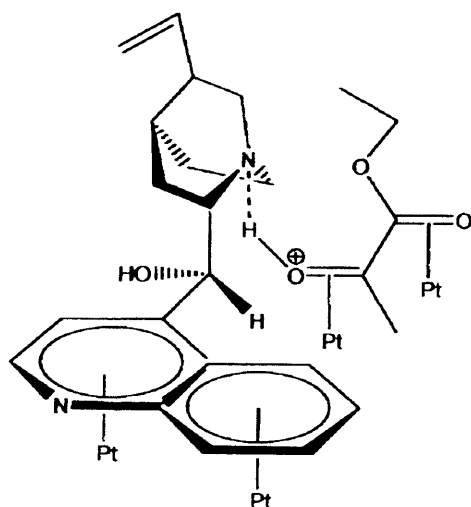


Figure 1.16 Reaction intermediate proposed by Wells for the heterogeneous enantioselective hydrogenation of ethyl pyruvate over cinchonidine modified platinum [72]. The intermediate is sometimes referred to as the “half-hydrogenated state”.

The half-hydrogenated state model correctly predicts the enantioselectivity of the reaction assuming that hydrogen is delivered from the metal side to the C=O group. It also predicts bond polarization due to the H-bond as an explanation for the rate acceleration [89, 72] by activating the C=O group towards hydrogenation.

### 1.8.2 The Baiker model

This model also describes a 1:1 interaction between alkaloid and the pyruvate [91] as an explanation of the enantioselectivity. The quinuclidine *N* is able to interact with the substrate as an electrophile after protonation. However, most of Baiker work was performed in acetic acid *i.e.* under protonated conditions of the chiral modifier. In non-acidic solution, the basic nitrogen is asserted to pick up a hydrogen atom from the Pt surface. This interaction is assumed to arise from the open conformation of the adsorbed alkaloid and pyruvate adsorbed flat *via* the  $\pi$ -system as shown in Figure 1.17, with a hydrogen bond between the protonated amine and the carbonyl group. The restricted rotation of adsorb Mepy leading to chiral product is the key element of this model. The steric blocking by aromatic part of alkaloid ensues correct orientation of Mepy.

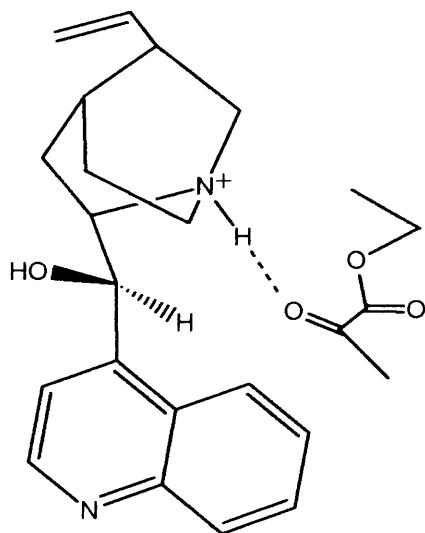


Figure 1.17 The Baiker model of enantiodifferentiation.

Calculations by the Baiker group suggest the possibility of formation of a bifurcated H-bond interaction with adsorbed pyruvate molecules (Figure 1.18) in both the pro-(*R*) and the pro-(*S*) configurations. Although both *syn* (*cis*) and *anti* (*trans*) configurations of substrate may interact with the modifier, the modifier complex is found to be less stable. In addition to the anti complex being more stable, it is also found that in the pro-(*S*) configuration, there was a repulsive interaction between the CD-quinoline ring and the ester portion of the alkyl group of the pyruvate ester. This leads to a difference in the stabilization energies between the pro-(*R*) and pro-(*S*) complexes and it is postulated that this difference could be taken into account for the rate enhancement and enantioinduction [88].

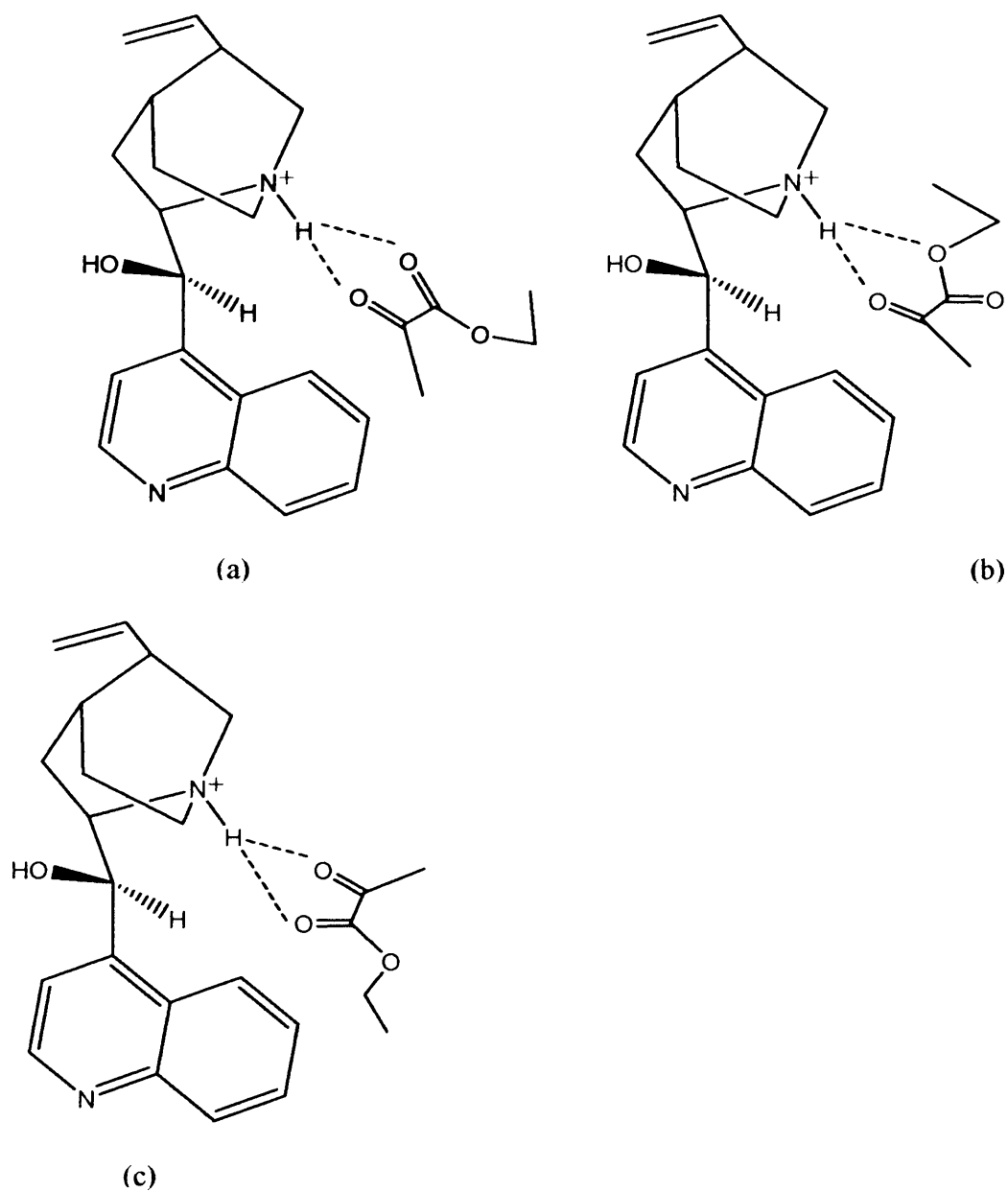


Figure.1.18 Substrate-modifier interactions proposed by Baiker. (a) CD: *cis* pyruvate interaction (b) CD: *cis* pyruvate interaction (Pro-*R*) (c) CD : *cis* pyruvate interaction (Pro-*S*)).

### 1.8.3 The Augustine model

In 1993 Augustine proposed that the cinchona alkaloid (CD) molecule was adsorbed *via* the *N* atom of the quinoline (edge-on) close to a Pt ad-atom where H and ethyl pyruvate (etpy) were also adsorbed [92]. A common element of this proposal is a “bidentate” complex between CD and the  $\alpha$ -ketoester leading to a six-membered ring as shown in Figure 1.19. In this proposal, the *N* and *O* of CD was proposed to interact with the C atoms of the keto carbonyl and ester carbonyl groups of the pyruvate ester, respectively. This suggestion is based on the observation that alcohols and amines predominantly react with activated ketones *via* nucleophilic attack at the carbonyl group. However, one of the major limitations of the model is that it cannot interpret the enantioselectivity observed when the chiral *N*-base modifier is protonated, *i.e.* the good *ee* achieved when for example, CD is replaced by CD.HCl [93], or the result of an even higher *ee* on methylation of the C<sub>9</sub>-OH group of CD (as in the case of *O*-methyl-CD(MeOCD)) or *O*-methyl-HCD(MeOHCD) [72]. Consequently, because the interaction between the “bidentate” complex and either of these modifiers would be sterically hindered the Augustine model has not found favour. The proposed active sites for hydrogenation *i.e.* unsaturated corner atoms and ad-atoms are also questionable when considering the yields achieved with colloidal Pt (consisting of particles) [94-96] or with the extended flat areas of heat treated Pt/alumina [74, 97].

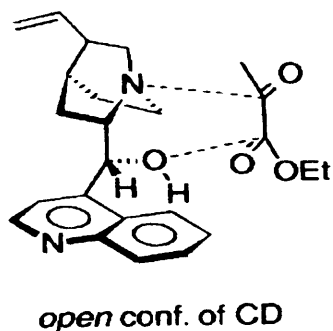


Figure 1.19 Reaction intermediate proposed by Augustine for the heterogeneous enantioselective hydrogenation of ethyl pyruvate over CD modified Pt [72].

#### 1.8.4 The Margitfalvi model

The proposed model suggests the formation of a reactant modifier 1:1 complex in solution *via* an electronic interaction of the aromatic ring of CD with the  $\pi$ -orbitals of the reactant [98-99]. The reactant CD complex may only adsorb on the Pt surface by its “unshielded” side as shown in Figure 1.20, favoring the predominate formation of one enantiomer, and thus termed the “shielding” model. Hence:

Complex in solution  $\rightleftharpoons$  adsorbed to catalyst surface.

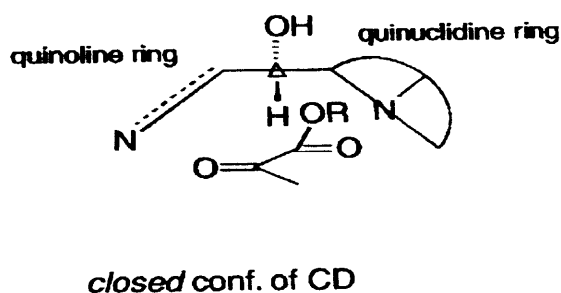


Figure 1.20 Reaction intermediate proposed by Margitfalvi for the heterogeneous enantioselective hydrogenation of ethyl pyruvate over CD modified Pt [72].

Furthermore, to facilitate an activating interaction of the quinuclidine *N* with the carbonyl carbon atom of pyruvate ester, CD must exist in a closed conformation. Although, it is very feasible for the reactant and the modifier to interact in solution, the complex cannot effect or control the enantioselection on the Pt surface. The disadvantage of this model is that it contradicts several of the experimental observations found for the Orito reaction such as:

- (i) The high *ee* observed once the quinuclidine *N* atom of CD is protonated.
- (ii) The observation made by Bartok and co-workers [100, 101], in which no *ee* was lost for the ethyl pyruvate hydrogenation when cinchona alkaloid was fixed in an open conformation, or explain the 76% *ee* afforded by the  $\alpha$ -isocinchonine, which primarily exists in an “anti-open” conformation [102]. However, the shielding model does assert that only the closed conformation of the modifier can provide enantiodifferentiation, while the open conformation of the modifier gives rise to the racemic product mixtures.
- (iii) In terms of a kinetic basis, the model is invalid as cited by two independent studies [103, 104].
- (iv) The shielding model also fails to adequately interpret the rate acceleration observed in the presence of trace amounts of chiral modifier [98].

As an example, Margitfalvi *et al.* achieved about 56% *ee* to (*R*)-lactate with a pyruvate/CD molar ratio of  $1.5 \times 10^5$  and a rate acceleration of 5.5 compared to unmodified reaction [73]. In addition, the low concentration of modifier ( $6.8 \times 10^{-6}$  M) limits the concentration of the proposed CD-pyruvate complex in solution. Regarding the adsorption rate of the reactant modifier complex, at this

low concentration, it is expected to be very low. Consequently, this will limit (by mass transport from solution to surface) the overall hydrogenation rate assuming a Langmuir-Hinshelwood mechanism [105]. Hence, to obtain the observed 5.5 fold rate acceleration, the intrinsic reaction rate should be higher by a factor of  $8 \times 10^5$  compared to the unmodified reaction, an unrealistic scenario.

### 1.8.5 The McBreen model

The most widely discussed mechanistic models are based on the formation of chemisorbed 1:1 complexes through H-bonding between the quinuclidine function of the cinchona modifier and the prochiral, keto-carbonyl, function of the substrate. Recently, McBreen *et al.* have proposed the two-point H-bonding model [106]. This model describes two H-bonding interactions as shown in Figure 1.21. The first interaction is an aromatic-carbonyl H-bonding interaction between the aromatic ring hydrogen atoms and the carbonyl group of the  $\alpha$ -ketoesters. The proposed interaction depends on surface science studies showing that this type of interaction, especially the C—H $\cdots$ O interactions between the adsorbed aromatics on Pt{111} and the carbonyl groups of coadsorbed molecules are possible [107], *i.e.* the metal surface activates the quinoline C-H bonds to exhibit hydrogen bonding towards the carbonyl of the  $\alpha$ -ketoester. A number of recent studies have been reported for the same interaction between tetrafluorobenzene and oxygenated clusters [108-110]. The second H-bonding interaction in the McBreen model is between the ester carbonyl O atom and the quinuclidine-N atom. In common with the majority of



previous models, the proposed model is based on the formation of 1:1 modifier-substrate interaction adsorbed on the Pt surface.

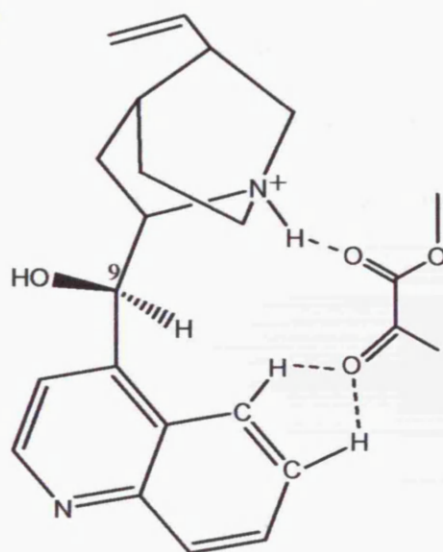
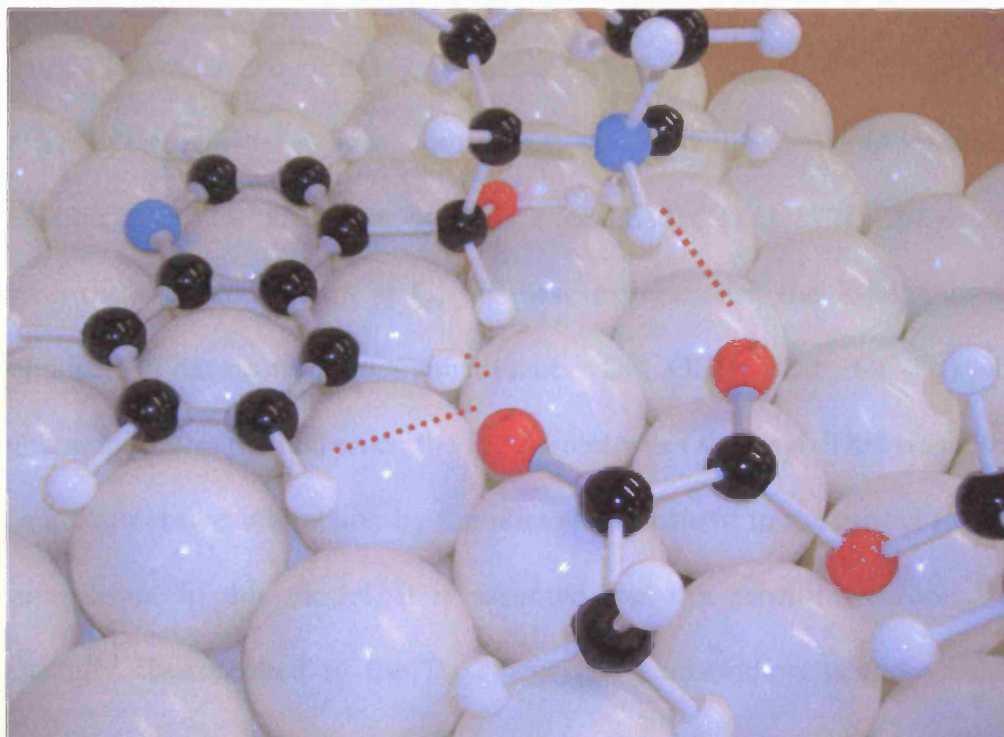


Figure 1.21 Upper: Real space schematic representing McBreen model: red = O, black = C, blue = N, small white = H, and large white = Pt surface, dotted line = H-bonding interaction. Lower: the two-point H-Bonding model as proposed by McBreen *et al.* [106].

The significance of this observation is that the two-point model predicts the correct enantioselectivity for reaction. Taking CD as an example, it can be seen that the formation of pro-(*S*) in the intermediate complex is expected to be sterically hindered by the substituents at C<sub>9</sub> (which is the OH group). Recently, Diezi *et al* reported a further important aspect of the C—H···O interaction in enantioselectivity as shown by their experiments. [111,112]. They used CD with different substituent at C<sub>9</sub>. In these experiments, the *R*-enantiomer was obtained in excess (when C<sub>9</sub> substituent = OH, OCH<sub>3</sub>, and OC<sub>2</sub>H<sub>5</sub>) while *S*-enantiomer was formed when the substituent was *O*-phenyl. This was attributed to a competitive interaction by the phenyl substituent to the aromatic-carbonyl interaction. In this model, it is assumed that the prochiral carbonyl is not strongly chemisorbed to the Pt, since strong adsorption would weaken the carbonyl-aromatic interaction. It should be noted that C—H···O acts parallel to the metal surface while the ester carbonyl H-bonding interaction with the quinuclidine-*N* takes almost perpendicular to the surface. Whether or not there are “realistic” assumption needs to be tested by theoretical calculations.

## 1.9 Solvents

Several parameters such as catalyst, hydrogen partial pressure and modifier concentration have been found to influence the enantiomeric excess (*ee*) and rate of adsorption in the Orito reaction. Of particular interest however is the solvents used because they can influence the catalytic behavior by affecting the solubility of reactants ( $\alpha$ -ketoesters, modifier and hydrogen) as well as interaction between modifier,  $\alpha$ -ketoester and the Pt surface. Ideally, a solvent with a dielectric constant  $\epsilon_r$  between 2-10 produces optimum enantiomeric excess [113]. Wells *et al.* have also experimentally confirmed that rates and enantioselectivities vary with the solvent used for modification and for enantioselective reaction. Blaser *et al.* [113], have shown that acids whose dielectric constants fit this range, often lead to the highest optical yields for hydrogenation of ethyl pyruvate over a cinchonidine modified Pt catalyst. Dichloromethane proved to have the greatest yield and enantiomeric excess [113]. Acetic acid ( $\epsilon_r = 6.2$ ) and toluene ( $\epsilon_r = 2.3$ ) are the most suitable solvents, as the former affords an *ee* reaching over 95% under optimized conditions [56, 114]. Under acetic acid conditions the quinuclidine *N*-atom of cinchonidine (CD) is known to be protonated [115]. Although, the use of alcohols, such as ethanol and propanol ( $\epsilon_r \approx 30$ ) can afford reasonably high *ee* they tend to be avoided because in the presence of basic modifier, the solvents undergo side reactions leading to the formation of undesired hemiketals [116].

## 1.10 Background to experimental methods used

In this thesis, enantioselective hydrogenations were carried out using an autoclave reactor. This reactor was used for high pressure hydrogenation (typically 35 bar). The normal operating pressure will be described in detail in Chapter Two.

### *1.10.1 Electrochemical methods*

Electrochemical experiments were performed using cyclic voltammetry (CV).

### *1.10.2 Voltammetry*

Voltammetry comprises a group of electroanalytical methods in which information about the analyte is derived from a measurement of current as a function of the applied potential to the working electrode [117,118]. Voltammetry is widely used by inorganic, physical and biological chemists, to investigate fundamental aspects of oxidation-reduction processes in various media, adsorption processes on surfaces, and electron transfer mechanisms at electrode surfaces. In this thesis, cyclic voltammetry (CV) will be used to study catalyst surface structure and composition.

### *1.10.3 Cyclic voltammetry*

In what follows, an outline will be given of the voltammetry of platinum in dilute sulphuric acid. In cyclic voltammetry, the current passing between the electrode of interest and a counter electrode is measured under the control of the potentiostat. The working electrode is subjected to a triangular potential sweep, whereby the potential rises from a start value  $E_i$  to a final value  $E_f$  then

returns back to the start potential at a constant potential sweep rate. The resulting voltammogram is shown in Figure 1.22 and depicts the variation in electric current engendered by the triangular potential wave form flowing from the working electrode (the electrode of interest) to a counter electrode. Any voltammogram peak can be used to determine the potentials at which electrochemical processes take place. The peak width and height for a particular process may depend on the sweep rate, electrolyte concentration and the electrode material [117, 118].

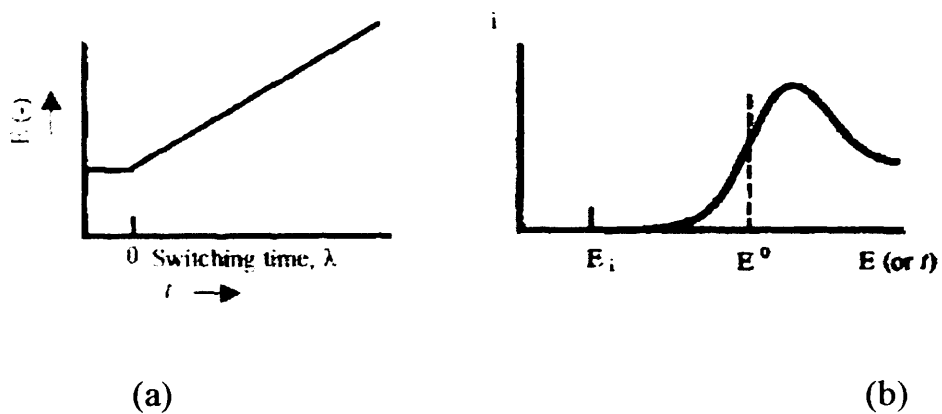
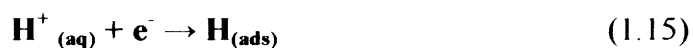


Figure 1.22 A schematic cyclic voltammogram of (a) Linear potential sweep; (b) resulting voltammogram. Reprinted from [118].

#### 1.10.4 Characterisation of CV from Pt surfaces

The adsorption of hydrogen ions from solution on platinum was investigated by Frumkin and Slygin in 1934 [119]. A monolayer of adsorbed hydrogen is formed between 0.0 – 0.3 V positive of the hydrogen equilibrium potential (0.0 V). Adsorption of hydrogen occurs according to equation 1.15.



Single crystal electrodes are electrodes whose surfaces are defined with respect to their crystallographic orientation [120]. Will was the first investigator to study the electrochemistry of single crystal platinum electrodes by means of cyclic voltammetry [121]. He assigned the hydrogen adsorption state observed on polycrystalline platinum at the more positive potential to strongly adsorbed hydrogen at {100} sites and the state at the less positive potential to weakly adsorbed hydrogen at {111} sites as judged from the analogous behaviour of an electrochemically activated Pt{100} and Pt{111} single crystal electrode [122]. A typical cyclic voltammogram for polycrystalline platinum in sulphuric acid is shown in Figure 1.23 [122].

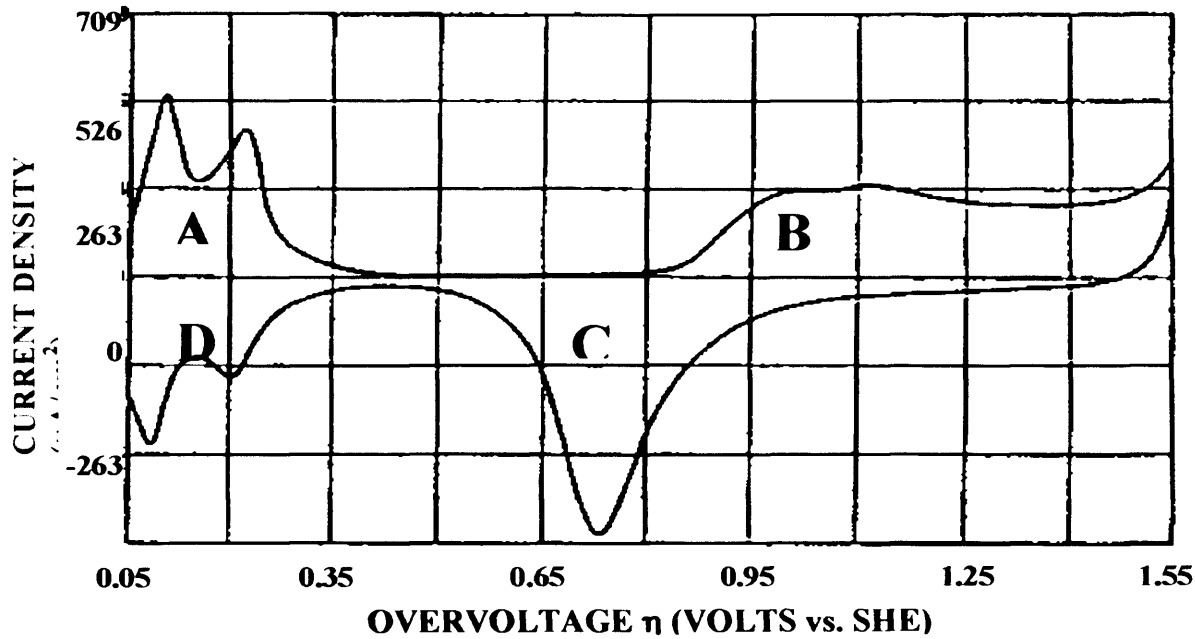


Figure 1.23 Cyclic voltammogram of a polycrystalline platinum electrode in sulphuric acid. Sweep rate =  $100\text{mVs}^{-1}$ . Reprinted from [122].

Figure 1.23 presents the cyclic voltammogram (CV) exhibited by a polycrystalline platinum electrode cycled in sulphuric acid. Two characteristic regions are evident:

- i. the hydrogen desorption and adsorption regions (A and D)
- ii. the oxide adsorption and desorption regions (B and C)

Region A of the voltammogram represents hydrogen desorption:

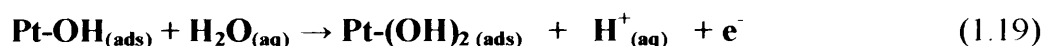
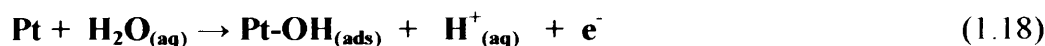


Electrons flow from the Pt-H covalent bond to the metal as a result of proton desorption, which generates a current each time this occurs. This generated current is proportional to the surface area of the Pt electrode.

Region D represents hydrogen adsorption which is the reverse of symmetrical about the potential axis and these processes are therefore reversible.

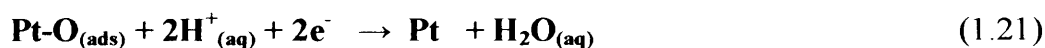


Region B is associated with adsorption of an oxide species to form an oxide surface. This occurs *via* place exchange between platinum atoms and adsorbed oxygen. These chemisorbed oxygen atoms may diffuse into the bulk of the electrode and form a non-stoichiometric oxide [123].



Normally on reaching about 1.55 V, the potential sweep is reversed. Potential excursions beyond 1.55 V result in the breakdown of the aqueous-electrolyte and production of oxygen gas. Similarly, potential excursions negative of 0.0 V result in hydrogen production.

Region C corresponds to the reduction of the oxide layer. It is important to note that regions B and C are not symmetrical about the potential axis and exhibit significant hysteresis, which indicates that the redox processes are not reversible.



The assignment of the Pt-H<sub>(111)</sub> states to specific crystallographic planes was accomplished by a combination of cyclic voltammetric and ultra-high vacuum (UHV) [124,125] studies. These studies confirmed Will's original assertions



for the assignment of the weakly and strongly bound states of atomic hydrogen. In order to take Will's original work further *i.e.* to assign specific voltammetric peaks to particular adsorption sites, it is necessary to be able to name individual adsorption sites. In what follows, a brief introduction to single crystal surface nomenclature will be provided since in this way, single crystal electrodes may be used subsequently to investigate adsorption and ultimately relate these processes to catalytic activity and selectivity.

### 1.11. Miller indices

The bulk crystal structure of most metals may be described as:

bcc	Body-centered cubic
fcc	Face-centered cubic
hcp	Hexagonal close packed

In most technological applications, metals are used either in a finely divided form (*e.g.* supported metal catalysts) or in a massive, polycrystalline form (*e.g.* electrodes and mechanical fabrications). Since metal surfaces possess structure sensitive properties, it is important to be able to characterise/identify the individual crystal planes that make up the surface of a metal crystallite since, depending on the nature of the plane (closed-packed, open, containing steps *etc.*), different surface chemistry may be expected. Therefore a method of unambiguously identifying a catalyst plane needs to be developed. The most commonly used nomenclature for this purpose is the Miller index. Miller indices are a vector representation for the orientation of an atomic plane in a crystal lattice and are defined as the reciprocals of the fractional intercepts

which the plane makes with the crystallographic axes. To determine the Miller index of a particular plane in a three-dimensional lattice, the following procedure is used [32,126-127]. Firstly, the intercepts of the plane with axes of the basis vectors  $\vec{a}$ ,  $\vec{b}$  and  $\vec{c}$  which define the unit cell of the crystal, are found (Figure 1.24). Secondly, the distances from the origin to the intercept points of the plane with  $\vec{a}$ ,  $\vec{b}$  and  $\vec{c}$  are evaluated as  $a$ ,  $b$  and  $c$ , respectively. The Miller index  $h, k, l$ , is defined as:

$$\frac{\overline{a}}{a}, \quad h, \quad \frac{\overline{b}}{b}, \quad k, \quad \frac{\overline{c}}{c} = l.$$

The Miller index is written as three numbers,  $(hkl)$ , one for each coordinate in three dimensional spaces [128]. When  $h, k$  or  $l$  take fractional values, the three indices are converted to the smallest integers having the same ratio as  $h$  to  $k$  to  $l$  by multiplying by a common factor, *e.g.*  $(2/4, 1/4, 1/4)$  becomes  $(2, 1, 1)$ . Where a “negative intercept” happens to result, this is indicated by placing a bar above the appropriate values of the index [129]. The three basal planes of the fcc crystal and the arrangements of the surface atoms in these Miller planes are shown in Figures 1.24 and 1.25. An example of CV’s for low Miller index planes of platinum prepared by using a flame-annealing method (heating them to 1000 °C in air and cooling in hydrogen) is shown in Figure 1.26 based on the preparation procedure developed by Clavilier in 1980 [130]. Figure 1.26 also shows a representation of a Pt nano-particle as a cubo-octahedron. Various terrace and step features of the nano-particle may be associated with the CV’s derived from electrochemical single crystal electrode studies.

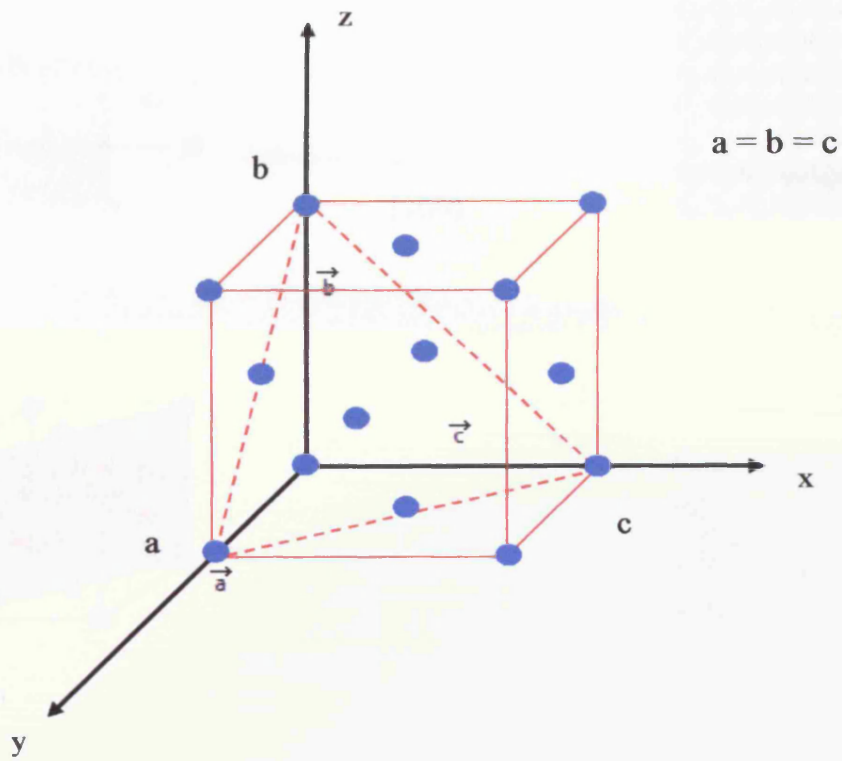


Figure 1.24 The three vectors  $\vec{a}$ ,  $\vec{b}$  and  $\vec{c}$  defining the crystal unit cell and the {111} Miller index plane (dotted triangle).

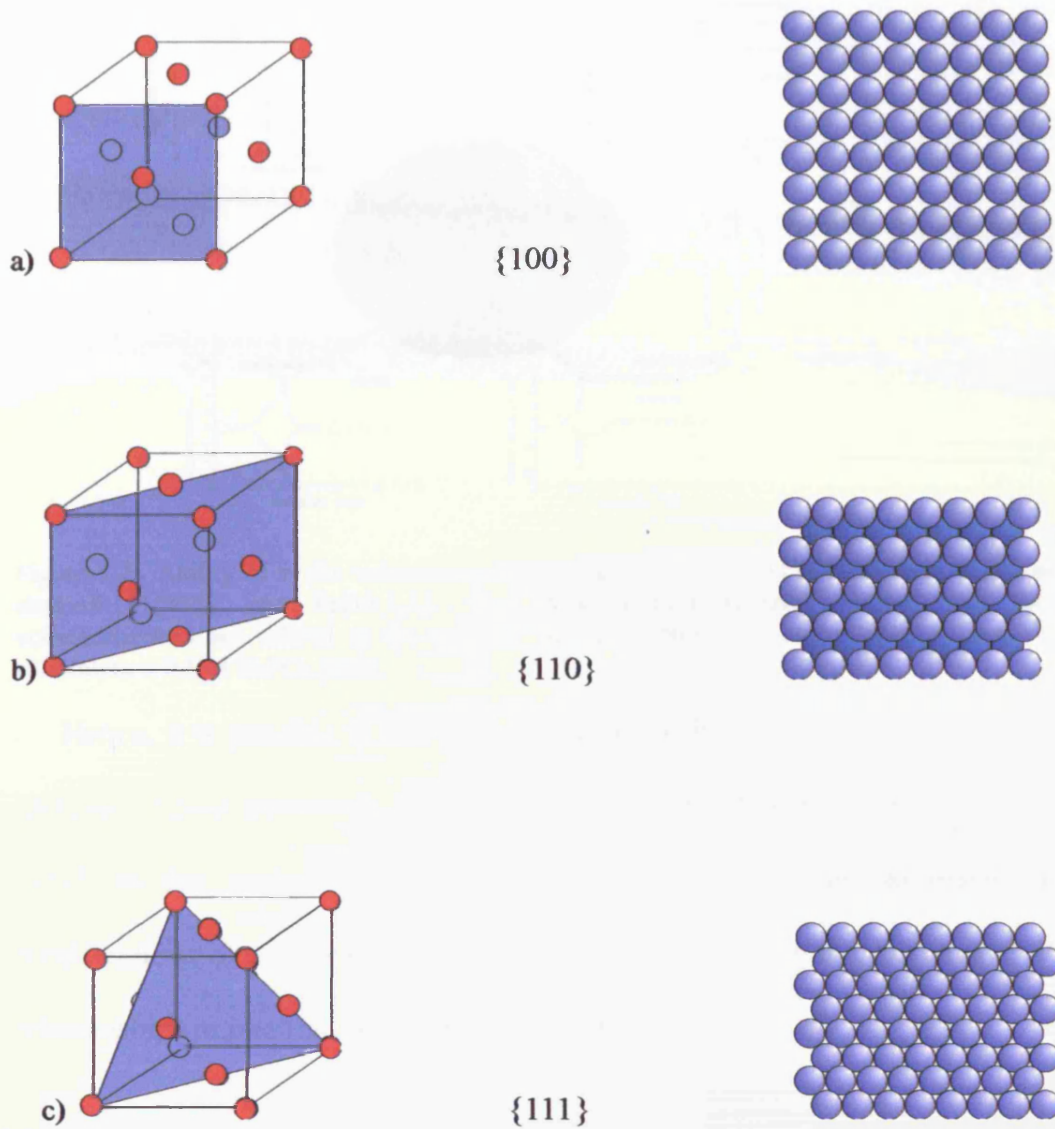


Figure 1.25 Low Miller index planes of a)  $\{100\}$ , b)  $\{110\}$ , and c)  $\{111\}$  and their corresponding surface structure for a face-centered cubic lattice.

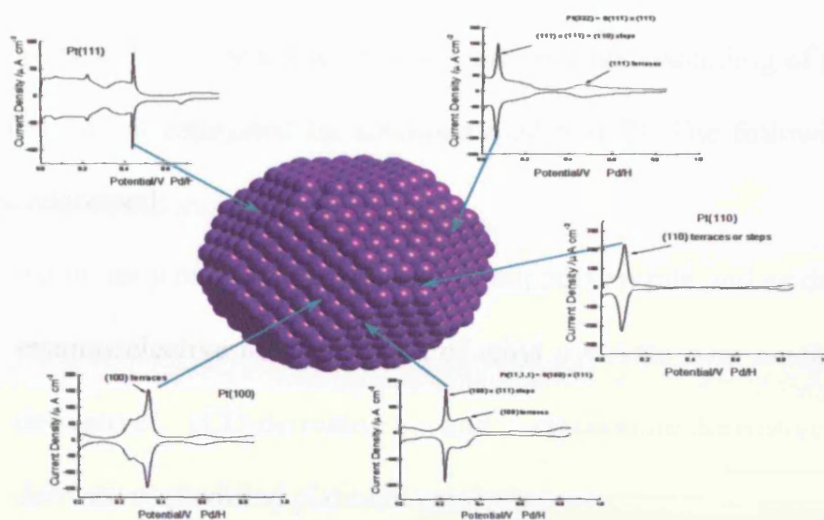


Figure 1.26 Ability of cyclic voltammograms to characterize P{111}, {100} and {110} and stepped Pt{332} and Pt{11,1,1}. The Pt-nanocluster (center) shows how these voltammograms are related to the exposed surface. Conditions: sweep rate =  $50 \text{ mVs}^{-1}$ , electrolyte =  $0.1 \text{ M H}_2\text{SO}_4$  [131].

Hence, it is possible to use CV to measure both the proportion (peak area) and typical peak potentials, of adsorption sites present at supported Pt catalyst [132]. In this study, electrochemical methods will be used to investigate modifications of supported Pt catalysts in order to observe structure-reactivity relationships in relation to the Orito-reaction.

## 1.12 Objectives

The objectives of this study were to advance our understanding of pyruvate ester hydrogenation catalyzed by cinchona-modified Pt. The following aims were to be addressed:

- a) To investigate the effect of catalyst support on rate and *ee* during the enantioselective hydrogenation of ethyl pyruvate over cinchonidine-derivative (CD-derivative) and cinchonine-derivative (CN-derivative) modified platinum catalysts.
- b) To investigate the influence of solvents on the rate and *ee* of enantioselective hydrogenation using various cinchona alkaloids as modifiers.
- c) To investigate the influences of thermal annealing and sintering on the rate and enantiomeric excess (*ee*) of the Orito reaction.
- d) To investigate the effect of bismuth adsorption on the title reaction by examining the effects of adsorbing Bi at steps, kink, and at terraces on *ee* and rate.
- e) To formulate the important features of a catalyst that produces high enantiomeric excess (*ee*) based on fundamental measurements.

### 1.13 References

- [1] M. Twigg, *Catalyst Handbook*. Manson Publisher, London, 1996.
- [2] G.C. Bond, *Heterogeneous Catalysis: Principles and Applications*. Oxford Chemistry, Oxford, New York, Clarendon, 1987.
- [3] J.J. Berzelius, *Edinburgh New Philosophical Journal.*, **XXI** (1836) 223.
- [4] I.M. Campbell, *Catalysis at surface*. Chapman & Hall, London, 1988.
- [5] P.B. Wells, *Surface Chemistry and Catalysis*. Kluwer Academic/Plenum Publisher, New York, 2002.
- [6] K. Campell and S.J. Thomson, *Prog. Surf. Membrane Sci.*, **9** (1975) 163.
- [7] A.E. Shilov, G.B. Shulpin, *Chem. Rev.*, **97** (1997) 2879.
- [8] P.B. Wells, A. Wilkinson, *Top. Catal.*, **5** (1998) 39.
- [9] R. Noyori, M. Koizumi, D. Ishii, T. Ohkuma, *Pure. Appl. Chem.*, **73** (2001) 227.
- [10] H.-U. Blaser, H.P. Jalett and F. Spindler, *J. Mol. Catal. A: Chemical*, **107** (1996) 85.
- [11] R. Noyori, T. Ohkuma, *Angew. Chem. Int. Ed. Engl.*, **40** (2001) 40.
- [12] P.K. Babu, P. Waszczuk, H.S. Kim, E. Oldfield, and A. Wieckowski, *J. Phys. Chem. B.*, **106** (2002) 9581.
- [13] Nie, Qian, Wu, Yan-hua, Wu, Chun, *J. American. Chem. Soc.*, **4** (2003) 172.
- [14] V. Ratovelomanana-Vidal and J.P. Genêt, *J. Organometal. Chem.*, **567** (1998) 163.

- [15] M.J. Burk, W. Hems, D. Herzberg, C. Malan and A. Zanotti-Gerosa, *Org. Lett.*, **26** (2000) 4173.
- [16] S. Jeulin, S. Dupratde Paule, V. Ratovelomanana-Vidal, J.P. Genêt, N. Champion and P. Dellis, *Pro. Natl. Acad. Sci. USA.*, **101** (2004) 5799.
- [17] D.G. Genov and D.J. Ager, *Angew. Chem. Int. Ed.*, **43** (2004) 2816.
- [18] J.F. Carpentier, F. Agbossou and A. Montreux, *Tetrahedron: Asym.*, **6** (1995) 39.
- [19] (a) M. Uchida, Y. Aoyaama, M. Tanabe, N. Yanagihara, Eda.; Ohta, A. *J. Electrochem. Soc.*, **142** (1995) 2572.
- (b) J.B Goodenough, A. Hamnett, B.J. Kennedy, R. Manoharan, S.A. Weeks, *J. Electroanal. Chem.*, **204** (1988) 133.
- (c) M. Wantanabe, M. Uchids, S. Motoe, *J. Electroanal. Chem.* **229** (1987) 395.
- [20] C.N. Hinshelwood, *The Kinetics of Chemical Change*. Clarendon Press, Oxford, 1940.
- [21] D.D. Eley, E.K. Rideal, *Nature*, **146** (1946) 401.
- [22] T. Engel, G. Ertl, *Adv. Catal.*, **28** (1979) 1.
- [23] G. Ertl, *Dynamics of Reactions at Surfaces*. Academic Press, Boston, 2000.
- [24] T. Engel, G. Ertl, *Oxidation of Carbon Monoxide, in the Chemical Physics of Solid Surfaces and Heterogeneous Catalysis*. Elsevier, Amsterdam, 1982.
- [25] S.T. Ceyer, W.L. Guthrie, T-H. Lin, G.A. Somorjai, *J. Chem. Phys.*, **78** (1983) 6982.



- [26] A. de Meijere, K.W. Kolasinski, E. Hasselbrink, *Faraday Discuss.* **96** (1993) 265.
- [27] C.C. Cheng, S.R. Lucas, H. Gutleben, W.J. Choyke, J.T. Yates Jr, *J. Am. Chem. Soc.*, **114** (1992) 1249.
- [28] K.R. Lykke and B.D. Kay, in *Laser Photoionization and Desorption Surface Analysis Technique-SPIE Proceedings*. SPIE, Bellingham, WA, 1990.
- [29] C.T. Rettner, *Phys. Rev. Lett.*, **69** (1992) 383.
- [30] G. Ertl, H. Knözinger, J. Weitkamp, *Handbook of Heterogeneous Catalysis. Catalytic Processes*, Wiley, 1997.
- [31] F. Rouquerol, J. Rouquerol, K. Sing, *Adsorption by Powders and Porous solid*. Academic Press, London, 1999.
- [32] G.A. Attard, C. Barnes, *Surfaces*. Oxford University Press, Oxford, New York, 1998.
- [33] M. Bowker, *The Basic and Applications of Heterogeneous Catalysis*. Oxford Chemistry Press, Oxford, 1998.
- [34] F. Zaera, *J. Phy. Chem. B.*, **106** (2002) 4043.
- [35] Y. Borodko, G.A. Somorjai, *Appl. Catal. A-Gen.*, **186** (1999) 355.
- [36] Ward, S. Robert, *Selectivity in Organic Synthesis*. John Wiley & Sons, Ltd, New York, 1999.
- [37] F. Thomas, Jr Degnan, *J. Catal.*, **216** (2003) 32.
- [38] S.C. Stinson, *C & EN*, 20 October, (1997) 38.
- [39] S.C. Stinson, *C & EN*, 21 September, (1998) 83.

- [40] G.M. Ramos Tombo, H.-U. Blaser, *in: Pesticide Chemistry and Bioscience*. Royal Society of Chemistry, Cambridge, 1999.
- [41] R. Noyori, *Chemtech.*, **22** (1992) 366.
- [42] C.G. Bond, *Chem. Soc. Rev.*, **4** (1991) 441.
- [43] Shi-Kai. Tain, Yonggan. Chen, Jianfeng. Hang, Liang. Hang, Paul McDaid, Li. Deng, *Acc. Chem. Research*, **37** (2004) 621.
- [44] Y. Orito, S. Imai and S. Niwa, *Collected papers of the 43<sup>rd</sup> Catalyst forum*, Japn., (1978) 30.
- [45] R.A. Hegstrom and D.K. Kondempudi, *Scientific American* (1990) 98.
- [46] J.B. Biot, *Bull. Soc. Philomath* (1815) 190.
- [47] L. Pasteur, *Acad. Sci.* **26** (1848) 535.
- [48] J.H. van't Hoff, *Arch. Neerl. Sci. Exacts. Nat.*, **9** (1874) 445.
- [49] J.A. Le Bel, *Bull. Soc. Com. Fr.*, **22** (1874) 337.
- [50] R.S. Cahn, C.K. Ingold, V. Prelog, *Angew. Chem. Int. Ed. Engl.*, **5** (1966) 385.
- [51] J. Clayden, N. Greeves, S. Warren, P. Wothers, *Organic Chemistry*. Oxford University Press, Oxford, 2001.
- [52] Y. Orito, S. Imai and S. Niwa, *J. Chem. Soc. Jpn.*, **8** (1979) 1118.
- [53] Y. Orito, S. Imai and S. Niwa, *J. Chem. Soc. Jpn.*, (1980) 670.
- [54] Y. Orito, S. Imai and S. Niwa, *J. Chem. Soc. Jpn.*, (1982) 137.
- [55] H.-U. Blaser, H.P. Jalett and J.T. Wiehl, *J. Mol. Catal.*, **68** (1991) 215.
- [56] H.-U. Blaser, M. Garland, and H.P. Jallet, *J. Catal.*, **144** (1993) 569.

- [57] D. Briggs, J. Dewing, A.G. Burden, R.B. Moyes, P.B. Wells, *J. Catal.*, **65** (1980) 31.
- [58] H.-U. Blaser, H.P. Jallet, D.M. Monti, J.F. Reber and J.T. Wehrli, *Stud. Surf. Sci. Catal.*, **41** (1988) 153.
- [59] H.-H. Blaser, H.P. Jallet, D.M. Monti, A. Baiker, J.T. Wehrl, *Stud. Surf. Sci. Catal.*, **67** (1991) 147.
- [60] M. Bartok, T. Bartok, G. Szollosi, K. Felfoldi, *Catal. Lett.*, **61** (1999) 57.
- [61] P.A. Meheux, A. Ibbotson and P.B. Wells, *J. Catal.*, **128** (1991) 387.
- [62] G. Bond, K.E. Simons, A. Ibbotson, P.B. Wells and D.A. Whan, *Catal. Today*, **12** (1992) 421.
- [63] H.-U. Blaser, H.P. Jallet, M. Studer, *J. Am. Chem. Soc.*, **122** (2000) 12675.
- [64] J.W. Geus, P.B. Wells, *J. Catal.*, **18** (1985) 231.
- [65] M.V. Arx, T. Mallat, A. Baiker, *Top. Catal.*, **19** (2002) 75.
- [66] H.-U. Blaser, *Chem. Commun.*, (2003) 293.
- [67] H.-U. Blaser, *Chem. Rev.*, **92** (1992) 935.
- [68] B. Minder, T. Mallat, A. Baiker, G. Wang, T. Heinz, A. Pfaltz, *J. Catal.*, **154** (1995) 371.
- [69] K.E. Simons, P.A. Meheux, S.P. Griffiths, I.M. Sutherland, P. Johnston, P.B. Wells, A.F. Carley, M.K. Rajumon, M.W. Roberts, A. Ibbotson, *Recl. Trav. Chim. Pays-Bas*, **133** (1994) 465.
- [70] N.F. Gold'schleger, V.V. Es'kova, A.E. Shilov, A.A. Shteinman, *Engl. Trans.*, **46** (1972) 785.

- [71] X. Li, Ph.D. Thesis, Cardiff University, 2001.
- [72] H.-U. Blaser, H.P. Jalett, M. Muller, M. Studer, *Catal. Today*, **37** (1997) 441.
- [73] J.L. Margitfalvi, E. Talas, M. Hegedus, *Chem. Commun.*, (1999) 645.
- [74] T. Mallat, S. Frauchiger, P.J. Kooyman, M. Schürch and A. Baiker, *Catal. Lett.*, **63** (1999) 121.
- [75] B. Török, K. Balázsik, M. Török, G. Szöllösi, M. Bartók, *Ultrasonics Sonochemistry*, **7** (2000) 151.
- [76] C. Leblond, J. Wang, J. Liu, A.T. Andrews, Y.K. Sun, *J. Am. Chem. Soc.*, **121** (1999) 4920.
- [77] B. Török, K. Felföldi, K. Balázsik, M. Bartók, *Chem. Commun.*, (1999) 1725.
- [78] M. Sutyinszki, K. Szöri, K. Felföldi, M. Bartók, *Catal. Lett.*, **81** (2002) 281.
- [79] M. Sutyinszki, K. Szöri, K. Felföldi, M. Bartók, *Catal. Commun.*, **3** (2002) 125.
- [80] K. Balázsik, K. Szöri, K. Felföldi, B. Török, M. Bartók, *Chem. Commun.*, (2000) 555.
- [81] M. Studer, S. Burkhardt, A. Findolese, H.-U. Blaser, *Chem. Commun.*, (2000) 1327.
- [82] G.Z. Wang, T. Mallat, A. Baiker, *Tetrahedron: Asym.*, **8** (1997) 2133.
- [83] N. Künzle, A. Szabó, M. Schürch, G. Wang, T. Mallat, A. Baiker, *Chem. Commun.*, (1998) 1377.

- [84] M. von Arx, T. Bürgi, T. Mallat, A. Baiker, *Chem. Eur.*, **8** (2002) 1430.
- [85] M. Studer, H.-U. Blaser, S. Burkhardt, *Adv. Synth. Catal.*, **344** (2002) 511.
- [86] E. Toukoniitty, P. Mäki-Arvela, M. Kuzma, A. Vilella, A. K. Neyestanaki, T. Salmi, R. Sjöholm, R. Leino, D. Y. Murzin, *J. Catal.*, **204** (2001) 281.
- [87] M. Studer, H.-U. Blaser, V. Okafor, *Chem. Commun.*, (1998) 1053.
- [88] T. Mallat, E. Orglmeister, and A. Baiker, *Chem. Rev.*, **107** (2007) 4863.
- [89] I. M. Sutherland, A. Ibbotson, R. B. Moyes and P. B. Wells, *J. Catal.*, **125** (1990) 77.
- [90] C. G. Bond, P. A. Meheux, A. Ibbotson and P. B. Wells, *Catal. Today*, **10** (1991) 371.
- [91] A. Baiker, *J. Mol. Catal. A: Chemical*, **155** (1997) 473.
- [92] R. L. Augustine, T. S. K. and L. K. Doyle, *Tetrahedron: Asym.*, **4** (1993) 1803.
- [93] A. Saus, K. Zimmermann and O. Gürtler, *Chem. Ztg.*, **155** (1991) 252.
- [94] X. Zuo, H. Liu and M. Liu, *Tetrahedron. Lett.*, **39** (1998) 1941.
- [95] X. Zuo, H. Liu, C. Guo and X. Yang, *Tetrahedron*, **55** (1999) 7787.
- [96] H. Bönemann and G. A. Baun, *Chem. Eur. J.*, **3** (1997) 1200.
- [97] B. Török, K. Bonazsik, G. Szöllösi, K. Felföldi and M. Bartók, *Chirality*, **11** (1999) 470.
- [98] J. L. Margitfalvi and E. Tfirst, *J. Mol. Catal. A*, **139** (1999) 81.

- [99] J.L. Margitfalvi, M. Hegedüs and E. Tfirst, *Stud. Surf. Sci. Catal.*, **101A** (1996) 241.
- [100] M. Bartók, K. Felföldi, G. Szöllösi and T. Bartók, *Catal. Lett.*, **61** (1999) 1.
- [101] M. Bartók, K. Felföldi, B. Török and T. Bartók, *Chem. Commun.*, **2605** (1998).
- [102] M. Bartók, K.B. Török, K. Balazsik and T. Bartók, *Catal. Lett.*, **73** (2001) 127.
- [103] H.-U. Blaser, H.P. Jalett, M. Garland, M. Studer, H. Thies and A. Wirth. Tijani, *J. Catal.*, **173** (1998) 282.
- [104] D.Y. Murzin, *Ind. Eng. Chem. Res.*, **36** (1997) 4784.
- [105] J.L. Margitfalvi, M. Hegedüs and E. Tfirst, *Tetrahedron: Asym.*, **7** (1996) 571.
- [106] S. Lavoie, M.-A. Laliberte, I. Temprano, P.H. McBreen, *J. Am. Chem. Soc.*, **128** (2006) 7588.
- [107] S. Lavoie, P.H. McBreen, *J. Phys. Chem. B.*, **109** (2005) 11986.
- [108] V. Venkatesan, A. Fujii, T. Ebata, N. Mikami, *Chem. Phys. Lett.*, **394** (2004) 45.
- [109] V. Venkatesan, A. Fujii, T. Ebata, N. Mikami, *Chem. Phys. Lett.*, **409** (2005) 57.
- [110] V. Venkatesan, A. Fujii, T. Ebata, N. Mikami, *Chem. Phys. Lett.*, **109** (2005) 915.
- [111] S. Diezi, T. Mallat, A. Szabo, A. Baiker, *J. Catal.*, **228** (2004) 162.

- [112] N. Bonalumi, A. Vargas, D. Ferri, T. Burgi, T. Mallat, A. Baiker, *J. Am. Chem. Soc.*, **127** (2005) 8467.
- [113] J.T. Wehrli, A. Baiker, D. M. Monti, H.-U. Blaser and H.P. Jalett, *J. Mol. Catal.*, **57** (1998) 245.
- [114] B. Török, K. Felföldi, G. Szakonyi, K. Balazsik and M. Bartók, *Catal. Lett.*, **52** (1998) 81.
- [115] D. Ferri, T. Bürgi and A. Baiker, *J. Chem. Soc. Perkin. Trans.*, **7** (1999) 1305.
- [116] B. Minder, T. Mallat, P. Skrabal and A. Baiker, *Catal. Lett.*, **29** (1994) 115.
- [117] E. Gileadi, E. Kirowa-Eisner, J. Penciner, *Interfacial Chemistry: An Experimental Approach*, Addison-Wesley, U. S. A, 1975.
- [118] A.J. Bard, L.R. Faulkner, *Electrochemical Methods, Fundamentals and Applications*. John Wiley & Sons, New York, 1980.
- [119] A.I. Slygin and A.N. Frumkin, *Acto. Physiochem. URSS*, **3** (1935) 791.
- [120] J.O'M. Bockris and S.U. M. Khan, *Surface electrochemistry, "A Molecular Level Approach"*. Plenum Press, New York and London, 1993.
- [121] F.G. Will, *J. Electrochem. Soc.*, **112** (1965) 451.
- [122] F.G. Will and C.F. Knorr, *Z. Electrochem.*, **64** (1960) 258.
- [123] B.E. Conway, B. Barnet, H. Angerstein-Kozłowska and B. Tilka, *J. Phys. Chem.*, **93** (1990) 8361.
- [124] K. Yamamoto, D.M. Kolb, R. Kotz and G. Lempfuhr, *J. Electroanal. Chem.*, **96** (1979) 233.

- [125] P.N. Ross, *J. Electroanal. Chem.*, **126** (1979) 67.
- [126] E.M. McCash, *Surface Chemistry*. Oxford University Press, Oxford, 2001.
- [127] A.R. West, *Basic Solid State Chemistry*. John Wiley & Sons, Ltd, England, 1999.
- [128] P.W. Atkins, *Physical Chemistry*. Oxford University Press, Oxford, Melbourne, Tokyo, 1994.
- [129] G.A. Somorjai, *Introduction to Surface Chemistry and Catalysis*. John Wiley & Sons, INC, New York, 1994.
- [130] J. Clavilier, R. Faure, G. Guinet, R. Durand, *J. Electroanal. Chem.*, **107** (1980) 205.
- [131] G.A. Attard, Ahmadi, D.J. Jenkins, O.A. Hazzazi, P.B. Wells, K.G. Griffin, P. Johnston, J.E. Gillies, *Chem. Phys. Chem.*, **4** (2003) 123.
- [132] G.A. Attard, J.E. Gillies, C.A. Harris, D.J. Jenkins, P. Johnston, M.A. Price, D.J. Watson, P.B. Wells, *Appl. Catal. A: General*, **222** (2001) 393.



**CHAPTER TWO**  
**EXPERIMENTAL**

## 2.1 Introduction

The enantioselective hydrogenation of  $\alpha$ -ketoesters such as ethyl pyruvate (etpy) to the corresponding *R*-lactate or *S*-lactate over cinchona alkaloid-modified platinum catalysts has been investigated. Various catalysts, modifiers, and reactants have been tested for the Orto reaction [1]. In this thesis most of the reactions were carried out using a standard procedure in which cinchona alkaloid, catalyst, substrate, and solvent were stirred together at the beginning of the reaction, under hydrogen ( $H_2$ ). In addition, hydrogenation of ethyl pyruvate using hydroquinine 4-chlorobenzoate, (from henceforth referred to as cinchonidine-derivative or CD-derivative) and hydroquinidine 4-chlorobenzoate, (from henceforth referred to as cinchonine-derivative or CN-derivative) (both obtained from Aldrich 98% purity) was investigated under various reaction conditions and used without further purification. The different catalysts used in this thesis were:

- Platinum supported on graphite (5% Pt/G),
- Platinum supported on silica (6.3% Pt/SiO<sub>2</sub>) (EUROPT-1),
- Platinum supported on alumina (5% Pt/Al<sub>2</sub>O<sub>3</sub>)

The products were analyzed and the enantioselectivities of reactions were investigated using chiral gas chromatography.

## 2.2 Materials

### 2.2.1. Catalysts

In the present study, three types of supported catalysts were used.

Platinum/graphite (Pt/G; 5%) was obtained from Johnson Matthey having a low surface area of  $2.1 \text{ m}^2 \text{ g}^{-1}$  with a mean platinum particle diameter of 14 nm. Platinum/silica (Pt/SiO<sub>2</sub>; 6.3%), was obtained from Johnson Matthey (standard reference catalyst EUROPT-1), having a surface area of  $185 \text{ m}^2 \text{ g}^{-1}$  and a mean platinum particle diameter of 2 nm. Platinum/alumina (Pt/Al<sub>2</sub>O<sub>3</sub>; 5%), was used both as received and after treatment at 700K in hydrogen from Engelhard (E 4759). The physical properties of this catalyst are reported to be as follows: Pt-content, 5% (w/w); Pt dispersion, 22%; mean Pt particle size, 4.5 nm; support,  $\gamma$ -Al<sub>2</sub>O<sub>3</sub>; specific surface area,  $168 \text{ m}^2 \text{ g}^{-1}$  [2].

### 2.2.2 Reactants and reagents

Ethyl pyruvate (etpy  $\geq 97\%$  purity) was obtained from Fluka. Modifiers such as hydroquinine 4-chlorobenzoate and hydroquinidine 4-chlorobenzoate (Figure 2.1) were obtained from Aldrich Chemicals and used without further purification. In this study, cinchonidine is mainly used for enantioselective hydrogenation (from henceforth, this reactant will be referred to as CD; 98% purity). Cinchonine, (from henceforth, this reactant will be referred to as CN; 98% purity) the near enantiomer of cinchonidine was used for a few experiments.

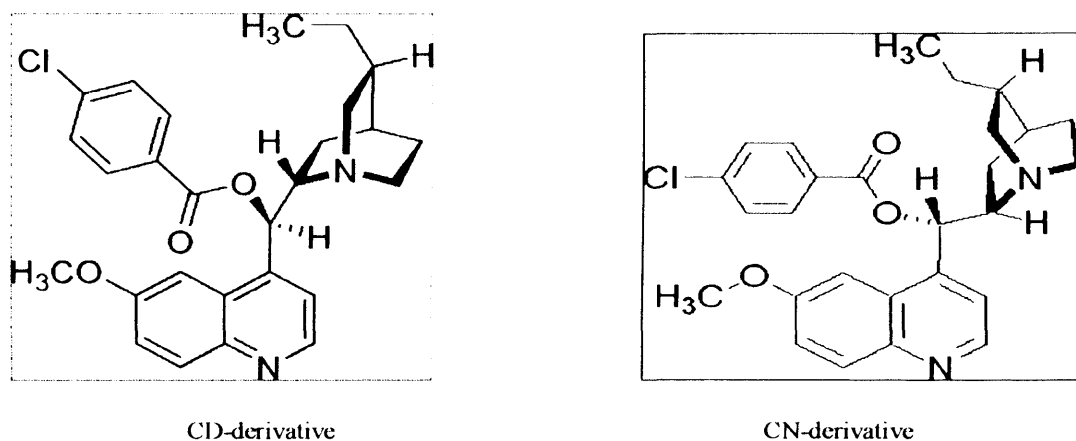


Figure 2.1. Structures of hydroquinine 4-chlorobenzoate (CD-derivative) and hydroquinidine 4-chlorobenzoate (CN-derivative).

Table 2.1. List of solvents, gases and other reactants used.

Reagent	Formula	Grade	Supplier
Bismuth nitrate	$\text{Bi}(\text{NO}_3)_3$	98+% <i>a.c.s</i>	Aldrich
Sulphuric acid	$\text{H}_2\text{SO}_4$	98%	Fisher Scientific
Potassium permanganate	$\text{KMnO}_4$	GBR	BDH
Hydrogen	$\text{H}_2$	99.995%	BOC Gases
Helium	He	99.995%	BOC Gases
Argon	Ar	99.995%	BOC Gases
5% Hydrogen/ Argon	5% $\text{H}_2$ / Ar	99.995%	BOC Gases
Air	$\text{O}_2$	High purity	BOC Gases
Nitrogen	$\text{N}_2$	High purity	BOC Gases
dichloromethane	$\text{CH}_2\text{Cl}_2$	99.9%	Fisher Scientific
Acetic acid	$\text{C}_2\text{H}_4\text{O}_2$	Glacial	Fisher Scientific

## 2.3 Apparatus

### 2.3.1. Autoclave reactor

Enantioselective hydrogenation experiments were carried out in a mini-reactor using a control tower supplied by Autoclave Engineers (Division of Snap-Tite, Ltd), as shown in Figure 2.2. The Autoclave Engineers reactor consisted of a 100 ml stainless steel vessel reactor equipped with a pressure gauge (1), a thermocouple, and a sealed mechanical stirrer driven by an integrated motor and magnetic drive unit. The stirrer and thermocouple were connected to the electronic control tower in order to control the stirrer speed and monitor the reaction temperature. Reactions took place in a 100 ml glass liner vessel (Figure 2.3). The vessel was attached into the body of reactor. A Teflon ring was placed between the vessel and the body of the reactor in order to prevent any gas leakage. A sealed mechanical impeller stirred the reactor and was driven by an integrated motor and magnetic drive unit. The reaction mixture was typically stirred at 1500 rpm.

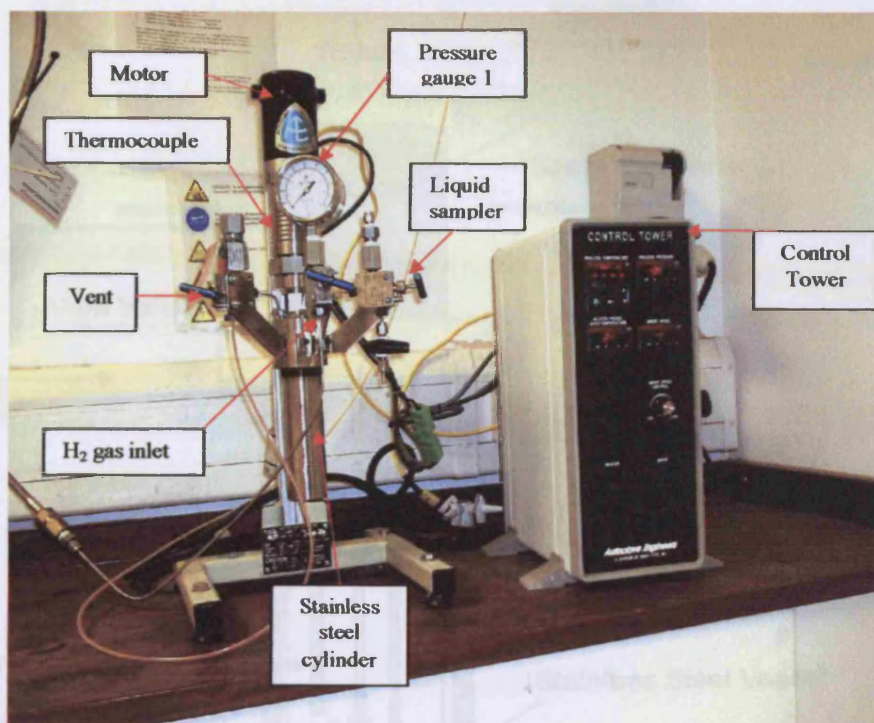


Figure 2.2 Autoclave reactor equipment used in enantioselective hydrogenation of ethyl pyruvate over modified catalysts.

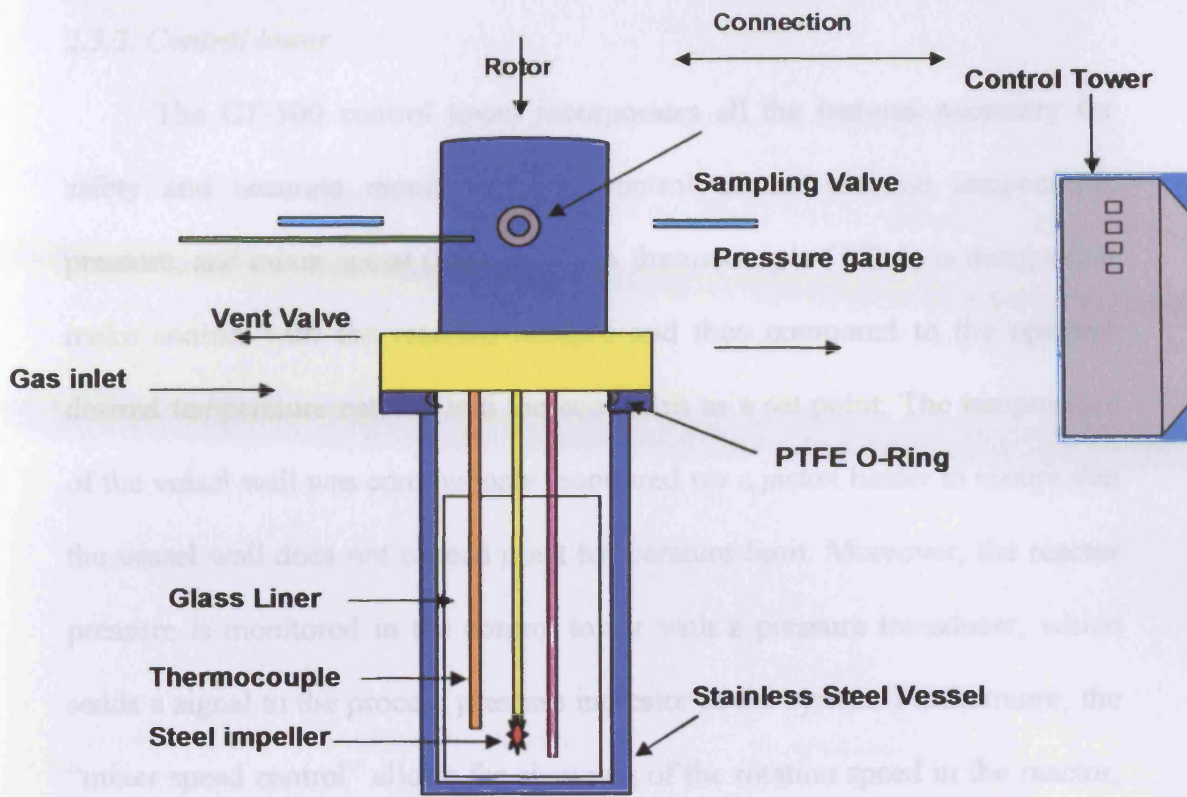


Figure 2.3 Schematic representation of the Autoclave Engineers reactor.



Figure 2.4 Control Tower ET-500

### 2.3.2. Control tower

The CT-500 control tower incorporates all the features necessary for safety and accurate monitoring and control of the reaction temperature, pressure, and mixer speed (Figure 2.4). A thermocouple (T/C-1) is designed to make contact with the reaction mixture and then compared to the operator desired temperature entered into the controller as a set point. The temperature of the vessel wall was continuously monitored *via* a jacket heater to ensure that the vessel wall does not exceed a net temperature limit. Moreover, the reactor pressure is monitored in the control tower with a pressure transducer, which sends a signal to the process pressure indicator in the system. Furthermore, the “mixer speed control” allows for changing of the rotation speed in the reactor, which is monitored on the “mixer speed” optical display.

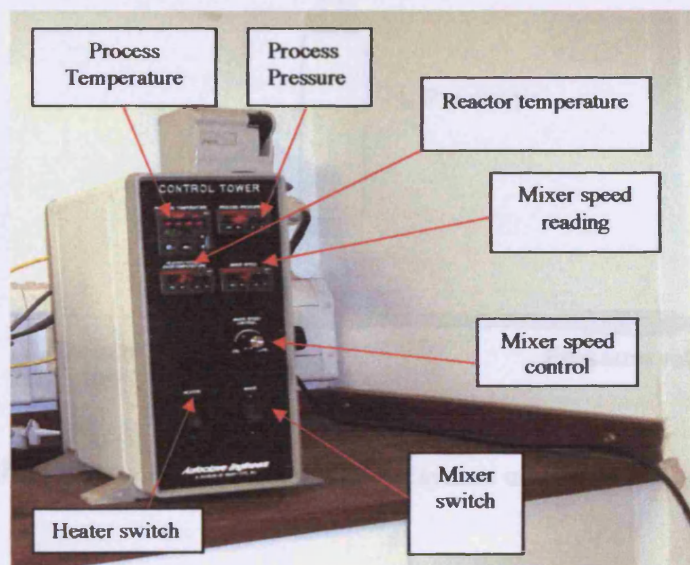


Figure 2.4. Control Tower CT-500.



### 2.3.3. Process gas flow diagram

The overall process flow for hydrogen ( $H_2$ ) is depicted in Figure 2.5. The progress of the catalytic reaction was monitored by a gas dosing system which was built in-house. The digital pressure display measures the change in the fixed volume gas reservoir, and was connected to high resolution data logger (ADC-16) processor and computer in order to measure the hydrogen uptake. The data recorded was then analysed using programmes such as Microsoft Excel<sup>TM</sup> or Microcal Origin<sup>TM</sup> [3].

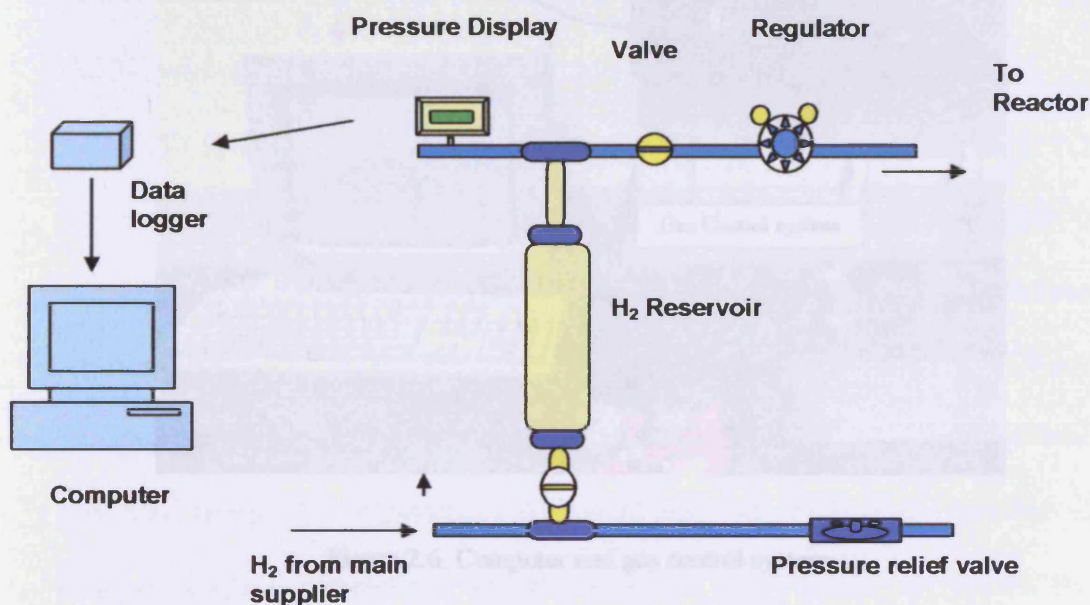


Figure 2.5. Schematic representation of gas dosing system used with the Autoclave reactor.

### 2.3.4. Control system

A computer is employed in various control and data-logging operations for the samples. An analogue to digital connection is used to collect data digitally relating to pressure changes as a function of time as the hydrogenation reaction proceeds Figure 2.6.

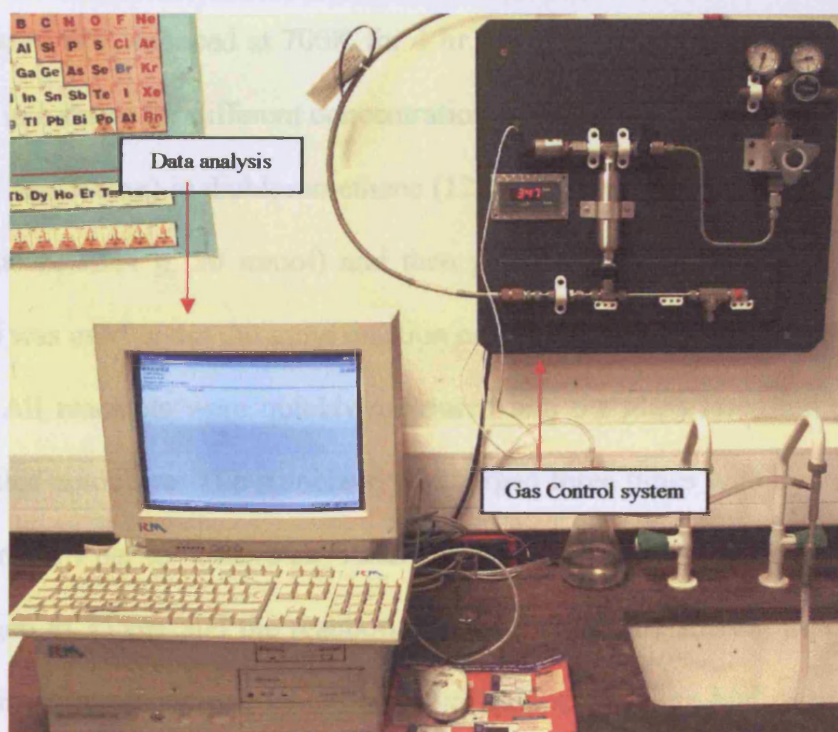


Figure 2.6. Computer and gas control system.

## 2.4. Experimental procedure

The reactor was cleaned rigorously before use by methanol reflux at 80°C for 2-5 h, and then tested with catalyst sample with known *ee* and conversion to ensure that reactor was clean after use by other workers. After each experiment, the reactor liner, stirrer, and vessel were thoroughly washed with acetone followed by dichloromethane and dried. Pt/graphite and Pt/alumina (5%) were fully reduced at 700K for 4 hr. Samples of catalysts (250mg) were stirred in a slurry for different concentrations of alkaloid (1, 2, 5, 10, 15, 20, 25, 30, 40, and 50 mg) in dichloromethane (12.5 ml), acetic acid (2.5 ml) and ethyl pyruvate (2.3224 g, 20 mmol) and then placed into the glass liner. Pt/silica (6.3%) was used under the same reaction conditions.

All reactants were quickly measured into the glass liner and placed in the sealed autoclave. The autoclave was purged three times with hydrogen to a pressure of 4 bar to remove air. After purging, the vessel was pressurised with hydrogen to 35 bar and the reaction was then started by stirring at 1500 rpm. To finish the experiment, the stirring was stopped and the hydrogen pressure was then released. The products were isolated from the reaction mixture and analysed by using chiral gas chromatography [4]. A typical H<sub>2</sub> uptake (bar) versus time (sec) curve over the course of catalytic reaction is shown in Figure 2.7.

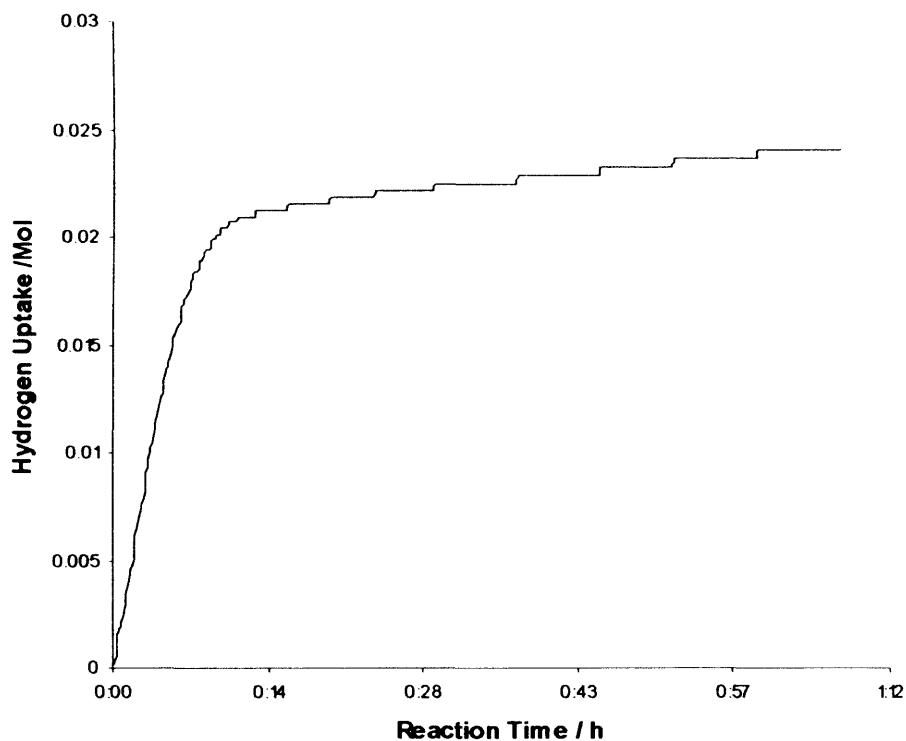


Figure 2.7 A typical H<sub>2</sub> uptake for the hydrogenation of ethyl pyruvate over Pt/G catalyst.

The figure shows a typical H<sub>2</sub> uptake curve for ethyl pyruvate hydrogenation in the presence of CD. The reaction profile is similar to previously reported measurements with a rapid uptake initially followed by a gradual plateau region [5-6]. The maximum rate was determined by measuring the initial slope of the H<sub>2</sub> uptake curve at time zero; it was also expressed as  $\text{mmol h}^{-1} \text{g}_{\text{cat}}^{-1}$ . Conversion was also measured using GC, which will be discussed later.

Table 2.2 Rate and enantioselectivity for blank reaction of ethyl pyruvate using Pt supported catalysts.

Solvent Modifier	DCM		Acetic acid	
	ee (%)	Rate	ee(%)	Rate*
Non	0	0.05	0.0	0.02

\* Rate mmol/g h

## 2.5 Product recovery

The catalyst was normally separated from the reaction mixture by filtration using Whatman (110 mm Ø) filter paper. The filtrate was then taken using a dropper plugged with cotton wool as additional filter, and transferred to a sample tube, stored and analysed by the use of chiral gas chromatography (GC).

## 2.6 Product analysis

### 2.6.1. Chiral gas chromatograph

A chiral gas chromatograph is a chemical analysis instrument that can be used in separating chemicals in a sample. The system used to analyze the products from enantioselective hydrogenation reaction of ethyl pyruvate with cinchona modified platinum catalysts was a Varian 3900, equipped with flame ionization detector (FID, Figure 2.8.). The capillary column used was a chiral  $\beta$ -cyclodextrin coated silica tube with dimensions 25m x 0.25mm. The software package *Star Chromatography Workstation* (Varian for windows) was used to process the data.

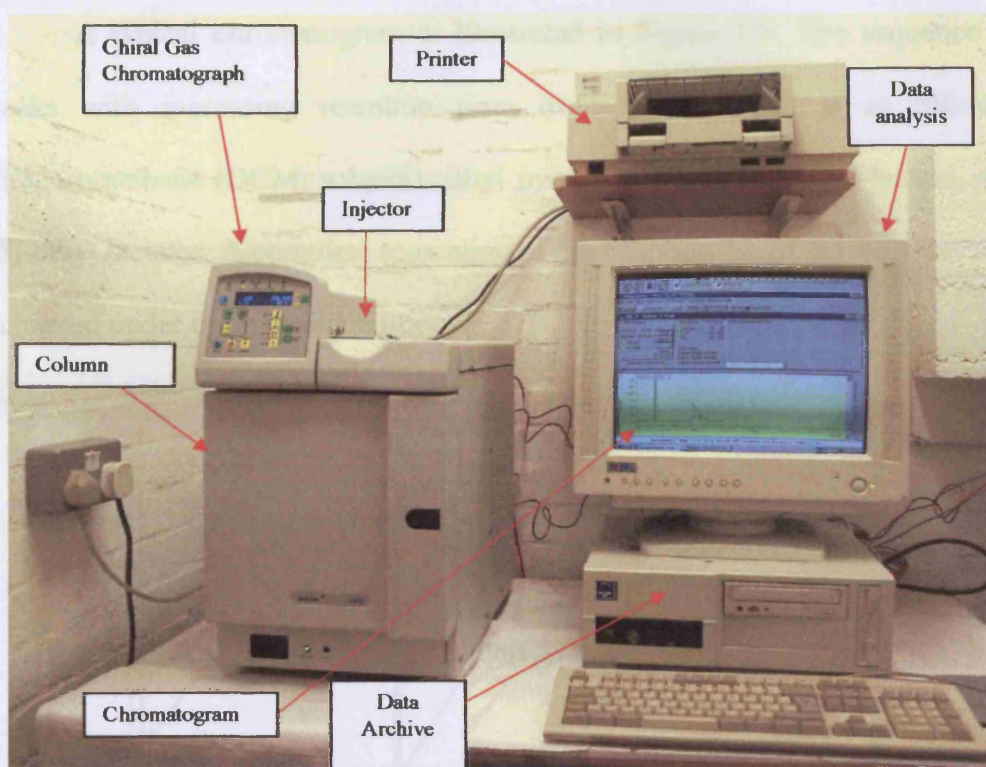


Figure 2.8 Chiral gas chromatograph.

From the filtered reaction solution described above (Section 2.5), a volume of  $0.1\mu\text{l}$  was taken and injected into the GC to obtain a good separation of products from ethyl pyruvate hydrogenation. The temperatures used in the GC were  $80^{\circ}\text{C}$  for the column (isothermal method) to separate the lactates. The detector and injector temperatures were set at  $200^{\circ}\text{C}$  and  $250^{\circ}\text{C}$  respectively. The injector provided a split ratio of 50:1 whilst maintaining a helium carrier gas flow rate of  $1\text{ ml min}^{-1}$  through the column. Splitter ratios and other gas flows were maintained by the use of electronic flow controllers within the instrument. Furthermore, no corrections for column response factor were applied to the GC data.

A typical chromatogram is illustrated in Figure 2.9. The sequence of peaks with increasing retention time from left to right is as follows: dichloromethane (DCM; solvent), ethyl pyruvate (Etpy), [*R*]-ethyl lactate, and [*S*]-ethyl lactates. A complete separation of the enantiomers of ethyl lactate was achieved under optimised conditions.

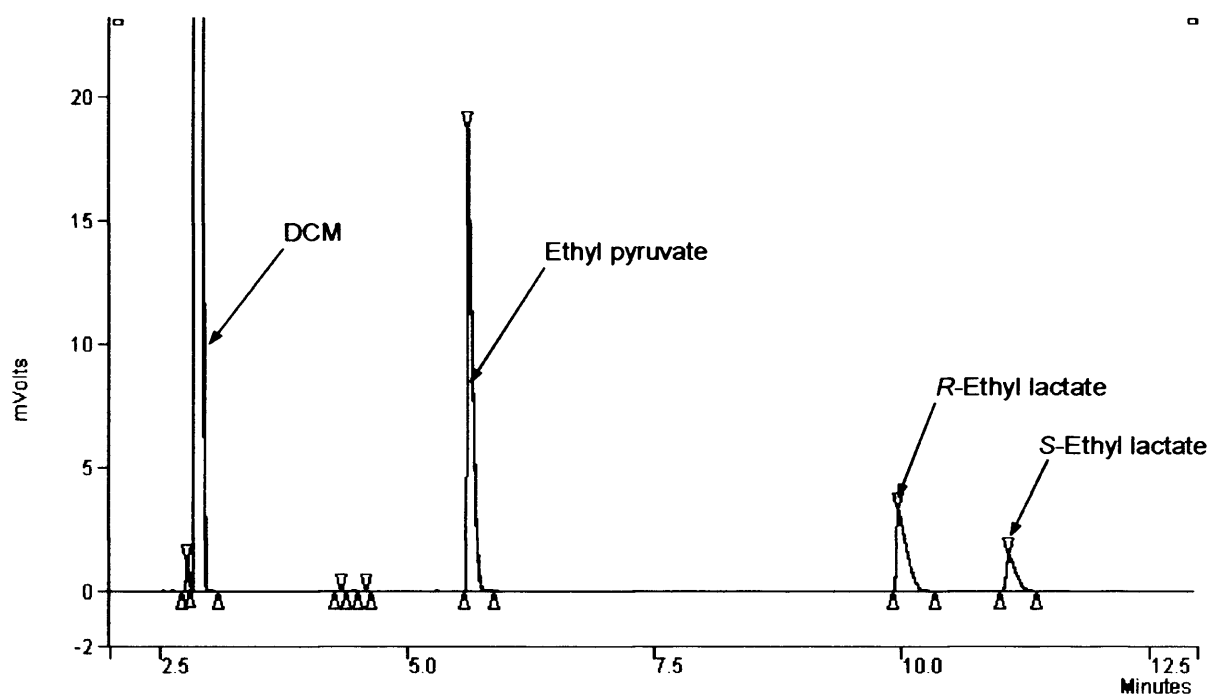


Figure 2.9 Chiral GC trace for elution of ethyl pyruvate, *R*- and *S*-ethyl lactate.

## 2.7 Analysis

### 2.7.1. Determination of enantiomeric excess (*ee*)

The enantiomeric excess (*ee*) could be determined using the following equation:

$$ee = \frac{[R]-[S]}{[R]+[S]} \times 100\% \quad (2.1)$$

Where  $[R]$  and  $[S]$  are the amounts of the enantiomeric products, respectively which were determined from the integrated peak area for  $[R]$ - and  $[S]$ -enantiomers in chiral GC analysis.

### 2.7.2. Determination of conversion

Conversion of the reaction could be determined using the following equation:

$$\text{Conversion (\%)} = \frac{[R]+[S]}{[R]+[S]+[Etpy]} \times 100 \quad (2.2)$$

Where  $[R]$ ,  $[S]$  and  $[Etpy]$  are respectively the integrated peak areas of  $[R]$ - and  $[S]$ -ethyl lactate and Etpy, respectively.



## **2.8 The electrochemical cell and data collection**

Cyclic voltammetry (CV) is a widely used technique and can give much information concerning the coverage and structure of a metal electrode surface as was highlighted in the Introduction of this thesis. It has been used to investigate metal deposition and to characterise the morphology of catalysts under investigation, and also to assess the effects of catalyst modification by ad-atom adsorption and thermal annealing. A schematic of the electrochemical cell is shown in Figure 2.10. The cell consists of the following parts: the working electrode, which was a platinum electrode and the removable palladium/hydrogen (Pd/H<sub>2</sub>) reference electrode which was housed in a small adjoining compartment to the working electrode. This reference maintains a stable and fixed reference potential of 50 mV versus a SHE (standard hydrogen electrode). The platinum mesh counter electrode is placed downstream from the working electrode in a luggin capillary. The main function of the counter electrode is to complete the electric circuit by measuring the current passing between it and the working electrode as a function of the potential measured.

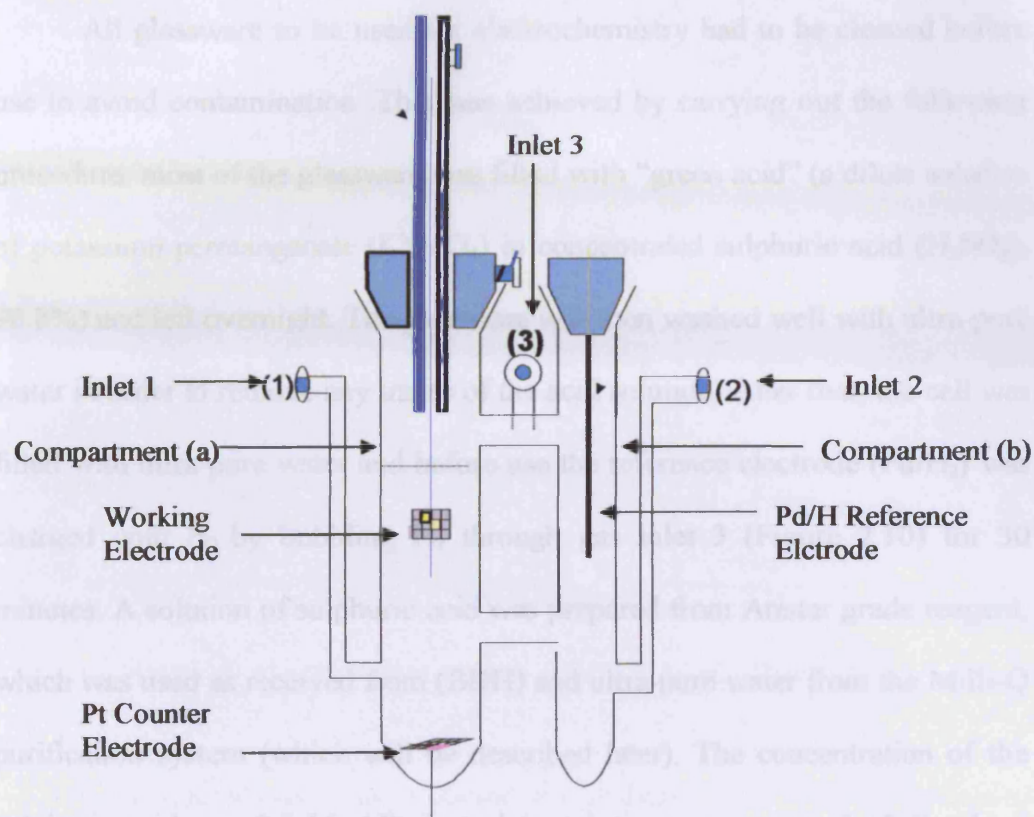


Figure 2.10 Schematic representation of electrochemical cell.

An electrochemical analyser was used to control the three electrodes to ensure that current only flows between the working electrode and counter electrode whilst the potential is applied between the working electrode and the reference electrode.

### 2.8.1. Electrochemical cell preparation procedure

All glassware to be used for electrochemistry had to be cleaned before use to avoid contamination. This was achieved by carrying out the following procedure: most of the glassware was filled with “green acid” (a dilute solution of potassium permanganate ( $\text{KMnO}_4$ ) in concentrated sulphuric acid ( $\text{H}_2\text{SO}_4$ , 98.8%) and left overnight. The glassware was then washed well with ultra-pure water in order to remove any traces of the acid solution. After that, the cell was filled with ultra-pure water and before use the reference electrode ( $\text{Pd}/\text{H}_2$ ) was charged with  $\text{H}_2$  by bubbling  $\text{H}_2$  through gas inlet 3 (Figure 2.10) for 30 minutes. A solution of sulphuric acid was prepared from Aristar grade reagent, which was used as received from (BDH) and ultra-pure water from the Milli-Q purification system (which will be described later). The concentration of the sulphuric acid was 0.5 M. All electrolyte solutions were purged of dissolved oxygen ( $\text{O}_2$ ) and carbon dioxide ( $\text{CO}_2$ ) by bubbling nitrogen ( $\text{N}_2$ ) through the electrochemical cell for 15-20 minutes. Catalyst (2.7 mg) was pressed onto a Pt mesh working electrode. This amount of catalyst had been found to give optimum electrochemical signal whilst avoiding problems of signal distortion associated with Ohmic drop [5]. After placing the platinum mesh with catalyst in the cell, the nitrogen gas line was then transferred to the gas inlet (gas inlet 2) to ensure that nitrogen is constantly flowing over the solution for the duration of the experiment. All connections were then checked and a cyclic voltammogram measurement was performed. The sweep rate during the experiment was either 10 or 50  $\text{mVs}^{-1}$  unless otherwise stated.

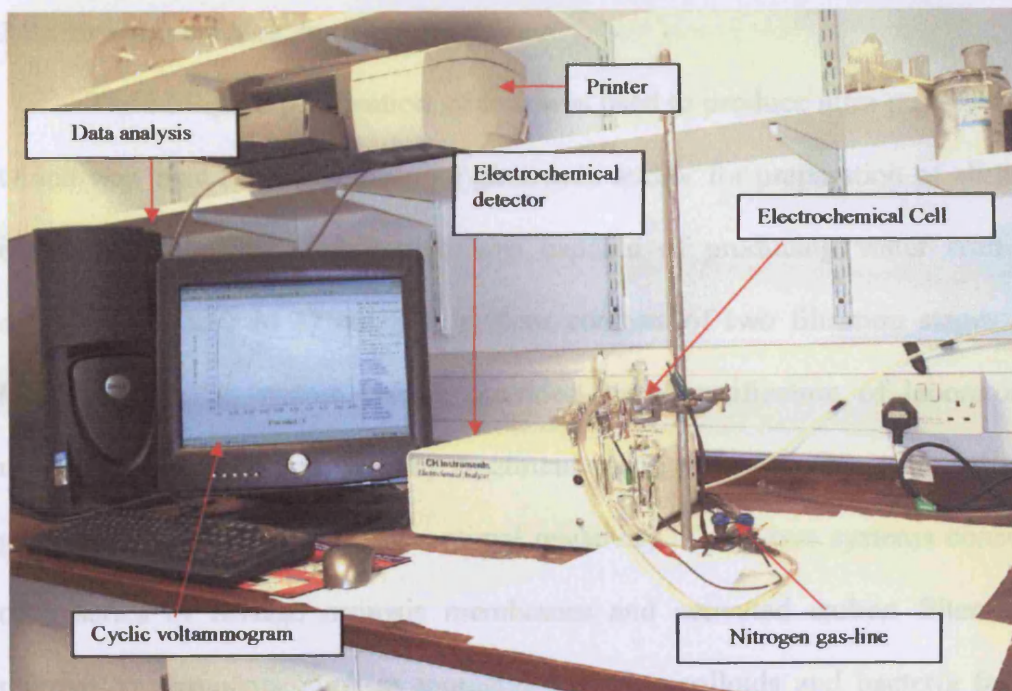


Figure 2.11 Equipment used for the collection of cyclic voltammogram.

A computer was used to obtain and analyse cyclic voltammograms as shown in Figure 2.11. The computer was connected to the electrochemical detector model 812 from CH instruments incorporating a potential wave generator.

## 2.9 Ultra-pure water purification system

The Millipore purification system was used to produce ultra-pure water, which was used either for cleaning glassware and/or for preparation of all the electrolyte solutions. The system was capable of producing water with a resistivity of 18.2 M  $\Omega$  cm. The system consists of two filtration stages: a Milli-RO 10 plus system, which provides initial purification of laboratory mains water supply followed by treatment using the Milli-Q system which gives the previously mentioned optimal resistivity. These two systems consist of a series of reverse osmosis membranes and activated carbon filters to remove contaminants, such as inorganic material, colloids and bacteria from the feed water. The purified water from the Milli-RO 10 plus was stored in a tank where it was connected to the Milli-Q system for further purification.

## 2.10 Distillation of ethyl pyruvate

The setup for a simple distillation is shown in Figure 2.12. A simple distillation apparatus consist of a boiling flask (round-bottom flask) attached to an adapter holding a thermometer (to determine the boiling temperature of the liquid). The adapter connects to a condenser into which cold water is constantly passed through. The condenser leads into a collection flask for the purified liquid. The procedure of distillation as follows:

- The apparatus was adjusted as in the Figure 2.12.
- Ethyl pyruvate (100 ml) was placed in the distilling flask.
- The distilling flask was connected to the condenser and covered with aluminium foil.

- The heating mantle was turned on and the temperature adjusted to 148-150°C (boiling point).
- The pure ethyl pyruvate was collected in the receiving flask.
- Once the liquid in the distilling flask was reduced to a minimum, and had darkened in color, the heating was stopped.
- The purified ethyl pyruvate was then kept in a closed sealed glass container in a refrigerator ready for use.

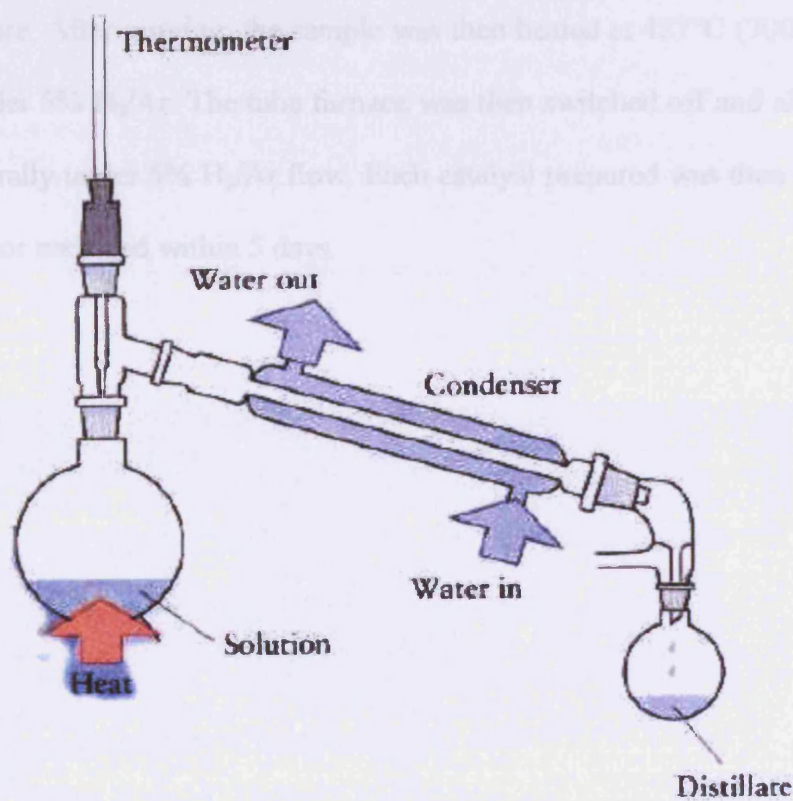


Figure 2.12 Apparatus used for distillation of ethyl pyruvate.

### 2.11 Apparatus used for catalyst reduction

Most catalyst samples of 5 % Pt/C (Johnson Matthey) and 5 % Pt/Al<sub>2</sub>O<sub>3</sub> (Engelhard) were pre-treated by reduction before use. The apparatus used for this purpose is shown in Figure 2.13. It utilised 5% H<sub>2</sub>/Ar (99.995%). Sintering was carried out as follows: 4.5 g of the catalyst sample were placed into a calcination boat as shown in Figure 2.14 and then this was placed into the Carbolite tube furnace (Pyrex) fitted with a quartz heating tube. Argon (99.995%) was passed over the catalyst for 30 minutes to remove air at room temperature. After purging, the sample was then heated at 427°C (700K), for 4 hours under 5% H<sub>2</sub>/Ar. The tube furnace was then switched off and allowed to cool naturally under 5% H<sub>2</sub>/Ar flow. Each catalyst prepared was then stored in a dessicator and used within 5 days.

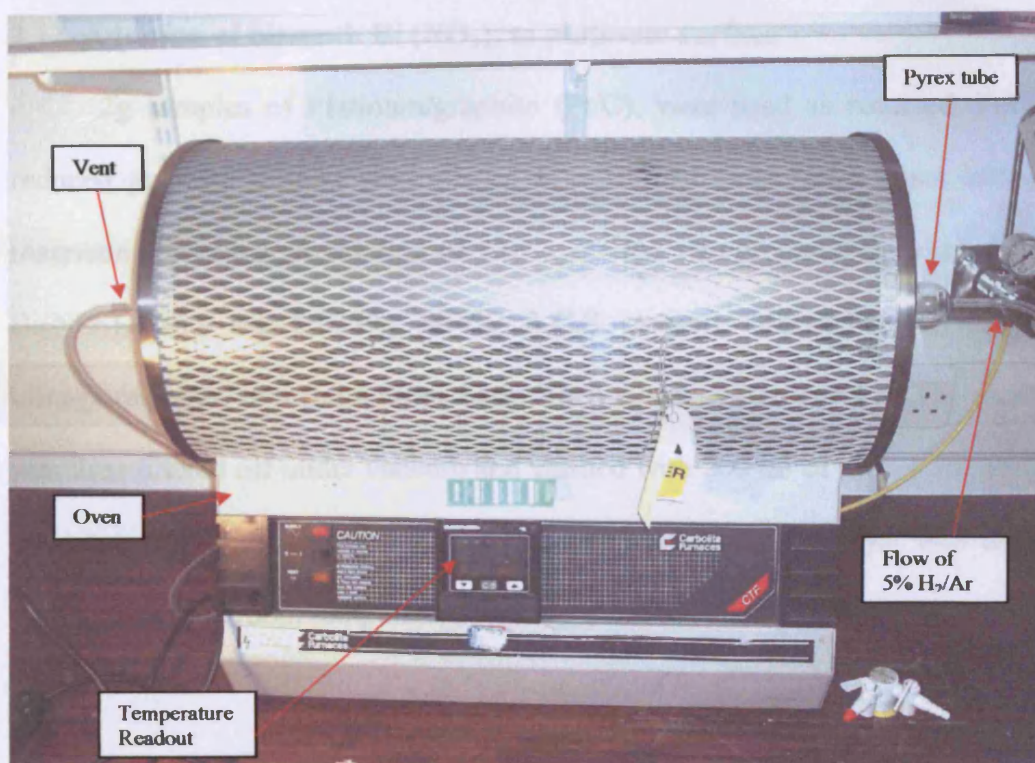


Figure 2.13 Furnace equipment used for catalyst reduction.

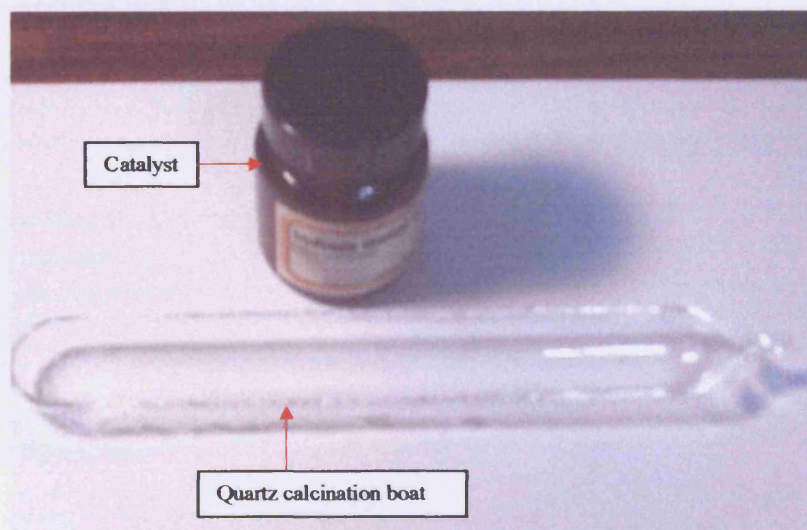


Figure 2.14 Calcination boat for use inside furnace.



### 2.12. Addition of bismuth $\text{Bi}(\text{NO}_3)_3$ to platinum surface

2g samples of Platinum/graphite (Pt/C), were used as received. Fully reduced graphite support were placed in a 100 ml evaporating basin with a magnetic stirrer bar. A solution of  $3.63 \times 10^{-4}$  M was prepared by addition of  $\text{Bi}(\text{NO}_3)_3$  (35.9 mg, 0.0359g; 98+%; A.C.S. reagent, Aldrich) in 250 ml of ultra-pure water, in a flat bottom flask. Then it was stirred for 4 h. The slurry was then filtered off under vacuum and washed with 200 ml of ultra-pure water three times to remove any remaining nitrate. Finally, the catalyst was dried under vacuum at room temperature overnight and used immediately [7].

## 2.13 Calculation of adsorbate coverage

### 2.13.1 Adsorbate coverage of Bi

The determination of surface coverage of adsorbate was calculated by measuring the integrated area below the voltammogram which represents the total charge  $Q$ . The total integrated area below the CV of the unmodified (clean) catalyst (Figure 2.15) can be considered as  $\theta_{\text{cat}} = 1$ . The decrease in the integrated area was attributed to adsorbate coverage. So the fractional adsorbate coverage can be determined by using the following equation:

$$\theta_{\text{ad}} = \frac{Q_{\text{clean}} - Q_{\text{mod}}}{Q_{\text{clean}}} \quad (2.3)$$

where:  $\theta_{\text{ad}}$  is the surface coverage of adsorbate in terms of  $\text{H}_{\text{UPD}}^*$  sites blocked,  $Q_{\text{clean}}$  is the total integrated charge for the clean catalyst, and  $Q_{\text{mod}}$  is the total integrated charge for the modified catalyst (Figure 2.16).  $\theta_{\text{ad}}$  may be considered as the fraction of free Pt sites remaining after adsorption.

$\text{H}_{\text{UPD}}^*$  = hydrogen under potential deposition corresponds to CV peaks in the range 0-0.3V (Pd/H). For polycrystalline Pt, this corresponds to 1 H atom per Pt site corresponding to a charge density of  $220 \mu\text{C cm}^{-2}$ .

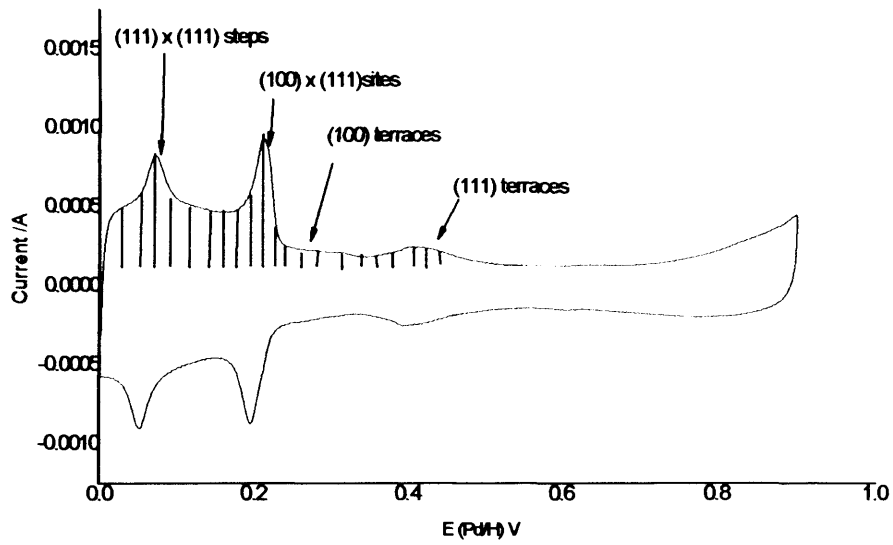


Figure 2.15 Voltammogram of the total integrated charge (shaded) for a clean Pt catalyst.

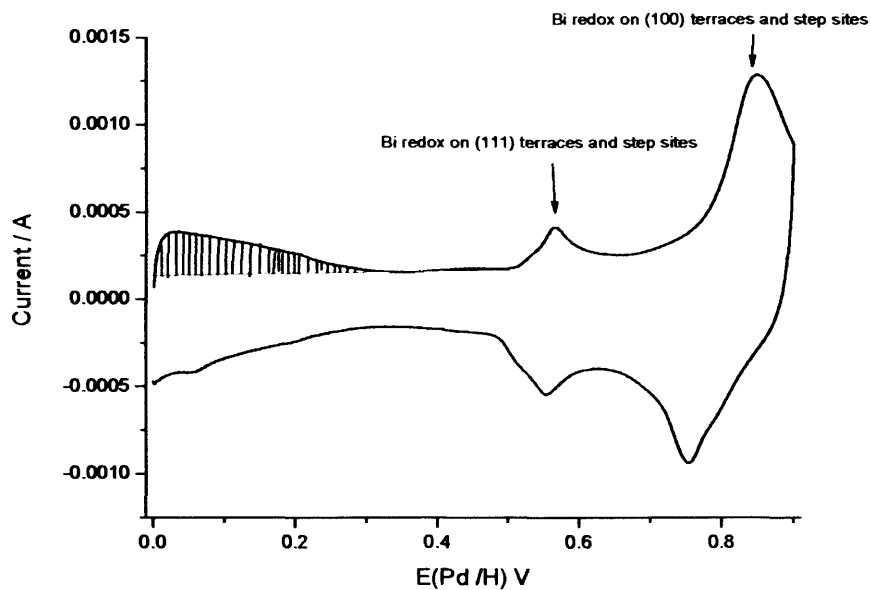


Figure 2.16 Voltammogram the total integrated charge (shaded) for bismuth modified Pt catalyst.

## 2.14 Reference

- [1] V. Mevellec, M. Christophe, J. Schulz, J.P. Rolland, and A. Roucoux, *J. Catal.*, **225** (2004) 1.
- [2] M. Bartók, G. Szollosi, K. Balázsik, T. Bartók, *J. Mol. Catal. A: Chem.*, **177** (2002) 299.
- [3] X. Li, K.P. R, P.B. Wells, and G.J. Hutchings, *Catal. Lett.*, **89** (2003) 3.
- [4] D. Watson, Ph.D. Thesis, Cardiff University, 2003.
- [5] H.-U. Blaser, H.P. Jalett and J. Wiehl, *J. Mol. Catal.*, **68** (1991) 215.
- [6] H.-U. Blaser, H.D. Jalett. M. Muller, S. Studer, *Catal. Today*, **37** (1997) 441.
- [7] N.F. Dummer, R. Jenkins, X. Li, S.M. Bawaked, P. McMorn, A. Burrows, C.J. Kiely, R.P.K. Wells, D.J. Willock, G. Hutchings, *J. Catal.*, **243** (2006) 165.

**CHAPTER THREE:  
RESULTS  
ENANTIOSELECTIVE  
HYDROGENATION OF ETHYL  
PYRUVATE CATALYSED BY  
PLATINUM ON GRAPHITE, SILICA  
AND ALUMINA**

### 3.1 Introduction

The primary objective of this chapter was to investigate the effect of reaction conditions, solvents, thermal annealing, the presence of CD-derivative and CN-derivative and sintering on the enantioselective hydrogenation of ethyl pyruvate, both distilled and non-distilled. Also, the effect of bismuth adsorption on the catalyst for title reaction was to be examined. In particular, the selective blocking of steps and chiral sites by Bi [1] and its effect on enantioselectivity was to be investigated in order to augment previous work by Albdulrahman [2].

### 3.2 Results of enantioselective hydrogenation of ethyl pyruvate (distilled and non-distilled) using Cinchonidine-derivative (CD-derivative) and Cinchonine-derivative (CN-derivative) modified 5% Pt/G

#### 3.2.1 Standard reaction on graphite

The activity of 5% Pt/G catalyst was investigated in the autoclave reactor with reference to standard enantioselective hydrogenation of ethyl pyruvate (etpy) and distilled etpy. Reactions were carried out over *in situ* modified 5% Pt/G at 25°C and at 35 bar H<sub>2</sub> in dichloromethane and acetic acid as the solvents. The corresponding enantiomeric excess (*ee*) and conversion of ethyl pyruvate for reactions carried out in dichloromethane is reported in Table 3.1. As received, the Pt/G catalyst with low amounts of CD-derivative exhibited a much lower enantiomeric excess than when using the same mass of CN-derivative (compare entries 1 and 2). In fact Figure 3.1 shows that, under reaction conditions, CN-derivative induced an optimum level of enantioselectivity at lowest loadings with negligible variation at high amounts of modifier. In contrast, the *ee* obtained using CD-derivative was strongly

correlated with modifier amount and actually reached an optimal, maximum *ee* at 20mg loading. All loadings of CD-derivative other than 20mg were found to be detrimental to optimal *ee*.

*Table 3.1 Comparison of enantiomeric excess (ee%) of etlac using CD-derivative and CN-derivative modified unsintered 5% Pt/G catalyst in dichloromethane.*

Entry	Amount of modifier (mg)	Enantiomeric excess (%) ( <i>R</i> )	Conversion (%)	Time Minutes	**Nominal rate mmol g <sup>-1</sup> h <sup>-1</sup>
1	1 CD-der	3.3	100	19*	5.26*
2	1 CN-der	29	87	125	0.69
4	2 CD-der	8	93.3	83	1.1
5	2 CN-der	26.2	100	167	0.59
6	10 CD-der	23	99	143	0.69
7	10 CN-der	30.2	100	73	1.36
8	20 CD-der	32	65	-	*
9	20 CN-der	31.1	100	67	1.49
10	30 CD-der	17	100	75	1.33
11	30 CN-der	30.4	96	68	1.41
12	40 CD-der	12.2	100	167	0.59
13	40 CN-der	30	100	158	0.63

\*Possible leak on system for this data.

\*\* Conversion/time

- N.A = Not available.

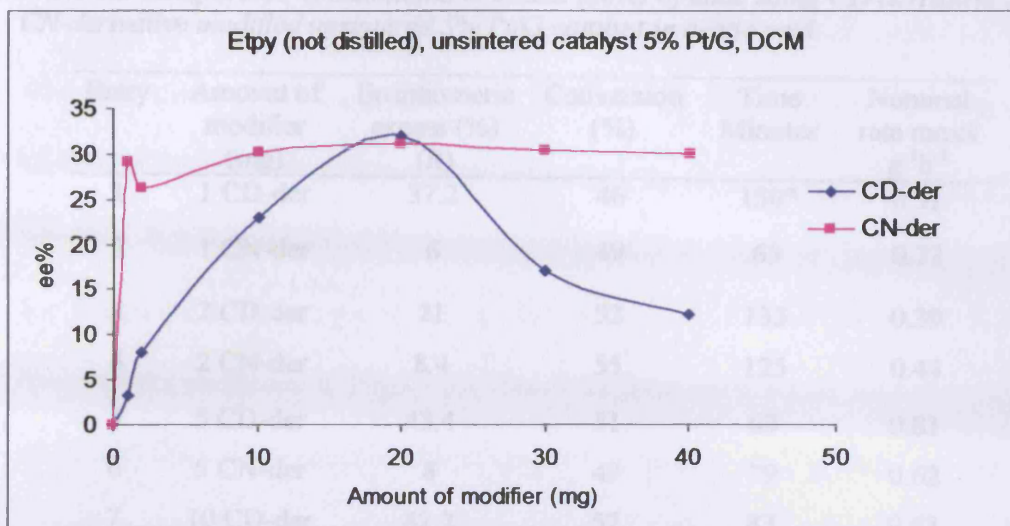


Figure 3.1 Enantiomeric excess in dichloromethane versus amount of modifier (mg). Unsintered 5% Pt/G catalyst.



*Table 3.2 Comparison of enantiomeric excess (ee%) of etlac using CD-derivative and CN-derivative modified unsintered 5% Pt/G catalyst in acetic acid.*

Entry	Amount of modifier (mg)	Enantiomeric excess (%) (R)	Conversion (%)	Time Minutes	Nominal rate mmol g <sup>-1</sup> h <sup>-1</sup>
1	1 CD-der	37.2	46	150*	0.31
2	1 CN-der	6	49	63	0.77
3	2 CD-der	21	52	133	0.39
4	2 CN-der	8.4	55	125	0.44
5	5 CD-der	43.4	51	63	0.81
6	5 CN-der	8	49	79	0.62
7	10 CD-der	42.2	52	83	0.63
8	10 CN-der	7	53	67	0.79
9	15 CD-der	43	56	96	0.58
10	15 CN-der	13	52	75	0.69
11	20 CD-der	27.3	86.3	67	1.3
12	20 CN-der	15	55	79	0.70
13	25 CD-der	47	63	67	0.94
14	25 CN-der	14	53	85	0.62
15	30 CD-der	39	52	83	0.62
16	30 CN-der	15	48	55*	0.87
17	35 CD-der	41	57	67	0.85
18	35 CN-der	17.1	59	88	0.67
19	40 CD-der	22	47	88	0.53
20	40 CN-der	14	43	75	0.57
21	50 CD-der	32	50	92	0.54
22	50 CN-der	20	56	63	0.89

\*- Possible leak on system for this data.

The choice of solvent has a marked effect on the rate of enantiomeric hydrogenation of carbonyl containing compounds [3]. The solvent (acetic acid) investigated was compared to dichloromethane under standard conditions. In

this case, acetic acid was used as a co-solvent, where 2.5 cm<sup>3</sup> of acetic acid was added to dichloromethane. Table 3.2 presents the effect of the solvents and modifiers on 5% Pt/G when dichloromethane and acetic acid were used together. It has been found that enantioselectivity depends on the solvent used for the reaction utilising different concentration of CD-derivative and differs from results presented in Figure 3.1. Solvents containing acetic acid were more effective than pure dichloromethane in affording *ee*, giving values of enantiomeric excess up to 47.0% (see Figure 3.2) using CD-derivative. For CN-derivative, the *ee* in this case reaches a maximum of only 20% (*R*). It has been proposed that a total or partial hydrogenolysis of the CN-derivative and CD-derivative under acidic reaction conditions to form CD and CN in solution takes place, according to work by Baiker and co-workers [4]. However, other workers disagree with this interpretation in that the expected hydrogenolysis products CD and CN could not be detected post-reaction [5-6].

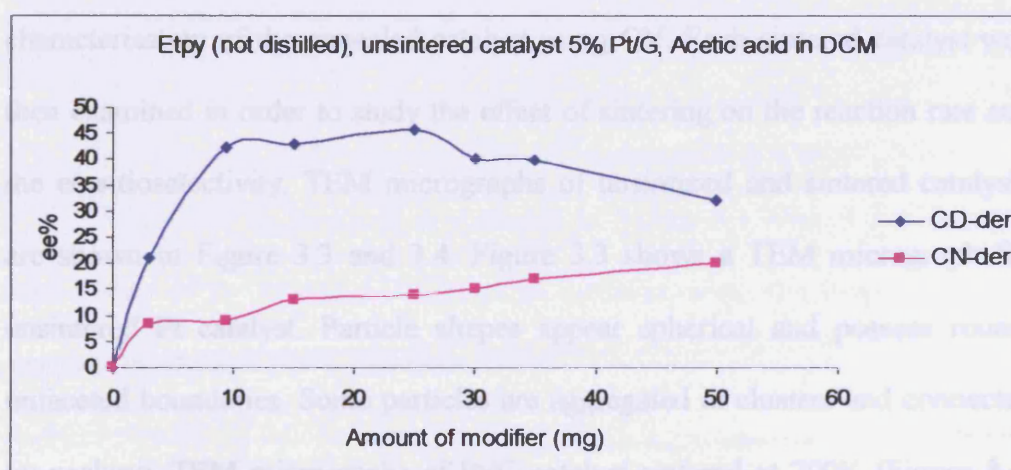


Figure 3.2 Enantiomeric excess versus amount of modifier (mg). Unsintered 5% Pt/G in acetic acid and dichloromethane mixture.

Hence, it is also noted that addition of acetic acid causes a reverse of the trend in *ee* found for dichloromethane with:

*ee* (DCM) using CN-derivative > *ee* (DCM) using CD-derivative

whereas:

*ee* (DCM/acetic acid) using CN-derivative < *ee* (DCM/acetic acid) using CD-derivative.

All modifiers give rise to an excess of *R*-etlac under present conditions in contrast to results expected using CN and CD.

### 3.2.2 Thermal annealing of Pt/G and its influence on enantioselective hydrogenation

The aim of this part of the investigation was to assess the effect of thermal annealing and sintering of Pt/G on the title reaction. Particular emphasis was placed on how changes in particle morphology would influence enantioselectivity. During the investigation, 5% Pt/G catalyst was annealed under 5% H<sub>2</sub>/Ar at 700K as described in Section 2.11 followed by characterisation of the annealed catalyst using CV. Each sintered catalyst was then examined in order to study the effect of sintering on the reaction rate and the enantioselectivity. TEM micrographs of unsintered and sintered catalysts are shown in Figure 3.3 and 3.4. Figure 3.3 shows a TEM micrograph for unsintered Pt catalyst. Particle shapes appear spherical and possess round, unfaceted boundaries. Some particles are aggregated in clusters and connected by necking. TEM micrographs of Pt/G catalyst sintered at 700K (Figure 3.4) show an increase in particles size and faceting. Hexagonal forms are orderly in shape and most particles are rather dispersed.

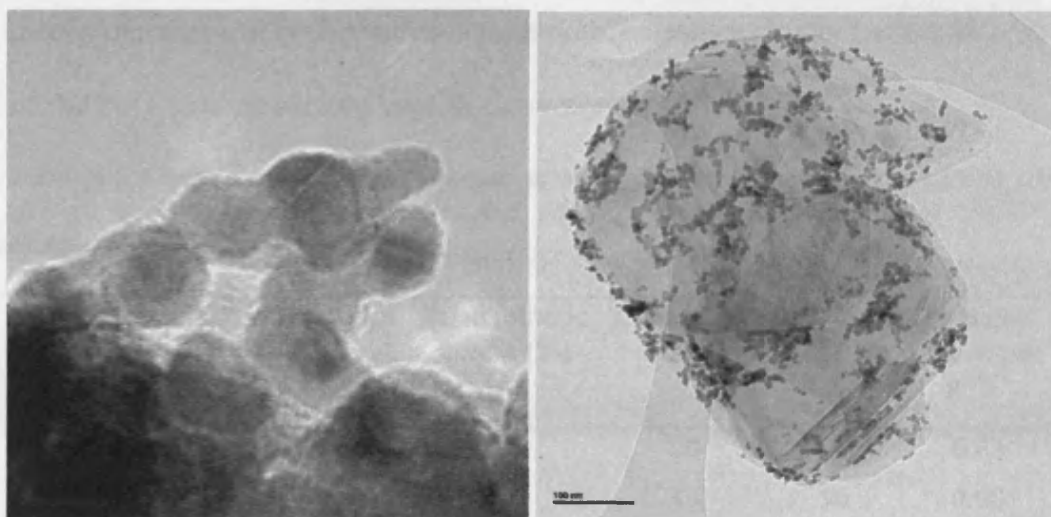


Figure 3.3 TEM micrographs of unsintered Pt/G catalyst.

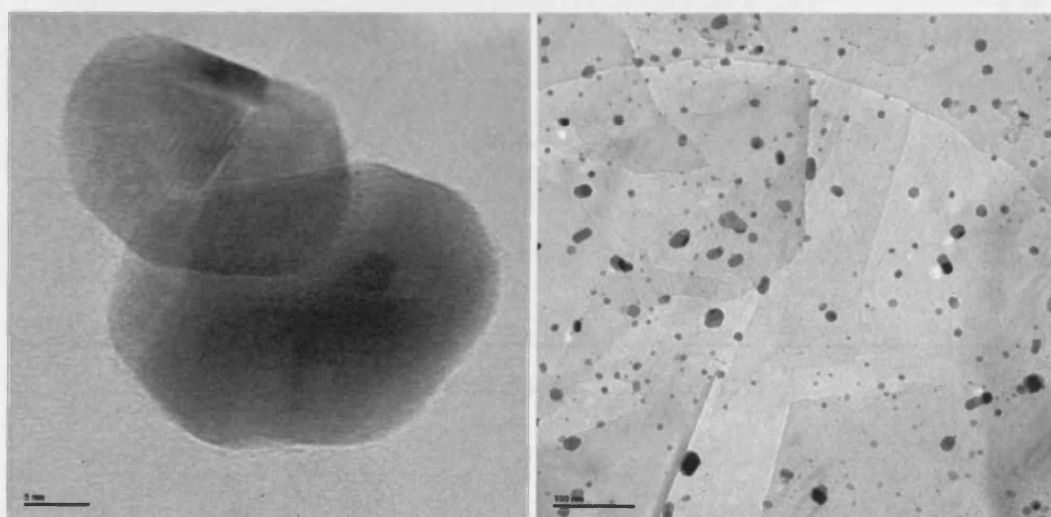


Figure 3.4 TEM micrographs of Pt/G catalyst sintered at 700K.

In contrast to trends in  $ee$  reported in Figure 3.1, Figure 3.5 shows a suppression of  $ee$  for the CD-derivative modifier when the Pt/G catalyst is sintered at 700K. The behaviour of the CN-derivative modifier is largely unchanged with an optimal  $ee$  of around 26% being reached at 10 mg loading, similar to what happens using the unsintered catalyst. Hence, it appears that in

dichloromethane, CD-derivative is remarkably sensitive to the surface structure of the Pt/G catalyst surface but CN-derivative is not.

Table 3.3 Enantiomeric excess observed in ethyl pyruvate hydrogenation using CD-derivative and CN-derivative modified 5% Pt/G catalyst sintered at 700K in dichloromethane.

Entry	Amount of modifiers (mg)	Solvent (ml)	Enantiomeric excess (%) ( <i>R</i> )	Conversion (%)	Time Minutes	Nominal rate mmol g <sup>-1</sup> h <sup>-1</sup>
1	5 CD-der	DCM	9.3	50	79	0.63
2	5 CN-der	DCM	25	49	50	0.98
3	10 CD-der	DCM	6.2	84	92	0.91
4	10 CN-der	DCM	26	48	46	1.04
5	15 CD-der	DCM	5.4	51	50	1.02
6	15 CN-der	DCM	24	66	63	1.04
7	30 CD-der	DCM	5.3	41	63	0.65
8	30 CN-der	DCM	24.4	71.4	67	1.07

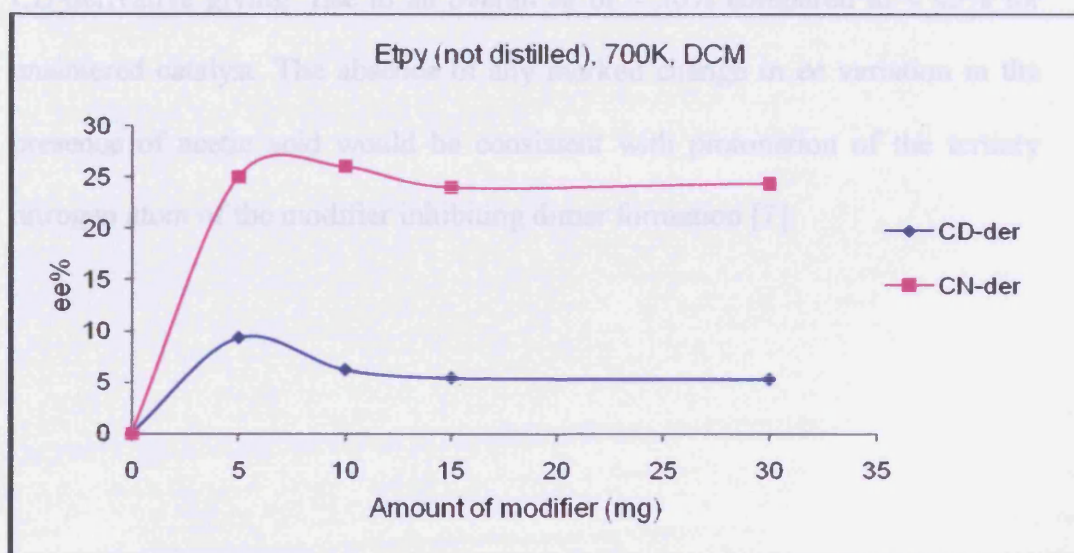


Figure 3.5 Enantiomeric excess in dichloromethane versus amount of modifier (mg). Pt/G catalyst sintered at 700K.

### 3.2.3 Enantioselective hydrogenation of distilled ethyl pyruvate over CD-derivative and CN-derivative-modified 5% Pt/G catalyst sintered at 700K in dichloromethane and acetic acid

When distilled etpy was used as substrate in dichloromethane instead of as-received etpy, differences in enantioselectivity were immediately observed for Pt/G catalysts sintered at 700K in hydrogen (Figure 3.6). The *ee* in *R*-etlac was almost the same irrespective of which modifier, CD-derivative or CN-derivative, was used. This means that using distilled etpy leads to a lowering of *ee* in the case of CN-derivative from 25% to 20% and an increase in *ee* from 9% to 19% for CD-der on 5% Pt/G in dichloromethane. This suggests that an impurity within the etpy is having a significant influence on overall *ee*. By impurity it could of course also mean a dimer of etpy [2]. In contrast, in the presence of acetic acid the 700K sintered Pt/G catalyst gave similar trends to those seen in Figure 3.2 for the unsintered catalyst using undistilled etpy, with CD-derivative giving rise to an overall *ee* of  $\approx 30\%$  compared to  $\approx 45\%$  for unsintered catalyst. The absence of any marked change in *ee* variation in the presence of acetic acid would be consistent with protonation of the tertiary nitrogen atom of the modifier inhibiting dimer formation [7].

*Summary table of ees observed in ethyl pyruvate (not distilled and distilled) hydrogenation using CD-derivative and CN-derivative modified unsintered 5% Pt/G catalyst and sintered at 700K in dichloromethane.*

Entry	Modifiers	ee (%) (R) non distilled etpy	ee (%) (R) distilled etpy
1	CN-der	25	20
2	CD-der	9	19

*Table 3.4 Enantiomeric excess observed in distilled ethyl pyruvate hydrogenation using CD-derivative and CN-derivative modified 5% Pt/G catalyst sintered at 700K in dichloromethane and acetic acid.*

Entry	Amount of modifiers (mg)	Solvent (ml)	Enantiomeric excess (%) (R)	Conversion (%)	Time Minutes	Nominal rate mmol g <sup>-1</sup> h <sup>-1</sup>
1	5 CD-der	DCM	19	7.3	71	0.10
2	5 CD-der	Acetic acid	30	11.2	50	0.22
3	30 CD-der	DCM	21	13	56	0.23
4	30 CD-der	Acetic acid	29.3	43.4	92	0.47
5	5 CN-der	DCM	16	8	-	-
6	5 CN-der	Acetic acid	3	18	54	0.33
7	30 CN-der	DCM	22	8	25*	0.32
8	30 CN-der	Acetic acid	9.2	18	33	0.54

\*- Possible leak on system for this data.

- N.A = Not available.

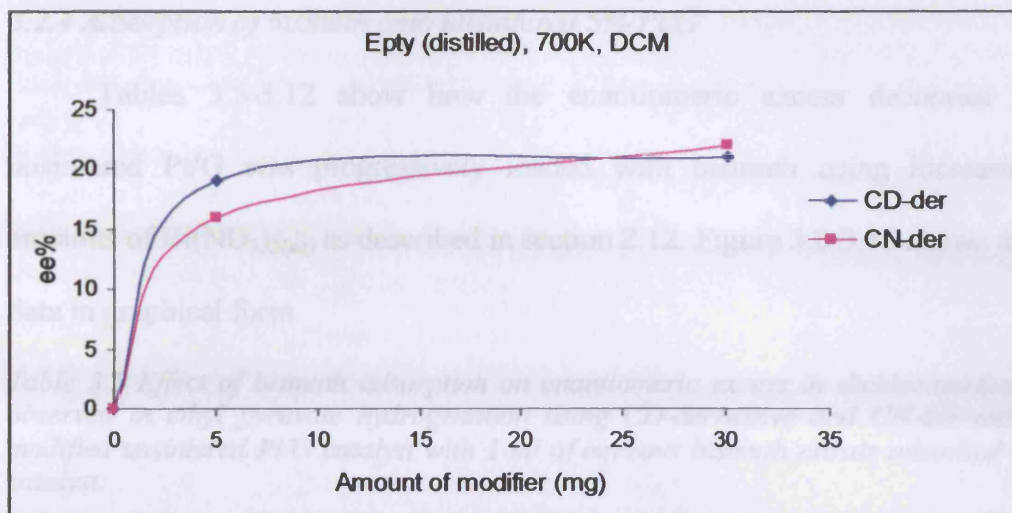


Figure 3.6 Enantiomeric excess in dichloromethane versus amount of modifier (mg). 5% Pt/G catalyst sintered at 700K.

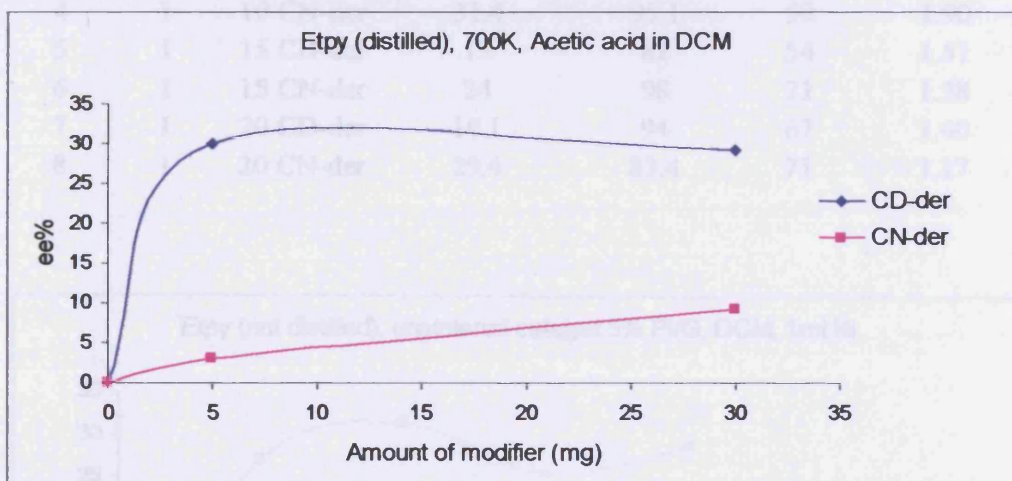


Figure 3.7 Enantiomeric excess in acetic acid versus amount of modifier (mg). Pt/G catalyst sintered at 700K.



### 3.2.4 Adsorption of bismuth onto unsintered 5% Pt/G

Tables 3.5-3.12 show how the enantiomeric excess decreases as unsintered Pt/G was progressively loaded with bismuth using increasing amounts of  $\text{Bi}(\text{NO}_3)_3(\text{aq})$  as described in section 2.12. Figure 3.8-3.15 shows this data in graphical form.

*Table 3.5 Effect of bismuth adsorption on enantiomeric excess in dichloromethane observed in ethyl pyruvate hydrogenation using CD-derivative and CN-derivative modified unsintered Pt/G catalyst with 1 ml of aqueous bismuth nitrate adsorbed on catalyst.*

Entry	Dosing volume $\text{Bi}/\text{cm}^3$	Amount of modifiers (mg)	Enantiomeric excess (%) ( <i>R</i> )	Conversion (%)	Time Minutes	Nominal rate $\text{mmol g}^{-1}\text{h}^{-1}$
1	1	5 CD-der	21.4	87	100	0.87
2	1	5 CN-der	27	90	54	1.67
3	1	10 CD-der	14.2	98	117	0.84
4	1	10 CN-der	31.4	95.1	50	1.90
5	1	15 CD-der	13	82	54	1.51
6	1	15 CN-der	24	98	71	1.38
7	1	20 CD-der	10.1	94	67	1.40
8	1	20 CN-der	29.4	83.4	71	1.17

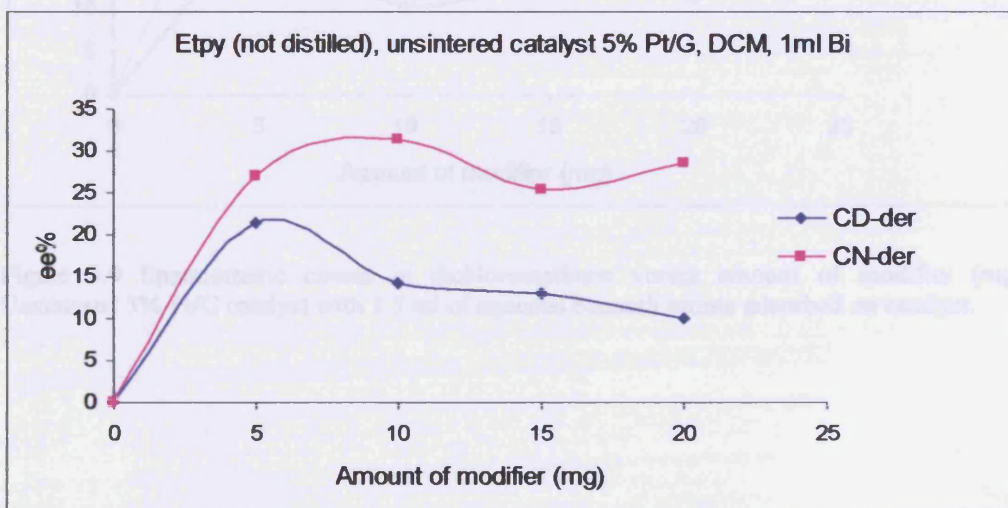


Figure 3.8 Enantiomeric excess in dichloromethane versus amount of modifier (mg). Unsintered 5% Pt/G catalyst with 1 ml of aqueous bismuth nitrate adsorbed on catalyst.

Table 3.6 Effect of bismuth adsorption on enantiomeric excess in dichloromethane observed in ethyl pyruvate hydrogenation using CD-derivative and CN-derivative modified unsintered Pt/G catalyst with 1.5 ml of aqueous bismuth nitrate adsorbed on catalyst.

Entry	Dosing volume Bi/cm <sup>3</sup>	Amount of modifiers (mg)	Enantiomeric excess (%) (R)	Conversion (%)	Time Minutes	Nominal rate mmol g <sup>-1</sup> h <sup>-1</sup>
1	1.5	5 CD-der	17.3	95	67	1.41
2	1.5	5 CN-der	31	91.4	42	2.17
3	1.5	10 CD-der	10.2	94.2	102	0.92
4	1.5	10 CN-der	31.2	93	42	2.21
5	1.5	15 CD-der	13.1	93.3	50	1.86
5	1.5	15 CN-der	33	89.3	43	2.07
6	1.5	20 CD-der	11.2	95.1	47	2.02
7	1.5	20 CN-der	32.4	93	-	-

- N.A = Not available.

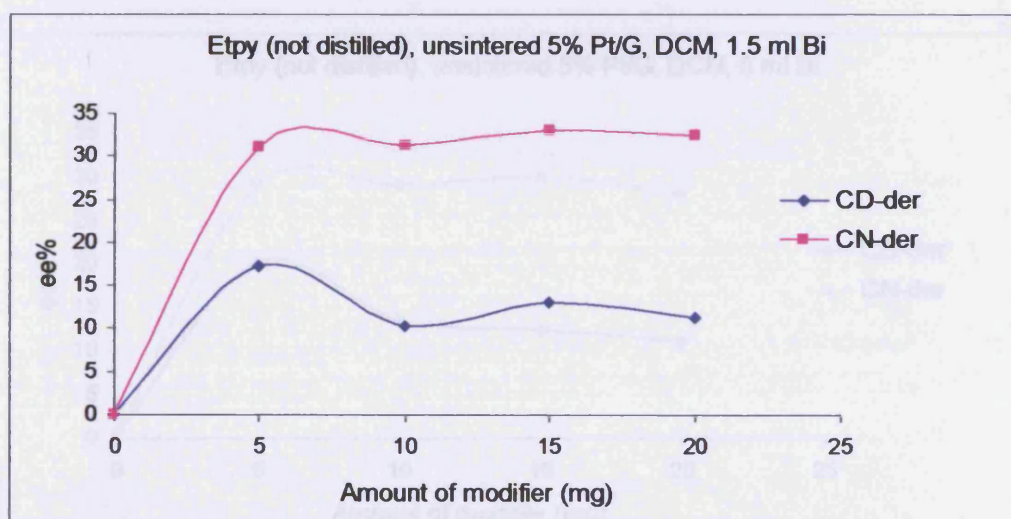


Figure 3.9 Enantiomeric excess in dichloromethane versus amount of modifier (mg). Unsintered 5% Pt/G catalyst with 1.5 ml of aqueous bismuth nitrate adsorbed on catalyst.

Table 3.7 Effect of bismuth adsorption on enantiomeric excess in dichloromethane observed in ethyl pyruvate hydrogenation using CD-derivative and CN-derivative modified unsintered Pt/G catalyst with 5 ml of aqueous bismuth nitrate adsorbed on catalyst.

Entry	Dosing volume Bi/cm <sup>3</sup>	Amount of modifiers (mg)	Enantiomeric excess (%) (R)	Conversion (%)	Time Minutes	Nominal rate mmol g <sup>-1</sup> h <sup>-1</sup>
1	5	5 CD-der	20.2	91.4	57	1.60
2	5	5 CN-der	29	91	58	1.57
3	5	10 CD-der	13.4	99	-	-
4	5	10 CN-der	29.1	90.4	57	1.58
5	5	15 CD-der	12.4	99	77	1.28
6	5	15 CN-der	30	95	58	1.64
7	5	20 CD-der	11	96.3	58	1.66
8	5	20 CN-der	28	95.1	-	-

- N.A = Not available.

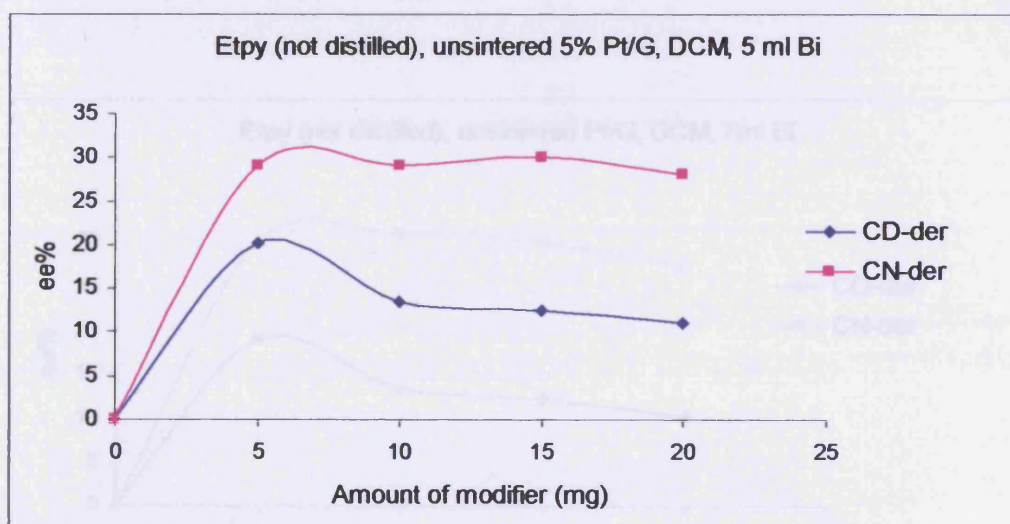


Figure 3.10 Enantiomeric excess in dichloromethane versus amount of modifier (mg). Unsintered 5% Pt/G catalyst with 5 ml of aqueous bismuth nitrate adsorbed on catalyst.

Table 3.8 Effect of bismuth adsorption on enantiomeric excess in dichloromethane observed in ethyl pyruvate hydrogenation using CD-derivative and CN-derivative modified unsintered Pt/G catalyst with 7 ml of aqueous bismuth nitrate adsorbed on catalyst.

Entry	Dosing volume Bi/cm <sup>3</sup>	Amount of modifiers (mg)	Enantiomeric excess (%) (R)	Conversion (%)	Time Minutes	Nominal rate mmol g <sup>-1</sup> h <sup>-1</sup>
1	7	5 CD-der	19	71.1	67	1.06
2	7	5 CN-der	30	93.1	58	1.60
3	7	10 CD-der	13.4	92.2	54	1.70
4	7	10 CN-der	31	92	50	1.84
5	7	15 CD-der	12.3	95.1	83	1.14
6	7	15 CN-der	30	95.2	108	0.88
7	7	20 CD-der	10.3	95	67	1.41
8	7	20 CN-der	27.2	89	54	1.64

N.A. Not available

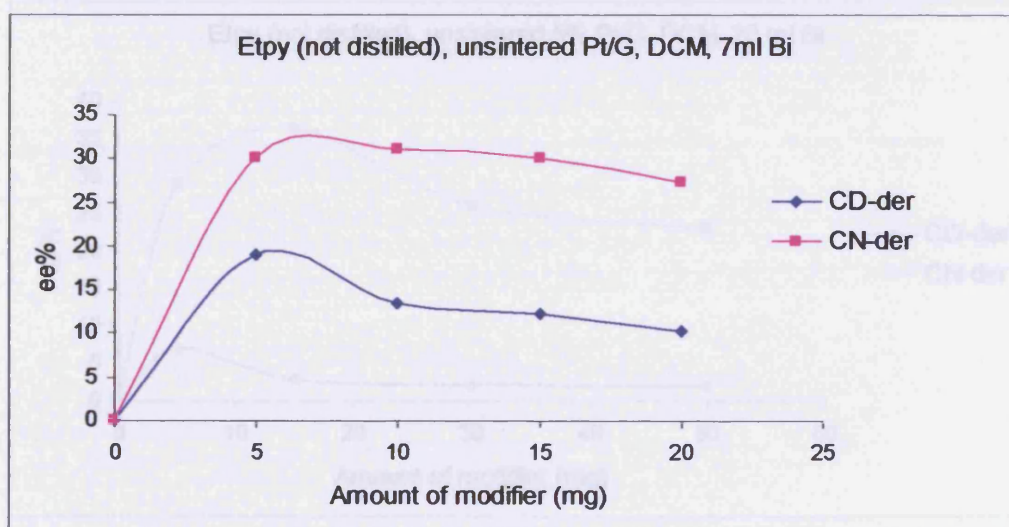
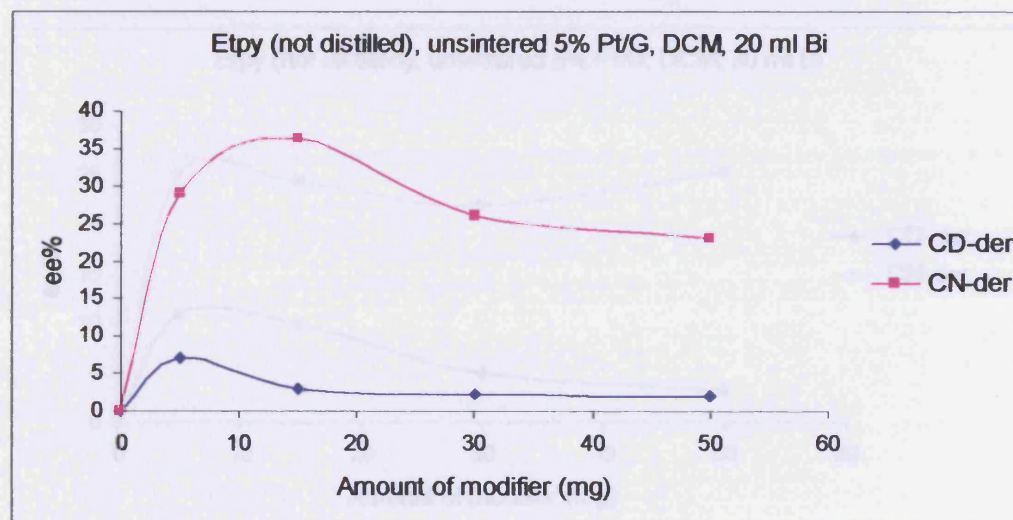


Figure 3.11 Enantiomeric excess in dichloromethane versus amount of modifier (mg). Unsintered 5% Pt/G catalyst with 7 ml of aqueous bismuth nitrate adsorbed on catalyst.

**Table 3.9** Effect of bismuth adsorption on enantiomeric excess in dichloromethane observed in ethyl pyruvate hydrogenation using CD-derivative and CN-derivative modified unsintered Pt/G catalyst with 20 ml of aqueous bismuth nitrate adsorbed on catalyst.

Entry	Dosing volume Bi/cm <sup>3</sup>	Amount of modifiers (mg)	Enantiomeric excess (%) ( <i>R</i> )	Conversion (%)	Time Minutes	Nominal rate mmol g <sup>-1</sup> h <sup>-1</sup>
1	20	5 CD-der	7.1	77	83	0.93
2	20	5 CN-der	29.1	32	50	0.64
3	20	15 CD-der	3	85.4	150	0.57
4	20	15 CN-der	36.4	17.3	25	0.69
5	20	30 CD-der	2.4	92.2	144	0.64
6	20	30 CN-der	26	6.3	-	-
7	20	50 CD-der	2	77	27	2.85
8	20	50 CN-der	23	4	121	0.03

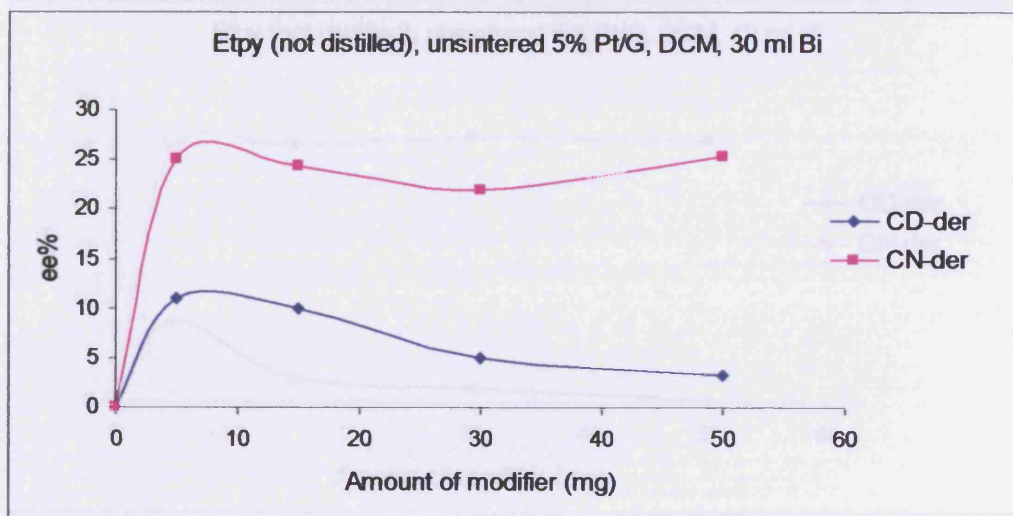
- N.A = Not available.



**Figure 3.12** Enantiomeric excess in dichloromethane versus amount of modifier (mg). Unsintered 5% Pt/G catalyst with 20 ml of aqueous bismuth nitrate adsorbed on catalyst.

**Table 3.10** Effect of bismuth adsorption on enantiomeric excess in dichloromethane observed in ethyl pyruvate hydrogenation using CD-derivative and CN-derivative modified unsintered Pt/G catalyst with 30 ml of aqueous bismuth nitrate adsorbed on catalyst.

Entry	Dosing volume Bi/cm <sup>3</sup>	Amount of modifiers (mg)	Enantiomeric excess (%) (R)	Conversion (%)	Time Minutes	Nominal rate mmol g <sup>-1</sup> h <sup>-1</sup>
1	30	5 CD-der	11	88	71	1.24
2	30	5 CN-der	25	96	96	1.00
3	30	15 CD-der	10	100	83	1.20
4	30	15 CN-der	24.3	98	75	1.31
5	30	30 CD-der	5	100	140	0.71
6	30	30 CN-der	22	91	42	2.17
7	30	50 CD-der	3.2	99.2	75	1.33
8	30	50 CN-der	25.3	92	75	1.23



**Figure 3.13** Enantiomeric excess in dichloromethane versus amount of modifier (mg). Unsintered 5% Pt/G catalyst with 30 ml of aqueous bismuth nitrate adsorbed on catalyst.

Table 3.11 Effect of bismuth adsorption on enantiomeric excess in dichloromethane observed in ethyl pyruvate hydrogenation using CD-derivative and CN-derivative modified unsintered Pt/G catalyst with 40 ml of aqueous bismuth nitrate adsorbed on catalyst.

Entry	Dosing volume Bi/cm <sup>3</sup>	Amount of modifiers (mg)	Enantiomeric excess (%) (R)	Conversion (%)	Time Minutes	Nominal rate mmol g <sup>-1</sup> h <sup>-1</sup>
1	40	5CD-der	8	99.4	77	1.29
2	40	5CN-der	25	97	58	1.67
3	40	15CD-der	2.4	96	42	2.29
4	40	15CN-der	25.4	98	63	1.55
5	40	30CD-der	1.3	99	54	1.83
6	40	30CN-der	26.3	98.3	47	2.09
7	40	50CD-der	0.13	100	63	1.59
8	40	50CN-der	26	98	42	233

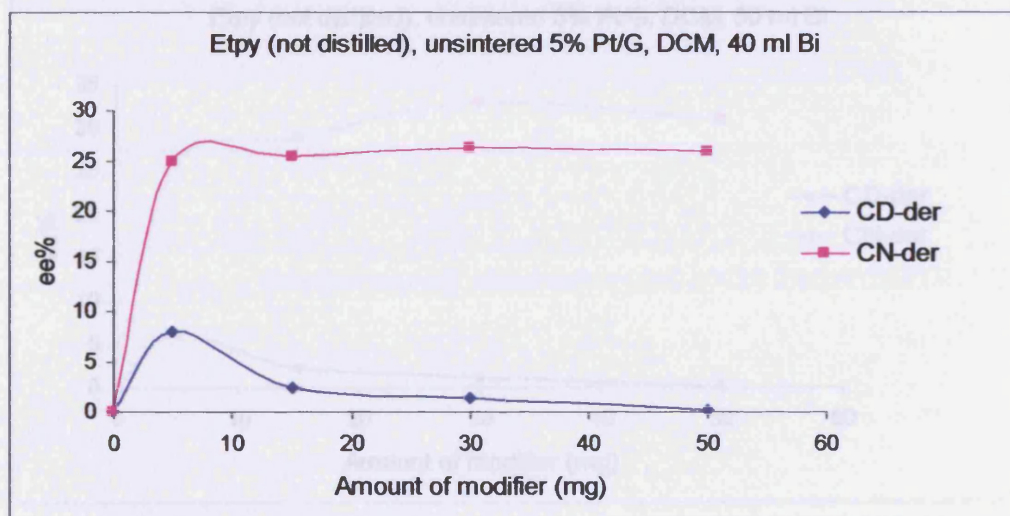
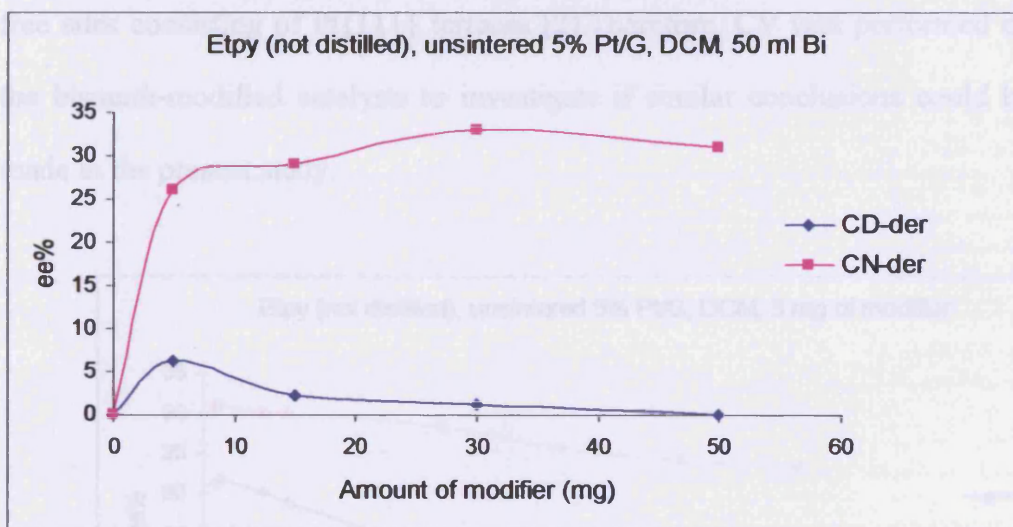


Figure 3.14 Enantiomeric excess in dichloromethane versus amount of modifier (mg). Unsintered 5% Pt/G catalyst with 40 ml of aqueous bismuth nitrate adsorbed on catalyst.

Some general trends may be observed from inspection of Figures 3.8-3.15. The addition of Bi<sup>3+</sup> to the unsintered catalyst has brought about a gradual decrease in ee using both CD-derivative and CN-derivative as modifiers.

**Table 3.12** Effect of bismuth adsorption on enantiomeric excess in dichloromethane observed in ethyl pyruvate hydrogenation using CD-derivative and CN-derivative modified unsintered Pt/G catalyst with 50 ml of aqueous bismuth nitrate adsorbed on catalyst.

Entry	Dosing volume Bi/cm <sup>3</sup>	Amount of modifiers (mg)	Enantiomeric excess (%) (R)	Conversion (%)	Time Minutes	Nominal rate mmol g <sup>-1</sup> h <sup>-1</sup>
1	50	5 CD-der	6.2	95	38	2.50
2	50	5 CN-der	26	96	58	1.66
3	50	15 CD-der	2.3	97.1	46	2.11
4	50	15 CN-der	29	88	42	2.10
5	50	30 CD-der	1.2	95.4	58	1.64
6	50	30 CN-der	33	100	58	1.72
7	50	50 CD-der	0.05	96	54	1.78
8	50	50 CN-der	31	98.1	39	2.52



**Figure 3.15** Enantiomeric excess in dichloromethane versus amount of modifier (mg). Unsintered 5% Pt/G catalyst with 50 ml of aqueous bismuth nitrate adsorbed on catalyst.

Some general trends may be observed from inspection of Figures 3.8-3.15. The addition of Bi to the unsintered catalyst has brought about a gradual decrease in *ee* using both CD-derivative and CN-derivative as modifiers



although CN-derivative always gives rise to the greatest value of *ee* and both modifiers continue to provide an excess of the *R*-enantiomer. In order to illustrate this effect, the variation in *ee* for both CD-derivative and CN-derivative in dichloromethane as a function of  $\text{Bi}(\text{NO}_3)_3(\text{aq})$  dosing volume at fixed modifier amount (5 mg and 15mg) is shown in Figures 3.16 and 3.16a. This data seems to suggest a loss of *ee* as Bi surface coverage increases. It will be recalled that this behaviour was also observed for Bi-modified 5% Pt/G catalyst using CD as chiral surface modifier [2]. In reference [2], CV was used to correlate Bi site adsorption with change in *ee*. In particular, the initial decrease in *ee* (and increase in rate) corresponded to blocking of defect sites such as steps and kinks whereas a lower overall *ee* was obtained from bismuth-free sites consisting of Pt{111} terraces [2]. Therefore, CV was performed on the bismuth-modified catalysts to investigate if similar conclusions could be made in the present study.

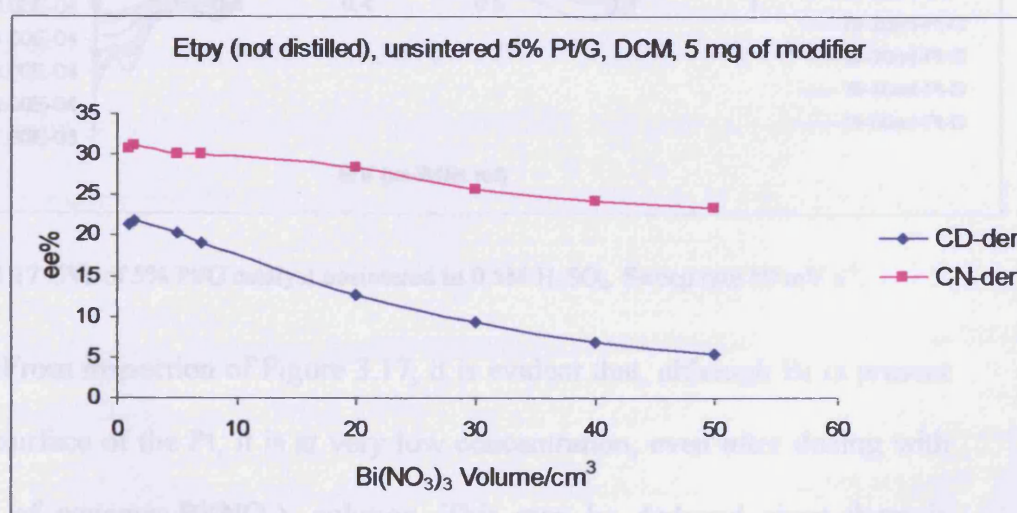


Figure 3.16 Adsorption of Bi on unsintered 5% Pt/G catalyst at 5 mg of modifier with 1, 1.5, 5, 7, 20, 30, 40 and 50 ml of aqueous bismuth nitrate adsorbed on catalyst.

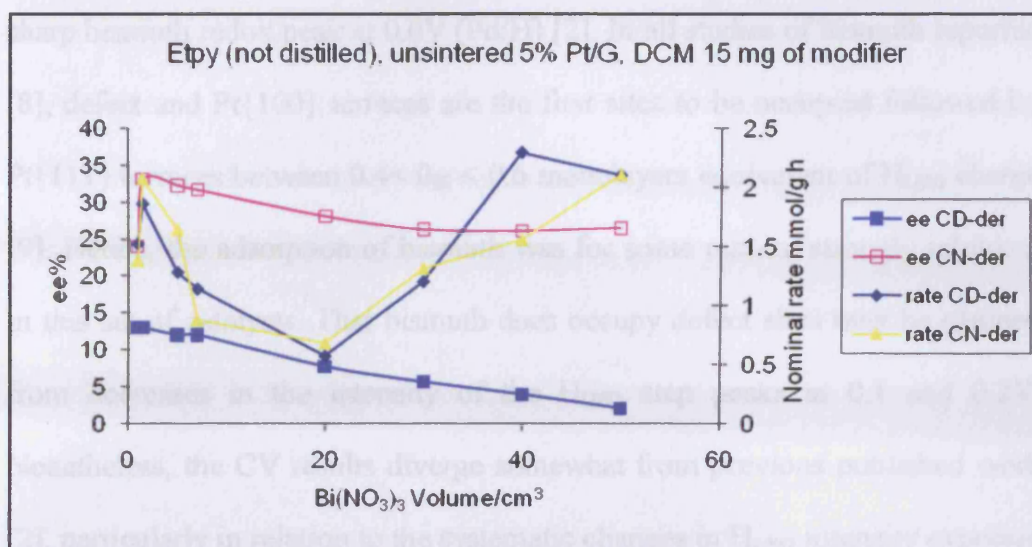


Figure 3.16 Hydrogenation of ethyl pyruvate. Nominal rate and enantiomeric excess versus the modifier concentration (unsintered 5% Pt/G catalyst in DCM).

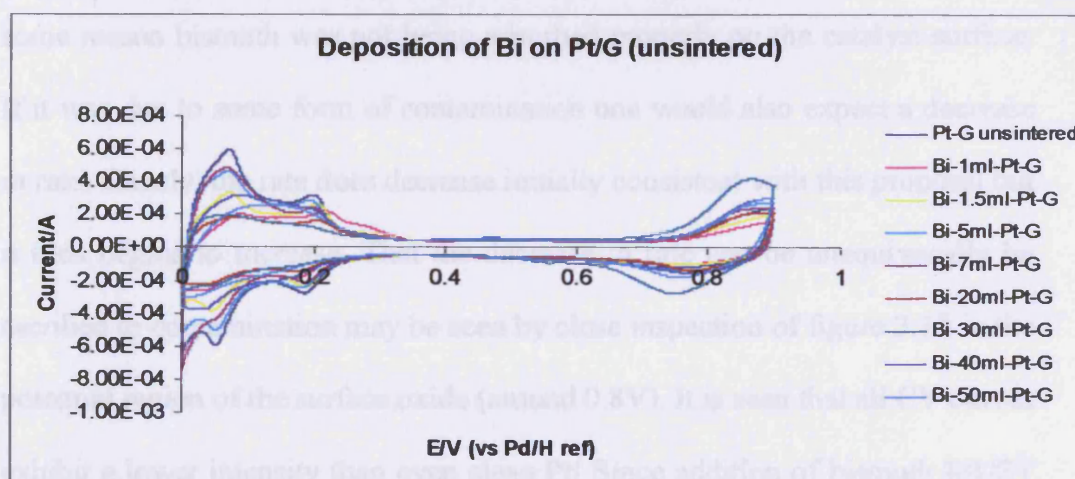


Figure 3.17 CVs of 5% Pt/G catalyst unsintered in 0.5M  $\text{H}_2\text{SO}_4$ . Sweep rate  $50 \text{ mV s}^{-1}$ .

From inspection of Figure 3.17, it is evident that, although Bi is present at the surface of the Pt, it is at very low concentration, even after dosing with 50 ml of aqueous  $\text{Bi}(\text{NO}_3)_3$  solution. This may be deduced since there is absolutely no sign of Bi adsorption at Pt{111} sites, as would be signified by a

sharp bismuth redox peak at 0.6V (Pd/H) [2]. In all studies of bismuth reported [8], defect and Pt{100} terraces are the first sites to be occupied followed by Pt{111} terraces between  $0.4 < \theta_{\text{Bi}} < 0.6$  monolayers equivalent of  $H_{\text{UPD}}$  charge [9]. Hence, the adsorption of bismuth was for some reason, strongly inhibited in this set of catalysts. That bismuth does occupy defect sites may be gleaned from decreases in the intensity of the  $H_{\text{UPD}}$  step peaks at 0.1 and 0.2V. Nonetheless, the CV results diverge somewhat from previous published work [2], particularly in relation to the systematic changes in  $H_{\text{UPD}}$  intensity expected as a function of Bi loading and corresponding increases in Bi-oxide features at 0.85V. Hence, it is possible that although measurements including CV and hydrogenation of etpy have been undertaken, the CV results indicate that for some reason bismuth was not being adsorbed properly on the catalyst surface. If it was due to some form of contamination one would also expect a decrease in rate. Clearly, the rate does decrease initially consistent with this proposal but it then begins to increase. That the decrease in rate can be unequivocally be ascribed to contamination may be seen by close inspection of figure 3.17 in the potential region of the surface oxide (around 0.8V). It is seen that all CV curves exhibit a lower intensity than even clean Pt! Since addition of bismuth MUST increase intensity over and above Pt contribution in this potential range, this means that the Pt in these data is contaminated by adatoms other than bismuth. The increase in rate as > 20ml of Bi solution is added to the Pt would be consistent with small amounts of Bi being eventually adsorbed and hence a corresponding increase in rate is observed. No evidence for multilayer Bi was

found in figure 3.17 since this would give rise to electrochemical stripping peaks between 0V and 0.15V (Pd/H). Therefore, in order to achieve a proper, systematic variation (and to find agreement with previous studies) the Bi adsorbed on unsintered Pt catalysts were discarded and a fresh series of Bi-modified catalysts were prepared in which the unsintered 5% Pt/G catalyst was heated at 700K in hydrogen in order to clean the surface completely before dosing Bi.

### 3.2.6 Adsorption of bismuth onto 5% Pt/G sintered at 700K

Table 3.13-3.20 shows the effect of bismuth loading on *ee* and conversion for etpy hydrogenation in dichloromethane using CD-derivative and CN-derivative as modifiers. Figure 3.18-3.25 shows graphically the changes in *ee* as a function of both modifier amount and bismuth dosing. In contrast to the previous data for the unsintered catalyst, significant changes in the enantioselective excess are observed as bismuth loading is increased. The most striking observation is the inversion of *ee* as a function of bismuth loading for the CD-derivative modifier. Conversions are observed to be rather low, probably due to the decreasing amount of free Pt as bismuth is dosed onto the catalyst surface. In Figure 3.26, the change in *ee* using CN-derivative and CD-derivative as modifiers is plotted for a constant modifier loading of 30mg and increasing amounts of bismuth. In Figure 3.27, the same plot is shown but with the variation altered for 5, 15 and 30 mg of modifier.

Table 3.13 Effect of Bismuth adsorption on enantiomeric excess in dichloromethane observed in ethyl pyruvate hydrogenation using CD-derivative and CN-derivative modified 5% Pt/G catalyst sintered at 700K pre-treated with 1 ml of aqueous bismuth nitrate adsorbed on catalyst.

Entry	Dosing volume Bi/cm <sup>3</sup>	Amount of modifiers (mg)	Enantiomeric excess (%) ( <i>R</i> )	Conversion (%)	Time Minutes	Nominal rate mmol g <sup>-1</sup> h <sup>-1</sup>
1	1	5 CD-der	13	15	42	0.36
2	1	5 CN-der	24	60	167*	0.36
3	1	15 CD-der	7.3	11.1	57	0.19
4	1	15 CN-der	30	20	167*	0.12
5	1	30 CD-der	3	15.1	47	0.32
6	1	30 CN-der	30.4	3	-	*

\*- Possible leak on system for this data.

- N.A = Not available.

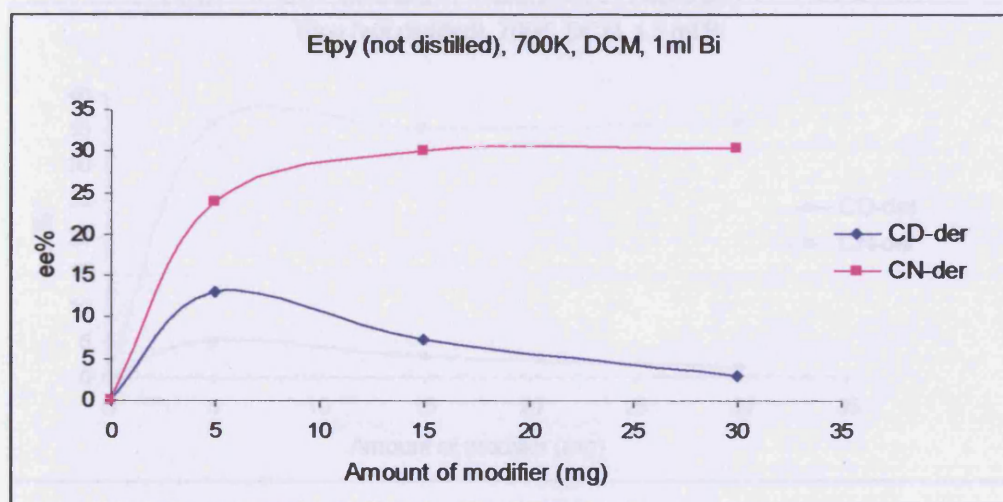


Figure 3.18 Enantiomeric excess in dichloromethane versus amount of modifier (mg). 5% Pt/G catalyst sintered at 700K with 1 ml of aqueous bismuth nitrate adsorbed on catalyst.

Table 3.14 Effect of Bismuth adsorption on enantiomeric excess in dichloromethane observed in ethyl pyruvate hydrogenation using CD-derivative and CN-derivative modified 5% Pt/G catalyst sintered at 700K pre-treated with 1.5 ml of aqueous bismuth nitrate adsorbed on catalyst.

Entry	Dosing volume Bi/cm <sup>3</sup>	Amount of modifiers (mg)	Enantiomeric excess (%) (R)	Conversion (%)	Time Minutes	Nominal rate mmol g <sup>-1</sup> h <sup>-1</sup>
1	1.5	5 CD-der	5.2	10	63	0.16
2	1.5	5 CN-der	36	4	65	0.06
3	1.5	15 CD-der	3	7.4	58	0.13
4	1.5	15 CN-der	35.3	4.4	57	0.08
5	1.5	30 CD-der	1.4	5.2	48	0.11
6	1.5	30 CN-der	36	4	-	-

- N.A = Not available.

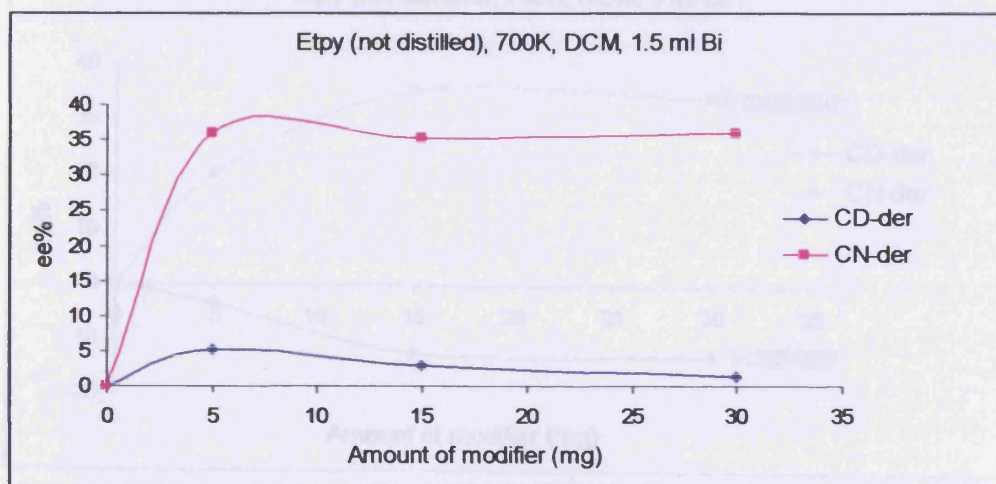
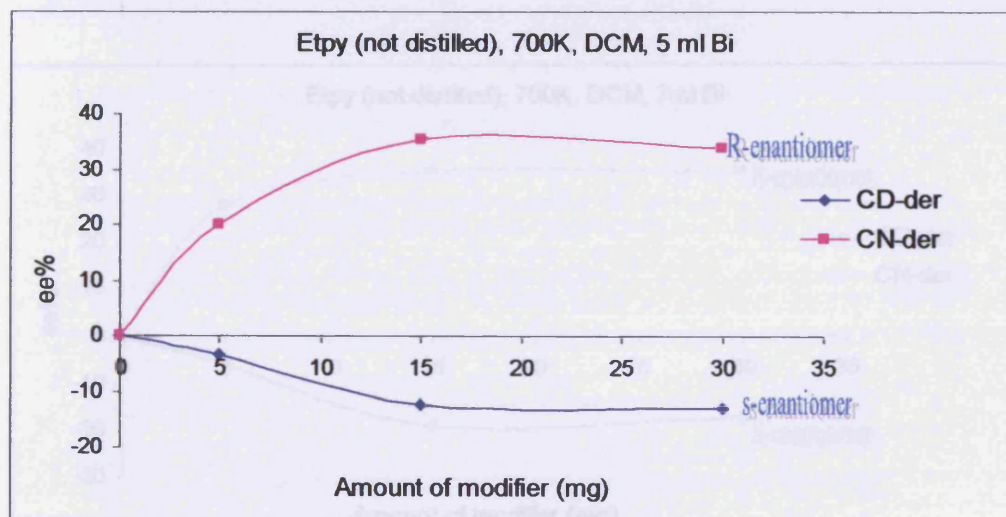


Figure 3.19 Enantiomeric excess in dichloromethane versus amount of modifier (mg). 5% Pt/G catalyst sintered at 700K with 1.5 ml of aqueous bismuth nitrate adsorbed on catalyst.

**Table 3.15** Effect of Bismuth adsorption on enantiomeric excess in dichloromethane observed in ethyl pyruvate hydrogenation using CD-derivative and CN-derivative modified 5% Pt/G catalyst sintered at 700K pre-treated with 5 ml of aqueous bismuth nitrate adsorbed on catalyst.

Entry	Dosing volume Bi/cm <sup>3</sup>	Amount of modifiers (mg)	Enantiomeric excess (%)	Conversion (%)	Time Minutes	Nominal rate mmol g <sup>-1</sup> h <sup>-1</sup>
1	5	5 CD-der	3.3 ( <i>S</i> )	19	54	0.35
2	5	5 CN-der	20 ( <i>R</i> )	2	46	0.04
3	5	15 CD-der	12.3 ( <i>S</i> )	9	52	0.17
4	5	15 CN-der	35.3 ( <i>R</i> )	7.3	-	-
5	5	30 CD-der	13 ( <i>S</i> )	12.3	-	-
6	5	30 CN-der	34 ( <i>R</i> )	8	54	0.15

- N.A = Not available.

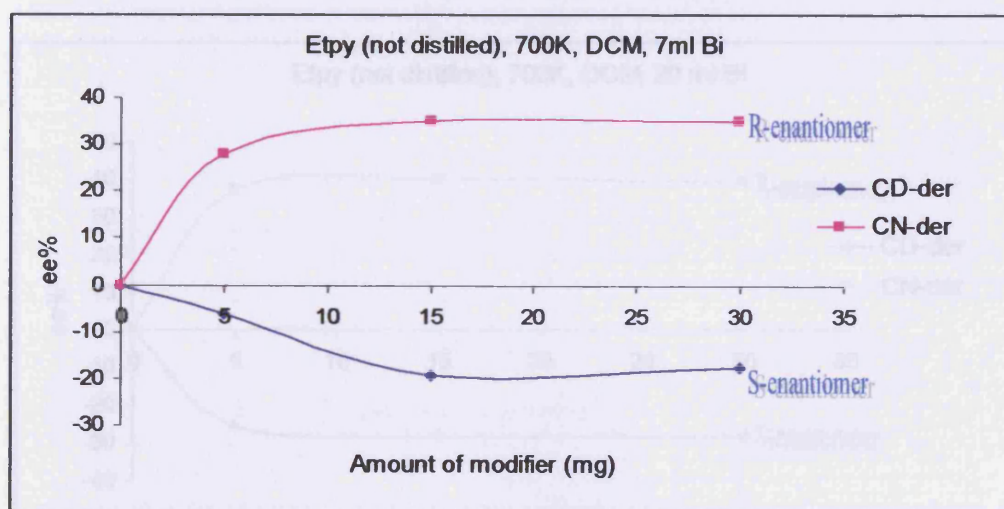


**Figure 3.20** Enantiomeric excess in dichloromethane versus amount of modifier (mg). 5% Pt/G catalyst sintered at 700K with 5 ml of aqueous bismuth nitrate adsorbed on catalyst.

**Table 3.16** Effect of Bismuth adsorption on enantiomeric excess in dichloromethane observed in ethyl pyruvate hydrogenation using CD-derivative and CN-derivative modified 5% Pt/G catalyst sintered at 700K pre-treated with 7 ml of aqueous bismuth nitrate adsorbed on catalyst.

Entry	Dosing volume Bi/cm <sup>3</sup>	Amount of modifiers (mg)	Enantiomeric excess (%)	Conversion (%)	Time Minutes	Nominal rate mmol g <sup>-1</sup> h <sup>-1</sup>
1	7	5 CD-der	6.1 ( <i>S</i> )	2	54	0.04
2	7	5 CN-der	28 ( <i>R</i> )	99	46	2.15
3	7	15 CD-der	19.2 ( <i>S</i> )	2	52	0.04
4	7	15 CN-der	35 ( <i>R</i> )	11	-	-
5	7	30 CD-der	17.4 ( <i>S</i> )	5.3	-	-
6	7	30 CN-der	35 ( <i>R</i> )	15	54	0.28

- N.A = Not available.



**Figure 3.21** Enantiomeric excess in dichloromethane versus amount of modifier (mg). 5% Pt/G catalyst sintered at 700K with 7 ml of aqueous bismuth nitrate adsorbed on catalyst.



Table 3.17 Effect of Bismuth adsorption on enantiomeric excess in dichloromethane observed in ethyl pyruvate hydrogenation using CD-derivative and CN-derivative modified 5% Pt/G catalyst sintered at 700K pre-treated with 20 ml of aqueous bismuth nitrate adsorbed on catalyst.

Entry	Dosing volume Bi/cm <sup>3</sup>	Amount of modifiers (mg)	Enantiomeric excess (%)	Conversion (%)	Time Minutes	Nominal rate mmol g <sup>-1</sup> h <sup>-1</sup>
1	20	5 CD-der	25.3 (S)	3.1	58	0.05
2	20	5 CN-der	37.2 (R)	13	54	0.24
3	20	15 CD-der	28 (S)	16.1	42	0.38
4	20	15 CN-der	40 (R)	14	58	0.24
5	20	30 CD-der	28.1 (S)	29	42	0.69
6	20	30 CN-der	39.4 (R)	52.2	50	1.04

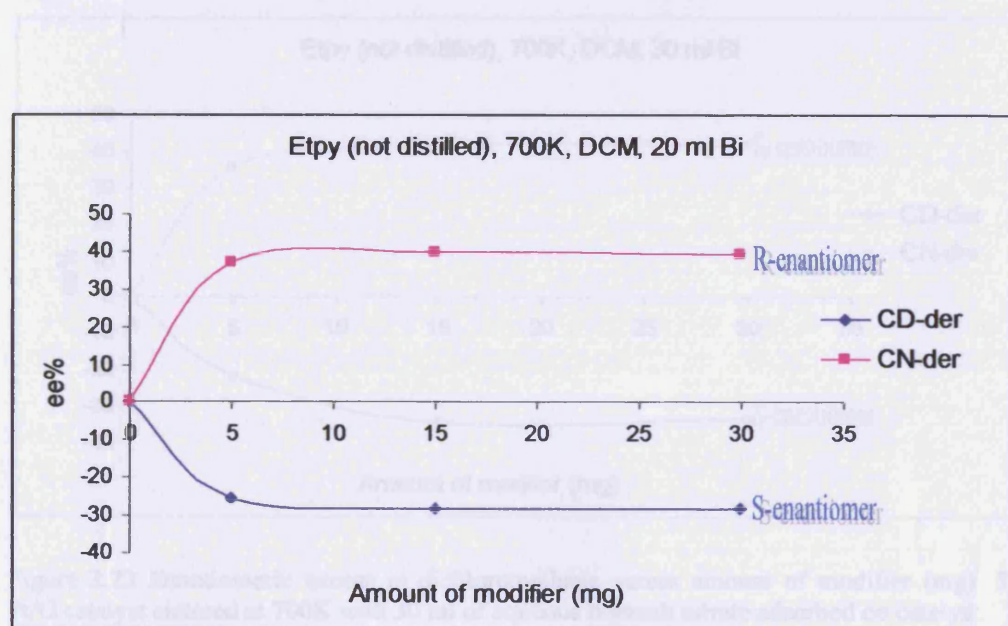
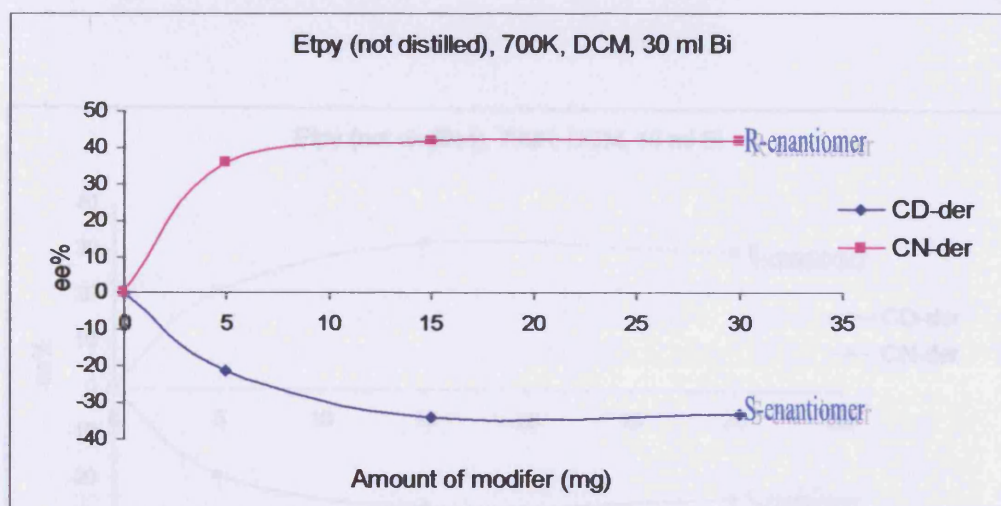


Figure 3.22 Enantiomeric excess in dichloromethane versus amount of modifier (mg). 5% Pt/G catalyst sintered at 700K with 20 ml of aqueous bismuth nitrate adsorbed on catalyst.

**Table 3.18** Effect of Bismuth adsorption on enantiomeric excess in dichloromethane observed in ethyl pyruvate hydrogenation using CD-derivative and CN-derivative modified 5% Pt/G catalyst sintered at 700K pre-treated with 30 ml of aqueous bismuth nitrate adsorbed on catalyst.

Entry	Dosing volume Bi/cm <sup>3</sup>	Amount of modifiers (mg)	Enantiomeric excess (%)	Conversion (%)	Time Minutes	Nominal rate mmol g <sup>-1</sup> h <sup>-1</sup>
1	30	5 CD-der	21.4 (S)	24.3	57	0.43
2	30	5 CN-der	36 (R)	40	63	0.63
3	30	15 CD-der	34 (S)	36	60	0.60
4	30	15 CN-der	42 (R)	51	50	1.02
5	30	30 CD-der	33 (S)	85.4	58	1.47
6	30	30 CN-der	42 (R)	71	61	1.16

N.A. = Not available



**Figure 3.23** Enantiomeric excess in dichloromethane versus amount of modifier (mg). 5% Pt/G catalyst sintered at 700K with 30 ml of aqueous bismuth nitrate adsorbed on catalyst.

Figure 3.24 Enantiomeric excess in dichloromethane versus amount of modifier (mg). 5% Pt/G catalyst sintered at 700K with 30 ml of aqueous bismuth nitrate adsorbed on catalyst.

Table 3.19 Effect of Bismuth adsorption on enantiomeric excess in dichloromethane observed in ethyl pyruvate hydrogenation using CD-derivative and CN-derivative modified 5% Pt/G catalyst sintered at 700K pre-treated with 40 ml of aqueous bismuth nitrate adsorbed on catalyst.

Entry	Dosing volume Bi/cm <sup>3</sup>	Amount of modifiers (mg)	Enantiomeric excess (%)	Conversion (%)	Time Minutes	Nominal rate mmol g <sup>-1</sup> h <sup>-1</sup>
1	40	5 CD-der	19 (S)	2	58	0.03
2	40	5 CN-der	21 (R)	3	79	0.04
3	40	15 CD-der	26.2 (S)	10	56	0.18
4	40	15 CN-der	32 (R)	8.1	54	0.15
5	40	30 CD-der	24 (S)	8.2	-	-
6	40	30 CN-der	30 (R)	7.4	58	0.13

- N.A = Not available.

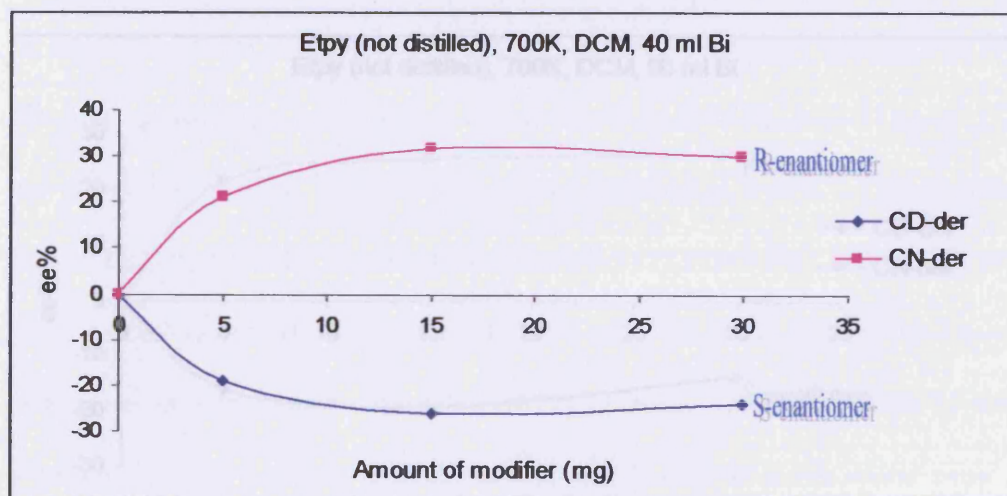


Figure 3.24 Enantiomeric excess in dichloromethane versus amount of modifier (mg). 5% Pt/G catalyst sintered at 700K with 40 ml of aqueous bismuth nitrate adsorbed on catalyst.

Table 3.20 Effect of Bismuth adsorption on enantiomeric excess in dichloromethane observed in ethyl pyruvate hydrogenation using CD-derivative and CN-derivative modified 5% Pt/G catalyst sintered at 700K pre-treated with 50 ml of aqueous bismuth nitrate adsorbed on catalyst.

Entry	Dosing volume Bi/cm <sup>3</sup>	Amount of modifiers (mg)	Enantiomeric excess (%)	Conversion (%)	Time Minutes	Nominal rate mmol g <sup>-1</sup> h <sup>-1</sup>
1	50	5 CD-der	16 (S)	3	50	0.06
2	50	5 CN-der	21.4 (R)	3	50	0.06
3	50	15 CD-der	19.3 (S)	3	42	0.07
4	50	15 CN-der	25.4 (R)	3.3	46	0.07
5	50	30 CD-der	14 (S)	1.3	-	-
6	50	30 CN-der	26.4 (R)	4	-	-

- N.A = Not available.

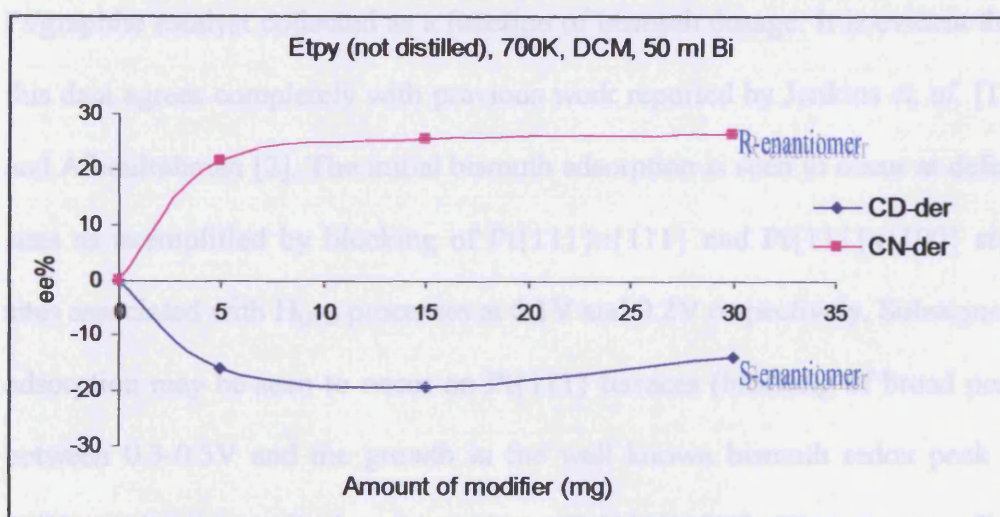


Figure 3.25 Enantiomeric excess in dichloromethane versus amount of modifier (mg). 5% Pt/G catalyst sintered at 700K with 50 ml of aqueous bismuth nitrate adsorbed on catalyst.

Inspection of Figure 3.26 and 3.27 indicates that optimal  $ee$  is obtained for a bismuth loading of between 20 and 30 cm<sup>3</sup> of bismuth solution and that this quantity of bismuth gives rise to a broad maximum in  $ee$  in the case of CN-derivative and a sharper maximum (but-opposite sign of  $ee$ ) for the CD-derivative. Similar behaviour has been reported by Hutchings *et al.*[10] for bismuth dosed Pt/Al<sub>2</sub>O<sub>3</sub> catalysts and it was speculated that bismuth could be occupying step sites at low coverages but terrace sites at higher coverages, although no evidence for this speculation was presented. The rate of the reaction also appears to pass through a maximum at a similar stage of Bi dosing (Figure 3.26). This is consistent with previous results showing that when all defect sites are blocked, the vacant Pt{111} terraces give rise to a greater rate of reaction [9,11]. In Figure 3.28 are the CVs of the heated 700K/H<sub>2</sub> 5% Pt/graphite catalyst collected as a function of bismuth dosage. It is evident that this data agrees completely with previous work reported by Jenkins *et al.* [12] and Abdurahman [2]. The initial bismuth adsorption is seen to occur at defect sites as exemplified by blocking of Pt{111}x{111} and Pt{111}x{100} step sites associated with H<sub>UPD</sub> processes at 0.1V and 0.2V respectively. Subsequent adsorption may be seen to occur on Pt{111} terraces (blocking of broad peak between 0.3-0.5V and the growth in the well known bismuth redox peak at 0.6V previously ascribed to bismuth on Pt{111}) [13]. The corresponding bismuth oxide redox peak for steps/Pt{100} terraces at 0.85V is observed to increase in magnitude as a function of bismuth loading. Further inspection of Figure 3.28 indicates that complete blocking of step sites occurs between 20

and 30 cm<sup>3</sup> of bismuth dosed. This is precisely where the maximum values of *ee* are recorded as mentioned previously. Clearly the inversion of *ee* for CD-derivative being reached at this bismuth coverage is consistent with speculations from Hutchings *et al.* [10] that CD-derivative is being forced to occupy differing adsorption sites, probably terraces instead of defects. However we will return to this point later when CD and CN as modifiers are considered. The variation in H<sub>UPD</sub> coverage/  $\theta_{Bi}$  as a function of bismuth dosing is presented in Table 3.22 based on equation 2.3 in section 2.13.

*Table 3.21 Effect of Bismuth adsorption on enantiomeric excess in dichloromethane observed in ethyl pyruvate hydrogenation using CD-derivative and CN-derivative modified 5% Pt/G catalyst sintered at 700K.*

Dosing volume Bi/cm <sup>3</sup>	5 CD-der ( <i>ee</i> %)	5 CN-der ( <i>ee</i> %)	15 CD-der ( <i>ee</i> %)	15 CN-der ( <i>ee</i> %)	30 CD-der ( <i>ee</i> %)	30CN-der ( <i>ee</i> %)
1	13 (R)	24 (R)	7.3 (R)	30 (R)	3 (R)	30.4 (R)
1.5	5.2 (R)	36 (R)	3 (R)	35.3 (R)	1.4 (R)	36 (R)
5	3.3 (S)	20 (R)	12.3 (S)	35.3 (R)	13 (S)	34 (R)
7	6.1 (S)	28 (R)	19.2 (S)	35 (R)	17.4 (S)	35 (R)
20	25.3 (S)	37.2 (R)	28 (S)	40 (R)	28.1 (S)	39.4 (R)
30	21.4 (S)	36 (R)	34 (S)	42 (R)	33 (S)	42 (R)
40	19 (S)	21 (R)	26.2 (S)	32 (R)	24 (S)	30 (R)
50	16 (S)	21.4 (R)	19.3 (S)	25.4 (R)	14 (S)	26.4 (R)

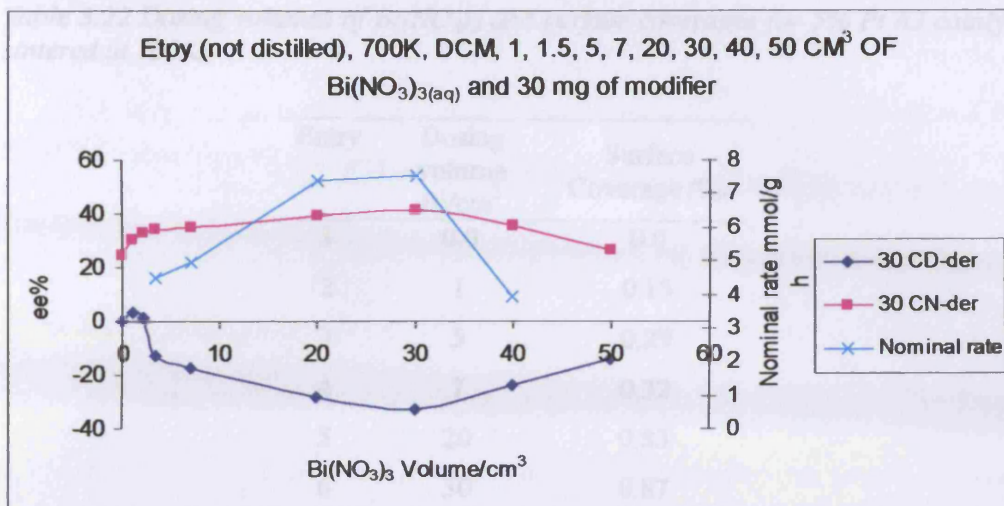


Figure 3.26 Adsorption of Bi on 5% Pt/G catalyst sintered at 700K and enantiomeric excess at 30 mg of modifier 1, 1.5, 5, 7, 20, 30, 40 and 50 ml of Bi solution. The variation in nominal rate is also depicted.

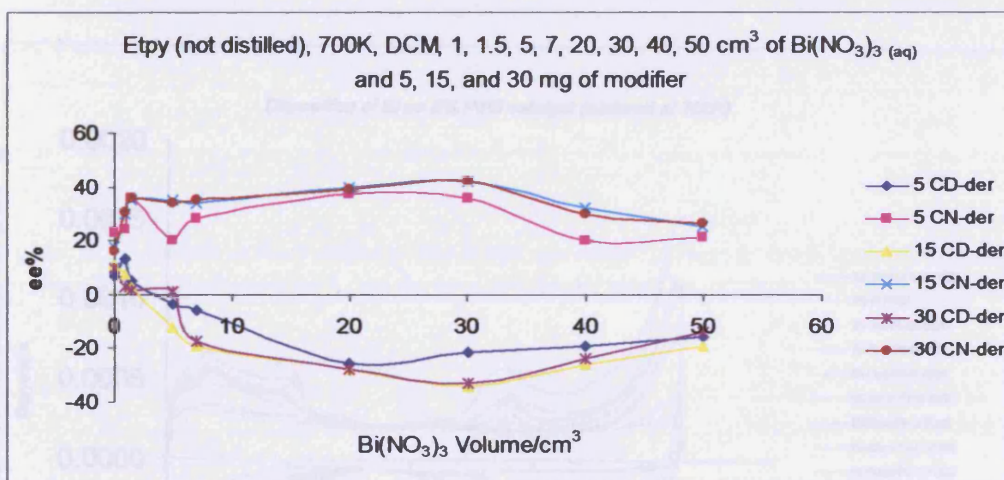


Figure 3.27 Enantiomeric excess in dichloromethane versus various concentration of bismuth with (CD-derivative and CN-derivative) modified 5% Pt/ G catalyst sintered at 700K.

Table 3.22 Dosing volumes of  $\text{Bi}(\text{NO}_3)_3$  and surface coverages for 5% Pt/G catalyst sintered at 700K.

Entry	Dosing volume $\text{Bi}/\text{cm}^3$	Surface Coverage $\theta_{\text{Bi}}$
1	0.0	0.0
2	1	0.15
3	5	0.29
4	7	0.32
5	20	0.83
6	30	0.87
7	40	0.85
8	50	0.88

Table 3.23 Equilibrium current observed in cyclic voltammetry hydrogenation using cyclohexene (CD) modified sintered 5% Pt/G catalyst in dichloromethane and sulfuric acid.

Entry	Amount of modifier ( $\mu\text{mol}$ )	Solvent	Equilibrium current ( $\mu\text{A}$ )	Conversion (%)	Time (min)	Reaction rate ( $\mu\text{mol/g h}$ )
1	0	$\text{H}_2\text{SO}_4$	0.0000	0	15	0
2	0.05	$\text{H}_2\text{SO}_4$	0.0005	5	15	0.0003
3	0.1	$\text{H}_2\text{SO}_4$	0.0010	10	15	0.0006
4	0.2	$\text{H}_2\text{SO}_4$	0.0020	20	15	0.0013
5	0.5	$\text{H}_2\text{SO}_4$	0.0040	40	15	0.0026
6	1.0	$\text{H}_2\text{SO}_4$	0.0080	80	15	0.0052
7	2.0	$\text{H}_2\text{SO}_4$	0.0160	160	15	0.0104
8	5.0	$\text{H}_2\text{SO}_4$	0.0320	320	15	0.0208
9	10.0	$\text{H}_2\text{SO}_4$	0.0640	640	15	0.0416
10	20.0	$\text{H}_2\text{SO}_4$	0.1280	1280	15	0.0832
11	30.0	$\text{H}_2\text{SO}_4$	0.1920	1920	15	0.1248
12	40.0	$\text{H}_2\text{SO}_4$	0.2560	2560	15	0.1664
13	50.0	$\text{H}_2\text{SO}_4$	0.3200	3200	15	0.2080
14	0	$\text{CH}_2\text{Cl}_2$	0.0000	0	15	0
15	0.05	$\text{CH}_2\text{Cl}_2$	0.0005	5	15	0.0003
16	0.1	$\text{CH}_2\text{Cl}_2$	0.0010	10	15	0.0006
17	0.2	$\text{CH}_2\text{Cl}_2$	0.0020	20	15	0.0013
18	0.5	$\text{CH}_2\text{Cl}_2$	0.0040	40	15	0.0026
19	1.0	$\text{CH}_2\text{Cl}_2$	0.0080	80	15	0.0052
20	2.0	$\text{CH}_2\text{Cl}_2$	0.0160	160	15	0.0104
21	5.0	$\text{CH}_2\text{Cl}_2$	0.0320	320	15	0.0208
22	10.0	$\text{CH}_2\text{Cl}_2$	0.0640	640	15	0.0416
23	20.0	$\text{CH}_2\text{Cl}_2$	0.1280	1280	15	0.0832
24	30.0	$\text{CH}_2\text{Cl}_2$	0.1920	1920	15	0.1248
25	40.0	$\text{CH}_2\text{Cl}_2$	0.2560	2560	15	0.1664
26	50.0	$\text{CH}_2\text{Cl}_2$	0.3200	3200	15	0.2080

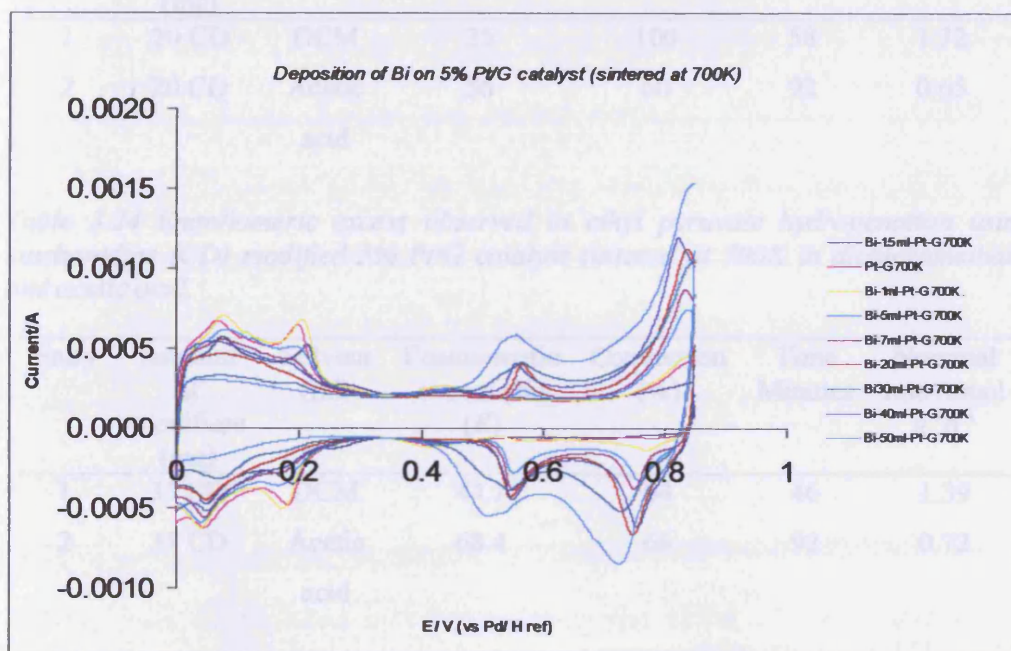


Figure 3.28 CVs of 5% Pt/G catalyst sintered at 700K in 0.5M  $\text{H}_2\text{SO}_4$ . Sweep rate  $50 \text{ mV s}^{-1}$ .



### 3.2.7 The influence of solvent on *ee* using cinchonidine (CD) and cinchonine (CN) as modifiers

A key concern of the present study is to compare CD-derivative/CN-derivative modifier behaviour with previous studies using CD and CN with clean and bismuth modified Pt supported catalyst [2, 9]. Hence, it is necessary to re-investigate some aspects of CD and CN behaviour for enantioselective hydrogenation, particularly solvent dependence of *ee* and conversion. In Table 3.23 and 3.24 are shown the *ee* and conversions obtained for unsintered and sintered 5% Pt/G respectively.

Table 3.23 Enantiomeric excess observed in ethyl pyruvate hydrogenation using cinchonidine (CD) modified unsintered 5% Pt/G catalyst in dichloromethane and acetic acid.

Entry	Amount of modifiers (mg)	Solvent (ml)	Enantiomeric excess (%) (R)	Conversion (%)	Time Minutes	Nominal rate mmol g <sup>-1</sup> h <sup>-1</sup>
1	20 CD	DCM	35	100	58	1.72
2	20 CD	Acetic acid	56	60	92	0.65

Table 3.24 Enantiomeric excess observed in ethyl pyruvate hydrogenation using cinchonidine (CD) modified 5% Pt/G catalyst sintered at 700K in dichloromethane and acetic acid.

Entry	Amount of modifiers (mg)	Solvent (ml)	Enantiomeric excess (%) (R)	Conversion (%)	Time Minutes	Nominal rate mmol g <sup>-1</sup> h <sup>-1</sup>
1	35 CD	DCM	44.1	64	46	1.39
2	35 CD	Acetic acid	68.4	66	92	0.72

It is evident from inspection of both Tables that acetic acid as solvent leads to an increase in *ee* and a decrease in nominal rate relative to the solvent dichloromethane. This behaviour has been reported previously [14] whereby

enhanced *ee* was ascribed to protonation of the tertiary nitrogen of CD leading to generation of the key  $\text{HCD}^+$ -etpy hydrogen bonded surface complex necessary for enantio-discrimination [14]. Although Blaser *et al.* [15] note that use of acetic acid as solvent affords a greater *ee* but lower rate compared with ethanol and toluene, no satisfactory explanation for this behaviour has yet been proposed.

### 3.2.8 Reaction of bismuthated catalysts in acetic acid

No studies of Orito-type reactions on bismuthated 5% Pt/G catalysts with acetic acid as solvent have been reported. Therefore, since solvent effects are known to be very important in influencing *ee*, it was thought interesting to make comparisons with earlier work by Jenkins *et al* [2] and Albdulrahman [9] on the influence of solvent on *ee* changes resulting from selectively blocking Pt sites with bismuth. To this end, a new series of bismuthated 5% Pt/G catalysts was prepared. Each catalyst was heated twice in 5%  $\text{H}_2/\text{Ar}$  at 700K as described in Section 2.11 followed by characterisation using CV. This procedure was undertaken due to possible ambiguities that may arise after dosing of Bi, for example could the Bi be only partially reduced after dosing? Also, water is a known accelerant of the Orito reaction [16] and therefore a second annealing step in hydrogen would ensure both complete reduction of bismuth, but also complete removal of water from the catalyst. Each sintered catalyst was investigated in order to study the effect of acetic acid on the reaction rate and the enantioselectivity and the results are shown in Table 3.25.

Table 3.25 Effect of Bismuth adsorption on enantiomeric excess observed in distilled ethyl pyruvate hydrogenation using cinchonidine (CD) modified 5% Pt/G catalyst heated twice at 700K with 5, 7, 15, 30, 50, 70 and 80 ml of Bismuth in Acetic acid.

Entry	Dosing volume Bi/cm <sup>3</sup>	Amount of modifiers (mg)	Enantiomeric excess (%) (R)	Conversion (%)	Time Minutes	Nominal rate mmol g <sup>-1</sup> h <sup>-1</sup>
1	5	5 CD	32	66	67	0.99
2	5	30 CD	41.1	40	46	0.87
3	7	5 CD	34	63.4	44	1.43
4	7	30 CD	40	69	48	1.44
5	15	5 CD	18.1	67.2	42	1.60
6	15	30 CD	24	74	29	2.55
7	30	5 CD	6.1	54	52	1.04
8	30	30 CD	8	61.4	38	1.61
9	50	5 CD	4.2	63	92	0.68
10	50	30 CD	3.2	55.1	92	0.60
11	70	5 CD	6	2	54	0.04
12	70	30 CD	5.1	1.4	42	0.03
13	80	5 CD	3.4	1.3	60	0.02
14	80	30 CD	3	1.4	83	0.02

\* Possible leak on system for this data

Figure 3.29-3.35 shows graphically the changes in *ee* as a function of bismuth loading for the “doubly sintered” Pt catalysts. In Figure 3.36 is plotted the changes in *ee* and nominal rate as a function of Bi loading for optimised modifier amount (30 mg). In agreement with earlier studies in DCM [2], the catalysts dosed with bismuth show a gradual loss of *ee* as bismuth coverage increases. In contrast however, enantiomeric excesses close to 0% are obtained (with very low conversions) at highest bismuth loadings (> 50 cm<sup>3</sup> dosing volume). The rate of reaction also is seen to pass through a clear maximum at 20ml bismuth dosing. In DCM, a gradual loss in *ee* was observed after the large

decrease associated with filling of defect/step sites [2,9] and a finite *ee* of between 20%-30% *ee* was observed even at relatively high ( $\theta_{\text{Bi}} > 0.5$ ) bismuth coverage. In order to clarify the issue of what sites are being blocked, it is necessary to understand the site occupancy by bismuth adatoms of the doubly sintered catalyst. Examination of Figure 3.37 which shows CVs of the doubly sintered catalysts shows that the voltammetric response obtained is practically identical to that shown in Figure 3.28 for the “singly-sintered” catalyst save for at higher bismuth loading ( $80 \text{ cm}^3 \text{ Bi}$ ). For this sample, complete blocking of all  $\text{H}_{\text{UPD}}$  sites is observed. Furthermore, a new redox peak at 0.75V is observed when a high coverage of bismuthated catalyst is prepared which has not so far been reported in the literature. This is a major departure from observations made by Abdurahman for high bismuth loading Pt/G catalyst sintered only once [9]. One can only speculate as to the origin of this new surface redox peak at the present time. It could reflect some sort of Bi-Pt alloyed phase [17] or perhaps some new “compression structure” [18] of the bismuth overlayer. Whatever its origin, it is completely inactive towards Orito type hydrogenation as signified in Table 3.25 by both an extremely low conversion and a negligible *ee*.

The behaviour of the bismuth-modified catalysts in acetic acid indicates a sharp fall in *ee* corresponding to filling of defect sites such as steps and Pt{100} terraces followed by a constant (low-almost zero) *ee* when only Pt{111} sites are free of bismuth. Hence, it is concluded that for free Pt{111} terraces on the catalyst :

$ee$  (CD in acetic acid) <  $ee$  (CD in dichloromethane)

Also, in both singly- and doubly-sintered catalysts, bismuth occupation of defect sites leads to a marked decrease in  $ee$ . The maximum in rate is also coincident with filling of defect sites leaving vacant Pt{111} terraces. These sites must be particularly active for hydrogenation although they form racemic product. The use of distilled EP and singly or doubly sintered catalysts has shown that the behaviour originally reported by Jenkins *et al.*, for unsintered bismuth-modified catalysts and sintered bismuth-modified catalyst by Albulrahman [9] has been reproduced. Hence, speculation concerning the presence of water as impurities in EP can be discarded as causing the change in  $ee$  for different site occupancies by bismuth.

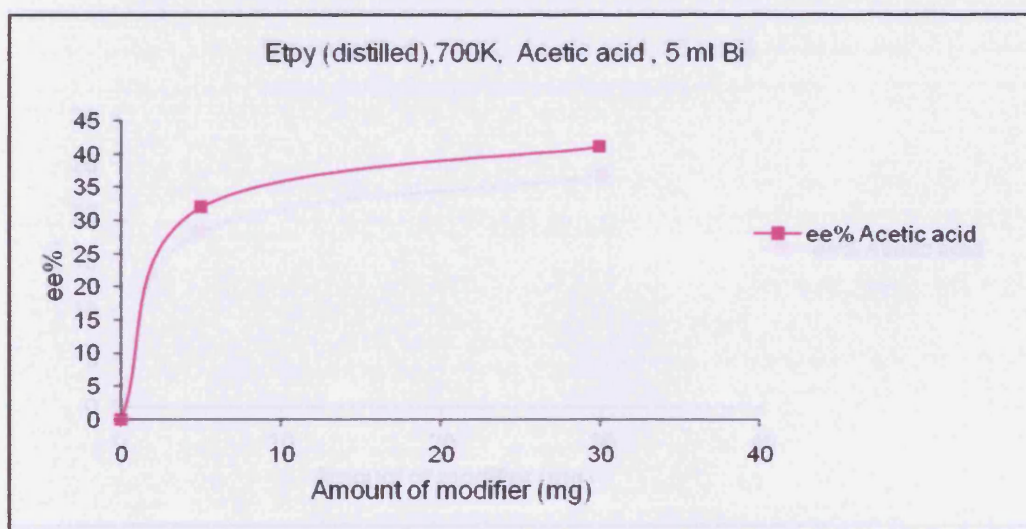


Figure 3.29 Enantiomeric excess in acetic acid versus amount of modifier (mg). 5% Pt/G catalyst sintered twice at 700K with 5 ml of aqueous bismuth nitrate adsorbed on catalyst.

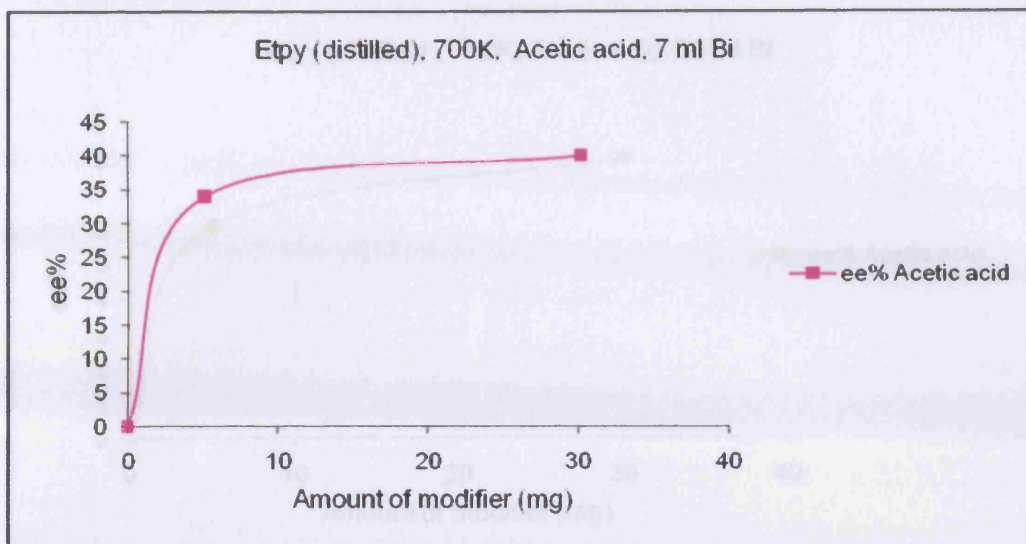


Figure 3.30 Enantiomeric excess in acetic acid versus amount of modifier (mg). 5% Pt/G catalyst sintered twice at 700K with 7 ml of aqueous bismuth nitrate adsorbed on catalyst.

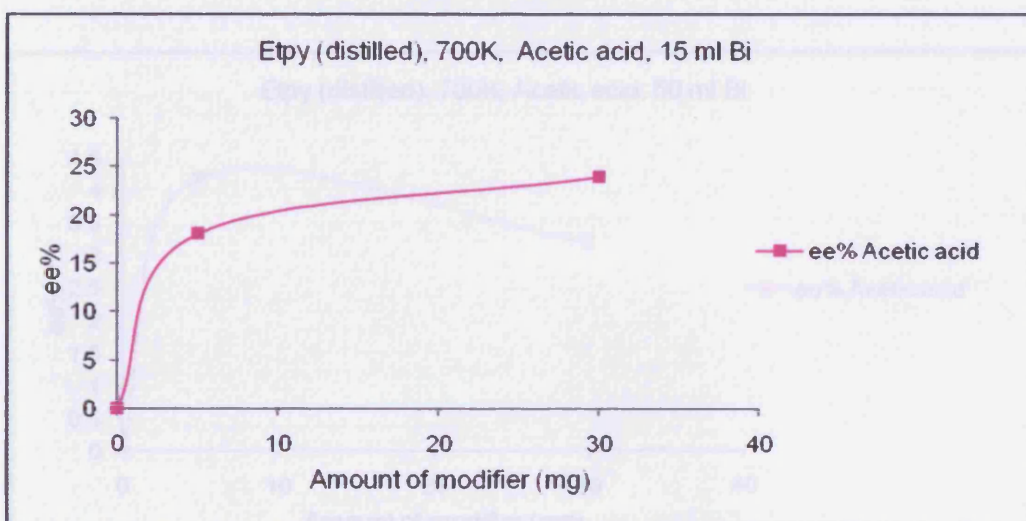


Figure 3.31 Enantiomeric excess in acetic acid versus amount of modifier (mg). 5% Pt/G catalyst sintered twice at 700K with 15 ml of aqueous bismuth nitrate adsorbed on catalyst.

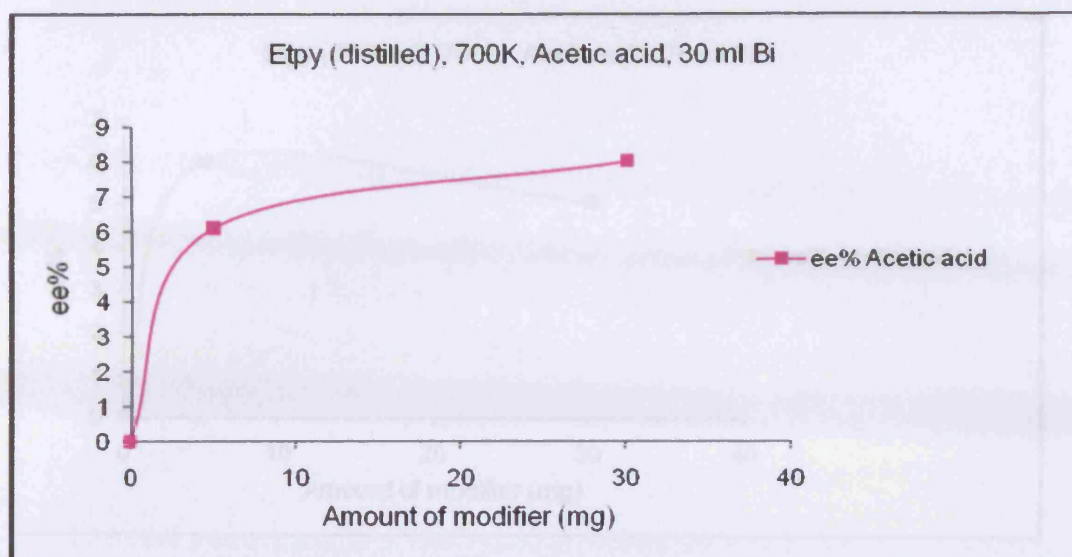


Figure 3.32 Enantiomeric excess in acetic acid versus amount of modifier (mg). 5% Pt/G catalyst sintered twice at 700K with 30 ml of aqueous bismuth nitrate adsorbed on catalyst.

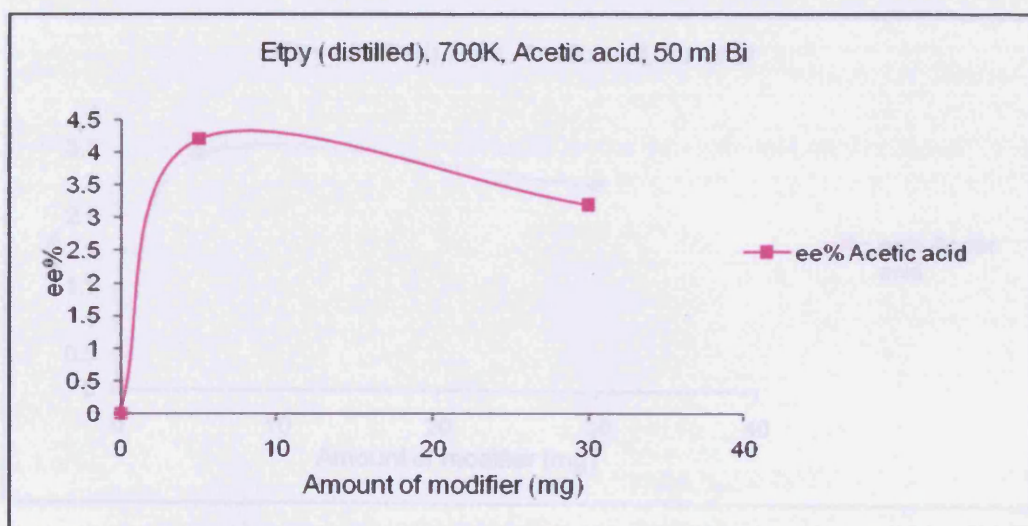


Figure 3.33 Enantiomeric excess in acetic acid versus amount of modifier (mg). 5% Pt/G catalyst sintered twice at 700K with 50 ml of aqueous bismuth nitrate adsorbed on catalyst.

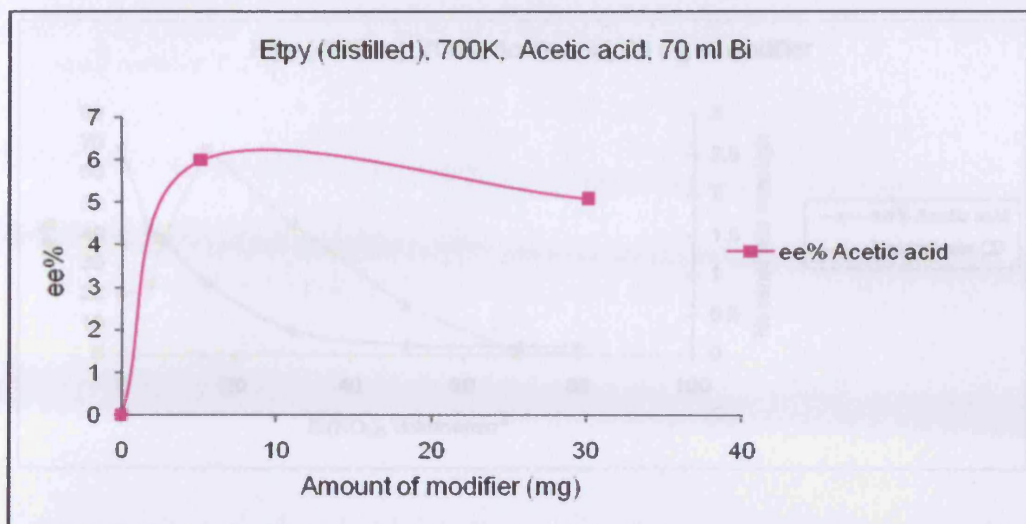


Figure 3.34 Enantiomeric excess in acetic acid versus amount of modifier (mg). 5% Pt/G catalyst sintered twice at 700K with 70 ml of aqueous bismuth nitrate adsorbed on catalyst.

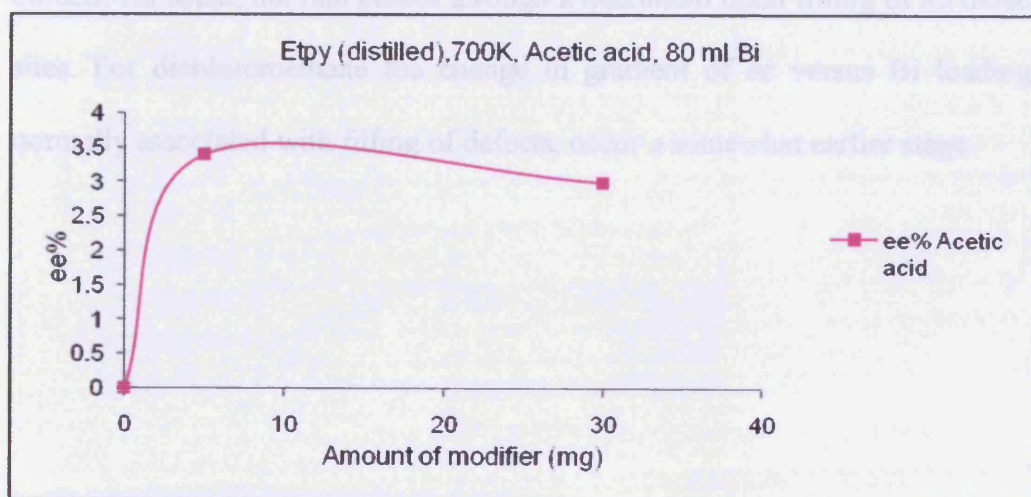


Figure 3.35 Enantiomeric excess in acetic acid versus amount of modifier (mg). 5% Pt/G catalyst sintered twice at 700K with 80 ml of aqueous bismuth nitrate adsorbed on catalyst.



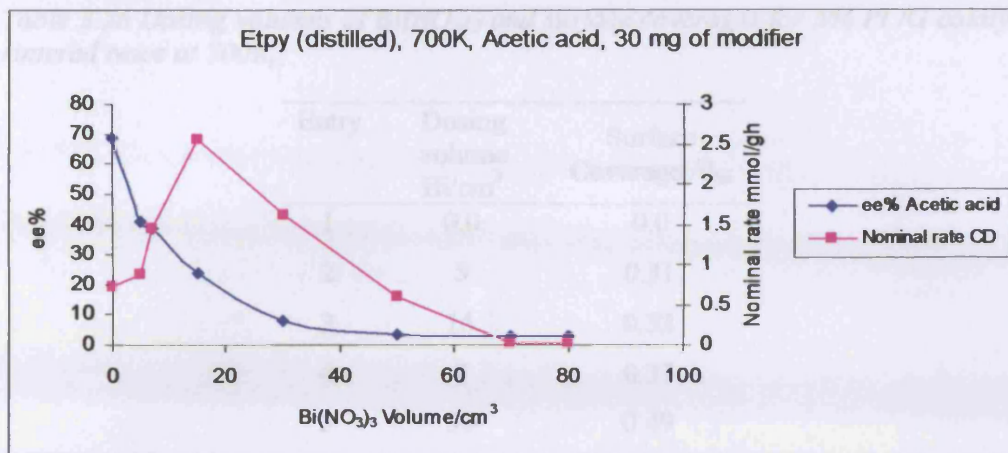


Figure 3.36 Enantiomeric excess in acetic acid and nominal rate versus various concentration of bismuth with (CD-modified 5% Pt/ G catalyst sintered twice at 700K.

Table 3.26 shows  $\text{Bi}(\text{NO}_3)_3$  dosing volumes and surface coverages calculated according to the method described in section 2.13.1. Figure 3.38 shows how  $ee$  and rate varies as a function of bismuth surface coverage. The coverage at which  $ee$  plateaus (close to 0%  $ee$ ) corresponds to blocking of all defects. As usual, the rate passes through a maximum upon filling of all defect sites. For dichloromethane the change in gradient of  $ee$  versus Bi loading, normally associated with filling of defects, occur a somewhat earlier stage.

Table 3.26 Dosing volumes of  $\text{Bi}(\text{NO}_3)_3$  and surface coverages for 5% Pt /G catalyst sintered twice at 700K.

Entry	Dosing volume $\text{Bi}/\text{cm}^3$	Surface Coverage $\theta_{\text{Bi}}$
1	0.0	0.0
2	5	0.31
3	15	0.32
4	7	0.37
5	30	0.49
6	50	0.54
7	70	0.61
8	80	0.71

Figure 3.36 Bi coverage on Pt surface (measured by cyclic voltammetry) for 5% Pt/G catalyst sintered at 700K.

### 3.2.3 The influence of Pt metal loading on electrocatalytic activity

Two more Pt/G catalysts were prepared in an identical fashion to the 5%

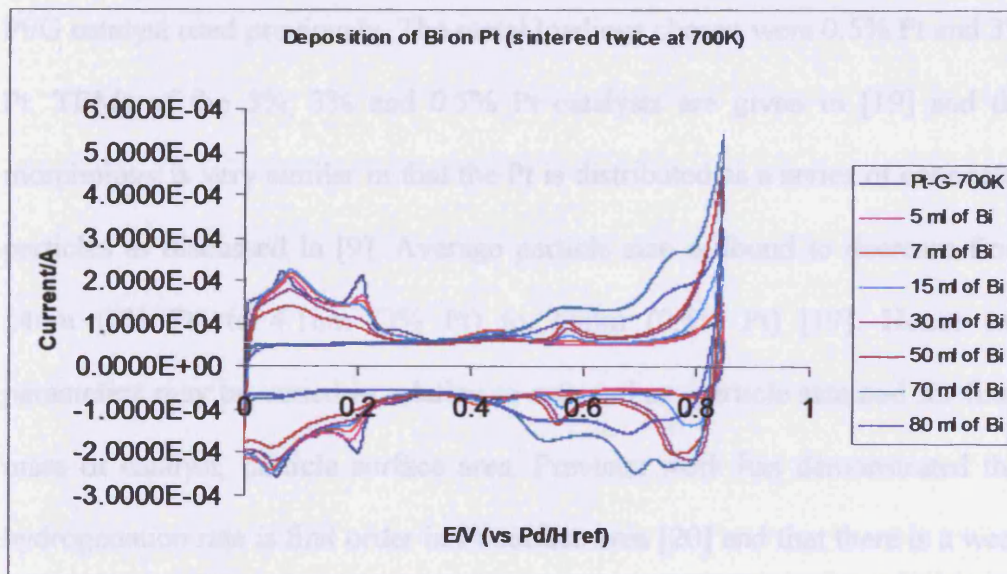


Figure 3.37 CVs of 5% Pt/G catalyst sintered twice at 700K in 0.5M  $\text{H}_2\text{SO}_4$ . Sweep rate 50  $\text{mV s}^{-1}$

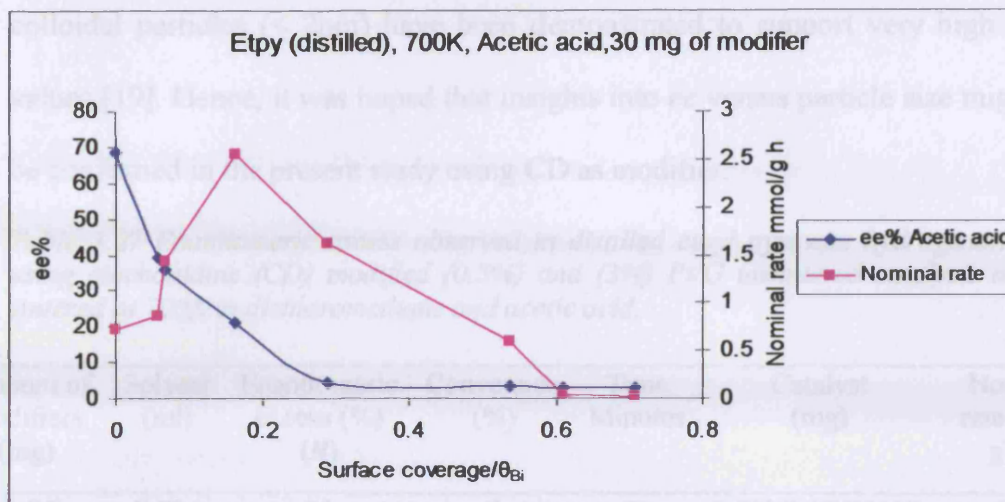


Figure 3.38 Bi coverage and enantiomeric excess versus nominal rate for 5% Pt/G catalyst sintered at 700K.

### 3.2.8 The influence of Pt metal loading on enantiomeric excess

Two more Pt/G catalysts were prepared in an identical fashion to the 5% Pt/G catalyst used previously. The metal loadings chosen were 0.5% Pt and 3% Pt. TEMs of the 5%, 3% and 0.5% Pt catalysts are given in [19] and the morphology is very similar in that the Pt is distributed as a series of connected particles as discussed in [9]. Average particle size is found to decrease from 14nm (5% Pt) to 4.1nm (3% Pt) to 2.9nm (0.5% Pt) [19]. Hence two parameters may be varied in relation to rate and *ee*, particle size and for fixed mass of catalyst, particle surface area. Previous work has demonstrated that hydrogenation rate is first order in Pt-surface area [20] and that there is a weak dependence of *ee* as a function of average particle size [20] but that for Pt particles less than 2nm, *ee* was reported to be low [20]. This was explained in terms of Pt particles being too small to support both CD and etpy/H<sub>2</sub> in the correct configuration to give high *ee* [21]. It should be noted that small

colloidal particles (< 2nm) have been demonstrated to support very high *ee* values [19]. Hence, it was hoped that insights into *ee* versus particle size might be confirmed in the present study using CD as modifier.

Table 3.27 Enantiomeric excess observed in distilled ethyl pyruvate hydrogenation using cinchonidine (CD) modified (0.5%) and (3%) Pt/G unsintered catalysts and sintered at 700K in dichloromethane and acetic acid.

Amount of modifiers (mg)	Solvent (ml)	Enantiomeric excess (%) (R)	Conversion (%)	Time Minutes	Catalyst (mg)	Nominal rate mmol g <sup>-1</sup> h <sup>-1</sup>
20 CD	DCM	39	6	73	0.5% Pt/G(700K)	0.08
20 CD	Acetic acid	64	22	92	0.5% Pt/G(700K)	0.24
20 CD	Acetic acid	54	78.3	29	0.5% Pt/G(300K)	2.7
20 CD	DCM	45	74	33	0.5% Pt/G(300K)	2.24
20 CD	Acetic acid	70	60	58	3% Pt/G (700K)	1.03
20 CD	DCM	47	99	50	3% Pt/G (700K)	1.98

Table 3.27 shows the effect of the solvents and the supports on 0.5% Pt/G and 3% Pt/G catalysts for sintered and unsintered catalysts when acetic acid and dichloromethane were used as solvents. It is seen from Table 3.27 that the unsintered 0.5% Pt catalyst gives an *ee* to the *R*-enantiomer of etlac of 45% in dichloromethane and 54% in acetic acid. This behaviour is identical to that shown by the standard unsintered 5% Pt/G in the present study and, for reactions in dichloromethane, the same outcome as reported by Jenkins [12] and Albulrahman [9]. It is also noted that conversion is good in both solvents. When sintered at 700K, the 3% Pt/G catalyst gives rise to enantiomeric excesses comparable with the 5% Pt/G catalyst (70% *ee* versus 68% *ee* in acetic and 47% *ee* versus 52% in dichloromethane). Finally, for the sintered

0.5% Pt/G catalyst, poor conversion is observed in both dichloromethane and acetic acid and values of *ee* slightly lower than those found for 5% Pt/G in acetic acid (64%) and dichloromethane (39%) are obtained. Therefore, two effects are noted from the 0.5% Pt catalyst:

- The smaller particle size leads to a slightly lower *ee*.
- For sintered 0.5% Pt/G, where surface area should be very low, very low conversion is also obtained.

Nonetheless, for all catalysts studied, *ee* is highest using acetic acid as solvent.

### 3.3 Enantioselective hydrogenation using EUROPT-1

In order to examine the role of catalyst support in the Orito reaction, a 6.3% Pt/SiO<sub>2</sub> catalyst was investigated. The catalyst used has previously been well characterised [22]. In reference [12] it had been speculated that the edges of the Pt nanoparticles might be the most enantioselective. Therefore, by changing support, this hypothesis could be tested in that the nature of the support should have a direct bearing on the outcome of the reaction. Previous work [2] had shown a dependence of *ee* on support for CD as a modifier but no investigations have been reported using CD-derivative and CN-derivative as modifier in this context.

#### 3.3.1 Standard reaction over EUROPT-1

Enantioselective hydrogenations over the 6.3% Pt/SiO<sub>2</sub> reference catalyst EUROPT-1 were used in this investigation. The standard reaction was the hydrogenation of 20 mmol of ethyl pyruvate in dichloromethane and acetic acid at 25°C at 35 bar H<sub>2</sub>. Catalyst, various concentrations of CD-derivative

and CN-derivative modifiers and reactant were placed in the reaction vessel as described in section 2.4 for the hydrogenation of ethyl pyruvate in the liquid phase. Examples of the resulting hydrogen uptake profiles are shown in Figure 3.39. The first stage is reported as 706 mmol/g cat/h (Table 3.28). This compares to the rate quoted in the literature of 1200 mmol g<sup>-1</sup>cat h<sup>-1</sup> as the maximum rate using CD instead of CD-derivative as modifier [23]. The enantiomeric excess at 100% conversion was 17.1% (*R*) as shown in Figure 3.40, which compares to the values in the literature of 42% [23].

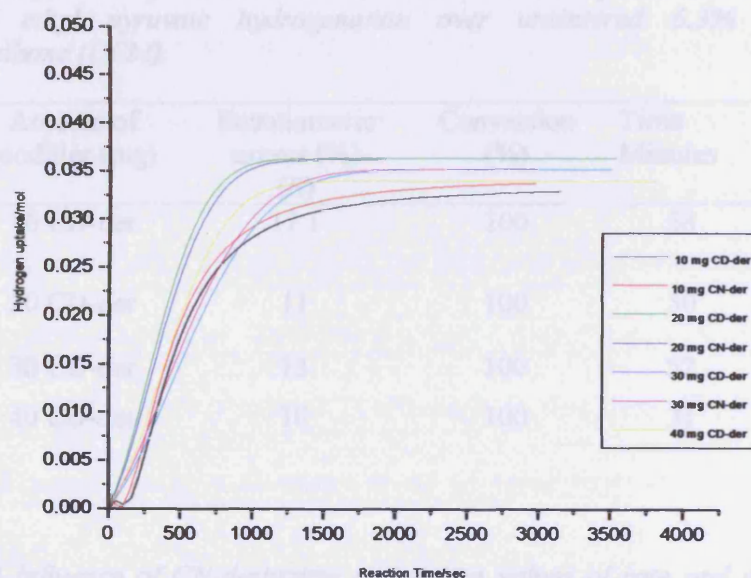


Figure 3.39 Hydrogen uptake curves versus time showing the rate of ethyl pyruvate hydrogenation over CD-derivative and CN-derivative modified unsintered 6.3% Pt/silica catalyst in dichloromethane.

Tables 3.28 and 3.29 show both the variation in rate and *ee* as a function of modifier concentration under standard conditions using dichloromethane as a solvent and Figure 3.40 the change in *ee* as a function of CN-derivative and CD-derivative amount. From Table 3.28-3.29 and Figure 3.40 it is evident that

the behaviour of the modifier using 5% Pt/G is similar to what is found here using silica supported Pt catalyst. For example, in dichloromethane at high modifier amounts, the *ee* (to *R*-etlac) using CN-derivative is greater than the *ee* (again to *R*-etlac) using CD-derivative (see 3.1-3.5). For CD-derivative there is a shallow increase in rate as modifier concentration increases, but for CN-derivative, rates are fairly constant. As for unsintered 5% Pt/G, the *ee* using CD-derivative passes through a maximum at 10 mg loading of modifier (Figure 3.40).

*Table 3.28 Influence of CD-derivative amount on values of rate and enantiomeric excess of ethyl pyruvate hydrogenation over unsintered 6.3% Pt/SiO<sub>2</sub> in dichloromethane (DCM).*

Entry	Amount of modifier (mg)	Enantiomeric excess (%) ( <i>R</i> )	Conversion (%)	Time Minutes	Maximum rate/mmol g <sup>-1</sup> h <sup>-1</sup>
1	10 CD-der	17.1	100	58	706
2	20 CD-der	11	100	50	840
3	30 CD-der	13	100	52	882
4	40 CD-der	10	100	31	928

*Table 3.29 Influence of CN-derivative amount on values of rate and enantiomeric excess of ethyl pyruvate hydrogenation over unsintered 6.3% Pt/SiO<sub>2</sub> catalyst in dichloromethane.*

Entry	Amount of modifier (mg)	Enantiomeric excess (%) ( <i>R</i> )	Conversion (%)	Time Minutes	Maximum rate/mmol g <sup>-1</sup> h <sup>-1</sup>
1	10 CN-der	14.2	100	54	760
2	20 CN-der	23	100	61	735
3	30 CN-der	23	100	65	767
4	40 CN-der	24.3	100	52	772

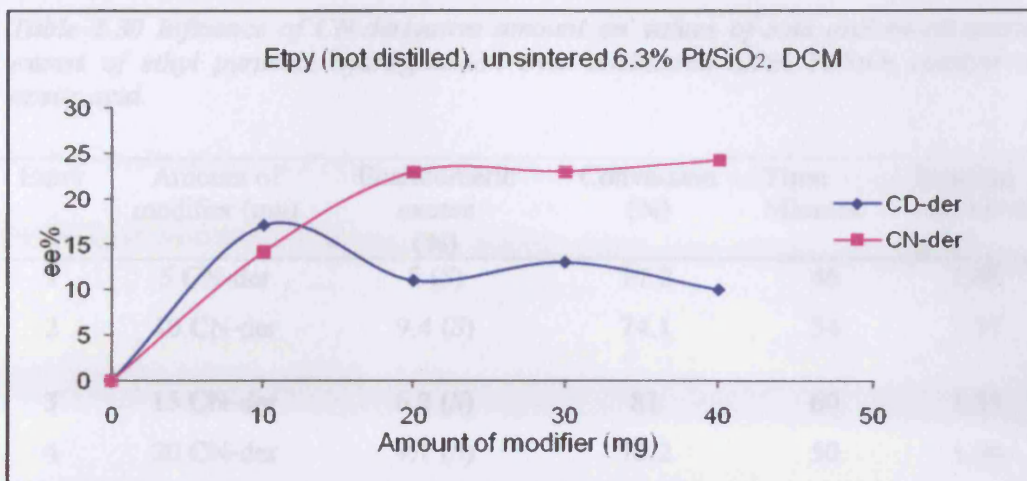


Figure 3.40 Enantiomeric excess versus amount of modifier (mg). Unsintered 6.3% Pt/silica catalyst in dichloromethane.

Table 3.30 shows *ee* and rate measurements in acetic acid /dichloromethane mixed solvent as a function of modifier amount and Figure 3.41 a graph of *ee* versus modifier amount. The most striking feature of Figure 3.41 in comparison with Figure 3.40 is the inversion of *ee* using CN-derivative and marked inversion in *ee* (to *R*-etlac) using CD-derivative. A similar effect was seen using 5% Pt/G (Figure 3.7) although, in that case, CN-derivative in acetic acid caused only a decrease in *ee* of etlac to  $\approx 5\%$  *R*, rather than inversion to *S*.



Table 3.30 Influence of CN-derivative amount on values of rate and enantiomeric excess of ethyl pyruvate hydrogenation over unsintered 6.3% Pt/SiO<sub>2</sub> catalyst in acetic acid.

Entry	Amount of modifier (mg)	Enantiomeric excess (%)	Conversion (%)	Time Minutes	Nominal rate/mmol g <sup>-1</sup> h <sup>-1</sup>
1	5 CN-der	5 (S)	77.2	46	1.68
2	10 CN-der	9.4 (S)	74.1	54	1.37
3	15 CN-der	6.2 (S)	81	60	1.35
4	20 CN-der	9.1 (S)	75.2	50	1.50
5	30 CN-der	3 (S)	81	58	1.40
6	40 CN-der	4 (S)	79.4	30	2.65

Hutchings *et al.*, [24] have suggested that there is a change in the conformation of the CD-derivative and CN-derivative as a function of both modifier solution concentration and *pH*. The change in the conformation of the chiral auxiliary is then thought to reflect a change in *ee*. However, in a recent paper by Baiker *et al.*, [4], it has been stated that the ether bond in the modifier undergoes hydrogenolysis in acetic acid under reaction conditions. Clearly, in the present context, this offers a simple explanation of previous findings in that CD and CN are being generated *in situ* from CD-derivative and CN-derivative such that, if the CD-derivative is in competition with CD for adsorption sites then clearly this will result in an apparent change in the sign of *ee*. Furthermore if the extent of hydrogenolysis was *pH* dependent or a function of the amount of CD-derivative added initially, one should expect interesting changes in *ee* to be observed in acetic acid since both species would be competing for surface sites. However, the low *ees* obtained here do not reflect the presence of CD and

CN since enantiomeric excesses should reach at least 60-70% using Pt/SiO<sub>2</sub> catalysts.

Table 3.31 Influence of CD-derivative amount on values of rate and enantiomeric excess of ethyl pyruvate hydrogenation over unsintered 6.3% Pt/SiO<sub>2</sub> catalyst in acetic acid.

Entry	Amount of modifier (mg)	Enantiomeric excess (%)	Conversion (%)	Time Minutes	Nominal rate/mmol g <sup>-1</sup> h <sup>-1</sup>
1	5 CD-der	31 (R)	79	52	1.51
2	10 CD-der	29 (R)	82	54	1.52
3	15 CD-der	34.1 (R)	77	40	1.93
4	20 CD-der	28 (R)	80	56	1.43
5	30 CD-der	31 (R)	76	36	2.11
6	40 CD-der	30.1 (R)	83	29	2.86

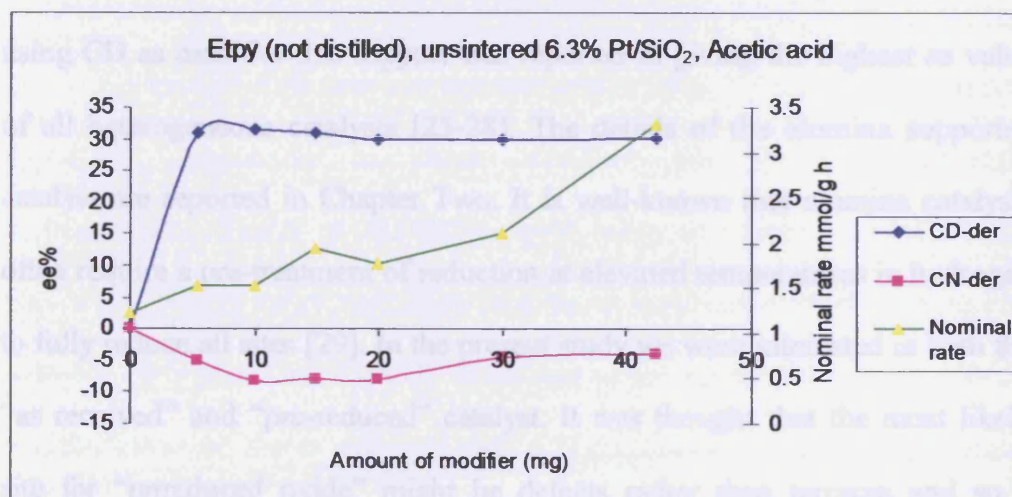


Figure 3.41 Enantiomeric excess and nominal rate versus amount of modifier (mg). Unsintered 6.3% Pt/silica catalyst in acetic acid.

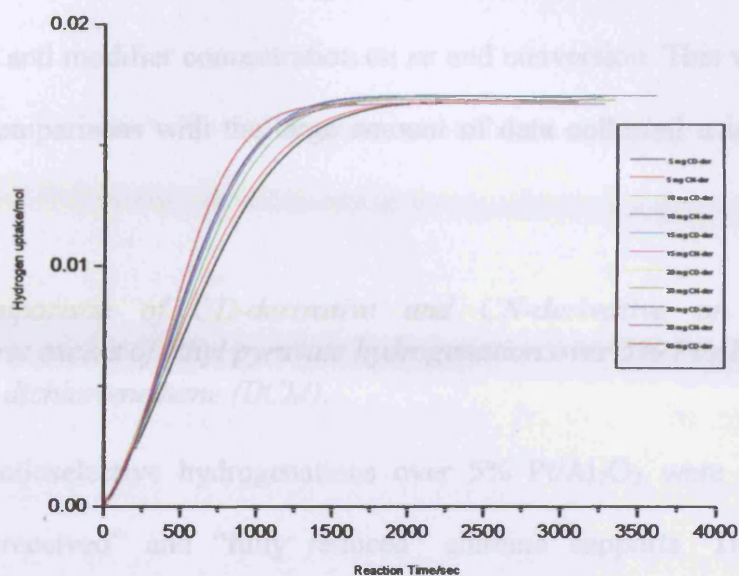


Figure 3.42 Hydrogen uptake curves versus time showing the rate of ethyl pyruvate hydrogenation over CD-derivative and CN-derivative modified unsintered 6.3% Pt/silica catalyst in acetic acid.

### 3.4 Enantioselective hydrogenation using 5% Pt/Al<sub>2</sub>O<sub>3</sub>

The third support to be investigated was alumina. In previous studies using CD as modifier this support was reported as giving the highest *ee* value of all heterogeneous catalysts [25-28]. The details of the alumina supported catalyst are reported in Chapter Two. It is well-known that alumina catalysts often require a pre-treatment of reduction at elevated temperatures in hydrogen to fully reduce all sites [29]. In the present study we were interested in both the “as received” and “pre-reduced” catalyst. It was thought that the most likely site for “unreduced oxide” might be defects rather than terraces and so a comparison between each might afford interesting differences. Of course both for alumina and silica supported catalysts (in previous section), it is not possible to perform CV measurements due to the non-conducting nature of

support. However, it was still thought important in this case to study bismuth adsorption and modifier concentration on *ee* and conversion. This was in order to make comparisons with the large amount of data collected using 5% Pt/G catalysts.

*3.4.1 Comparison of CD-derivative and CN-derivative on values of enantiomeric excess of ethyl pyruvate hydrogenation over 5% Pt/Al<sub>2</sub>O<sub>3</sub> catalyst at 300K in dichloromethane (DCM).*

Enantioselective hydrogenations over 5% Pt/Al<sub>2</sub>O<sub>3</sub> were carried out using “as-received” and “fully reduced” alumina supports. The standard reaction was the hydrogenation of 20 mmol of ethyl pyruvate in dichloromethane and acetic acid at 25°C under 35 bar H<sub>2</sub>. Catalyst, various concentrations of CD-derivative and CN-derivative modifiers and reactant were placed in the reaction vessel as described in section 2.4 for the hydrogenation of ethyl pyruvate in the liquid phase over a 5% Pt/Al<sub>2</sub>O<sub>3</sub> catalyst.

Tables 3.32-3.33 shows *ee* and conversion using CD-derivative and CN-derivative respectively as chiral modifiers for the enantioselective hydrogenation of etpy in dichloromethane using as received 5% Pt/Al<sub>2</sub>O<sub>3</sub>. Figure 3.43 shows the *ee* variations observed in graphical form. In comparison with 5% Pt/G and 3.6% Pt/SiO<sub>2</sub>, behaviour is as expected in that at optimal modifier amount, the *ee* obtained with CN-derivative is greater than that of CD-derivative (both giving excess of *R*-etlac). The results are commensurate with Pt/SiO<sub>2</sub> (Figure 3.40) including what appears to be a maximum at 5 mg of CD-derivative. Rates are reasonable with all reactions going to almost 100% completion.

In Tables 3.34-3.35 are listed *ee* and conversion data for the same reaction conditions but using an acetic acid/DCM mixed solvent. Again a familiar trend is observed (see for example Figure 3.2 and 3.41). Protonation of the modifier leads to an enhancement in the *ee* obtained using CD-derivative and a marked decrease in *ee* using CN-derivative. In contrast to Pt/SiO<sub>2</sub> however, the *ee* obtained with CN-derivative in acetic acid always gives rise to an excess of the *R*-enantiomer as found with 5% Pt/G. The maximum *ee* obtained using CD-derivative was 28% (Pt/SiO<sub>2</sub> ~ 32% and unsintered Pt/G 44%) so there does appear to be a significant influence of support on *ee*. The *ees* obtained with CN-derivative do not differ significantly as the support is varied (Pt/Al<sub>2</sub>O<sub>3</sub> ≈ 10% *R*, Pt/SiO<sub>2</sub> ≈ 10% *S* and Pt/G ≈ 12% *R*) although the Pt/SiO<sub>2</sub> result is exceptional.

Table 3.32 Influence of CD-derivative amount on values of enantiomeric excess of ethyl pyruvate hydrogenation over unsintered 5% Pt/Al<sub>2</sub>O<sub>3</sub> catalyst in dichloromethane (DCM).

Entry	Amount of modifier (mg)	Enantiomeric excess (ee) (%) (R)	Conversion (%)	Time Minutes	Nominal rate/mmol g <sup>-1</sup> h <sup>-1</sup>
1	5 CD-der	13	96	38	2.52
2	10 CD-der	10	80	117	0.68
3	15 CD-der	7	93	110	0.85
4	20 CD-der	8.2	84.3	102	0.83
5	30 CD-der	6	86	31	2.77
6	40 CD-der	6	91.1	121	0.75
7	50 CD-der	6.4	97	125	0.77

Table 3.33 Influence of CN-derivative amount on values of enantiomeric excess of ethyl pyruvate hydrogenation over unsintered 5% Pt/Al<sub>2</sub>O<sub>3</sub> catalyst in dichloromethane (DCM).

Entry	Amount of modifier (mg)	Enantiomeric excess (%) (R)	Conversion (%)	Time Minutes	Nominal rate/mmol g <sup>-1</sup> h <sup>-1</sup>
1	5 CN-der	13.4	99.1	150	0.66
2	10 CN-der	16.4	90.1	*	*
3	15 CN-der	18	93.2	121	0.77
4	20 CN-der	17	83.2	118	0.70
5	30 CN-der	18	94	123	0.76
6	40 CN-der	18	94	149	0.63
7	50 CN-der	19	91.2	117	0.78

\*- Possible leak on system for this data.

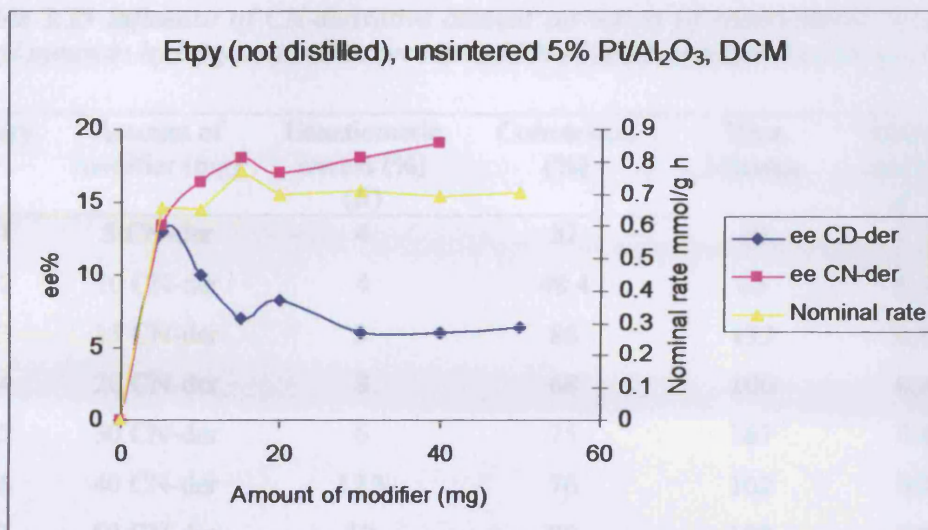


Figure 3.43 Enantiomeric excess in dichloromethane and nominal rate versus amount of modifier (mg). Unsintered 5% Pt/alumina catalyst.

Table 3.34 Influence of CD-derivative amount on values of enantiomeric excess of ethyl pyruvate hydrogenation over unsintered 5% Pt/Al<sub>2</sub>O<sub>3</sub> catalyst in acetic acid.

Entry	Amount of modifier (mg)	Enantiomeric excess (%) (R)	Conversion (%)	Time Minutes	Nominal rate/mmol g <sup>-1</sup> h <sup>-1</sup>
1	5 CD-der	24.3	60	121	0.50
2	10 CD-der	28	57	108	0.53
3	15 CD-der	26.4	55	118	0.47
4	20 CD-der	23.2	46	108	0.42
5	30 CD-der	26.1	82	135	0.61
6	40 CD-der	23	70	92	0.76
7	50 CD-der	21	65	88	0.74

Table 3.35 Influence of CN-derivative amount on values of enantiomeric excess of ethyl pyruvate hydrogenation over unsintered 5% Pt/Al<sub>2</sub>O<sub>3</sub> catalyst in acetic acid.

Entry	Amount of modifier (mg)	Enantiomeric excess (%) (R)	Conversion (%)	Time Minutes	Nominal rate/mmol g <sup>-1</sup> h <sup>-1</sup>
1	5 CN-der	4	37	50	0.74
2	10 CN-der	4	48.4	63	0.76
3	15 CN-der	3	88	133	0.66
4	20 CN-der	8	68	100	0.68
5	30 CN-der	6	75	167	0.45
6	40 CN-der	12.3	76	102	0.75
7	50 CN-der	12	80	108	0.74

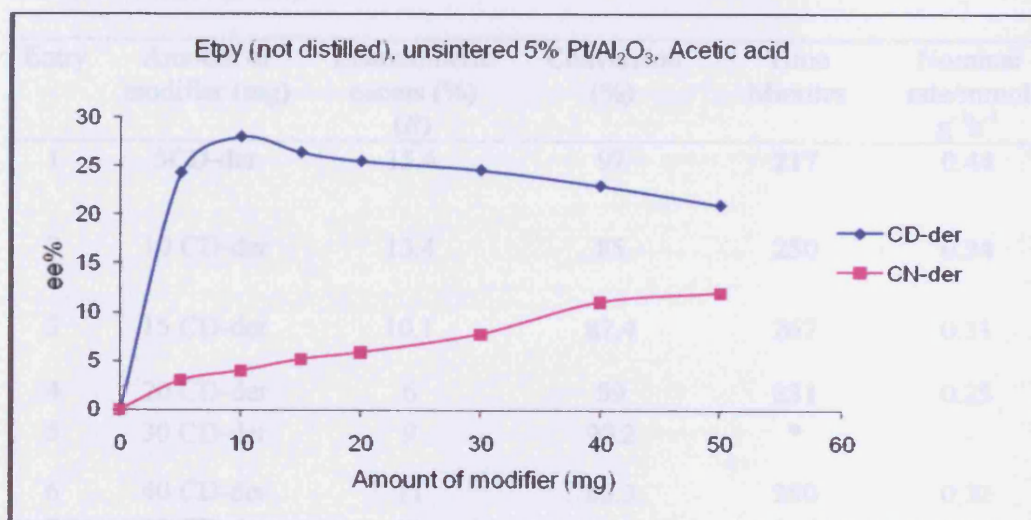


Figure 3.44 Enantiomeric excess in acetic acid versus amount of modifier (mg). Unsintered 5% Pt/alumina catalyst.



### 3.4.2 Comparison of CD-derivative and CN-derivative on values of enantiomeric excess of ethyl pyruvate hydrogenation over 5% Pt/Al<sub>2</sub>O<sub>3</sub> catalyst at 700K in acetic acid

In order to compare the properties of the “as received” and sintered Al<sub>2</sub>O<sub>3</sub> supported catalysts, experiments were performed on the fully reduced Pt/Al<sub>2</sub>O<sub>3</sub> (treated at 700K in hydrogen). It was hoped that any differences observed might be ascribed to the presence of tenaciously held metal oxides in the as-received catalyst. Their removal would be facilitated by heating in hydrogen. It was speculated that such oxides would be present at defect sites rather than terraces.

*Table 3.36 Influence of CD-derivative amount on values of enantiomeric excess of ethyl pyruvate hydrogenation over 5% Pt/Al<sub>2</sub>O<sub>3</sub> catalyst sintered at 700K in dichloromethane (DCM).*

Entry	Amount of modifier (mg)	Enantiomeric excess (%) ( <i>R</i> )	Conversion (%)	Time Minutes	Nominal rate/mmol g <sup>-1</sup> h <sup>-1</sup>
1	5CD-der	15.4	97	217	0.44
2	10 CD-der	13.4	85	250	0.34
3	15 CD-der	10.1	82.4	267	0.31
4	20 CD-der	6	59	231	0.25
5	30 CD-der	9	90.2	*	-
6	40 CD-der	11	80.3	250	0.32
7	50 CD-der	11	83.1	267	0.31

\*- Possible leak on system for this data.

- Not available.

Table 3.37 Influence of CN-derivative amount on values of enantiomeric excess of ethyl pyruvate hydrogenation over 5% Pt/Al<sub>2</sub>O<sub>3</sub> catalyst sintered at 700K in dichloromethane (DCM).

Entry	Amount of modifier (mg)	Enantiomeric excess (%) (R)	Conversion (%)	Time Minutes	Nominal rate/mmol g <sup>-1</sup> h <sup>-1</sup>
1	5 CN-der	10	91	267	0.34
2	10 CN-der	10	76	192	0.40
3	15 CN-der	11.3	94	163	0.58
4	20 CN-der	10.4	83	175	0.47
5	30 CN-der	13	76.3	133	0.57
6	40 CN-der	14	85.3	-	-
7	50 CN-der	14	82	208	0.39

-N.A = Not available.

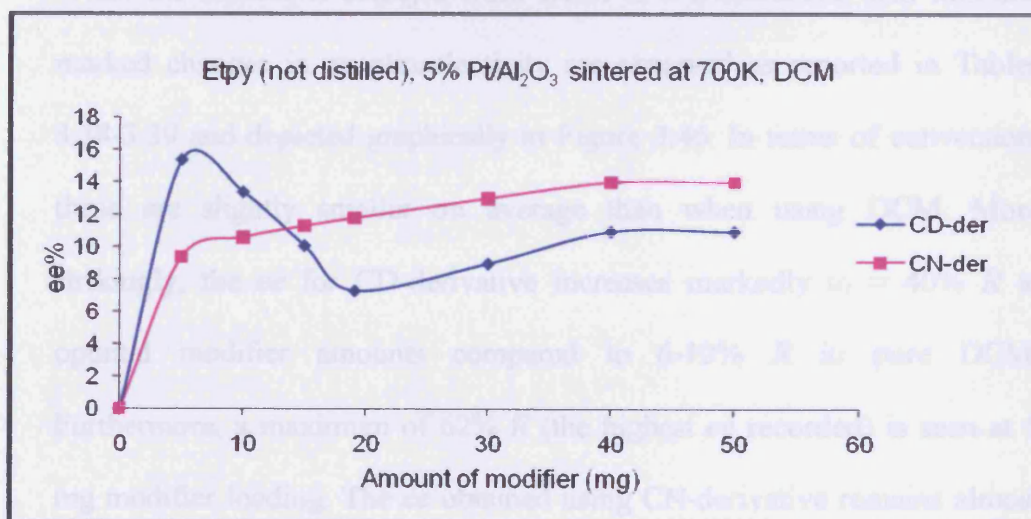


Figure 3.45 Enantiomeric excess in dichloromethane versus amount of modifier (mg). 5% Pt/alumina catalyst sintered at 700K.

Tables 3.36 and 3.37 list *ee* and conversion data for CD-derivative and CN-derivative respectively in DCM and Figure 3.45 shows how the *ee* in particular varies with modifier amount. In comparison with the results shown in Figure 3.43, the *ee* results in Figure 3.45 show that after heating in hydrogen the CN-derivative *ee* is decreased slightly from  $\approx 18\% R$  to  $\approx 11\% R$  and for CD-derivative, the *ee* is increased from  $\approx 6\% R$  to  $\approx 10\% R$ . The “maximum” at 5 mg of CD-derivative is still observed after heat treatment at 700K but instead of being 14% *R* in Figure 3.43 it is now 16.8% *R* in Figure 3.45. This is well-within experimental error so overall, in DCM only marginal changes have been observed although the *ee* using CN-derivative has been decreased. No significant changes in conversion were observed. When the solvent is changed from DCM to a DCM/acetic acid mixture, marked changes in enantioselectivity are observed as reported in Tables 3.38-3.39 and depicted graphically in Figure 3.46. In terms of conversion, these are slightly smaller on average than when using DCM. More strikingly, the *ee* for CD-derivative increases markedly to  $\approx 40\% R$  at optimal modifier amounts compared to 6-10% *R* in pure DCM. Furthermore, a maximum of 62% *R* (the highest *ee* recorded) is seen at 5 mg modifier loading. The *ee* obtained using CN-derivative remains almost unchanged upon annealing at 700K at just over 10% *R*.

*Table 3.38 Influence of CD-derivative amount on values of enantiomeric excess of ethyl pyruvate hydrogenation over 5% Pt/Al<sub>2</sub>O<sub>3</sub> catalyst sintered at 700K in acetic acid.*

Entry	Amount of modifier (mg)	Enantiomeric excess (%) (R)	Conversion (%)	Time Minutes	Nominal rate/mmol g <sup>-1</sup> h <sup>-1</sup>
1	5 CD-der	62	64	233	0.97
2	10 CD-der	43	85.2	142	0.50
3	15 CD-der	36.2	52.4	152	0.34
4	20 CD-der	45.1	54	213	0.25
5	30 CD-der	38	89	133	0.67
6	40 CD-der	38.4	77	125	0.62
7	50 CD-der	29	73	*	-

\*- Possible leak on system for this data.

- Not available.

*Table 3.39 Influence of CN-derivative amount on values of enantiomeric excess of ethyl pyruvate hydrogenation over 5% Pt/Al<sub>2</sub>O<sub>3</sub> catalyst sintered at 700K in acetic acid.*

Entry	Amount of modifier (mg)	Enantiomeric excess (%) (R)	Conversion (%)	Time Minutes	Nominal rate/mmol g <sup>-1</sup> h <sup>-1</sup>
1	5 CN-der	15	40	300	0.13
2	10 CN-der	9	71	217	0.33
3	15 CN-der	12	85	*	-
4	20 CN-der	12	94	185	0.51
5	30 CN-der	11.1	82	179	0.46
6	40 CN-der	5	56	250	0.22
7	50 CN-der	6	64.1	192	0.33

\*- Possible leak on system for this data.

- Not available.

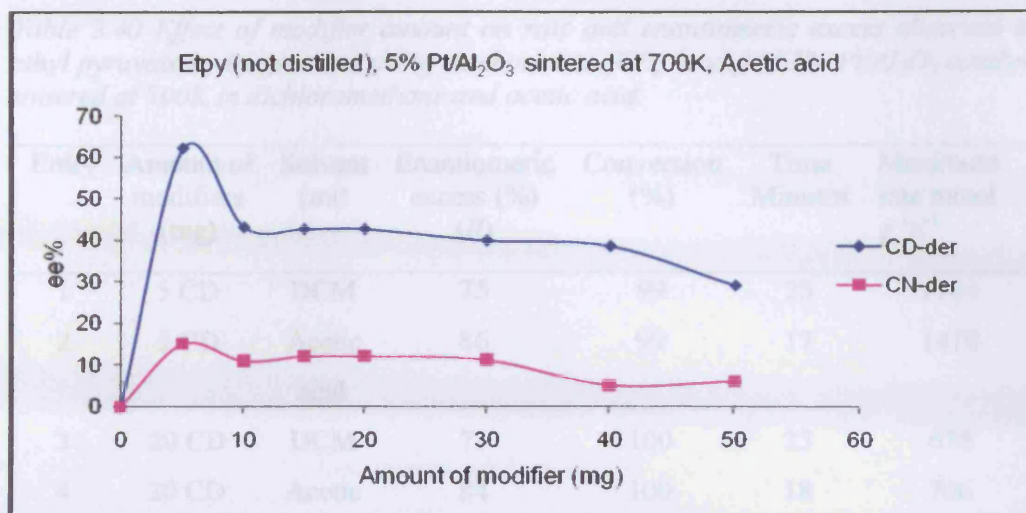


Figure 3.46 Enantiomeric excess in acetic acid versus amount of modifier (mg). 5% Pt/alumina catalyst sintered at 700K.

The exceptional results obtained using CD-derivative and CN-derivative with Pt/alumina catalysts prompted the re-examination of Pt/alumina but using CD and CN as modifiers. This experiment had never been performed at Cardiff and would make a good comparison with previous work on Pt/G and Pt/alumina using CD-derivative and CN-derivative. It is reported in the literature that Pt/alumina in acetic acid gives rise to the highest value of *ee* [30].

Table 3.40 Effect of modifier amount on rate and enantiomeric excess observed in ethyl pyruvate hydrogenation using cinchonidine (CD) modified 5% Pt/Al<sub>2</sub>O<sub>3</sub> catalyst sintered at 700K in dichloromethane and acetic acid.

Entry	Amount of modifiers (mg)	Solvent (ml)	Enantiomeric excess (%) ( <i>R</i> )	Conversion (%)	Time Minutes	Maximum rate mmol g <sup>-1</sup> h <sup>-1</sup>
1	5 CD	DCM	75	99	25	1764
2	5 CD	Acetic acid	86	99	17	1470
3	20 CD	DCM	73	100	23	678
4	20 CD	Acetic acid	84	100	18	706

Table 3.40 and Figure 3.47 show the effect of modifier concentration on the enantiomeric excess observed in ethyl pyruvate hydrogenation over cinchonidine (CD) modified 5% Pt/Al<sub>2</sub>O<sub>3</sub> catalyst sintered at 700K in dichloromethane and acetic acid. When hydrogenation is carried out with CD modified 5% Pt/Al<sub>2</sub>O<sub>3</sub> catalyst (entries 1-4), a high conversion and *ee* were obtained. The resulting hydrogen uptake profile is shown in Figure 3.48. The rate of the first stage is reported as 1764 mmol g<sup>-1</sup> h<sup>-1</sup> as shown in Table 3.40. The enantiomeric excess at 100% conversion was 84% (*R*) as shown in Figure 3.45.

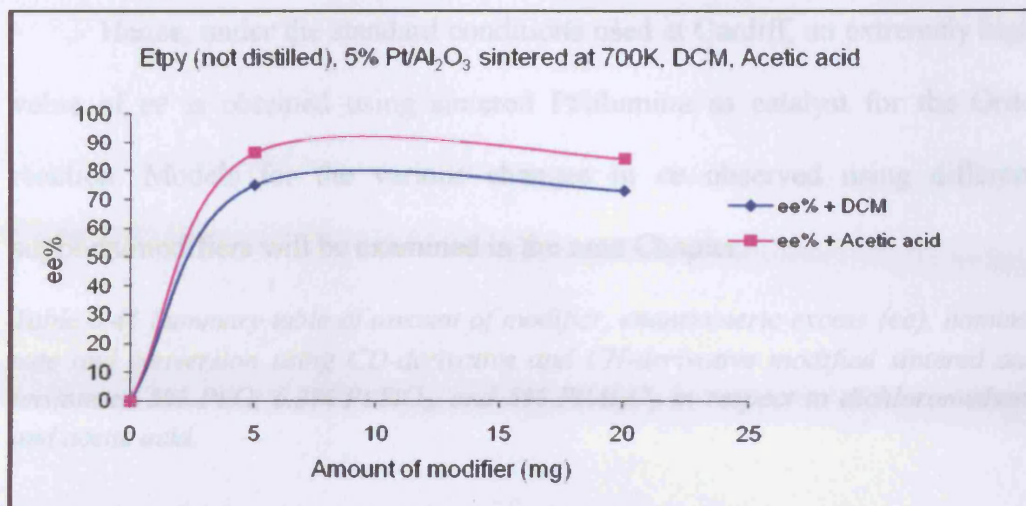


Figure 3.47 Enantiomeric excess in acetic acid and dichloromethane versus amount of modifier (mg). 5% Pt/alumina catalyst sintered at 700K.

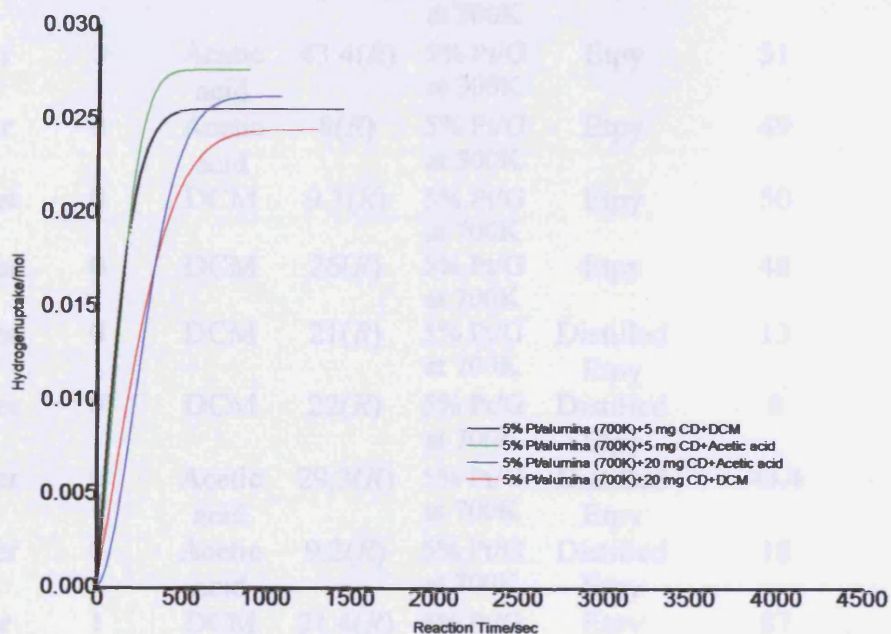


Figure 3.48 Hydrogen uptake curves versus time showing the rate of ethyl pyruvate hydrogenation over CD-modified 5% Pt/alumina catalyst sintered at 700K in dichloromethane and acetic acid.

Hence, under the standard conditions used at Cardiff, an extremely high value of *ee* is obtained using sintered Pt/alumina as catalyst for the Orito reaction. Models for the various changes in *ee* observed using different supports/modifiers will be examined in the next Chapter.

*Table 3.41 Summary table of amount of modifier, enantiomeric excess (ee), nominal rate and conversion using CD-derivative and CN-derivative modified sintered and unsintered 5% Pt/G, 6.3% Pt/SiO<sub>2</sub>, and 5% Pt/Al<sub>2</sub>O<sub>3</sub> in respect to dichloromethane and acetic acid.*

Modifier (mg)	Dosing volume Bi/cm <sup>3</sup>	Solvent (ml)	<i>ee</i> (%)	Catalyst (mg)	Substrate (mmol)	Conversion (%)	Nominal rate mmol/g h
2CD-der	0	DCM	8( <i>R</i> )	5% Pt/G at 300K	Etpy	93.3	1.12
2CN-der	0	DCM	26.2( <i>R</i> )	5% Pt/G at 300K	Etpy	100	0.69
5CD-der	0	Acetic acid	43.4( <i>R</i> )	5% Pt/G at 300K	Etpy	51	0.81
5CN-der	0	Acetic acid	8( <i>R</i> )	5% Pt/G at 300K	Etpy	49	0.62
10CD-der	0	DCM	9.3( <i>R</i> )	5% Pt/G at 700K	Etpy	50	0.63
10CN-der	0	DCM	26( <i>R</i> )	5% Pt/G at 700K	Etpy	48	1.04
30CD-der	0	DCM	21( <i>R</i> )	5% Pt/G at 700K	Distilled Etpy	13	0.23
30CN-der	0	DCM	22( <i>R</i> )	5% Pt/G at 700K	Distilled Etpy	8	0.32
30CD-der	0	Acetic acid	29.3( <i>R</i> )	5% Pt/G at 700K	Distilled Etpy	43.4	0.47
30CN-der	0	Acetic acid	9.2( <i>R</i> )	5% Pt/G at 700K	Distilled Etpy	18	0.55
5CD-der	1	DCM	21.4( <i>R</i> )	5% Pt/G at 300K	Etpy	87	0.87
5CN-der	1	DCM	27( <i>R</i> )	5% Pt/G at 300K	Etpy	90	1.67
15CD-der	50	DCM	2.3( <i>R</i> )	5% Pt/G at 300K	Etpy	97.1	2.10
15CN-ser	50	DCM	29( <i>R</i> )	5% Pt/G at 300K	Etpy	88	2.10
5CD-der	5	DCM	3.3( <i>S</i> )	5% Pt/G at 700K	Etpy	19	0.35



5CN-der	5	DCM	20(R)	5% Pt/G at 700K	Etpy	2	0.04
30CD-der	50	DCM	14(S)	5% Pt/G at 700K	Etpy	1.3	-
30CN-der	50	DCM	26.4(R)	5% Pt/G at 700K	Etpy	4	-
10CD-der	0	DCM	17.1(R)	6.3% Pt/SiO <sub>2</sub> at 300K	Etpy	100	1.72
10CN-der	0	DCM	14.2(R)	6.3% Pt/SiO <sub>2</sub> at 300K	Etpy	100	1.85
20CD-der	0	Acetic acid	28(R)	6.3% Pt/SiO <sub>2</sub> at 300K	Etpy	80	1.43
20CN-der	0	Acetic acid	9.1(S)	6.3% Pt/SiO <sub>2</sub> at 300K	Etpy	75.2	-
5CD-der	0	DCM	13(R)	5% Pt/Al <sub>2</sub> O <sub>3</sub> at 300K	Etpy	96	2.52
5CN-der	0	DCM	13.4(R)	5% Pt/Al <sub>2</sub> O <sub>3</sub> at 300K	Etpy	99.1	0.66
10CD-der	0	Acetic acid	28(R)	5% Pt/Al <sub>2</sub> O <sub>3</sub> at 300K	Etpy	57	0.53
10CN-der	0	Acetic acid	4(R)	5% Pt/Al <sub>2</sub> O <sub>3</sub> at 300K	Etpy	48.4	0.76
5CD-der	0	DCM	15.4(R)	5% Pt/Al <sub>2</sub> O <sub>3</sub> at 700K	Etpy	97	0.44
5CN-der	0	DCM	10(R)	5% Pt/Al <sub>2</sub> O <sub>3</sub> at 700K	Etpy	91	0.34
5CD-der	0	Acetic acid	62(R)	5% Pt/Al <sub>2</sub> O <sub>3</sub> at 700K	Etpy	64	0.27
5CN-der	0	Acetic acid	15(R)	5% Pt/Al <sub>2</sub> O <sub>3</sub> at 700K	Etpy	40	0.13

- Not available.

In Chapter Three, experimental data for the enantioselective hydrogenation of ethyl pyruvate under standard reaction conditions as a function of catalyst sintering, catalyst support, modifier type, modifier amount,

solvent (DCM and acetic acid) and also the influence of bismuth surface coverage and EP distillation was reported. That significant variation in both *ee* and rate as a function of these experimental parameters is observed (Table 3.41) supports the fact that Orito-type surface reactions are intrinsically complex. The aim of the next Chapter will be to delineate a number of trends that may lead to new insights into the behaviour of different chiral surface modifiers and more particularly, allow prediction of catalyst behaviour within a consistent model of enantiodifferentiation. The ultimate *ee* reached for Orito-type heterogeneous catalysis must be, according to most workers in the field (the exception being Margitfalvi and co-workers [30-32]) strongly surface structure dependent [3, 25, 33-36] and the convolution of rate at particular adsorption sites together with an intrinsic *ee* associated with individual adsorption sites is a guiding theme within the Cardiff group [2, 9, 37].

### 3.5 References

- [1] G.A. Attard, A.Ahmadi, J.Feliu, A. Rodes, *Langmuir*, **15** (1999) 2420.
- [2] D.J. Jenkins, A.M.S. Alabdulrahman, G.A. Attard, K.G. Griffin, P.Johnston, P.B. Wells, *J. Catal.*, **234** (2005) 230.
- [3] H.-U. Blaser, H.P. Jalett and J. Wiehl, *J. Mol. Catal.*, **68** (1991) 215.
- [4] M. von Arx, T. Mallat, and A. Baiker, *J. Catal.*, **202** (2001) 169.
- [5] X. Li, N.F. Dummer, R.L. Jenkins, R.P.K. Wells, P.B. Wells, D.J. Willock, S.H. Taylor, P. Johnston and G.J. Hutchings, *Catal. Lett.*, **96** (2004) 147.
- [6] T. Burgi and A. Baiker, *J. Am. Chem. Soc.*, **120** (1998) 12920.
- [7] M.V. Arx, T. Mallat, T. Bürgi, A. Baiker, *Chem. Eur. J.*, **8** (2002) 1430.
- [8] E. Herrero, V. Climent, J.M. Feliu, *Electrochem. Comm.*, **2** (2000) 636.
- [9] A.M.S. Alabdulrahman. Ph.D. Thesis, Cardiff University, 2007.
- [10] N.F. Dummer, R. Jenkins, X. Li, S.M. Bawaked, P. McMorn, A. Burrows, C.J. Kiely, R.P. K. Wells, D.J. Willock, G.J. Hutchings, *J. Catal.* **243** (2006) 165.
- [11] D.J. Jenkins. Ph.D. Thesis, Cardiff University, 2003.
- [12] G.A. Attard, D.J. Jenkins, O.A. Hazzazi, P.B. Wells, J.E. Gillies, K.G. Griffin, P. Johnston, *Catalysis in Application, Roy.Soc. Chem.*, (2003) 70.
- [13] J. Clavilier, K. El Achi, A. Rodes, *Chem. Phys.*, **141** (1990) 1.
- [14] B. Minder, T. Mallat, P. Skrabal, A. Baiker, *Catal. Lett.*, **29** (1994) 115.
- [15] H.-U. Blaser, A.P. Jalett, W. Lottenbach and M. Studer, *J. A. C. S.*, **122** (2000) 12675.

- [16] J.L. Margitfalvi, I. Kolosova, E. Tálás, S. Göbölös, *Appl. Catal. A: General*, **154** (1997) 1.
- [17] J. Sanabria-Chinchilla, H. Abe, F.J. DiSalvo, H.D. Abruña, *Surf. Sinc.*, **602** (2008) 1830.
- [18] G.A. Attard, A. Ahmadi, D.J. Jenkins, O.A. Hazzazi, P.B. Wells, K.G. Griffin, P. Johnston, J.E. Gillies, *Chem. Phys. Chem.*, **4** (2003) 123.
- [19] M. Price. Ph.D. Thesis, Cardiff University, 2000.
- [20] A. Baiker, H. Baris, M. Erbudak, F. Vanini., *Proc.- Int. Congr. Catal.*, **4** (1988) 1928.
- [21] Omar.A. Hazzazi. Ph.D. Thesis, Cardiff University, 2002.
- [22] J.W. Geus, P.B. Wells, *Appl. Catal.*, **18** (1985) 231.
- [23] J.A. Slipszenko, S.P. Griffiths, P. Johnston, K.E. Simons, W.A.H. Vermeer and P.B. Wells, *J. Catal.* **179** (1998) 267.
- [24] R.L. Jenkins, N.F. Dummer, X.Li, S.M. Bawaked, P. McMorn., R.P.K. Wells, A. Burrows, J.C. Kiely, G.J. Hutchings, *Catal. Lett.*, **110** (2006) 135.
- [25] A. Baiker, *J. Mol. Catal. A*, **163** (2000) 205.
- [26] H.-U. Blaser, J.P. Jalett, M. Müller and M. Studer, *Catal. Today*, **37** (1997) 441.
- [27] P.B. Wells and A.G. Wilkinson, *Top. Catal.*, **5** (1998) 39.
- [28] M. von Arx, T. Mallat and A. Baiker, *Top. Catal.*, **19** (2002) 75.
- [29] X. Li, R.P. K, P.B. Wells, G.J. Hutchings, *Catal. Lett.*, **89** (2003) 163.
- [30] J.L. Margifalvi and M. Hegedüs, *J. Mol. Catal. A: Chem.*, **107** (1996) 281.

- [31] J.L. Margitfalvi and E. Tfirst, *J. Mol. Catal. A*, **139** (1999) 81.
- [32] J.L. Margitfalvi, M. Hegedüs and E. Tfirst, *Stud. Surf. Sci. Catal.*, **101A** (1996) 241.
- [33] A. Baiker, *J. Mol. Catal. A: Chemical*, **155** (1997) 473.
- [34] H.-U. Blaser, *Chem. Commun.*, (2003) 293.
- [35] M. Bartók, K. Felföldi, G. Szöllösi and T. Bartók, *Catal. Lett.*, **61** (1999) 1.
- [36] M. Bartók, K. Felföldi, B. Török and T. Bartók, *Chem. Commun.*, **2605** (1998).
- [37] D.J. Watson. Ph.D. Thesis, Cardiff University, 2003.

**CHAPTER FOUR**  
**DISCUSSION**

## 4.1 Introduction

In what follows, interpretation of the experimental data presented in Chapter Three will be expounded based on ideas concerning differential adsorption at different sites. Cyclic voltammetry in particular has allowed for detailed scrutiny of catalyst adsorption sites giving rise to enantioselectivity and therefore, new insights into structure-selectivity relationships.

## 4.2 The structural reaction model used to interpret *ee* changes

A model is proposed to interpret the variations in *ee* reported in Chapter Three based on a number of assumptions listed below. Each assumption has been justified from inspection of the experimental data and these justifications will be given subsequently. Two cases are considered: reaction of individual platinum adsorption sites in DCM and reaction in the presence of acetic acid.

### 4.2.1 Reaction in DCM of CD-derivative and CN-derivative

- i. CD-der adsorption at steps/defects gives excess of *R*-etlac at around 40% *ee*.
- ii. CD-der adsorption at Pt{111} terraces gives *S*-excess of etlac at around 40% *ee*.
- iii. CN-der adsorption at steps/defects gives excess of *S*-etlac but with low *ee*.
- iv. CN-der adsorption at Pt{111} terraces gives excess of *R*-etlac at medium *ee* (10% < *ee* < 40%).

4.2.2 Reaction in DCM of CD and CN

- i. CD adsorption at steps gives rise to excess of *R*-etilac with high *ee* (>70%).
- ii. CD adsorption at Pt{111} terraces gives rise to excess of *R*-etilac with medium *ee* (20% < *ee* < 40%).
- iii. CN adsorption at steps gives rise to excess *S*-etilac with high *ee* (>70%).
- iv. CN adsorption at Pt{111} terraces gives rise to *S*-etilac excess with medium *ee* (20% < *ee* < 40%).

4.2.3 Reaction in the presence of acetic acid of CD-derivative and CN-derivative

- i. [HCD-der]<sup>+</sup> adsorption at steps gives excess *R*-etilac at around 40% *ee*.
- ii. [HCD-der]<sup>+</sup> adsorption at Pt{111} terraces gives excess *S*-etilac at low *ee* (around 10% *ee* or less).
- iii. [HCN-der]<sup>+</sup> adsorption at steps gives low excess of *S*-etilac at around 10% *ee*.
- iv. [HCN-der]<sup>+</sup> adsorption at Pt{111} terraces gives excess of *R*-etilac at low *ee* (again around 0% *ee* or less).



#### 4.2.4 Reaction in presence of acetic acid of CD and CN

- i.  $[\text{HCD}]^+$  adsorption at steps gives excess of *R*-etlac at high *ee* (> 70%).
- ii.  $[\text{HCD}]^+$  adsorption at Pt{111} terraces gives excess *R*-etlac at very low *ee* (around 0%-5% *ee*).
- iii.  $[\text{HCN}]^+$  adsorption at steps gives excess of *S*-etlac at high *ee* (>70%).
- iv.  $[\text{HCN}]^+$  adsorption at Pt{111} terraces gives excess *S*-etlac at very low *ee* (around 0%-5% *ee*).

#### 4.2.5 Model justification

##### 4.2.5.1 Justification of assumptions listed in 4.2.2 and 4.2.4

Previous work using bismuth modified supported platinum catalysts [1-2] had demonstrated that there was a direct correlation between the filling of step/defect Pt adsorption sites and the fall in *ee* obtained in DCM/CD for EP hydrogenation under standard conditions. The very gradual fall in *ee* upon further loading of bismuth adatoms leading to the blocking of Pt{111} terrace sites (reported in references [1-2]) was ascribed to enantioselective hydrogenation occurring at Pt{111} terraces in DCM with an overall, maximum *ee* of between 20% and 40%.

Unpublished work by the Cardiff group has also demonstrated a similar enantioselectivity trend using CN as modifier as a function of Bi loading [3]. Hence, the assumption listed in 4.2.2 may be asserted on the basis of previous site-blocking experiments. The magnitude of the maximum *ee* obtainable from

Pt{111} terraces has been shown to be a strong function of the terrace width with large terrace widths (at least 8 atoms wide based on the intensity of the Pt{111} CV contributions) giving rise to an *ee* value of 40% [1]. The most interesting results concerning CD and CN however are found when the same bismuth site-blocking experiment is repeated in acetic acid containing solvents. From figure 3.36, it is evident that the *ee* obtainable from the Pt{111} terraces of the catalyst is now much lower than before with an overall *ee* close to 0% being exhibited. This means that the protonated versions of CN and CD appear unable to induce any sort of enantiodiscrimination when adsorbed on Pt{111} terraces. This suggests that the CD adsorbed at different Pt sites is sensitive to the nature of the activation process on the keto-group of EP. In the Baiker model [4], a key assumption is that it is the protonated tertiary nitrogen of the CD, acting as an electrophile that leads to hydrogen bonding to the activated carbonyl group of EP.

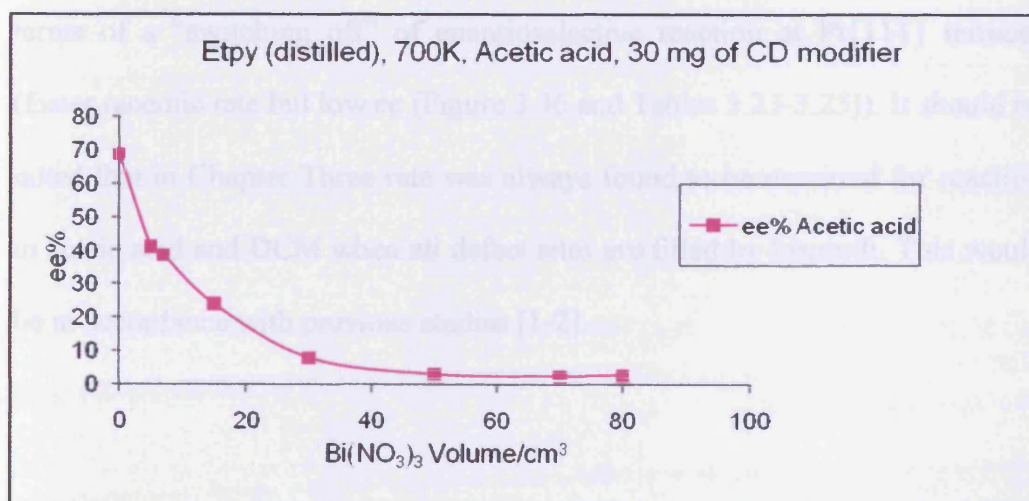


Figure 3.36 Enantiomeric excess in acetic acid versus various concentration of bismuth with (CD-modified 5% Pt/ G catalyst sintered twice at 700K.

Clearly, from the present results, on Pt{111} terraces at least, this cannot be the activating, enantiodifferentiating step since no *ee* should result. Recent work using high resolution NMR by Bartok studied the solution phase complexation between EP and CD and ketopantalactone (KPL) and CD [5]. The data suggested strongly that a nucleophilic interaction leading to enantiodifferentiation is taking place *via* the unprotonated lone pair of the tertiary nitrogen of the quinuclidine and the activated carbonyl of EP.

The present study suggests a phenomenon somewhat more complex. Nucleophilic interactions may well be leading to enantiodifferentiation at terraces (see previous DCM [1-2] and acetic acid results in Figure 3.36) but for step sites, protonation of CD does not appear to be detrimental to the overall *ee*. In fact slightly higher *ee* (but lower rate) is found both in the present work and previous studies [6-9]. An explanation for the slightly higher *ee* observed for EP hydrogenation in acetic acid relative to DCM may now be put forward in terms of a “switching off” of enantioselective reaction at Pt{111} terraces (faster racemic rate but low *ee* (Figure 3.36 and Tables 3.23-3.25)). It should be noted that in Chapter Three rate was always found to be maximal for reaction in acetic acid and DCM when all defect sites are filled by bismuth. This would be in accordance with previous studies [1-2].

#### 4.2.5.2 Assumptions 4.2.1 and 4.2.3

Inspection of Figures 3.26 and 3.27 show that when all step/defect sites are blocked by bismuth, for CD-derivative and CN-derivative in DCM, the enantioselective excesses in etlac obtained from vacant Pt{111} sites are approximately 32% *R*- and 40% *S*-respectively. Hence, assumption ii) of 4.2.1 is justified and to some extent assumption iv). However, unlike for CD and CN, CN-derivative and CD-derivative give rise to an increase in *ee* as step/defect sites are blocked. The only possible rationalization of this behaviour is that *CN-derivative and CD-derivative give rise to opposite enantioselective excesses when adsorbed at terrace and defect sites*. The reasons for such a change will be explored later. Hence, for catalyst surfaces free of bismuth and assuming equal rates of hydrogenation at all sites, the overall *ee* measured must reflect the balance of adsorption of modifier at step and terrace sites. Therefore, in the case of CD-derivative in DCM, the very low value of *ee* (0% *ee*) at clean Pt indicates that step/defect sites afford an *ee* of approximately 40% *ee* in *R*-etlac (assumption i) of 4.2.1). If CN-derivative behaviour in Figures 3.26 and 3.27 is now considered, a somewhat different interpretation may be formulated. Indeed, it must still be the case that CN-derivative adsorption at step/defect sites affords an *ee* of opposite sense to adsorption at terraces since when these sites are blocked by bismuth, the overall *ee* increases. However, the magnitude of this increase is much smaller than for CD-derivative and moreover, even for clean Pt surface free of bismuth, an *ee* of 25% *R*- is observed indicating that the terrace contribution is “winning out” over the step/defect. Hence, in estimating

the *ee* being generated at step/defect sites by adsorption of CN-derivative, it is asserted that this must be significantly less than the magnitude of the *ee* being generated by CD-derivative adsorbed at step/defect sites. Hence, assumption iii) of 4.2.1 is justified.

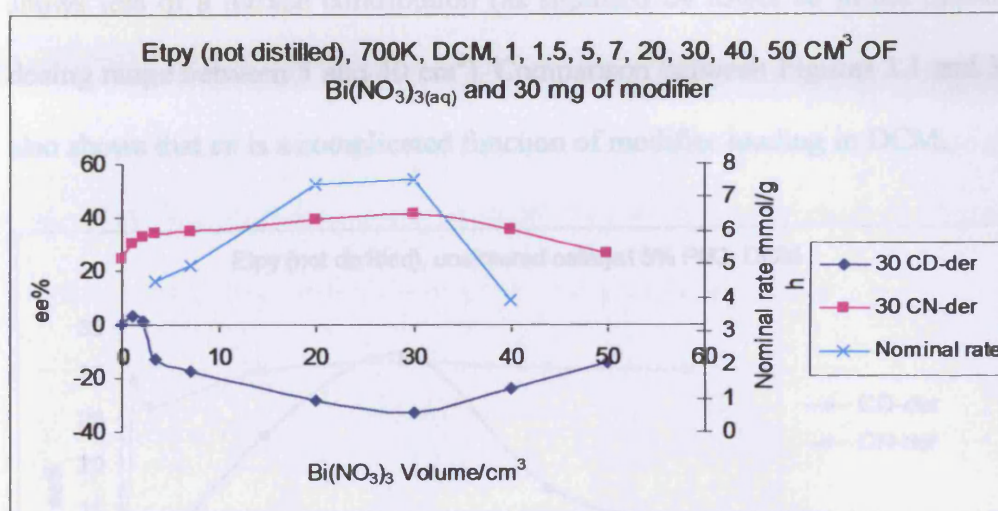


Figure 3.26 Adsorption of Bi on 5% Pt/G catalyst sintered at 700K and enantiomeric excess at 30 mg of modifier 1, 1.5, 5, 7, 20, 30, 40 and 50 ml of Bi solution. The variation in nominal rate is also depicted.

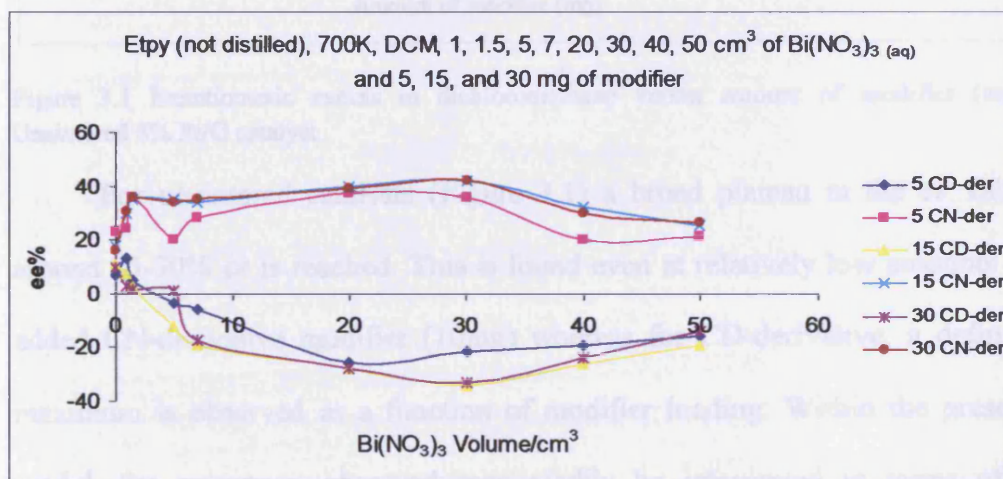


Figure 3.27 Enantiomeric excess in dichloromethane versus various concentration of bismuth with (CD-derivative and CN-derivative) modified 5% Pt/ G catalyst sintered at 700K.

The present discussion refers to an optimal loading of modifier of typically 15-30mg in all experiments (see Figures 3.26 and 3.27). However, evidence for slight variations from these trends at low alkaloid loadings (5mg) may be gleaned from Figure 3.27 whereby the lower loading consistently shows less of a terrace contribution (as signified by lower *ee* in the bismuth dosing range between 5 and 40 cm<sup>3</sup>). Comparison between Figures 3.1 and 3.5 also shows that *ee* is a complicated function of modifier loading in DCM.

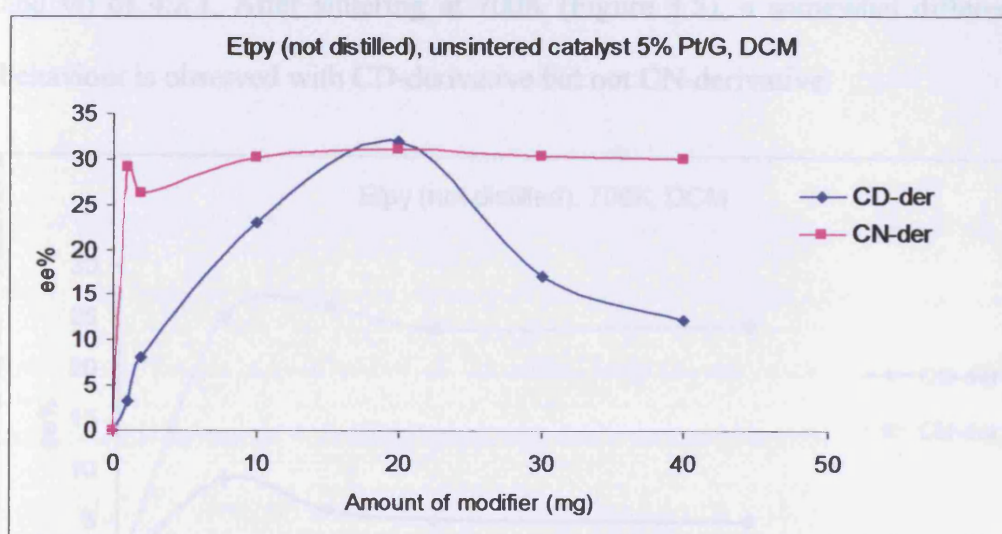


Figure 3.1 Enantiomeric excess in dichloromethane versus amount of modifier (mg). Unsintered 5% Pt/G catalyst.

For unsintered catalysts (Figure 3.1) a broad plateau in the *ee* value around 25-30% *ee* is reached. This is found even at relatively low amounts of added CN-derivative modifier (10mg) whereas for CD-derivative, a definite maximum is observed as a function of modifier loading. Within the present model, the maximum observed may readily be interpreted in terms of a preference for CD-derivative to adsorb at step sites initially, followed by subsequent population of terraces at greater modifier concentrations. This

behaviour was also speculated to be occurring in the study by Hutchings *et al* using the same CD-derivative and CN-derivative modifiers [10]. For CN-derivative, the low *ee* exhibited for step adsorption has already been noted and clearly the value of *ee* observed in this case may be attributed to a dominance of control over *ee* at terraces even though step sites may also be being occupied by CN-derivative at the same time. Hence, even a small amount of adsorption at terraces should lead to an *ee* corresponding to *R*-excess by assumption iii) and vi) of 4.2.1. After sintering at 700K (Figure 3.5), a somewhat different behaviour is observed with CD-derivative but not CN-derivative.

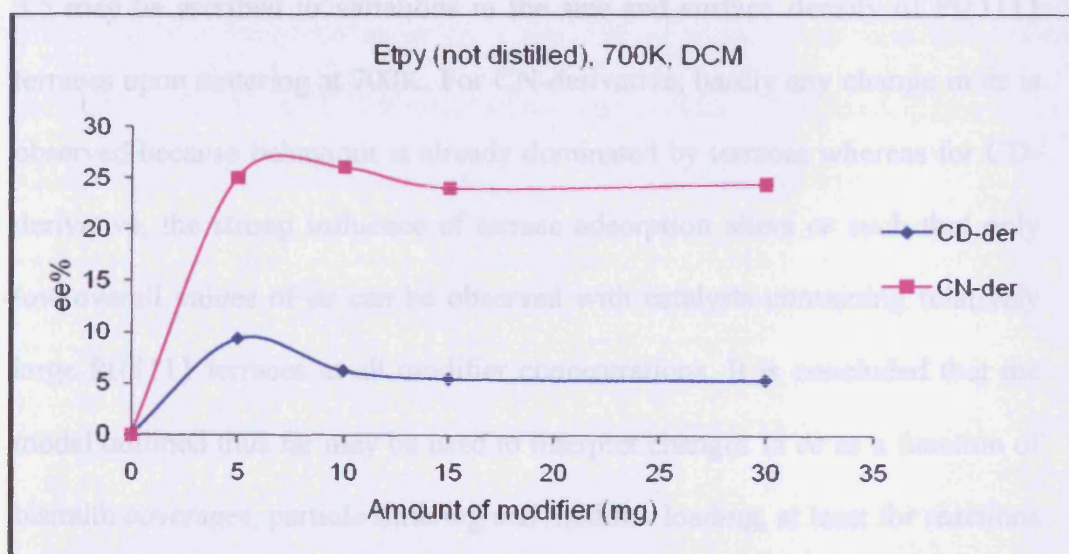


Figure 3.5 Enantiomeric excess in dichloromethane versus amount of modifier (mg). Pt/G catalyst sintered at 700K.

So for CN-derivative, the overall *ee* is decreased by perhaps 1-2% but the trend observed of a plateau being reached at low modifier loadings is still reproduced again signifying the greater contribution to overall *ee* from terraces in this case even though step sites may also be being occupied. For CD-derivative, the maximum seen in Figure 3.1 is now no longer observed and

instead a plateau in  $ee$  is reached at low modifier coverage which corresponds to a significant decrease in  $ee$  relative to the unsintered catalyst. In order for this behaviour to be rationalized within the present model, a much greater contribution from CD-derivative adsorbed on terraces must be occurring when the catalyst is sintered. From previous studies [1, 11] and the present work, the increase in the average Pt{111} terrace width upon sintering 5% Pt/graphite catalysts is well-established associated with a shift to more negative potentials of the "Pt{111}" electrosorption peak at 0.5V(Pd/H) together with an increase in Pt{111} peak magnitude. Hence, the differences reported in Figures 3.1 and 3.5 may be ascribed to variations in the size and surface density of Pt{111} terraces upon sintering at 700K. For CN-derivative, hardly any change in  $ee$  is observed because behaviour is already dominated by terraces whereas for CD-derivative, the strong influence of terrace adsorption alters  $ee$  such that only low overall values of  $ee$  can be observed with catalysts containing relatively large Pt{111} terraces at all modifier concentrations. It is concluded that the model outlined thus far may be used to interpret changes in  $ee$  as a function of bismuth coverages, particle sintering and modifier loading, at least for reactions occurring in DCM. For interactions of CD-derivative and CN-derivative with etpy/catalyst in acetic acid containing solvents, the extension of the model is more difficult because no measurements could be performed on bismuthated catalysts due to both time and material constraints (the batch of 5% Pt/G catalyst used throughout the study was completely consumed and a fresh batch could not be obtained from Johnson Matthey). Hence, a definitive value of  $ee$



in acetic acid for CD-derivative and CN-derivative modifiers adsorbed on Pt{111} terraces (by selectively adsorbing bismuth) was not obtained. In spite of this, it is possible to piece together the most likely contributions by step/defect and terrace sites to overall *ee* by inspection of data taken in DCM and then subsequently repeated in DCM/acetic acid. In particular, a simple interpretation of these variations is obtained if a similar assumption of low, but non-zero *ee* for protonated modifiers adsorbed on Pt{111} sites is made as for the cases of CD and CN.

From a comparison between Figures 3.1 and 3.2 for unsintered catalyst, it is seen that the trend in *ee* as a function of modifier amount for CD-derivative in DCM and DCM/acetic acid is very similar with a gradual increase in overall *ee* to the *R*-etlac enantiomer up to 20mg of CD-derivative.

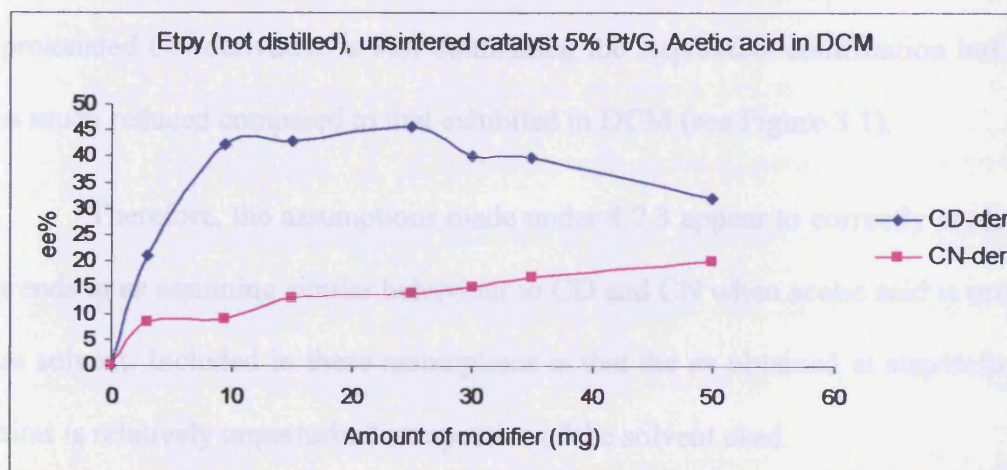


Figure 3.2 Enantiomeric excess versus amount of modifier (mg). Unsintered 5% Pt/G in acetic acid and dichloromethane mixture.

The differences however occur at higher modifier amounts whereby in DCM this was assumed to correspond to greater occupation of terraces relative

to step/defect sites leading to a marked maximum. In the presence of acetic acid, although the maximum is present, it is much less well marked with only a very small decrease of some 5-7% *ee* at highest modifier amounts (50mg). This would be entirely consistent with a much lower *ee* contribution from Pt{111} terraces occupied by protonated CD-derivative modifiers. The slight increase in *ee* at the maximum from 30% *ee* (Figure 3.1) to 40% *R*-(Figure 3.2) up to 20mg of modifier added would also be explicable within a model of low *ee* for protonated CD-derivative on Pt{111} terraces as found with CN and CD. In contrast, because CN-derivative on Pt{111} is also predicted to give rise to similar behaviour, a marked decrease in overall *ee* is to be expected for CN-derivative in the presence of acetic acid (much lower terrace contribution to overall *ee*). From Figure 3.2, this is precisely what one observes. That a low *R*-excess is still observed means that the *ee* derived from adsorption on terraces of protonated CN-derivative is still dominating the step/defect contribution but it is much reduced compared to that exhibited in DCM (see Figure 3.1).

Therefore, the assumptions made under 4.2.3 appear to correctly predict trends in *ee* assuming similar behaviour to CD and CN when acetic acid is used as solvent. Included in these assumptions is that the *ee* obtained at step/defect sites is relatively unperturbed irrespective of the solvent used.

## 4.2.6 The impact of EP distillation on enantiomeric excess

From comparison between Figures 3.5 and 3.6, it is evident that there was a significant change in the enantiomeric excess using distilled EP instead of as-received EP.

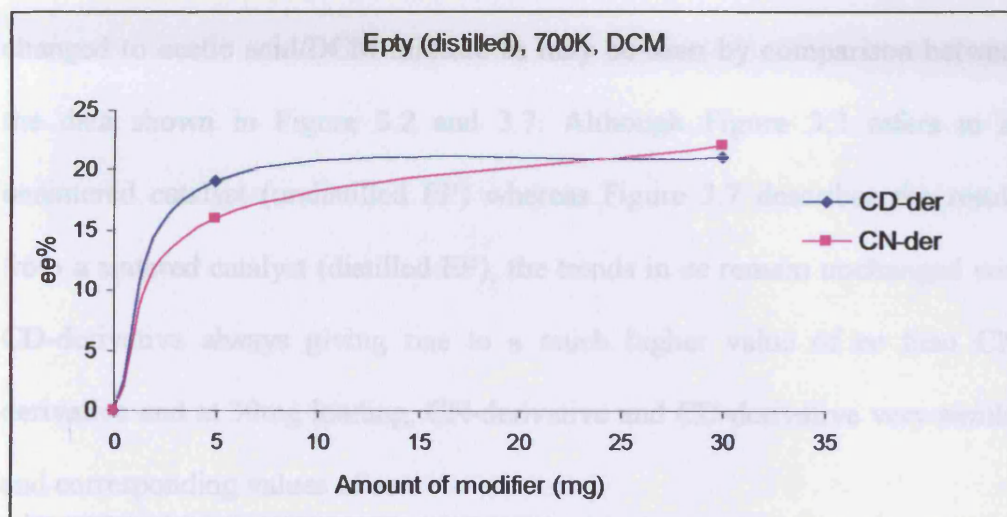


Figure 3.6 Enantiomeric excess in dichloromethane versus amount of modifier (mg). 5% Pt/G catalyst sintered at 700K.

For CD-derivative, an increase in *ee* from 5% to 20% *R*-etlac is observed after distillation of the substrate with all other parameters remaining constant (DCM solvent, catalyst sintered at 700K, identical reaction pressure, catalyst loading and EP concentration). Within the present model of enantioselectivity, an increase in *ee* for CD-derivative in DCM would mean that a greater influence of CD-derivative at steps was occurring. Since, it is known that impurities present in undistilled EP such as dimeric, aldol and other condensation products may form [4, 12], it is speculated that for freshly distilled EP, the concentration of such impurities is much reduced and they are no longer adsorbing at step/defect sites in competition with CD-derivative

leading to a lower overall *ee*. In a similar way, the *ee* from CN-derivative going down slightly from 25% to 20% would also be consistent with a “freeing-up” of more step sites for distilled EP since a greater step/defect contribution should give rise to an excess of *S*-etlac according to assumption 4.2.1 iii). However, the effect described above is not observed when the solvent is changed to acetic acid/DCM mixture as may be seen by comparison between the data shown in Figure 3.2 and 3.7. Although Figure 3.2 refers to an unsintered catalyst (undistilled EP) whereas Figure 3.7 describes the results from a sintered catalyst (distilled EP), the trends in *ee* remain unchanged with CD-derivative always giving rise to a much higher value of *ee* than CN-derivative and at 30mg loading, CN-derivative and CD-derivative very similar and corresponding values of *ee*.

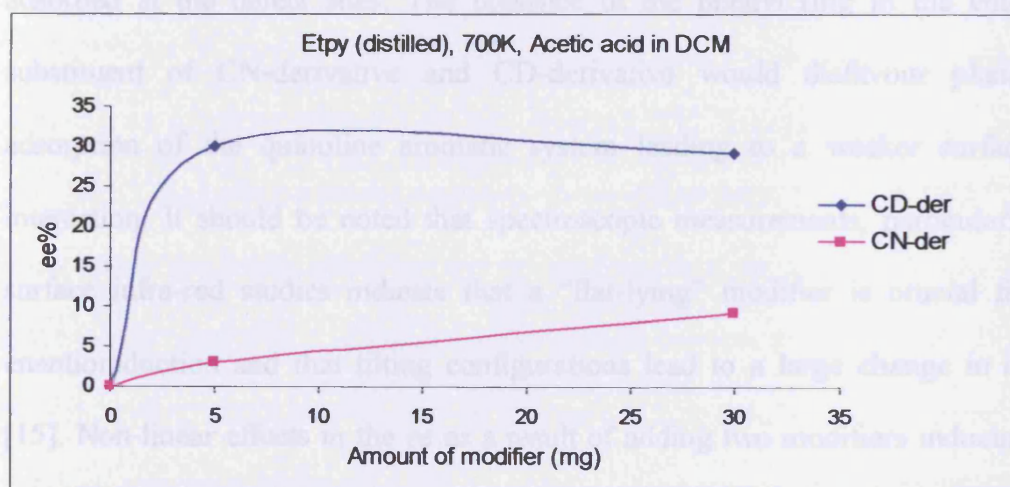


Figure 3.7 Enantiomeric excess in acetic acid versus amount of modifier (mg). Pt/G catalyst sintered at 700K.

Hence, even if there were impurities present in the as-received EP, the action of acetic acid is to inhibit their influence on the overall *ee*. The reasons

for this could be that the presence of acid inhibits the formation of further dimeric product *in situ* that would normally form due to base catalysed (alkaloid) dimerisation [13, 14]. It may also be that the protonated version of the alkaloid modifier competes for platinum sites more successfully with these impurities, irrespective of whether or not they were there initially (undistilled) or formed *in situ*. According to Baiker, base-catalysed EP dimer formation is completely inhibited in acetic acid due to protonation of the nucleophilic quinuclidine nitrogen atom [13]. Although distillation of EP had no effect on *ee* when the modifiers CD and CN were used [1], there is evidently an influence when CD-derivative and CN-derivative are used. It is speculated that CD and CN adsorb more strongly than CD-derivative and CN-derivative at platinum surfaces and can therefore readily displace any small amounts of impurity adsorbed at the defect sites. The presence of the phenyl ring in the ether substituent of CN-derivative and CD-derivative would disfavour planar adsorption of the quinoline aromatic system leading to a weaker surface interaction. It should be noted that spectroscopic measurements, particularly surface infra-red studies indicate that a “flat-lying” modifier is crucial for enantioinduction and that tilting configurations lead to a large change in *ee* [15]. Non-linear effects in the *ee* as a result of adding two modifiers inducing opposite enantiodifferentiation also support the contention that the presence of a phenyl-ether substituent to CD strongly inhibits adsorption [16, 17].

The present discussion does not detract from the majority of the findings reported in this thesis using as-received EP since the model that has been

developed to interpret *ee* readily explains all of the experimental data. However, in retrospect, because of the assumed weakness of the surface-modifier interaction in the case of CD-derivative and CN-derivative relative to CD and CN, it would have been best to use freshly distilled EP in all measurements.

#### 4.2.7 Particle size effects

In addition to 5% Pt/G catalysts, 0.5% and 3% Pt/G catalysts were also investigated. The influence of particle size, metal loading and solvent effects in relation to changes in *ee* were examined as a result of changing metal loading (and consequently particle size). It was concluded that only marginal changes in *ee* were found as a function of particle size with the decrease in overall *ee* being observed for the 0.5% Pt/G catalyst relative to the other two catalyst. This behaviour was consistent with previous studies in which a weak dependence of *ee* on particle size was reported [18]. In addition, acetic acid was found to provide superior *ee* values compared to those found in DCM. It was notable that both conversion and *ee* was low when the 0.5% Pt/G catalyst was sintered at 700K and reacted in DCM. An interpretation of this result would be that although the average Pt particle size would almost certainly increase as a result of sintering, the overall Pt surface area of the catalyst would decrease. It has been noted previously [11] that a collapse in conversion often results for low surface area catalysts (for example 5% Pt/G sintered at 1000K [11]) and in order to compensate for this effect, more catalyst needed to be added in order to obtain reasonable conversion. It is speculated therefore that

there is some sort of mass transport limit associate with low surface area of catalyst in the Cardiff high pressure reactor and when this phenomenon is observed, mass compensation (addition of large amounts of catalyst) should be employed.

#### *4.2.8 Variation of catalyst support*

For Orito-type catalysis, there is ample evidence in the literature of a strong influence of the support on *ee* [6, 19]. In the present study, for the first time this effect is examined in relation to catalyst modification using CD-derivative and CN-derivative as chiral auxiliaries.

## 4.2.8.1 Pt/Silica

From Figure 3.40, the variation of  $ee$  with modifier amount for a Pt/silica catalyst in DCM follows closely the behaviour exhibited by unsintered Pt/G (Figure 3.1).

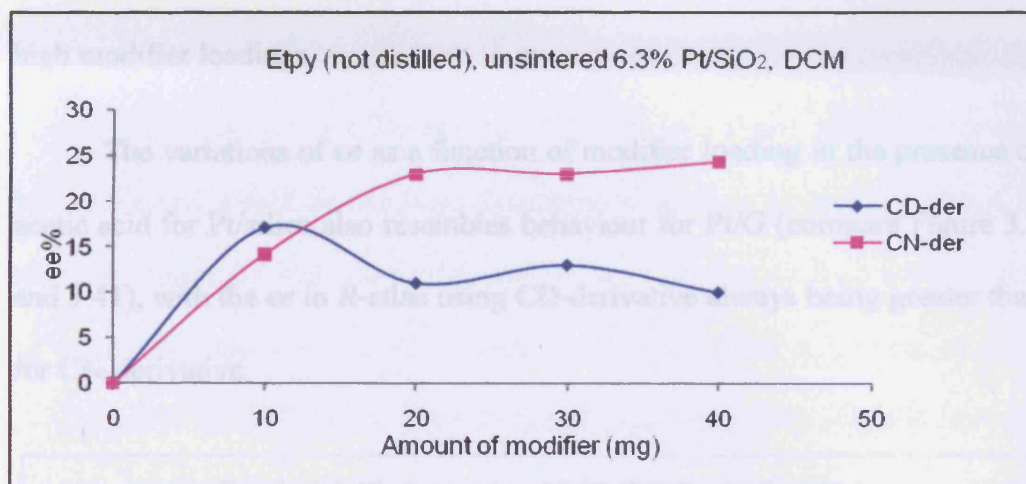


Figure 3.40 Enantiomeric excess versus amount of modifier (mg). Unsintered 6.3% Pt/silica catalyst in dichloromethane.

For example, CD-derivative passes through a definite maximum in  $ee$  as modifier loading increases whereas the trend for CN-derivative is of a gradual rise in  $ee$  to a plateau at highest loadings. At this stage CN-derivative always displays a greater  $ee$  to  $R$ -etlac than CD-derivative. The absolute values of  $ee$  at the different stages of modifier loading are also very similar for CN-derivative; if slightly lower for CD-derivative on Pt/silica. However, because of the generally close similarity in behaviour between the two supports, it is suggested that the same model as described earlier to explain these trends holds. To recap, for CD-derivative, adsorption at steps is dominant at low modifier loadings giving rise to an excess of  $R$ -etlac. However, as modifier



amount increases, a greater contribution from terrace sites (*S*-etlac) to the overall *ee* is observed. Hence the *ee* passes through a maximum. For CN-derivative in DCM, the same model pertains but because the *ee* always gives rise to an excess of *R*-etlac, it is necessary to assume that the *ee* from steps is low (assumption 4.2.1. iii)) and terraces dominate the overall *ee*, particularly at high modifier loadings.

The variations of *ee* as a function of modifier loading in the presence of acetic acid for Pt/silica also resembles behaviour for Pt/G (compare Figure 3.2 and 3.41), with the *ee* in *R*-etlac using CD-derivative always being greater than for CN-derivative.

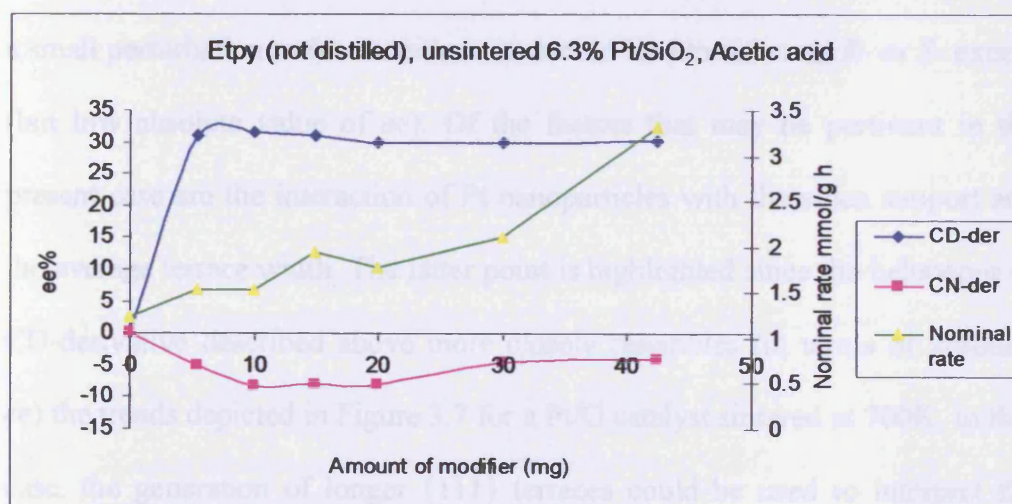


Figure 3.41 Enantiomeric excess versus amount of modifier (mg). Unsintered 6.3% Pt/silica catalyst in acetic acid.

However, for Pt/silica, the CN-derivative actually causes a *switch to an overall ee giving rise to S-etlac with acetic acid*. Within, the present model, these changes are ascribed to a “deactivation” of CD-derivative and CN-derivative when protonated and adsorbed on Pt{111} sites. Hence an overall

increase in  $ee$  is seen for CD-derivative upon adding acetic acid for both Pt/G and Pt/silica because step adsorption of modifier dominates the overall  $ee$  (to give  $R$ -etlac). In the case of CN-derivative, this model also holds true. However, in contrast to what was observed using Pt/G where terrace influence still controls the overall  $ee$  (since step/defect sites should only give rise to low  $ee$  to  $S$ -etlac), the step/defect sites at Pt/silica must dominate the enantioselectivity compared to terraces. It is still only about 5%  $S$ -etlac excess but it is a real effect. Hence, the silica support appears to promote  $ee$  (to  $S$ -etlac) at defect/step sites on the Pt catalyst nanoparticles. In fact, because low  $ee$  is speculated to occur for CN-derivative adsorbed either at terraces or steps in acetic acid, the balance between the two effects is probably very delicate and a small perturbation to favour either site would lead to either an  $R$ - or  $S$ - excess (but low absolute value of  $ee$ ). Of the factors that may be pertinent in the present case are the interaction of Pt nanoparticles with the silica support and the average terrace width. The latter point is highlighted since the behaviour of CD-derivative described above more closely resembles (in terms of absolute  $ee$ ) the trends depicted in Figure 3.7 for a Pt/G catalyst sintered at 700K. In that case, the generation of longer  $\{111\}$  terraces could be used to interpret the changes observed from going from unsintered (Figure 3.2) to sintered Pt/G catalysts. If this interpretation is extended to Pt/silica, it suggests that the extended Pt $\{111\}$  terraces present in the Pt/silica catalyst are similar in dimension to those encountered for sintered Pt/G. For DCM, this difference between Pt/G and Pt/silica would only manifest itself in marginal changes since

in DCM, steps dominate  $ee$ . In fact one would predict that the maximum in  $ee$  observed for Pt/silica in DCM as a function of modifier loading might occur at a somewhat lower absolute  $ee$  than observed with Pt/G (unsintered). Inspection of Figures 3.1 and 3.40 show that indeed, this is the case and also affords an explanation of the slightly lower  $ee$  for CD-derivative in DCM in Figure 3.40 compared to Figure 3.1. Since, a longer average Pt{111} terrace would be expected to give an even greater excess of  $R$ -etlac in acetic acid (assumption 4.2.3 iv)), the generation of an  $S$ -excess cannot be ascribed to the longer average Pt{111} terraces of Pt/silica compared to Pt/G (unsintered). Hence, the greater contribution of step/defect sites to  $ee$  is speculated to be due to perturbation by the silica support of such sites at the perimeter of the supported Pt nanoparticle such that the generation of  $S$ -etlac at steps is enhanced compared even to reaction on extended {111} terraces.

#### 4.2.8.2 Pt/alumina

Pt on alumina catalysts are known to require thermal pre-treatment in hydrogen in order to obtain the highest level of activity [12]. Such pre-treatment suggests that in the “unsintered” state, certain adsorption sites are not available for reaction. Based on surface science [18] and electrochemical studies [20, 21] it is reported that defect/step sites of platinum afford the most tenaciously held oxide moieties and it has been speculated that if this is indeed the case, then for alumina, the greater activity in thermally reduced catalysts is caused by reduction of such sites to pure platinum. In the present context, the models being developed to interpret changes in  $ee$  for alkaloid modified Orito-

chemistry depend crucially on the relative availability and activity of various fundamental step/defect and terrace sites. Therefore Pt/alumina affords an intriguing test of the models in relation to catalyst morphology.

In Figure 3.43 is shown *ee* as a function of CD-derivative and CN-derivative amount in DCM on unsintered Pt/alumina. The data resembles closely previous findings on Pt/G (Figure 3.1) and Pt/silica (Figure 3.40) showing an increase in *ee* up to a plateau for CN-derivative and a marked maximum in *ee* for CD-derivative. CD-derivative always gives a lower *ee* than CN-derivative at high loading.

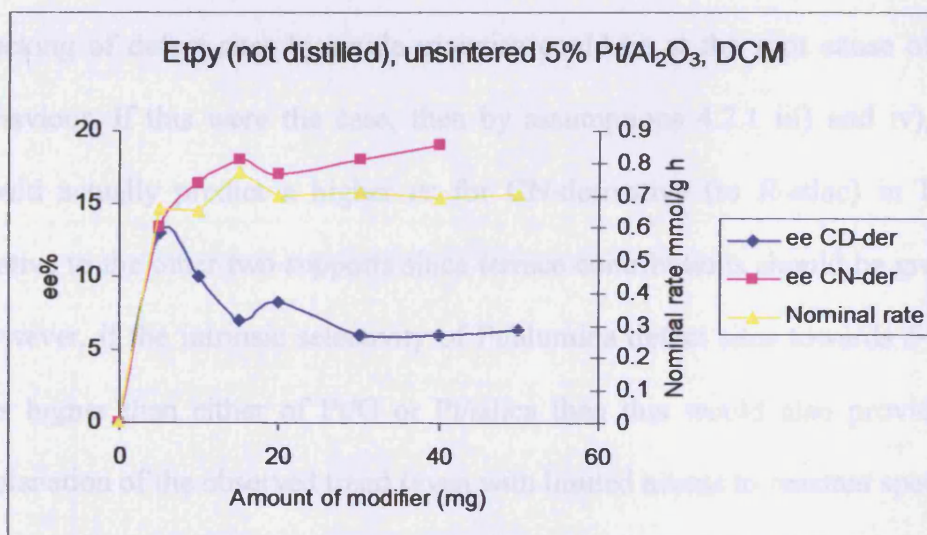


Figure 3.43 Enantiomeric excess in dichloromethane versus amount of modifier (mg). Unsintered 5% Pt/alumina catalyst.

Hence, as before, a model for CD-derivative adsorption at step sites for low modifier loading followed by population of terrace sites can be used to interpret the observed behaviour. Similarly, for CN-derivative, the low value of *ee* at both terrace and step sites but with terrace sites tipping the *ee* in favour of

an *R*-etlac excess would explain the trend observed with Pt/alumina. In contrast to Figures 3.1 and 3.40 however, in Figure 3.43 the absolute values of *ee* on unsintered Pt/alumina are all smaller (for CN-derivative around 18% *R* on Pt/alumina compared to 28% *R*- for Pt/G (unsintered) and 24% *R*- for Pt/silica. For CD-derivative at high loadings around 7% *R*- on Pt/alumina compared to 10% *R*- on Pt/G (unsintered) and 10% *R*- on Pt/silica). Hence for CD-derivative, there is little variation of *ee* with support in DCM whereas for CN-derivative there is a significant decrease in *ee* in the case of alumina, presumably again due to the critical balance between step/defect and Pt{111} terrace contributions for this modifier. It is difficult to say whether partial blocking of defect sites by oxide moieties could be at the root cause of this behaviour. If this were the case, then by assumptions 4.2.1 iii) and iv), one would actually predict a higher *ee* for CN-derivative (to *R*-etlac) in DCM relative to the other two supports since terrace contributions should be greater. However, if the intrinsic selectivity of Pt/alumina defect sites towards *S*-etlac was higher than either of Pt/G or Pt/silica then this would also provide an explanation of the observed trend (even with limited access to reactant species). It is already well reported that Pt/alumina catalysts afford the highest *ee* for the Orito reaction when using CN and CD as modifiers [12]. A test of this hypothesis would be that if after thermal annealing to remove oxide moieties from defects/steps, the *ee* obtained using CN-derivative actually decreased, then the full selectivity of the step sites towards *S*-etlac production should become available. Inspection of Figure 3.45 shows that indeed this is the case

with a fall in *ee* using CN-derivative being observed for the 700K/hydrogen annealed sample compared to unsintered catalyst. For CD-derivative, a slight increase in *ee* at highest modifier loading from approximately 6% to 10% after annealing Pt/alumina at 700K in hydrogen would also be consistent with a greater influence of steps than before to the overall *ee* although it should be noted that the trend for CD-derivative with unsintered catalyst (Figure 3.43) is very similar with a marked maximum again being observed at low modifier loadings. For unsintered Pt/alumina in acetic acid (Figure 3.44), very similar behaviour to that described for Pt/G and Pt/silica is seen with a marked decrease in *ee* being observed for CN-derivative and a significant increase in *ee* using CD-derivative.

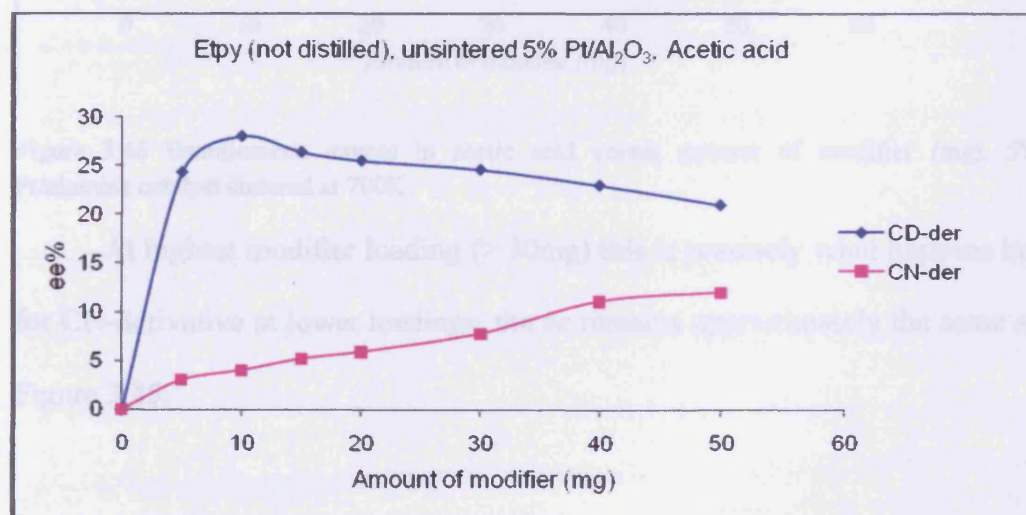


Figure 3.44 Enantiomeric excess in acetic acid versus amount of modifier (mg). Unsintered 5% Pt/alumina catalyst.

Both trends are well explained in terms of fast racemic reaction using CD-derivative and CN-derivative at terrace sites when protonated as proposed

for Pt/G and Pt/silica. Unlike Pt/silica however, this time no *ee* towards *S*-etlac was observed for CN-derivative and behaviour resembled more closely Pt/G. If this behaviour corresponds to slightly blocked step sites by oxide moieties then full reduction of these species should lead to a still larger increase in the *ee* towards *R*- etlac in the case of CD-derivative and a lower *ee* in the case of CN-derivative. Inspection of Figure 3.44 shows that this is largely what happens.

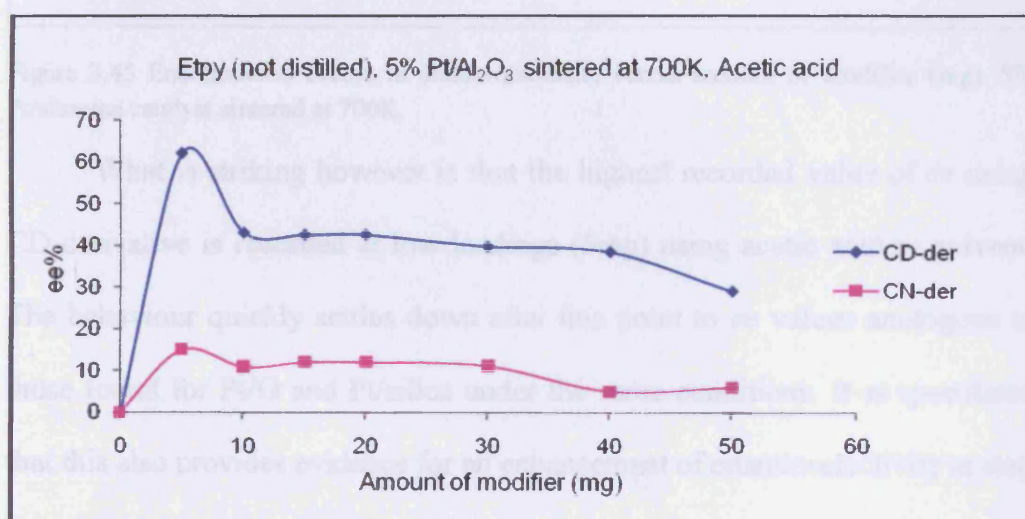


Figure 3.46 Enantiomeric excess in acetic acid versus amount of modifier (mg). 5% Pt/alumina catalyst sintered at 700K.

At highest modifier loading (> 30mg) this is precisely what happens but for CN-derivative at lower loadings, the *ee* remains approximately the same as Figure 3.45.

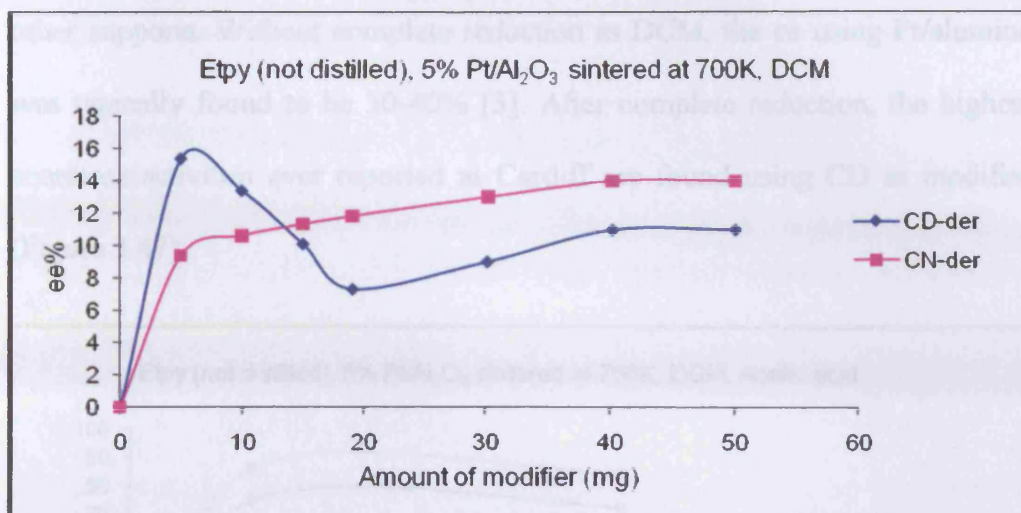


Figure 3.45 Enantiomeric excess in dichloromethane versus amount of modifier (mg). 5% Pt/alumina catalyst sintered at 700K.

What is striking however is that the highest recorded value of *ee* using CD-derivative is recorded at low loadings (5mg) using acetic acid as solvent. The behaviour quickly settles down after this point to *ee* values analogous to those found for Pt/G and Pt/silica under the same conditions. It is speculated that this also provides evidence for an enhancement of enantioselectivity at step sites adjacent to the alumina oxide support over and above that exhibited by either Pt/G or Pt/silica since at low loadings of CD-derivative; step site adsorption is thought to dominate (see earlier discussion in relation to Pt/G). Hence, it does appear that partial reduction of step/defect sites does give rise to important but (within the present context) explicable changes in *ee* again highlighting the key role played by these sites in generating high values of *ee*.

It has been reported that Pt/alumina should give higher *ee* than any other support [12]. Hence, it was thought prudent to test this hypothesis under Cardiff standard conditions using CD as modifier in order to compare with the



other supports. Without complete reduction in DCM, the *ee* using Pt/alumina was typically found to be 30-40% [3]. After complete reduction, the highest enantioselectivities ever reported at Cardiff are found using CD as modifier (Figure 3.47).

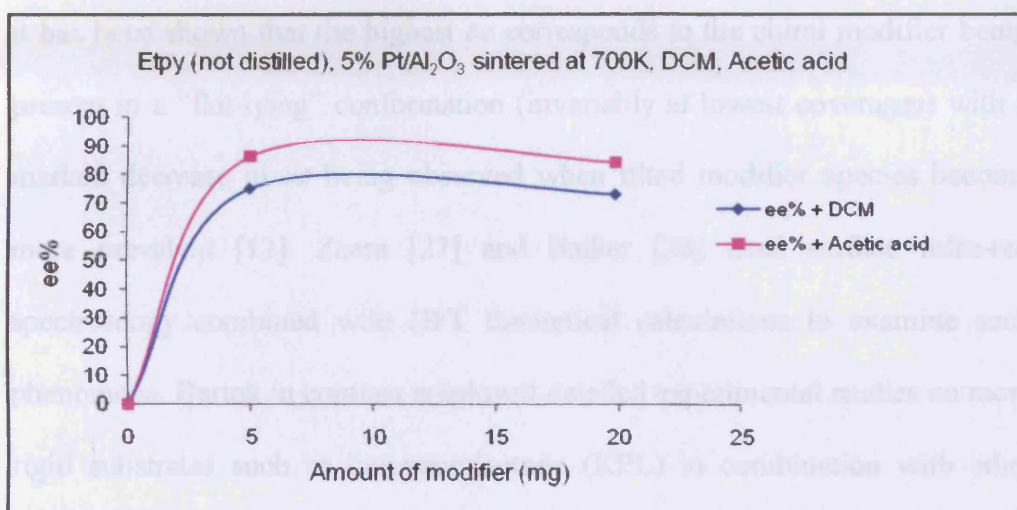


Figure 3.47 Enantiomeric excess in acetic acid and dichloromethane versus amount of modifier (mg). 5% Pt/alumina catalyst sintered at 700K.

These are typically 86% in acetic acid and 74% in DCM. Hence the literature results are reproduced which lends strength to measurements being performed here but also highlights that if the assumptions in 4.2.4 i) and ii) are correct, a simple explanation of this trend is afforded. The existing model of changes in modifier configuration as a function of solvent type, or rather dielectric constant [22] suffers from two weaknesses. The first being that modifier configurations in solution may not necessarily reflect the modifier configuration at the surface that induces *ee*. Second, although acetic acid possesses a rather large dielectric constant, it still gives rise to the highest *ee* of all solvents [6, 23].

### 4.3 Possible configurations of modifier in controlling enantioselectivity

Recent work, particularly by Zaera [24], Baiker [25] and Bartok [26] has emphasized the importance of the orientation of the modifier on the Pt catalyst surface being correlated with *ee* for ethyl pyruvate hydrogenation. In particular, it has been shown that the highest *ee* corresponds to the chiral modifier being present in a “flat-lying” conformation (invariably at lowest coverages) with a marked decrease in *ee* being observed when tilted modifier species become more prevalent [12]. Zaera [27] and Baiker [28] used surface infra-red spectroscopy combined with DFT theoretical calculations to examine such phenomena. Bartok in contrast employed detailed experimental studies on more rigid substrates such as ketopantolactone (KPL) in combination with ether derivatives of CN, CD, quinidine and quinine in different solvents (and also DFT) to propose a new model of enantiodifferentiation based on the “tilt angle” of modifier [29] and also the “attack” angle of the nitrogen lone pair on the quinuclidine moiety with the activated carbonyl group of the substrate [29]. Hence, stereochemical control based on an approximately open-3 configuration of the surface modifier docking at a variable tilt angle with the substrate is proposed to control the overall *ee* as a function of modifier structure. In extreme cases of “bulky” ether substituents attached to the CD or CN, inversion of overall *ee* can be observed [30]. In the present context, it has been shown that *ee* can be changed significantly (and even inverted in acetic acid solvent using silica supported Pt) as a function of modifier concentration. To explain this, a model based on differential adsorption at step/defects or terraces

has been proposed. If instead, changes in tilt angle *alone* were responsible for this behaviour (the tacet assumption in such models being that all adsorption is taking place on “flat” surfaces) it could not explain the specific correlations between bismuth site occupation and changes in *ee* reported in the present study. Nonetheless, it still has to be explained as to why protonation of CD leads to a marked decrease in *ee* at Pt{111} sites but little change in *ee* occurs for adsorption at defects/steps, a crucial aspect of the present study.

In what follows, a model for the interpretation of *ee* changes when CD-der and CN-der *and their protonated forms* adsorb at terrace and step sites will be given incorporating the notion of the “tilt” angle of the quinoline ring. It should be noted that the question of why the tilt angle should be a significant factor has not really been addressed as yet. It has simply been found empirically to be correlated with *ee* [24]. It is proposed here that the reason for this effect may be rationalised by reference to the recent model proposed by McBreen *et al* [31] for enantioinduction based on hydrogen bonding interactions between EP and CD. It will be recalled (Figure 1.20) that in McBreen’s speculation; the enantio-directing influence of CD was based on a two point model. The carbonyl of the ester substituent of EP formed a hydrogen bond with the quinuclidine nitrogen of CD with the keto- carbonyl of EP hydrogen bonding with hydrogen atoms of the quinoline substituent *previously activated by their interaction with the Pt surface*. Clearly, if the second interaction is important, the tilt angle of the quinoline will be crucial in determining the magnitude of this interaction (since the degree of electron

withdrawal by the metal surface depends on overlap of its  $\pi$ -system with  $d$ -orbitals). Hence, it is proposed that any tilting away from the “flat lying” configuration of the chiral modifier will lead to loss of control of the stereo-directing influence of the modifier and a decrease in overall  $ee$ .

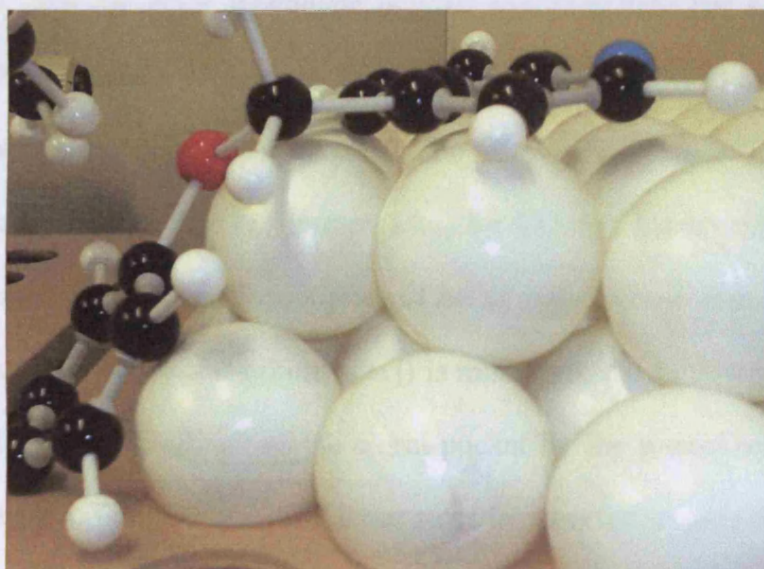


Figure 4.1 Real space schematic representing CD-derivative adsorbed at step-kink site; red = O, black = C, blue = N, small white = H, and large white = Pt surface.

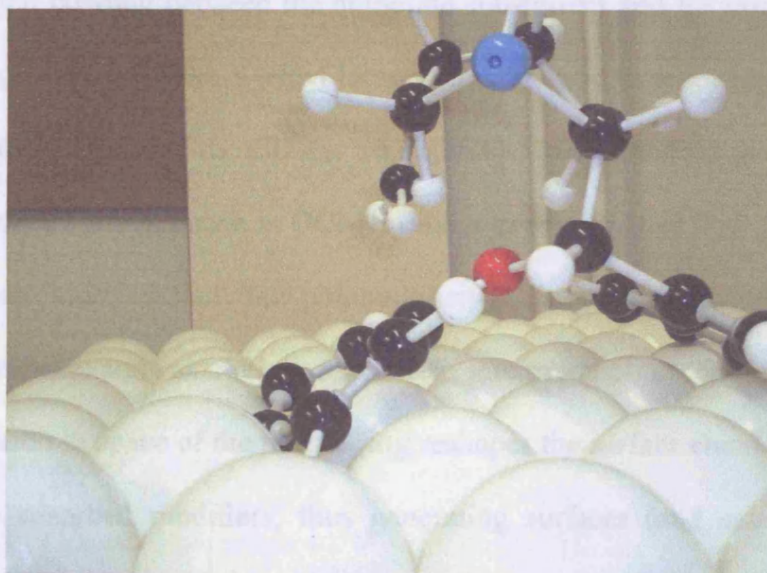


Figure 4.2 Real space schematic representing CD-derivative adsorbed at a flat Pt{111} terrace; red = O, black = C, blue = N, small white = H, and large white = Pt surface.

Figure 4.1 shows how CD-der might adsorb at a step-kink site adjacent to the support (*i.e.* at the rim of the supported Pt nanoparticle) and Figure 4.2 the adsorption of the same molecule at a flat Pt{111} terrace. It is evident that in the former, the quinoline substituent is lying perfectly flat along the Pt{111} terrace with the ether substituent bonded approximately flat against the two atom high step site. In contrast, for adsorption on the Pt{111} terrace it is very difficult for the quinoline substituent to lie flat to the surface. This means that when adsorbed on Pt{111} terrace sites, for CD-der, the crucial activation of the quinoline hydrogen atoms (caused by strong electron coupling of the *pi*-system with the metal *d*-orbitals [31]) is much reduced (although we shall see later that the “crowding” of the chiral pocket by the phenyl substituent may also be important). Hence, CD-der at steps is expected to give the same chiral induction as CD (because CD also lies flat) and this is indeed the case (assumptions 4.2.1. i) and 4.2.3.i)). In CD-der on Pt{111}, the absence of hydrogen bonding between the quinoline substituent and EP presumably leads to the generation of the *S*- ethyl lactate product upon hydrogenation of EP. But what arrangement of the CD-der on Pt{111} terraces should give rise to 40% *ee* towards *S*-ethyl lactate in DCM? Baiker *et al* [28] used both DFT and ATR IR spectroscopy to study this point explicitly. Their conclusion was as follows: “Experiments and calculations support an interpretation according to which the orientation in space of the phenyl ring reshapes the surface chiral space formed by the adsorbed modifiers, thus generating surfaces (and catalysts) having different, in some cases even opposite enantioselective properties, without

altering the absolute configuration of the modifier.” That is, the movement of the phenyl ring reconfigures the chiral space available for docking.

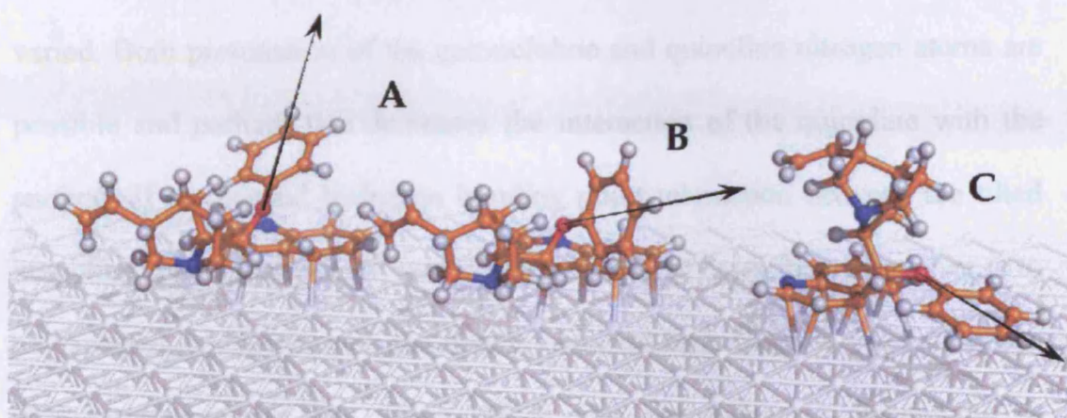


Figure 4.3 Three relevant surface conformations of PhOCD, the differences being in a range of *ca.* 2 kcal/mol. Note that in conformers (B) and (C) the phenyl ring is close to the metal and can interfere in the interaction with the substrate, while in conformation (A) the chiral space is similar to that of CD. Reproduced from reference [32].

According to reference [32] “In the case of Figure 4.3A, it is apparent that the phenyl cannot interfere with an incoming substrate, since it lies above the quinoline ring. This absence of the phenyl ring close to the metal reactive site virtually reproduces the chiral space displayed by CD. On the contrary, in the other case (Figure 4.3B and 4.3C) the phenyl ring can hinder the access to some metal sites close to the modifier, which are critical for the docking of the incoming substrate.” It should be noted that in Figure 4.3, the most important configurations responsible for chiral induction actually involve a flat lying quinoline system so “McBreen-like” hydrogen bonding interactions should be possible! Hence, if we assume that such configurations are responsible for the generation of an excess in *S*-ethyl lactate, why should this *ee* decrease

significantly in acidic solvents (this fact also being true of CD adsorbed on Pt{111} terraces) according to assumptions 4.2.3 ii) and 4.2.4 ii) respectively? We speculate that in fact when protonated, both CD and CD-der tilt when adsorbed on Pt{111} planes! The reasons for this effect could be wide and varied. Both protonation of the quinuclidine and quinoline nitrogen atoms are possible and perhaps this decreases the interaction of the quinoline with the surface? If the second hydrogen bonding point interaction between the tilted quinoline substituent and EP was weakened in both cases then a lower *ee* is to be expected, consistent with the results obtained here. Clearly, when adsorbed at a step/defect site, the tilting effect does not appear to change the *ee* (assumptions 4.2.3 i) and 4.2.4.i)). In order to accommodate this result, one has to further speculate that the chiral space available when modifiers are adsorbed at the step/defect site at the perimeter of the Pt nanoparticle and support is not compromised to the extent it is when molecular tilting occurs on a two dimensional plane. The above interpretation must also apply to CN-der and CN when using acidic solvents. Clearly, a spectroscopic study comparing CD/CN adsorption in aprotic solvents [33] with adsorption in protic solvents would be useful here to confirm the present speculations. Although no vibrational studies have been published of CD in acetic acid, unpublished Raman spectroscopy studies of CD adsorbed on Pt electrodes in sulphuric acid under hydrogenating conditions demonstrate conclusively that ring modes that should be invisible if planar adsorption was occurring are observed irrespective of CD coverage [34]. Hence, in contrast to Zaera [33] using aprotic solvents, the disappearance of

CD ring breathing vibrational modes was never observed in the *in situ* electrochemical studies. Hence, the model proposed, based on lesser or greater interaction of quinoline H atoms (H-bonding) appears to be compatible with all of the experimental findings reported in the present study, the studies by Jenkins [2] and Albdulahrahman [1] and the studies by Hutchings *et al* [30].



#### 4.4 References

- [1] A.M.S. Alabdulrahman. Ph.D. Thesis, Cardiff University, 2007.
- [2] D.J. Jenkins. Ph.D. Thesis, Cardiff University, 2003.
- [3] G.A. Attard and S.F. Elkhaseh, *unpublished results*.
- [3] J.L. Margifalvi and M. Hegedüs, *J. Mol. Catal. A: Chemical*, **107** (1996) 281.
- [4] A. Baiker, *J. Mol. Catal. A: Chemical*, **155** (1997) 473.
- [5] M. Bartók, K. Balázsik, I. Bucsí, Gy. Szöllösi, *J. Mol. Catal. A: Chemical*, **280** (2008) 87.
- [6] H.-U. Blaser, H.P. Jalett and J. Wiehl, *J. Mol. Catal.*, **68** (1991) 215.
- [7] H.-U. Blaser, *Chem. Commun.*, (2003) 293.
- [8] M. Bartók, K. Felföldi, G. Szöllösi and T. Bartók, *Catal. Lett.*, **61** (1999) 1.
- [9] M. Bartók, K. Felföldi, B. Török and T. Bartók, *Chem. Commun.*, **2605** (1998).
- [10] N.F. Dummer, R. Jenkins, X. Li, S.M. Bawaked, P. McMorn, A. Burrows, C.J. Kiely, R.P. K. Wells, D.J, G.J. Hutchings, *J. Catal.* **243** (2006) 165.
- [11] D.J. Watson. Ph.D. Thesis, Cardiff University, 2003.
- [12] Baiker, *J. Mol. Catal.*, **163** (2000) 205.
- [13] D. Ferri, T. Bürgi and A. Baiker, *J. Chem. Soc. Perkin. Trans.*, **7** (1999) 1305.
- [14] B. Minder, T. Mallat, P. Skrabal and A. Baiker, *Catal. Lett.*, **29** (1994) 115.

- [15] K. Szőri, K. Balázsik, K. Felföldi, I. Bucsi, S. Cserényi, G. Szöllősi, E. Vass, M. Hollósi, M. Bartók, *J. Mol. Catal. A: Chemical*, **294** (2008) 14.
- [16] S. Diezi, T. Mallat, A. Szabo, A. Baiker, *J. Catal.*, **228** (2004) 162.
- [17] S. Diezi, Szabó, T. Mallat, A. Baiker, *Tetrahedron: Asym.*, **14** (2003) 2573.
- [18] T. Mallat, S. Frauchiger, P. J. Kooyman, M. Schürch and A. Baiker., *Catal. Lett.*, **63** (1999) 121.
- [19] H.-U. Blaser, H.P. Jalett, W. Lottnbach, M. Studer, *J. Am. Chem. Soc.*, **122** (2000) 1275.
- [20] N.P. Lebedeva, M.T. M. Koper, E. Herroero, J.M Feliu, R.A. van Santen, *J. Electroanal. Chem.*, **487** (2000) 37.
- [21] N.P. Lebedeva, A. Rodes, J.M Feliu, M.T. M. Koper, and R.A. van Santen, *J. Phys. Chem., B* **106** (2002) 9863.
- [22] J.T. Wehrli, A. Baiker, D. M. Monti, H.-U. Blaser and H.P. Jalett, *J. Mol. Catal.*, **57** (1998) 245.
- [23] B. Török, K. Felföldi, G. Szakonyi, K. Balázsik and M. Bartók, *Catal. Lett.*, **52** (1998) 81.
- [24] L. Mink, Z. Ma, R.A. Olsen, J.N. James, D.S. Sholl, L.J. Mueller, F. Zaera, *Top. Catal.*, **48** (2008) 120.
- [25] E. Orglmeister, T. Bürgi, T. Mallat, A. Baiker, *J. Catal.*, **232** (2005) 137.
- [26] M. Bartók, M. Sutyinszki, K. Felföldi, *J. Catal.*, **220** (2003) 207.
- [27] Z. Ma, I. Lee and F. Zaera, *J. Am. Chem. Soc.*, **129** (2007) 51.
- [28] A. Vargas, S. Reimann, S. Diezi, T. Mallat, A. Baiker, *J. Mol. Catal. A: Chemical*, **282** (2008) 1.

- [29] K. Balázsik, I. Bucsí, S. Cserényi, G. Szöllősi, M. Bartók, *J. Mol. Catal. A: Chemical*, **285** (2008) 84.
- [30] X. Li, N.F. Dummer, R. Jenkins, R.P. K. Wells, P.B. Wells, D.J. Willock, S.H. Taylor, P. Johnston, G.J. Hutchings, *Catal. Lett.*, **96** (2004) 147.
- [31] S. Lavoie, M.-A. Laliberte, I. Temprano, P.H. McBreen, *J. Am. Chem. Soc.*, **128** (2006) 7588.
- [32] A. Vargas, D. Ferri, N. Bonalumi, T. Mallat, and A. Baiker, *Angew. Chem. Int. Ed.*, **46** (2007) 3905.
- [33] Z. Ma, F. Zaera, *J. Phys. Chem. B* **109** (2005) 406.
- [34] G.A. Attard and R.J. Taylor, *unpublished results*.

**CHAPTER FIVE**  
**SUMMARY AND**  
**FUTURE WORK**

## 5.1 Summary and future work

Certain aspects of the enantioselective hydrogenation of  $\alpha$ -ketoesters (etpy) (Orito reaction) over cinchona-modified Pt/G, Pt/SiO<sub>2</sub> and Pt/Al<sub>2</sub>O<sub>3</sub> have been investigated in detail. The significant backbone of this study was to examine the influence of catalysts on the title enantioselective reaction in the presence of ether-derivatives of the modifier CD and CN by selectively blocking step, kink, and terrace sites by bismuth adatoms and then to test activity and selectivity. The solvent dependence of the enantiomeric excess for the hydrogenation is interpreted in terms of the conformational behaviour of cinchona alkaloids particularly the “tilt” angle of the quinoline with respect to the surface. The Pt{111} terrace sites showed an interesting effect on enantiomeric excess whereby a loss of *ee* for the protonated modifier was observed. It is also deduced that hydrogenation of ethyl pyruvate affords an enantiomeric excess to *R*-(*S*-) ethyl lactate in DCM if CD-der (CN-der) is adsorbed at step/defect sites whereas an excess of *S*- (*R*-) ethyl lactate results from adsorption of CD-der (CN-der) at Pt{111} terrace sites. From the results obtained it appears that blockage of kink and step sites have a more significant effect on enantiomeric excess than occupation by bismuth of terrace sites. The influence of particle size, metal loading and solvent effects in relation to changes in *ee* were examined as a result of changing metal loading (and consequently particle size). It was noted that only marginal changes in *ee* were found as a function of particle size with the a decrease in overall *ee* being observed for the 0.5% Pt/G catalyst relative to the other two catalyst.

Taken together, the results and models proposed in the present study afford a straightforward and reasonably clear description of a complex surface reaction. Predictions stemming from the invocation of McBreen's model to interpret enantioselectivity have been challenged recently by Baiker [1] in that modifiers such as quinidine and quinine (containing as they do a methoxy substituent at one of the critical "H-bonding" positions on the quinoline element of the modifier) still give rise to high *ee* even though sterically, a decrease in *ee* would perhaps be expected? Hence, future experiments to verify the veracity of the McBreen model would include the synthesis of organic analogue molecules of CD and CN that would preclude entirely any H-bonding interactions by the quinoline with the substrate. The prediction would be that such modifiers would give rise to very low *ee*. Another aspect of the present interpretation of changes in *ee* (as a function of *pH* for example) would be an *in situ* study of CD, CN and other modifiers adsorbed on platinum single crystals in acetic acid solvents. In particular, an *in situ* NEXAFS study like those performed previously by Lambert *et al* [2] under UHV conditions would be most useful (using flame-annealed Pt electrodes and fluorescence detection of X-ray absorption in a thin layer configuration). The observation predicted would be of "flat-lying" quinoline group under aprotic solvents and a "tilted" version with acetic acid. One could always extrapolate such measurements to real catalysts using selective blocking by bismuth of all step/defect sites leaving only Pt{111} terrace sites free. However, RAIRS or SERS should be used instead of NEXAFS in this case since the surface selection rule would ensure that only

vibrational modes giving rise to a change in dipole moment perpendicular to the surface will be observed. It would also be very interesting to investigate other prochiral substrates in Orito-type surface hydrogenation in order to explore further the influence of selective blocking of platinum adsorption sites by bismuth. Will similar trends found with ethyl pyruvate be observed and if not, why not? In particular, non-enolisable substrates such as ethyl benzoyl formate might offer an interesting way of probing keto-enol tautomerism in the surface chemistry of the Orito reaction. Substrates that might afford a “crowding” of the chiral space around the quinuclidine/quinoline of the modifier might also prove interesting, particularly if the degree of activation of the keto-carbonyl determines the magnitude of the H-bonding interactions. In this context, STM studies of modifiers coadsorbed with substrates in which this parameter is controlled might reveal a correlation between the extent of “docking” *via* H-bonding interactions (both quinuclidine and quinoline) and *ee* under real conditions of reaction (high pressure, solvent *etc*). The vexed question here to be answered would be:

“Is the Orito reaction mechanism specific to ethyl pyruvate or is it “universal” irrespective of modifier/substrate combination?”

Perhaps it is striving for an answer to this question that future work should be directed.

## **5.2 References**

- [1] T. Mallat, E. Orglmeister, A. Baiker, *Chem. Rev.*, **107** (2007) 4863.
- [2] J.M. Bonello, F.J. Williams, R.M. Lambert, *J. Am. Chem. Soc.*, **125** (2003) 2723.